Report Prepared by:
Dr. Francisco J. Presuel–Moreno
With
Rolando Bencosme
Kazi Hoque
Manzurul Nazim
Dr. Amirkhosro Kazemi
Dr. Fujian Tang

Final Report

Corrosion Propagation of Carbon Steel Rebars in High Performance Concrete
BDV27–977–08

Submitted to
Florida Department of Transportation Research Center
605 Suwannee Street
Tallahassee, Florida 32399

Submitted by
Francisco Presuel–Moreno
Principal Investigator
Department of Ocean and Mechanical Engineering
Center for Marine Materials
Florida Atlantic University – Sea Tech

101 North Beach Road
Dania Beach, Florida 33004

November 2018

Disclaimer

The opinions, findings, and conclusions expressed in this publication are those of the author and not necessarily those of the State of Florida Department of Transportation.

Units Conversion Page

APPROXIMATE CONVERSIONS TO SI UNITS				
Symbol	**When You Know**	**Multiply By**	**To Find**	**Symbol**
		LENGTH		
in	inches	25.4	millimeters	mm
ft	feet	0.305	meters	m
yd	yards	0.914	meters	m
mi	miles	1.61	kilometers	km
		AREA		
in^2	square inches	645.2	square millimeters	mm^2
ft^2	square feet	0.093	square meters	m^2
yd^2	square yard	0.836	square meters	m^2
ac	acres	0.405	hectares	ha
mi^2	square miles	2.59	square kilometers	km^2
		VOLUME		
fl oz	fluid ounces	29.57	milliliters	mL
gal	gallons	3.785	liters	L
ft^3	cubic feet	0.028	cubic meters	m^3
yd^3	cubic yards	0.765	cubic meters	m^3
	NOTE: volumes greater than 1000 L shall be shown in m^3			
		MASS		
oz	ounces	28.35	grams	g
lb	pounds	0.454	kilograms	kg
T	short tons (2000 lb)	0.907	megagrams (or "metric ton")	Mg (or "t")
		TEMPERATURE (exact degrees)		
°F	Fahrenheit	5 (F-32)/9 or (F-32)/1.8	Celsius	°C
		ILLUMINATION		
fc	foot-candles	10.76	lux	lx
fl	foot-Lamberts	3.426	$candela/m^2$	cd/m^2
		FORCE and PRESSURE or STRESS		
lbf	poundforce	4.45	newtons	N
lbf/in^2	poundforce per square inch	6.89	kilopascals	kPa

APPROXIMATE CONVERSIONS FROM SI UNITS				
Symbol	**When You Know**	**Multiply By**	**To Find**	**Symbol**
		LENGTH		
mm	millimeters	0.039	inches	in
m	meters	3.28	feet	ft
m	meters	1.09	yards	yd
km	kilometers	0.621	miles	mi
		AREA		
mm^2	square millimeters	0.0016	square inches	in^2
m^2	square meters	10.764	square feet	ft^2
m^2	square meters	1.195	square yards	yd^2
ha	hectares	2.47	acres	ac
km^2	square kilometers	0.386	square miles	mi^2
		VOLUME		
mL	milliliters	0.034	fluid ounces	fl oz
L	liters	0.264	gallons	gal
m^3	cubic meters	35.314	cubic feet	ft^3
m^3	cubic meters	1.307	cubic yards	yd^3
		MASS		
g	grams	0.035	ounces	oz
kg	kilograms	2.202	pounds	lb
Mg (or "t")	megagrams (or "metric ton")	1.103	short tons (2000 lb)	T
		TEMPERATURE (exact degrees)		
°C	Celsius	1.8C+32	Fahrenheit	°F
		ILLUMINATION		
lx	lux	0.0929	foot-candles	fc
cd/m^2	$candela/m^2$	0.2919	foot-Lamberts	fl
		FORCE and PRESSURE or STRESS		
N	newtons	0.225	poundforce	lbf
kPa	kilopascals	0.145	poundforce per square inch	lbf/in^2

*SI is the symbol for the International System of Units. Appropriate rounding should be made to comply with Section 4 of ASTM E380.
(Revised March 2003)

Technical Report Documentation Page

1. Report No.	2. Government Accession No.	3. Recipient's Catalog No.
4. Title and Subtitle Corrosion Propagation of Carbon Steel Rebars in High Performance Concrete		5. Report Date August 2018
		6. Performing Organization Code FAU–OE-cmM–08–3
7. Author(s) Francisco J. Presuel–Moreno, Rolando Bencosme, Kazi Hoque, Manzurul Nazim, Dr. Amirkhosro Kazemi, Dr. Fujian Tang.		8. Performing Organization Report No. BDV27–977–08
9. Performing Organization Name and Address Center for Marine Materials Florida Atlantic University – SeaTech 101 North Beach Road Dania Beach, Florida 33004		10. Work Unit No. (TRAIS)
		11. Contract or Grant No. BDV27–977–08
12. Sponsoring Agency Name and Address Florida Department of Transportation 605 Suwannee Street, MS 30 Tallahassee, FL 32399		13. Type of Report and Period Covered Final Report December 21, 2015 – November 15, 2018
		14. Sponsoring Agency Code
15. Supplementary Notes		

16. Abstract

A better understanding of the corrosion propagation of carbon steel rebar embedded in high performance concrete is needed. The project aim was to fill some of the knowledge gaps. The study used samples exposed outdoors (now) for over 24 years to wet/dry cycles with seawater. The concrete of these samples can be considered high performance concrete because in some of the mixes prepared, the fly ash content ranged from 20 percent to 50 percent, and in other mixes, the amount of silica fume was varied. The corrosion rate was monitored over 18 months using a commercial rebar potential and rebar corrosion rate monitoring device.

Accelerated chloride transport was applied via electromigration to samples exposed indoors. Electromigration worked well to accelerate the initiation of corrosion. The indoor samples had concrete covers that ranged from 5 cm to 0.8 cm. The length of the solution reservoir ranged from 2.5 cm to 17 cm. Four types of samples were prepared in 2016, and samples prepared as part of previous research efforts were also used. The concrete composition in some of the samples was 50 percent blast furnace slag; in others, 20 percent fly ash. A smaller number of samples were prepared with 20 percent fly ash and 8 percent silica fume, a similar number of samples were prepared with 50 percent blast furnace slag and 20 percent fly ash. The rebar potentials, polarization resistance, and solution resistance were monitored after installing the solution reservoirs. More than a year's worth of data was used to assess the corrosion propagation stage.

Selected samples were identified for forensic analysis from both indoor and outdoor samples. The concrete surface was assessed, and in some cases, cracks were present. The rebars were cleaned, and the mass fraction loss determined (for those with significant mass loss) and compared to the measured corrosion rate.

It was found that cracks occurred on some of the specimens cast with high performance concrete and that the duration of the corrosion propagation that caused the cracks was a few years. (If the corrosion initiation is considered from a large potential drop, the duration would be longer if the corrosion propagation is counted from when a more gradual rebar potential drop started).

Corrosion appears to have initiated at small sites and did not appear to have grown significantly on samples subjected to accelerated chloride transport as part of this project.

17. Key Word	18. Distribution Statement		
Reinforced Concrete, High Performance Concrete, Corrosion Initiation, Corrosion Propagation, Forensic Examination, Pitting Factor, Exposure Time.			
19. Security Classif. (of this report) Unclassified	20. Security Classif. (of this page) Unclassified	21. No. of Pages 248	22. Price

Form DOT F 1700.7 (8–72) Reproduction of completed page authorized

Acknowledgments

The authors are indebted to the FDOT State Materials Office (SMO) for assisting in preparing new reinforced concrete samples, conducting several tests at SMO, and assistance during the field visits for this study, in particular, Mr. Ivan Lasa, Mr. Ronald Simmons, and several SMO technicians (Dennis Baldi, Teresa Risher, Cody Owen), personnel of the concrete laboratory at SMO. The author also acknowledges the assistance of several students who worked as graduate/undergraduate research assistants at FAU–SeaTech marine materials and corrosion lab during the duration of this project.

Executive Summary

The main objective of the project was to better understand the corrosion propagation that takes place on carbon steel rebars that are embedded in high-performance concrete. Some of the bridges that were built in Florida during the mid to late 1980s and early 1990s could soon reach an age in which the chloride concentration at the rebar trace could potentially initiate corrosion. There have been reports that suggest that the rebar corrosion rate (once corrosion has initiated) is lower on concrete with higher resistivity. This in part might be due to the smaller macrocell and the smaller throwing power. It is important to differentiate between the concrete bulk resistivity and the solution resistance (and corresponding resistivity) that is measured between the reinforcing steel and the concrete surface as obtained by a corrosion rate measuring device. The bulk resistivity of high-performance concrete can change significantly depending on the moisture content, age, and curing condition, but even under saturated conditions, the bulk resistivity is typically greater than 10 kΩ. The resistivity (obtained from solution resistance based on geometry) measured by a device in the field or on a lab specimen can be quite different. In part due to the rebar presence that reduces the resistivity value measured (see previous publication for FDOT (F. Presuel-Moreno, Liu, and Suarez 2010)), but also it could be due in part to chloride buildup (and subsequent moisture increase due to chlorides being hygroscopic) or a combination of both. Once corrosion has progressed for sometime such that a crack forms and remains wet, an additional reduction could develop in the solution resistance with a corresponding resistivity drop. In contrast, during the dry season, the concrete resistivity can increase significantly.

Samples were prepared as part of this investigation with four different concrete compositions. There were three sets of older samples that were also used as part of this investigation. A set of older samples was exposed outdoors and has been subjected to wet/dry cycles with seawater for over 24 years (F Presuel-Moreno et al. 2013). These samples had binary compositions (20% to 50% fly ash or silica fume in slurry form ranging from 6% to 25%) with a water to cementitious-material ratio (w/cm) of 0.37. The concrete cover for these samples was either 1.9 cm or 3.2 cm. Single rebar and four-rebar specimens were prepared in 2008 and 2009 as part of a different research work (F. Presuel-Moreno, Liu, and Suarez 2010). The concrete cover for these samples was 5 cm (top rebar layer), and the concrete composition had a w/cm of 0.41 and three cementitious compositions: ordinary Portland cement (OPC), OPC+fly ash (FA), and OPC+FA+silica fume (SF). Finally, single rebar specimens were prepared in 2006 as a part of previous research (Tanner 2006), but mortar was used instead of concrete (two compositions were prepared, but samples described here are those with OPC+FA and w/cm of 0.37). The mortar cover for these samples was 0.8 cm. Composition details can be found in the experimental section.

Except for the samples that have been exposed for more than 24 years, most other samples were subjected to electromigration. A solution reservoir was installed, and a 10% NaCl solution was added. The electromigration accelerates the chloride transport from the top reservoir towards the rebar. Electromigration took place once the concrete samples were several months to several years old. The passive layer is expected to have formed on the rebar on most specimens (concrete samples prepared in 2016 with slag and FA+SF might not have fully formed the passive layer due to high moisture content at the rebar depth). The experimental section describes how the electromigration was applied.

An interesting finding that should be kept in mind is that the chloride threshold was found to be lower for concrete that contains supplementary cementitious materials. This was observed in samples exposed outdoors for over 24 years. The application of electromigration also produces an ionic current that polarizes the rebar to a more noble potential (when the rebar is not corroding). This polarization could allow corrosion to initiate at a lower chloride concentration. An exception to the prior statement occurs if the ionic polarization stimulated a film to form that is associated with anodic protection (either corrosion product buildup or buildup of products that form due to the reactions that take place at more noble potentials). If the exception occurs, it can take some additional time for corrosion to initiate even when the electromigration is removed (as the layer needs to either dissolve into the concrete matrix and/or the chlorides need to reach the rebar surface). Moreover, corrosion would not initiate if not enough chlorides reach the rebar trace (i.e., if the chloride threshold is not exceeded).

On samples exposed outdoors, cracks appeared on a few reinforced concrete samples prepared with concrete OPC only, OPC + calcium nitrate, and binary mixes made from fly ash (20%, 35%, 50%) and OPC, and binary mixes that contain OPC and silica fume. Several of the samples exposed outdoors to seawater for 24 years showed a significant amount of corrosion (based on the forensic analysis and i_{corr} measurements), but just six samples showed cracks.

For samples tested indoors, the corrosion appeared to initiate on most samples subjected to electromigration during the evaluation period. A summary of the observations made on terminated indoor samples follows. Rebars of older mortar samples showed corrosion sites (before cleaning) similar to the solution reservoir lengths. The rebars with 5-cm cover showed corrosion at locations other than under the solution reservoir. For these samples, the solution reservoir was installed on the troweled side. In some cases, very small corrosion sites (or no corrosion) were observed on the rebar surface below the solution reservoir. For the samples subjected to electromigration, two of the mortar samples showed cracks and two of the samples with 5-cm concrete cover (1B1 and 1A1 – OPC only on both) also developed cracks. There were three other mortar samples that showed cracks, but these samples were not subjected to

electromigration. Corrosion started more than 10 years ago on these latter samples, but the samples were stored for several years with no solution in the reservoir.

Regarding the terminated rebars from samples prepared as part of this project, the corrosion sites were significantly smaller than the solution reservoir. In some cases, rebar corrosion took place on the surface extending outside of the concrete (no shrinkage wrap was initially installed). The duration of the corrosion propagation was not long enough to cause cracks in most of the indoor samples. No cracks were observed on any of the samples prepared in 2016.

Given enough time, corrosion will initiate and propagate on carbon steel rebar embedded in high–performance concrete, and given enough time, it can reach a point at which cracks or corrosion stains will reach the surface. The corrosion sites appear to be more localized than that observed on reinforced concrete with no cementitious admixtures.

The combined use of a smaller solution reservoir and electromigration appears to be a good method to achieve local corrosion with a small anode and a large cathode similar to what is observed in the field. Longer periods of electromigration appear to be needed to allow corrosion to initiate on a larger section under the solution reservoir.

Table of Contents

List of Figures

List of Tables

Chapter 1 – Introduction and Literature Review

Corrosion initiation of reinforcing steel embedded in concrete has been investigated for several decades. The corrosion propagation of carbon steel embedded in high–performance concrete is not understood well. This study was performed to gain a better understanding of the corrosion propagation of carbon steel rebar embedded in high–performance concrete. This chapter contains a brief background, followed by a literature review.

Reinforcement steel corrosion is one of the main causes of reinforced concrete (RC) structural deterioration. Steel corrosion in RC structures is a slow process, which can be broadly divided into three stages as schematically shown in Figure 1 (Tuutti 1982). Stage I is the corrosion initiation stage (also known as the time to corrosion initiation), corresponding to the transport process (e.g. diffusion) of aggressive ions such as chloride or carbon dioxide through the concrete cover. The duration of this stage is dependent on environmental factors, concrete cover properties, and the surface conditions of steel reinforcement. Stage II is the corrosion propagation stage, which is mainly affected by environmental and concrete cover factors and interactions with the surrounding reinforcement. The slope of this deterioration rate is dependent on the corrosion rate of steel reinforcement. Stage III corresponds to the RC structure (or multiple components within a structure) reaching a predetermined limit state (e.g., 10% area spalling, or 20% cross-section loss of the reinforcement).

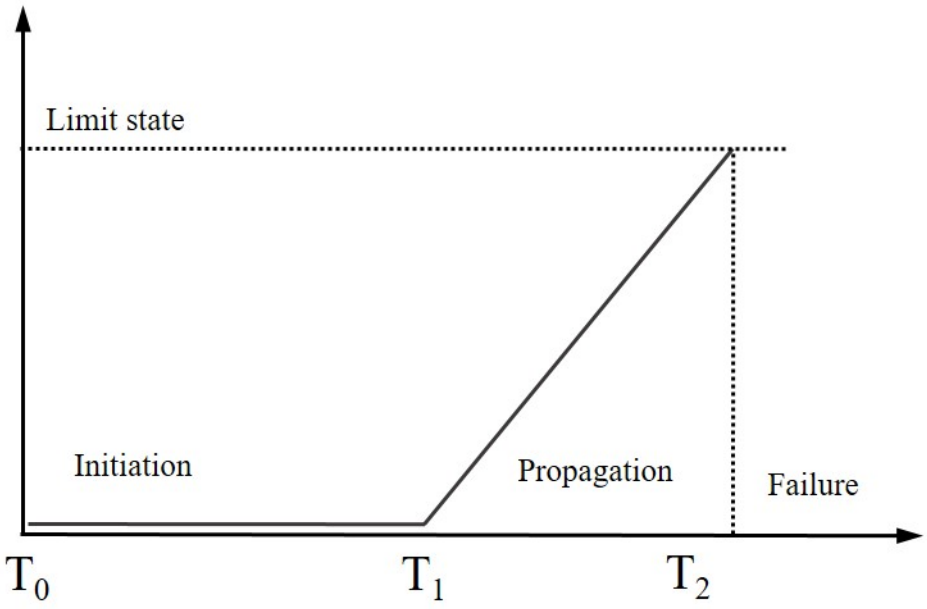

Figure 1. Schematic illustration of corrosion–induced structural deterioration(Tuutti 1982)

Compared with stage I, stage II is much more complicated. It is typically assumed that stage II only last a few years (e.g., five to ten years). The use of high–performance admixtures such as fly ash, silica fume, blast–furnace slag not only delay the corrosion initiation time (T_1) in stage I, but it is believed to reduce the corrosion rate in stage II, which then could result in an extended

service life. A reduced corrosion rate during the propagation stage would also delay reaching the limit service state that triggers reaching stage III.

1.1. – Corrosion monitoring techniques

Several methods are used to evaluate corrosion of steel bar in concrete structures. In this section, a brief introduction is given on the four most widely used techniques for assessing corrosion of reinforced concrete structures, including open circuit potential, corrosion rate, concrete resistivity, and chloride concentration.

1.1.1 – Open circuit potential

Open circuit potential (OCP) is the simplest technique to evaluate corrosion activity in RC structures. Due to its simplicity and easy operation, it is widely used on site for engineering practice. ASTM C876–15(ASTM C876-15, 2015) specify the criteria for corrosion activity evaluation based on copper sulfate reference electrode as shown in Table 1. The potential values corresponding to saturated calomel electrode (SCE) and Ag/AgCl electrodes are also listed. These values assumed that the reinforced concrete is exposed to atmospheric conditions.

Table 1. OCP vs. corrosion activity

mV vs. Cu/CuSO4 (ASTM C876)	mV vs. SCE	mV vs. Ag/AgCl	Probability of corrosion
OCP > –200	OCP > –126	OCP > –106	90% no corrosion
–200 ≥ OCP ≥ –350	–126 ≥ OCP ≥ –276	–106 ≥ OCP ≥ –256	Uncertain
–350 > OCP	–276 > OCP	–256 > OCP	90% active corrosion

However, its reading is influenced by many factors such as concrete surface conditions (patch repair, organic coatings or contamination), rebar surface condition (epoxy–coated, galvanized), cathodic protection system or stray current effects. Gu and Beaudoin(Gu and Beaudoin 1998) summarized the influence of various parameters on effective half-cell potential readings. High moisture content tends to shift the rebar potential to quite negative values due to oxygen concentration limitations. Additionally, the corrosion potential only gives the probability of corrosion activity, and could not give quantitative or direct evaluation such as corrosion rate.

1.1.2 – Corrosion rate

Corrosion rate can be measured through a number of methods. One of the most widely used and nondestructive methods for RC structures is the linear polarization resistance (LPR).

The LPR method is based on the theory that the polarization curve near the corrosion potential is linear. A small current is applied from a counter electrode (CE) and the amount required to achieve a definite variation of the potential is recorded and monitored with a reference electrode. Using the Stern–Geary equation (Stern and Geary 1957), instantaneous polarization resistance can be calculated from the measurement and transformed into the total corrosion current (I_{corr}). The corrosion current density i_{corr} is obtained by dividing the total corrosion current I_{corr} by the corroding area. If the corrosion is uniform, this calculation may be adequate where large parts of the surface area are corroded. But, in the case of localized corrosion, only small pits or small

corrosion spots are affected by corrosion and the quantification may not be as precise. The local current density inside a pit is significantly higher than the average value for the steel area affected by the measurement, and as a result corrosion rate would be underestimated (Hornbostel, Larsen, and Geiker 2013; Morris et al. 2002).

The ohmic drop is the influence that the concrete resistance can have on the measured polarization resistance between the reference electrode and the working electrode (rebar). If the concrete resistivity is relatively high, a major error can be made during the measurement. For example, the polarization resistance might reflect the concrete resistance rather than the corrosion rate. To avoid this situation, it is commonly suggested to correct LPR measurements for the ohmic drop. Currently, instruments with sophisticated facilities for automatic iR compensation are commercially available. Depending upon the concrete measuring problem, alternating current and current interrupt techniques are used to compensate for changing resistance (Oelßner, Berthold, and Guth 2006). Table 2 summaries the corrosion activity of steel bar in concrete with respect to both corrosion rate and corrosion resistance R_{ct} (assuming uniform corrosion). The galvanostatic pulse is another technique that is used to assess and monitor corrosion of reinforcing steel (Newton and Sykes 1988)·(Law, Millard, and Bungey 1999), this method is described in the experimental section.

Table 2. Corrosion rate/resistance vs. corrosion activity (Law, Millard, and Bungey 1999)

Corrosion activity	Corrosion rate ($\mu A/cm^2$)	R_{ct} ($k\Omega\ cm^2$)
Very high	10 – 100	0.25 – 2.5
High	1.0 – 10	2.5 – 25
Moderate/Middle		
Low	0.1 – 1.0	25 – 250
Negligible/passive	< 0.1	>250

1.1.3 – Concrete resistivity

The resistivity of concrete is closely related to the corrosion rate especially after corrosion initiation; since the ion transport between anodes and cathodes on the steel surface is dependent on the surrounding concrete resistivity. However, its reading is also affected by a number of factors such as concrete geometry, cover thickness, or presence of steel bars. Despite these uncertainties, it is known that active corrosion areas with low concrete resistivity will be associated with a relatively high corrosion rate, in part due to the macrocell effect. Table 3 gives the correlations between the concrete resistivity and the likelihood of significant corrosion. It is important to note that some articles report solution resistance or solution resistance per unit area, instead of resistivity units. Devices often measure the resistivity of the cover concrete, between an electrode placed on the surface and the reinforcement. The resistivity measured this way could be significantly different from the bulk concrete resistivity.

Table 3. Concrete resistivity vs. corrosion activity.(Ahmad 2003)

Resistivity (ohm-cm)	Likelihood of significant corrosion
<5000	Very high
5000 – 10, 000	High
10,000 – 20, 000	Low/Moderate
> 20,000	Low

In addition to these methods designed for resistivity measurement, the concrete resistivity can also be measured through electrochemical impedance spectroscopy (EIS). EIS is a powerful nondestructive technique used for corrosion monitoring and measurement; it not only provides corrosion information at the electrolyte–steel interface where corrosion occurs but also gives concrete cover properties such as concrete resistance and capacitance. Concrete resistance values can be converted to resistivity if the cell constant due to geometry is known (or is calculated). The solution and polarization resistance are usually obtained by fitting the measured impedance spectrum with an equivalent electrical circuit model. The solution resistance is the value that can be converted to concrete resistivity if the cell constant is known.

1.1.4 – Chloride concentration

Most of the steel reinforcement corrosion happens in RC structures subjected to de-icing salt or located in marine/coastal environments. Therefore, chloride is one of the most aggressive chemicals causing steel corrosion. Extensive research has been carried out to study chloride-induced corrosion in RC structures. Transportation of chloride in concrete has three different mechanisms, including capillary absorption, migration, and diffusion, which is the most dominant mechanism.

The effect of chloride penetration on the service life of RC structures mainly occurs in stage I. However, it may affect the corrosion rate in stage II. A high chloride concentration in concrete may reduce the concrete resistivity of the cover concrete, consequently resulting in a change in the corrosion morphologies from localized corrosion to uniform corrosion. High chloride concentration might make the corroding site more stable.

It is widely accepted that chloride ions are responsible for causing local passive layer breakdown and initiating the corrosion of reinforcing bars once a critical concentration, Cl_{TH}, has been exceeded. Cl_{TH} is very important in the evaluation of the service life of reinforced structures as it determines how long it will take to initiate the corrosion process. Many variables of the concrete mix properties, such as cement type, cementitious amount, water to cement ratio, concrete pore structure solution pH, rebar composition, surface condition, etc., affect the value of Cl_{TH}(Morris, Vico, and Vázquez 2004). This explains why the Cl_{TH} values reported in the literature have a wide range. According to Glass and Buenfeld(Glass and Buenfeld 1997; Morris, Vico, and Vázquez 2004), chloride threshold levels are best presented as a total content (bound plus free chlorides) expressed relative to the weight of cement. The values of Cl_{TH} reported in Glass and Buenfeld review varied within a wide range (0.17–2.5%) relative to the weight of cement(U. M. Angst et al. 2011; Morris, Vico, and Vázquez 2004).

1.2 – Objectives

The primary objective of this literature review was to find what has been reported regarding the corrosion of steel bar embedded in ordinary Portland cement concrete as well as in high–performance concrete (mixes with fly ash, silica fume, blast–furnace slag). The selected publications presented a range of geometries, concrete compositions, chloride sources, environments, and periods of testing. The primary parameters that were collected included corrosion potential, corrosion rates (sometimes reported as polarization resistance values Rp/Rc), and concrete resistivity (or concrete solution resistance). The focus is mainly on investigations in which the chlorides penetrated via diffusion or via accelerated chloride transport, instead of articles in which chlorides were included in the concrete mix. In addition, the relationships or

correlations between corrosion parameters such as corrosion potential and corrosion rate and concrete resistivity were analyzed. This chapter provides some insights into the applicability and limitation of these parameters and their correlations in evaluating the corrosion conditions in the propagation stage. A list of symbols used is provided in Appendix A.

1.3 – Experimental details reported in the reviewed publications

1.3.1 – Specimen geometry and setup

Various concrete specimen geometries were prepared and tested in the literature (Elsener 2005; González, Miranda, and Feliu 2004; Ahmad and Ahmad 2014; Montemor, Simões, and Salta 2000; Garcés et al. 2010; Saraswathy and Song 2006; Choi, Kim, and Lee 2006; Monticelli et al. 2016b, 2016a; Criado et al. 2016; Miranda et al. 2005; Ip, n.d.; Yeau and Kim 2005; Huang, Chang, and Wu 1996; Kayali and Zhu 2005; Morris et al. 2002), including slab, prism, cube, and cylinder. Two of the most used specimens geometry to perform corrosion measurements are prisms and cylinders. Figure 2 shows some specimen geometries tested by other researchers to investigate the corrosion of the steel bar in concrete. For each specimen, different numbers of steel bars were embedded depending on the shape and size of the specimen. For cylinder specimen, one bar centered in the middle is the most used type. For prism specimen, multiple steel bars are usually embedded for corrosion observation.

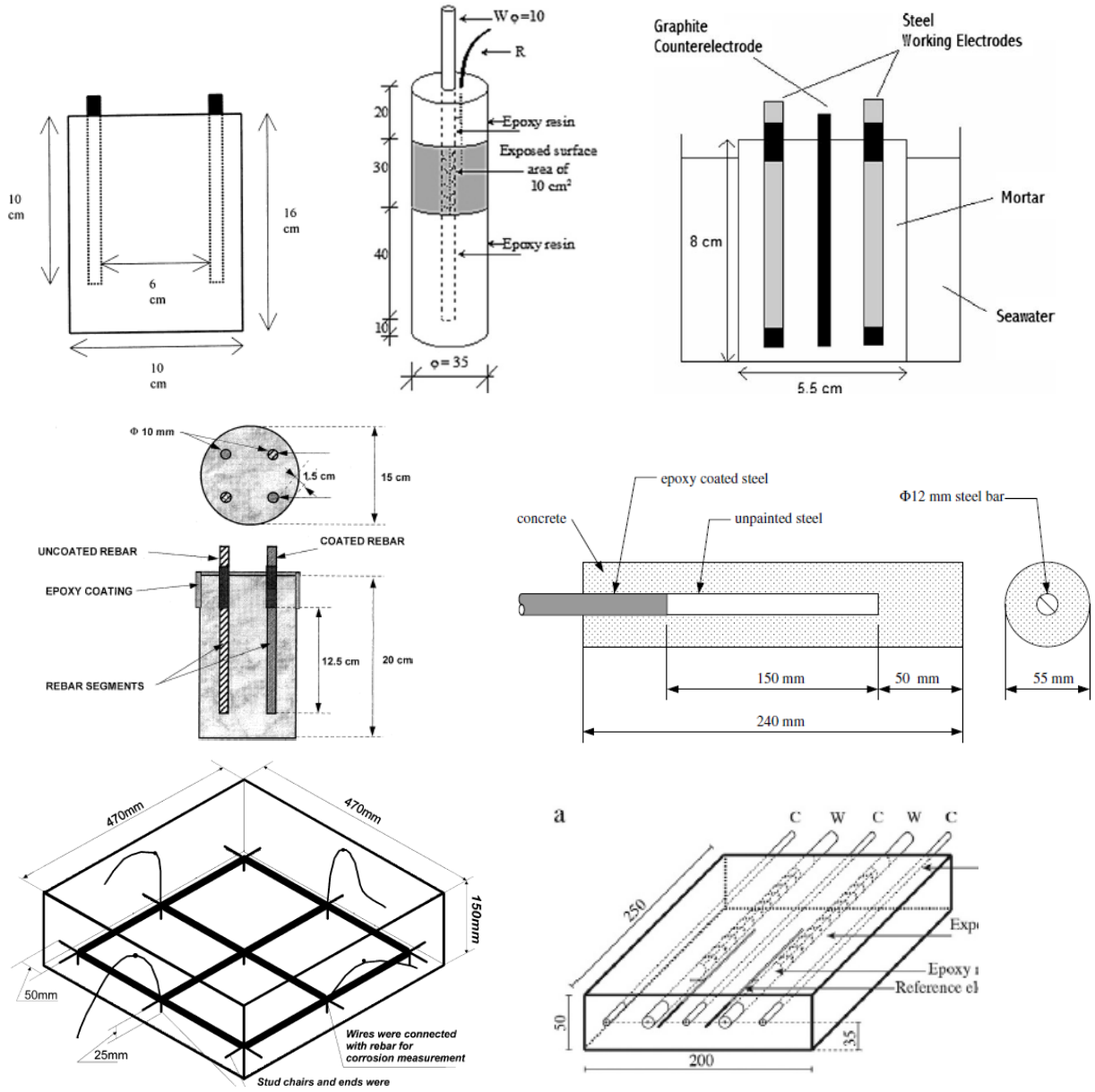

Figure 2. Different sample geometries found in the literature search.

Table 4 summarizes the specimen parameters from the literature such as geometry, size, rebar diameter, concrete cover thickness, and quantities of specimens prepared and tested.

Table 4. Specimen geometry and specimen details.

Reference	Specimen Type	Specimen Size (mm)	Rebar Diameter (mm)	Exposed Area (cm^2)	Cover Depth (mm)	# of Specimens
(González, Miranda, and Feliu 2004)	Slab	114×300 ×400	8	334	30	2
(Criado et al. 2016)	Bridge girder	Full scale	–	–	30	–
(Ahmad and Ahmad 2014)	Prism	100×300×65	12	56.5	26	10
(Morris et al. 2002)	Cylinder	Ø 150 ×200	10	40	15	8
(Montemor, Simões, and Salta 2000)	Prism	100×100×300	10	32.2	10	–
(Garcés et al. 2010)	Prism	20×55×80	6	9	7	>8
(Saraswathy and Song 2006)	Cylinder	Ø 50 ×50	6	8.5	22	48
(Choi, Kim, and Lee 2006)	Cylinder	Ø 55 ×240	12	57.68	21.5	>6
(Monticelli et al. 2016b)	Slab	200×250×50	10	74	20	>3
(Monticelli et al. 2016a)	Cylinder	Ø 35 ×100	10	10	12.5	16
(Criado et al. 2016)	Prism	80×55×20	10	10	5	–
(Miranda et al. 2005)	Prism	80×55×20	7	10	8	6
(Ip, n.d.)	Slab	114×300×400	13	102	56	6
(Yeau and Kim 2005)	Block	150×150×150	–	–	10/20/30	8
(Huang, Chang, and Wu 1996)	Cylinder	Ø 50 ×80	10	22.8	20	15
(Kayali and Zhu 2005)	slab	470×470×150	12	–	25	6

1.3.2 – Mix design and proportions

Most of the specimens found in the literature are concrete. However, a number of them used mortar especially when the specimens were small. Ordinary Portland cement Type I is the most used cement, and type IV was also used by some researchers. For high–performance concrete, admixtures used were fly ash, silica fume, and blast–furnace slag. These cementitious admixtures were added to the mix in different proportions. For fly ash, the percentage ranged from 0% to 50%, it ranged from 0% to 10% for silica fume, and from 0% to 55% for slag cement. Some specimens were also made with two admixtures for example: fly ash and silica fume (ternary mixes). The water to cement or water to binder ratios ranged from 0.24 to 0.65 found in the literature reviewed (Elsener 2005; González, Miranda, and Feliu 2004; Ahmad and Ahmad 2014; Morris et al. 2002; Montemor, Simões, and Salta 2000; Garcés et al. 2010; Saraswathy and Song 2006; Choi, Kim, and Lee 2006; Monticelli et al. 2016b, 2016a; Criado et al. 2016; Miranda et al. 2005; Ip, n.d.; Yeau and Kim 2005; Huang, Chang, and Wu 1996; Kayali and Zhu 2005). The water to binder is also known as water to cementitious (w/cm). In some publications, the fly ash is reported to have been processed using different treatment methods, such as grounded or magnetic method. Table 5 lists the source, type of sample, cement type, cementitious admixtures if present, and the water to binder (i.e., cement plus admixtures) ratio.

1.3.3 – Corrosion evaluation techniques

Different methods were used by the researchers to evaluate corrosion activity in concrete specimens as summarized in Table 6. Corrosion potential is the most widely used, almost every publication related to steel bar corrosion has the potential data. The reference electrodes for corrosion potential measurement include SCE, CSE, Ag/AgCl, or titanium. Corrosion rates were calculated using linear polarization resistance, or by gravimetrical analysis. Concrete resistivity was measured through different techniques: four electrodes, two electrodes, or extracted from impedance data. In some publications, the solution resistance was reported and not the concrete resistivity, still, the reported values give a sense of the concrete cover resistivity.

1.3.4 – Exposure conditions

Various methods have been used to initiate the corrosion of the lab specimens. Two of the most used methods are partially or fully immersed in a solution with chlorides (e.g., 3.5% NaCl solution or seawater), or subjected to cyclic wetting-drying cycles. Other methods to accelerate corrosion initiation include: placing the samples in a room at elevated temperature and high humidity or fog room. Carbonation has also been used. Additionally, some experiments exposed the specimens outdoors close to the shore, and in another investigation, the specimens were placed at the seashore. Table 7 lists some of the exposure conditions found in the literature. The exposure duration lasted from 30 days to 1000 days dependent on the specimens and the experiment design.

Table 5. Mix designs

Ref	Type	Cement	Admixtures	water-to-binder ratio
(González, Miranda, and Feliu 2004)	Concrete	OPC	–	0.50
(Elsener 2005)	Concrete	OPC	–	–
(Ahmad and Ahmad 2014)	Concrete	OPC	–	0.45
(Morris et al. 2002)	Concrete	OPC	–	0.40/0.60
(Montemor, Simões, and Salta 2000)	Concrete	OPC	FA (15%, 30%, 50%)	0.57
(Garcés et al. 2010)	Concrete	OPC	FA (30%; T0, T60, TNM, TM)	0.50/0.70
(Saraswathy and Song 2006)	Mortar	OPC	FA (10%, 20%, 30%, 40%; AFA, PFA, TFA, CFA)	0.45
(Choi, Kim, and Lee 2006)	Concrete	OPC	FA (20%)	0.31/0.35/0.50
(Monticelli et al. 2016b)	Concrete	OPC	FA	0.35/0.52
(Monticelli et al. 2016a)	Mortar	OPC	FA	0.52
(Criado et al. 2016)	Mortar	OPC	AAFA	–
(Miranda et al. 2005)	Mortar	OPC	FA	0.35/0.55
(Ip, n.d.)	Concrete	OPC	Slag (0%, 25%, 50%)	0.45
(Yeau and Kim 2005)	Concrete	OPC	Slag (55%)	0.42
(Huang, Chang, and Wu 1996)	Concrete	OPC	FA (10%, 20%) Slag (15%, 30%)	0.35/0.45/0.55
(Kayali and Zhu 2005)	Concrete	OPC	FA SF	0.24/0.31/0.60

Note: "–" was used when a value was not available or not listed

Table 6. Techniques used to evaluate corrosion

Reference	OCP	Corrosion rate or Polarization resistance	EIS	Galvanostatic pulse	Concrete resistivity or Concrete solution resistance
(González, Miranda, and Feliu 2004)	×	×	×	–	–
(Elsener 2005)	×	–	–	×	–
(Ahmad and Ahmad 2014)	–	×	–	–	×
(Morris et al. 2002)	×	×	–	–	×
(Montemor, Simões, and Salta 2000)	×	–	×	–	–
(Garcés et al. 2010)	×	×	–	–	–
(Saraswathy and Song 2006)	×	×	×	–	–
(Choi, Kim, and Lee 2006)	×	–	×	–	–
(Monticelli et al. 2016b)	×	×	–	–	–
(Monticelli et al. 2016a)	×	×	×	–	–
(Criado et al. 2016)	×	×	×	–	–
(Miranda et al. 2005)	×	×	–	–	–
(Ip, n.d.)	×	×	–	–	×
(Yeau and Kim 2005)	×	–	–	–	–
(Huang, Chang, and Wu 1996)	×	×	–	–	–
(Kayali and Zhu 2005)	×	×	–	–	–

Note: "–" indicates it was not reported, "×" indicates it was reported

Table 7. Sample exposure conditions

Ref	Exposure conditions	Measurement period
(González, Miranda, and Feliu 2004)	The slab was dry; before the test, a small wet pad was applied for one week; a big wet pad was used for another week	Less than 1 month
(Elsener 2005)	On-site; Leaking salt water from the traffic lane	Around one week
(Ahmad and Ahmad 2014)	Fully immersed in 5.0 % NaCl solution	–
(Morris et al. 2002)	Seashore; immersed in 3.5 % NaCl solution	–
(Montemor, Simões, and Salta 2000)	Partially immersion (6 cm deep); fully immersion in 3% NaCl solution	Around 600 days
(Garcés et al. 2010)	Partially immersed in seawater (7 cm deep)	Around 200 days
(Saraswathy and Song 2006)	15 days wetting, 15 days drying cycle in 3% NaCl solution	Around 20 months
(Choi, Kim, and Lee 2006)	Fully immersion in 3.5 % NaCl solution	Around 250 days
(Monticelli et al. 2016b)	Partially immersed in 3.5 wt% NaCl solution	Around 100 days
(Monticelli et al. 2016a)	Wetting–drying cycles in 3.5% NaCl solution	Around 100 days
(Criado et al. 2016)	Partially immersed in 3.5 wt% NaCl solution	Around 250 days
(Miranda et al. 2005)	Room temperature, humidity>90%	Around 100 days
(Ip, n.d.)	Wetting–drying cycles in 3.5% NaCl solution	Around 320 days
(Yeau and Kim 2005)	3 days wetting in 3% NaCl solution, 4 days drying	Around 220 days
(Huang, Chang, and Wu 1996)	Fully immersed in 3.5% NaCl solution	Around 1800 hours
(Kayali and Zhu 2005)	Partially submerged in 20,000 ppm chloride	Around 600 days

1.4 – Case studies

This section describes case studies on the steel reinforcement corrosion in concrete. Depending on the use of different high–performance admixtures, the studies were divided into four subsections. Cases related to the corrosion of rebars in ordinary Portland cement concrete are

presented first; followed by cases of rebar steel corrosion in concrete with fly ash; the third subsection describes cases of steel corrosion in concrete with blast–furnace slag; and the last subsection reports selected cases of steel corrosion in concrete with two or more admixtures like fly ash and silica fume. In each case study described below, the investigators, the publication details, the specimen details (e.g., specimen geometry, mix proportion), exposure condition, and results are described.

1.4.1 – Ordinary Portland cement

Case I: J.A. Gonzalez, J.M. Miranda, S. Feliu, "Consideration on reproducibility of potential and corrosion rate measurements in reinforced concrete", Corrosion Science 46 (2004) 2467–2485. (González, Miranda, and Feliu 2004)

Two cement mortar slabs of 133 × 133 × 7 cm, as depicted in Figure 3, manufactured more than a decade ago with a cement/sand/water ratio of 1/3/0.5. One slab was manufactured without additives, to represent passive structures, and the other was manufactured with the addition of 3% $CaCl_2$ by cement mass, in order to simulate the behavior of active structures. Thirteen bars of 0.8 cm diameter were embedded at 9 cm intervals in each slab, crossing from side to side. The zone where the bars emerged into the atmosphere was isolated with insulating tape in order to prevent differential aeration phenomena. The methods used include corrosion potential, corrosion rate (from LPR), and concrete resistivity.

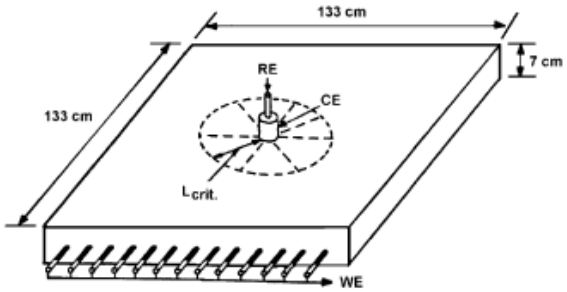

Figure 3. Specimen geometry

Figure 4 shows the correlations between corrosion potential, corrosion rate and concrete resistivity for the slab without the addition of $CaCl_2$. The corrosion potential measured in this study ranged from –200 mV/SCE to 300 mV/SCE, the corrosion rate varied from 0.01 to 0.08 $\mu A/cm^2$, and a high concrete resistivity 550 kΩ.cm was also measured (when dry). It can be observed from the figure that a more negative OCP is related to a high corrosion rate, and lower concrete resistivity. It is noted that the tests were started with a very dry mortar, after the slabs had been exposed for a number of years to an indoor atmosphere of very low relative humidity, normally less than 50%. At first, only the surface under the small counter electrode was wetted, using a pad that was soaked in water several times a day and covered with an impermeable plastic in order to prevent evaporation into the atmosphere. After one week, all the surface of the slabs was covered with large wet pads protected by impermeable plastics, which were only removed during the corrosion tests. The large concrete resistivity is attributed to the dry conditions.

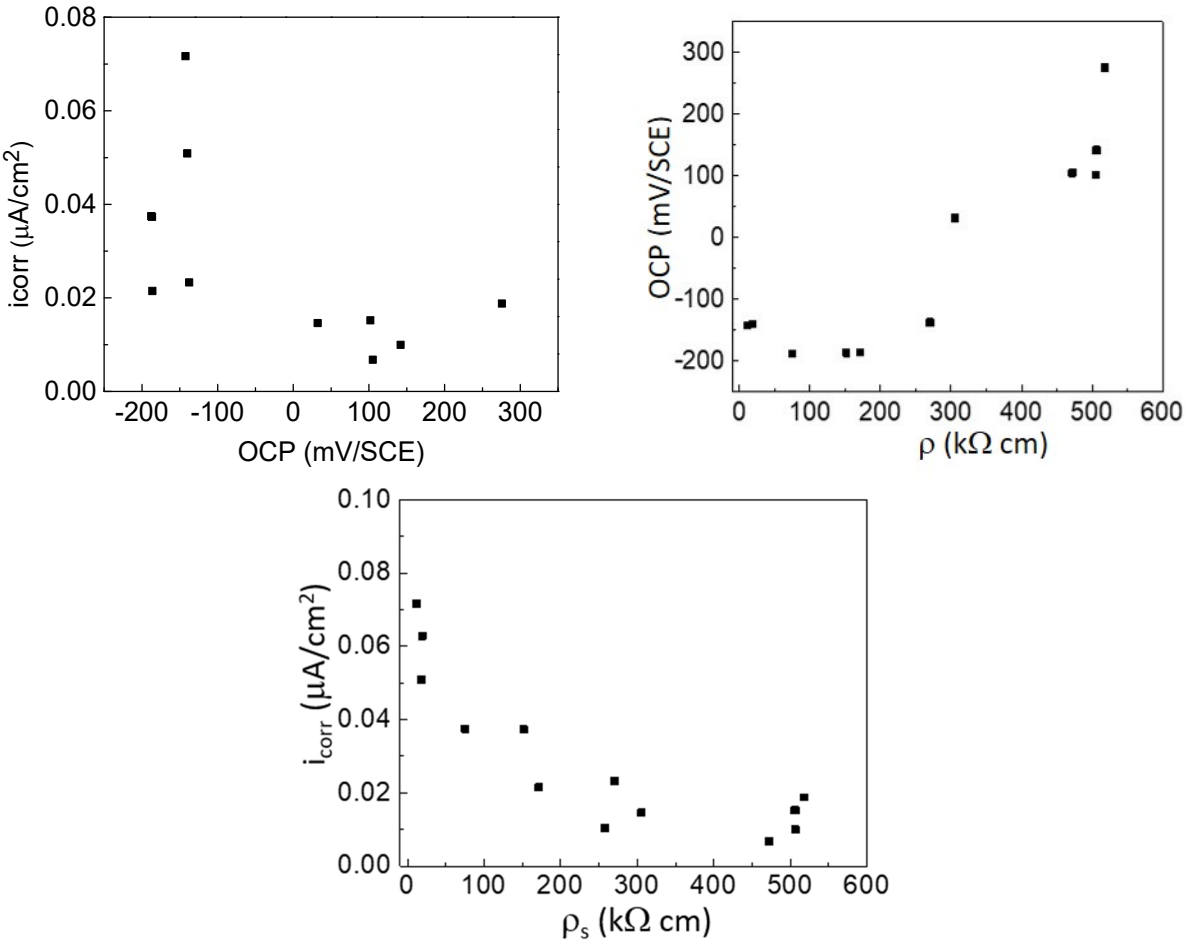

Figure 4. Correlations between OCP, corrosion rate, and concrete resistivity.

Case II: B. Elsener, "Corrosion rate of steel in concrete–Measurements beyond the Tafel law", Corrosion Science 47 (2005) 3019–3033. (Elsener 2005)

The tests were performed on the outside of a reinforced girder of a post-tensioned bridge built in 1965, where at several points corrosion of the reinforcement had started due to leaking salt water from the traffic lane. Several measuring points with different corrosion potential, from corroding zones (–0.4 V_{CSE}) to passive zones (+0.05 V_{CSE}) were used for the measurements. At every measuring point, several galvanostatic pulses with currents between 20 and 100 μA were applied. The counter electrode used had a diameter of 14 cm. Concrete cover depth was 30 mm. The temperature during the measurements was 6 °C.

Figure 5 shows the results and correlation of OCP, polarization resistance and solution (ohmic) resistance. It is obvious that a negative OCP corresponds to a low polarization resistance and a low solution resistance.

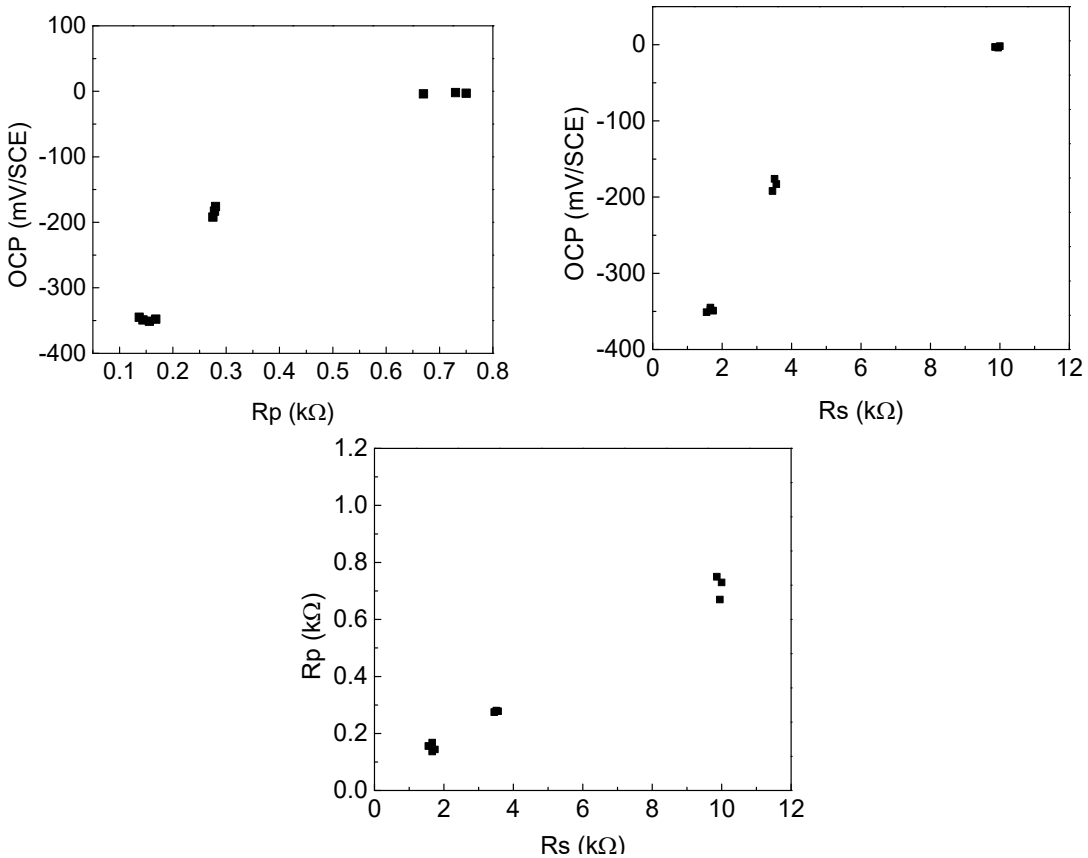

Figure 5. Correlations between OCP, polarization resistance, and solution resistance (area polarized ≈150 cm^2).

Case III: Shamsad Ahmad, "An experimental study on the correlation between concrete resistivity and reinforcement corrosion rate, Anti–Corrosion Methods and Materials, 61(3)", 2014: 158–165.
(Ahmad and Ahmad 2014)

The purpose of this paper was to explore the possibility of establishing an empirical correlation between concrete resistivity and reinforcement corrosion rate utilizing the experimental data generated by measuring corrosion current density of reinforced concrete specimens subjected to chloride-induced corrosion at different levels of concrete resistivity. To generate concrete resistivity vs corrosion current density data in a wide range, ten reinforced concrete specimens were prepared and allowed to corrode under severe chloride exposure as indicated in Figure 5. After significantly corroding the specimens, the specimens were removed from the chloride exposure and were subjected to different moisture levels for achieving variation in the resistivity of concrete. This methodology allowed for a good number of resistivity vs. corrosion rate data. It is noted that the corrosion loss during the test was not quantified. The purpose of this study was to investigate the correlation between corrosion rate and concrete resistivity. (The authors only mentioned that ten reinforced concrete specimens were corroded to different degrees under exposure to 5% NaCl solution).

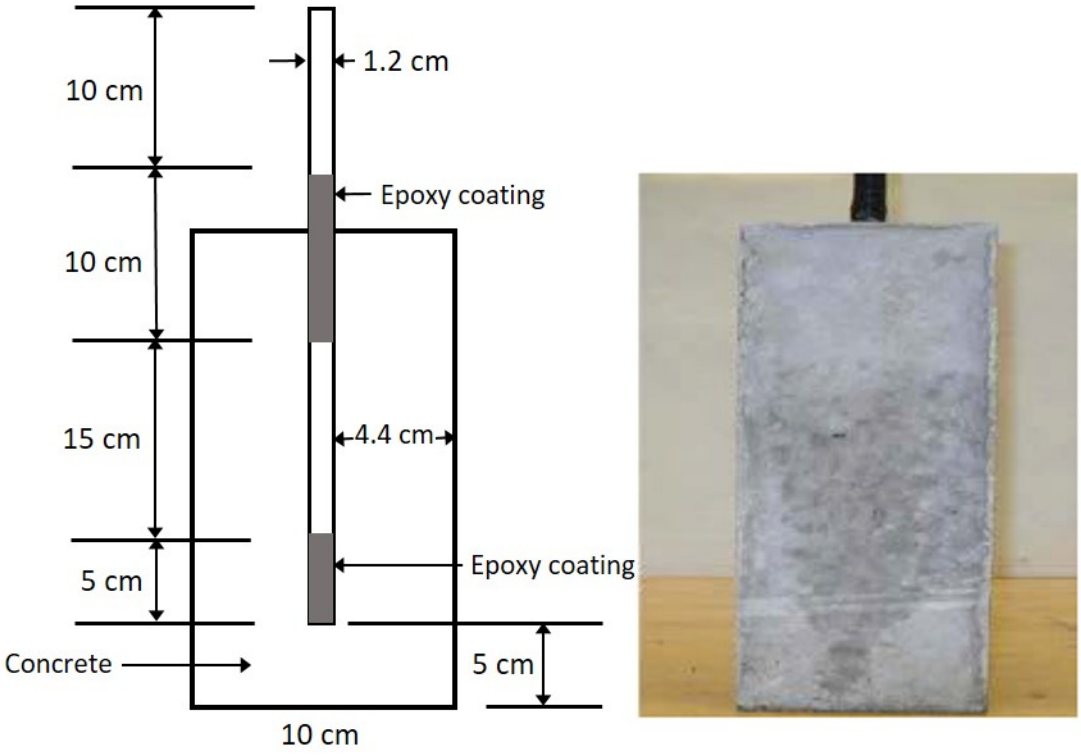

Figure 6. Specimen details.

Ten reinforced concrete specimens were corroded to different degrees under exposure to 5% NaCl solution. Before testing the specimens for concrete resistivity and corrosion current density at different moisture contents, specimens were first immersed in water for 48 hours so that the pores inside the specimen may be saturated with moisture. Then they were taken out of the water and after 30 minutes, their weights were measured and they were tested for resistivity and corrosion current density. The weight measurement and testing for resistivity and corrosion current density were simultaneously continued with a time interval of 30 minutes until the specimens reached their constant weights. After completion of the testing cycles, the specimens were oven–dried for 24 hours and their dry weights were taken. Using the moist weights taken at different times of testing and dry weights that were taken at the end of testing, the moisture contents were calculated. Resistivity was measured by a two-probe method, and corrosion current density was measured using the LPR method.

Figure 7 shows the result of concrete resistivity and corrosion rate as a function of concrete moisture. With an increase in the concrete moisture, the concrete resistivity decreased exponentially as shown in Figure 7a. The corrosion rate increased with an increase of the concrete moisture. The relationship between the concrete resistivity and the corrosion rate is evident; with an increase in the concrete resistivity, the corrosion rate of steel bar decreased.

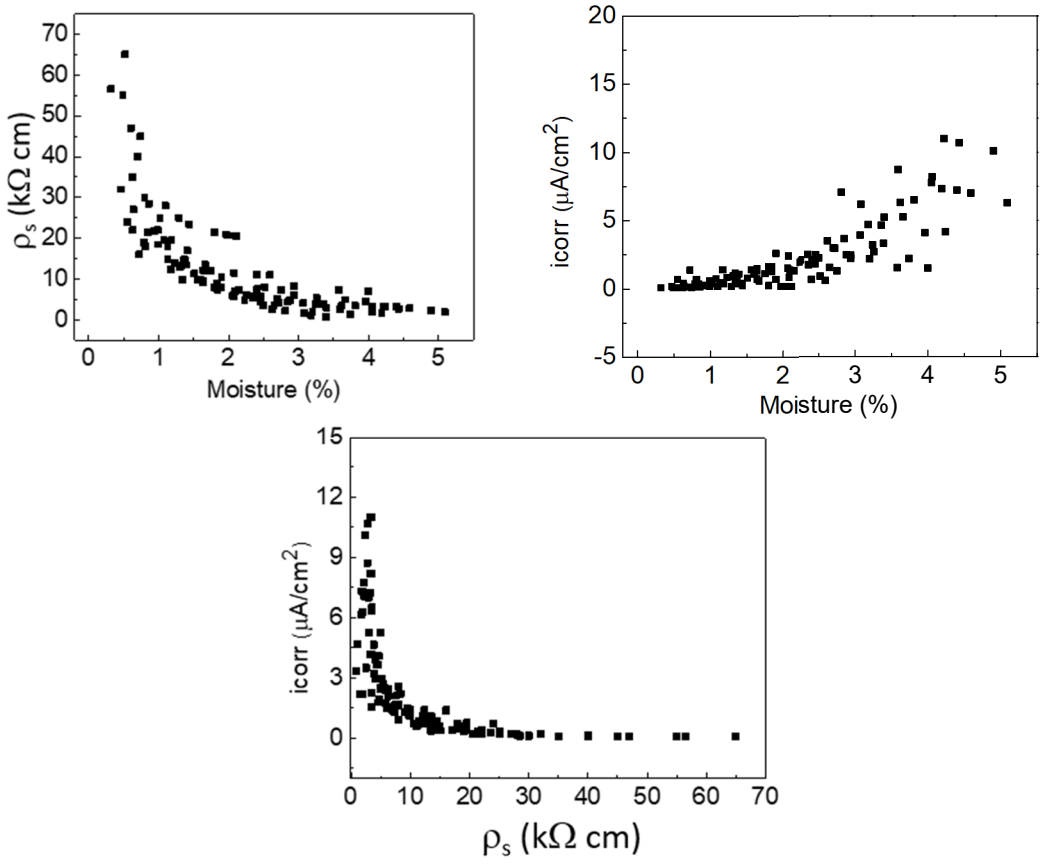

Figure 7. Correlations between corrosion rate, concrete resistivity, and moisture.

Case IV: W. Morris, A. Vico, M. Vazquez, S.R. de Sanchez, "Corrosion of reinforcing steel evaluated by means of concrete resistivity measurements", Corrosion Science 44 (2002) 81–99.(Morris et al. 2002).

The corrosion behavior of reinforcing steel bars in four different concrete mix designs commonly used at coastal cities in Argentina is studied. Two exposure conditions were investigated: seashore environment and partially immersed in a saline solution. Two water to cement ratios were selected for the study. Cylinder concrete specimens containing four rebar segments positioned in a way such that a 1.5-cm concrete cover was achieved as shown in Figure 8. The rebar segments were 20 cm long with a diameter of 1 cm and present an exposed area of 40 cm^2.

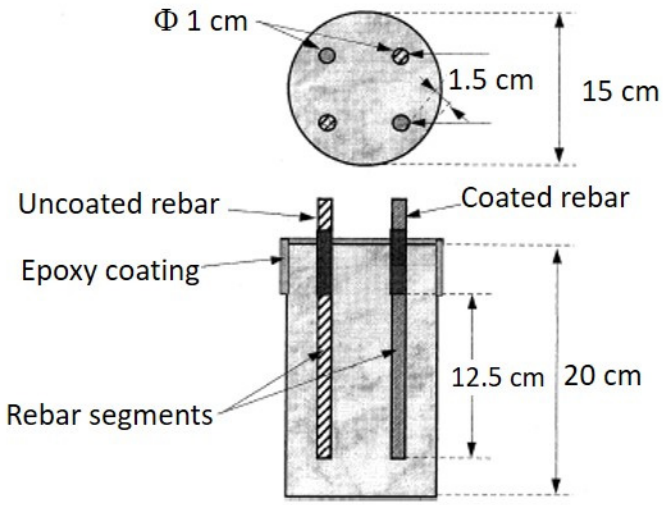

Figure 8. Specimen details.

Table 8 shows the mix design for four different specimens. Two types of sand were used including river sand and sea sand. For specimen C, NaCl was also added to the mix. Two exposure conditions, referred to as seashore and immersed, were evaluated. Four specimens per each mix design were prepared. Specimen exposed to the seashore after a conditioning period of 90 days in the laboratory environment. Another group of specimens was partially immersed in 3.5 wt.% NaCl solution after a conditioning period in the laboratory for 60 days. The test lasted for around 1000 days.

Table 8. Concrete mix design

Mix design	A	B	C	D
W/C	0.60	0.40	0.60	0.60
Cement content (kg/m^3)	300	400	300	300
River sand (kg)	–	–	851	858
Sea sand (kg)	858	789	–	–
River rock (kg)	1003	1042	1003	1003
Sodium chloride (kg)	–	–	7.4	–
Superplastisizer (%)	1.0	2.5	–	–

Figure 9 shows the correlations between OCP, corrosion rate, and concrete resistivity for specimens at the seashore. Figure 10 shows their correlations for specimens immersed in salt water. The corrosion rate measured reached 10 μA/cm^2 for steel immersed in a salt solution. It can also be observed that a negative OPC correspond to a high corrosion rate and a low concrete resistivity for all specimens.

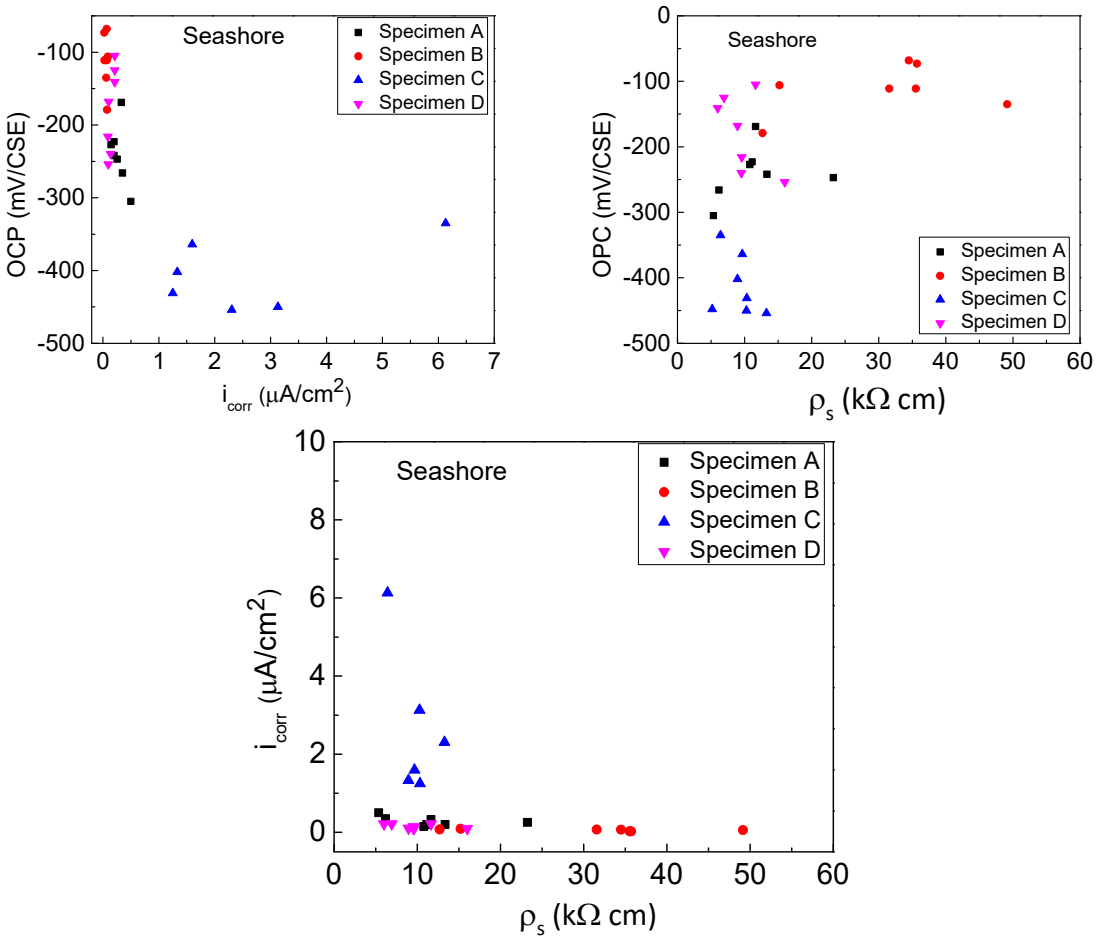

Figure 9. Correlations between OCP, corrosion rate, and concrete resistivity for specimens located at the seashore.

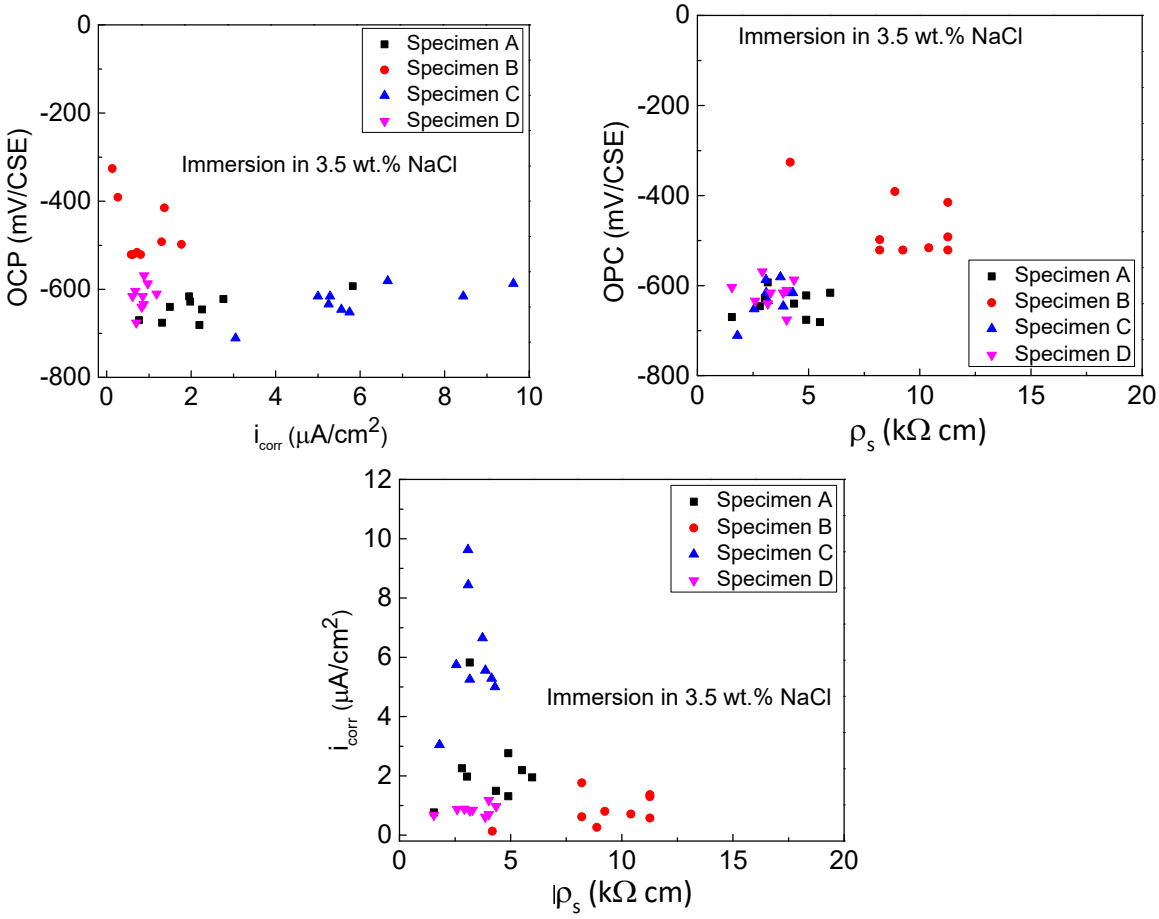

Figure 10. Correlations between OCP, corrosion rate, and concrete resistivity for specimens in 3.5% NaCl solution.

1.4.2 – Studies that included fly ash

Case I: M.F. Montemor, A.M.P. Simies, M.M. Salta, "Effect of fly ash on concrete reinforcement corrosion studied by EIS, Cement and Concrete Composites 22 (2000) 175–185 (Montemor, Simões, and Salta 2000).

In this study, the corrosion process of steel embedded in concrete with various amounts of fly ash (up to 50% of the total binder) was tested under complete and partial immersion, in sodium chloride solution. The corrosion process was followed by monitoring of open circuit potential (OCP) and electrochemical impedance spectroscopy (EIS).

Ordinary Portland cement and type–C fly ash were used in concrete preparation. The mixing proportions were the following: Portland cement plus fly ash: 350 kg; water: 200 liters; sand: 1400 kg; aggregates: 360 kg. Fly ash was added in partial substitution of Portland cement in the proportions of 50%, 30% and 15 (wt %). Samples with no fly ash were also prepared. The water/binder ratio was in all cases 0.57.

Two commercial steel bars with a diameter of 1 cm, previously polished with a 600 silicon carbide (SiC) grit emery paper to remove the mill scale/rust on the surface, were embedded in

each concrete block, with a concrete cover of 1 cm (Fig. 11). With this geometry, the distance between the inner surfaces of the steel bars was 6 cm and the embedded area of each electrode was 32.2 cm^2. Concrete blocks were cured during one week in a high humidity chamber before immersion in the aggressive solutions.

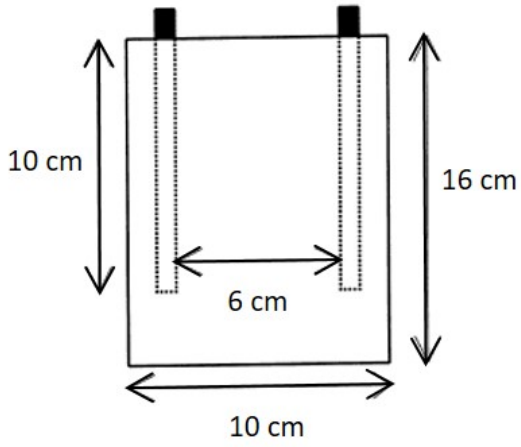

Figure 11. Specimen geometry.

Reinforced concrete blocks were either vertically immersed to a depth of 6 cm (partial immersion) or fully immersed in a 3 wt % NaCl solution in distilled water. Under these conditions only chloride-induced corrosion occurred, since the high content of water impeded carbonation of the concrete. Electrochemical tests were made during immersion, and blocks were broken at the end of the tests, for visual inspection. A minimum of two blocks for each condition was tested.

Figure 12 shows the evolution of OCP, concrete resistivity and charge transfer resistance with immersion time. It can be observed that with an increase in the immersion time, both the OCP and the charge transfer resistance decreased. Particularly after 60 days of immersion, a sudden drop of OCP and charge transfer resistance occurred. This is believed to be due to the initiation of corrosion. It also noted that the addition of fly ash increased the corrosion resistance of the steel bar, especially for concrete with 30% fly ash addition.

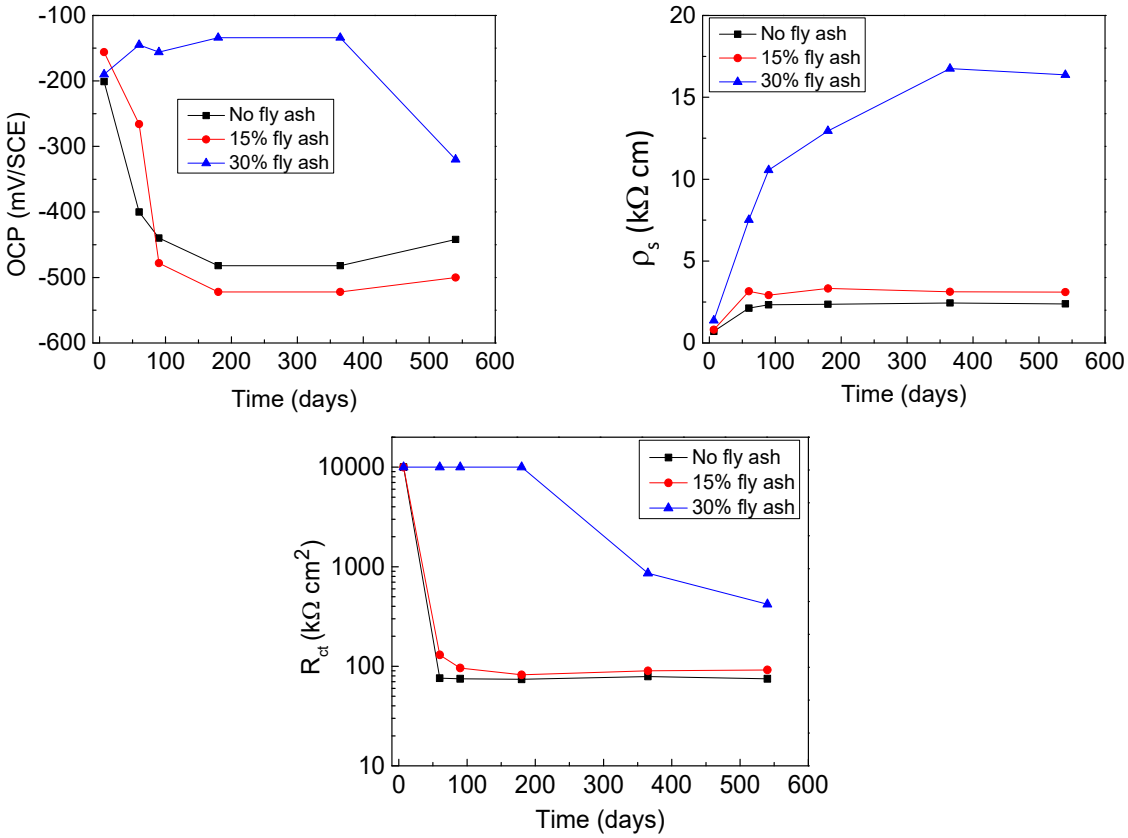

Figure 12. Corrosion parameters evolution with time.

Figure 13 shows the correlations between OPC, concrete resistivity and R_{ct} for specimens with various amounts of fly ash. No obvious relations were observed between these three parameters.

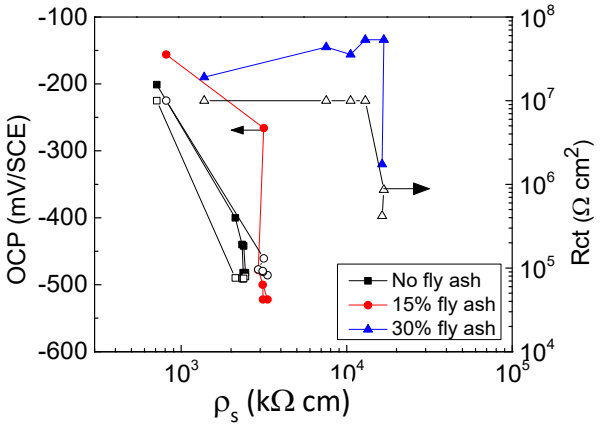

Figure 13. Corrosion parameters correlations.

Case 2: P. Garces, L.G. Andion, E. Zornoza, M. Bonilla, J. Paya, The effect of processed fly ashes on the durability and the corrosion of steel rebars embedded in cement–modified fly ash mortars, Cement and Concrete Composites 32 (2010) 204–210 (Garcés et al. 2010).

This paper deals with the study of corrosion of reinforcing steel bars embedded in Portland cement mortars containing different types of fly ash. The fly ashes used were obtained by physicochemical treatments of an original F class fly ash to modify its magnetic properties and reduce its particle size. An original fly ash (T0) and three types of modified ashes were tested according to treatment duration and magnetic properties (T60, ground fly ash; TNM, non-magnetic fraction; TM, magnetic fraction). Corrosion tests on reinforced mortar specimens with and without different types of fly ashes, cured at 40°C, and under accelerated carbonation conditions and seawater immersion, have been performed in order to obtain conclusions on durability. From the corrosion point of view, the addition of TNM in mortars showed to be much more effective than the addition of the original T0 fly ash.

The specimens for corrosion tests were prismatic, 2 × 5.5 × 8 cm, and contained two identical bars of carbon steel (D=6 mm). A graphite bar embedded in the middle was used as a counter-electrode. The resulting thickness of the mortar cover for the electrodes was 7 mm. The mortar specimens were prepared in the laboratory at 20°C and 80% R.H. After demolding, 24 h later, test specimens were immersed in water for 28 days of curing period at 40°C, to ensure that pozzolanic reaction was well advanced.

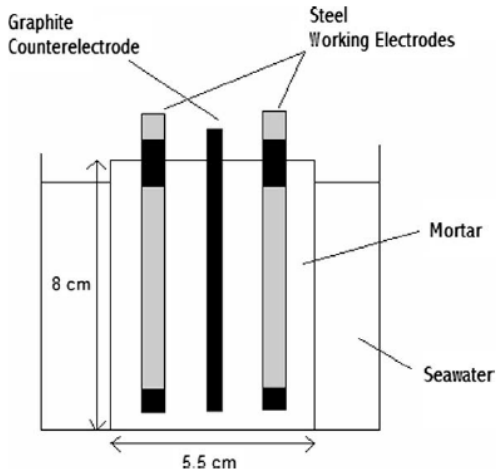

Figure 14. Specimen geometry

Low-calcium fly ash (class F according to ASTM C-618) from the thermoelectric power plant Andorra-Teruel (Spain) was used to obtain the various fractions of modified fly ashes: T0, original fly ash; T60, original fly ash ground for 60 min; TM, magnetic fraction of the original fly ash; and TNM, non–magnetic fraction of the original fly ash. Cement type CEM I 42.5R (OPC) was used. Silica sand and distilled water were always employed. The mortar combined one part (by mass) of cement and three parts of sand. Different mortars were prepared using a ratio of water to cement plus fly ash of 0.5 and 0.7. Fly ash replaced 30% of the cement (by mass).

After the curing period (28 days, RH = 100%, 40°C), water-saturated samples (two for each fly ash type) were partially immersed in seawater, being the immersion depth 7 cm to avoid contact between the seawater and the external part of the rebars.

The electrochemical technique used to measure the instantaneous corrosion rate, I_{corr}, was the polarization resistance technique, through the well-known Stern-Geary formula, $I_{corr} = B/Rp$. I_{corr}

was calculated assuming values of B = 26 mV for corroding steel or 52 mV for passive steel. Rp and corrosion potential (E_{corr}) were periodically measured during the time of the experiment, and also the weight loss was measured, for each electrode, at the end of the test. All potentials are vs. a saturated calomel reference electrode (SCE). A potentiostat galvanostat EG&G Model 362 was used. I_{corr} data were calculated as average values of four measurements (two specimens, two electrodes each).

Figure 15 shows the change of OCP and corrosion rate over time and the correlations between OCP and corrosion rate. With an increase of time, the OCP decreased and the corrosion rate increased slowly. With a high corrosion rate, a more negative OCP was obtained.

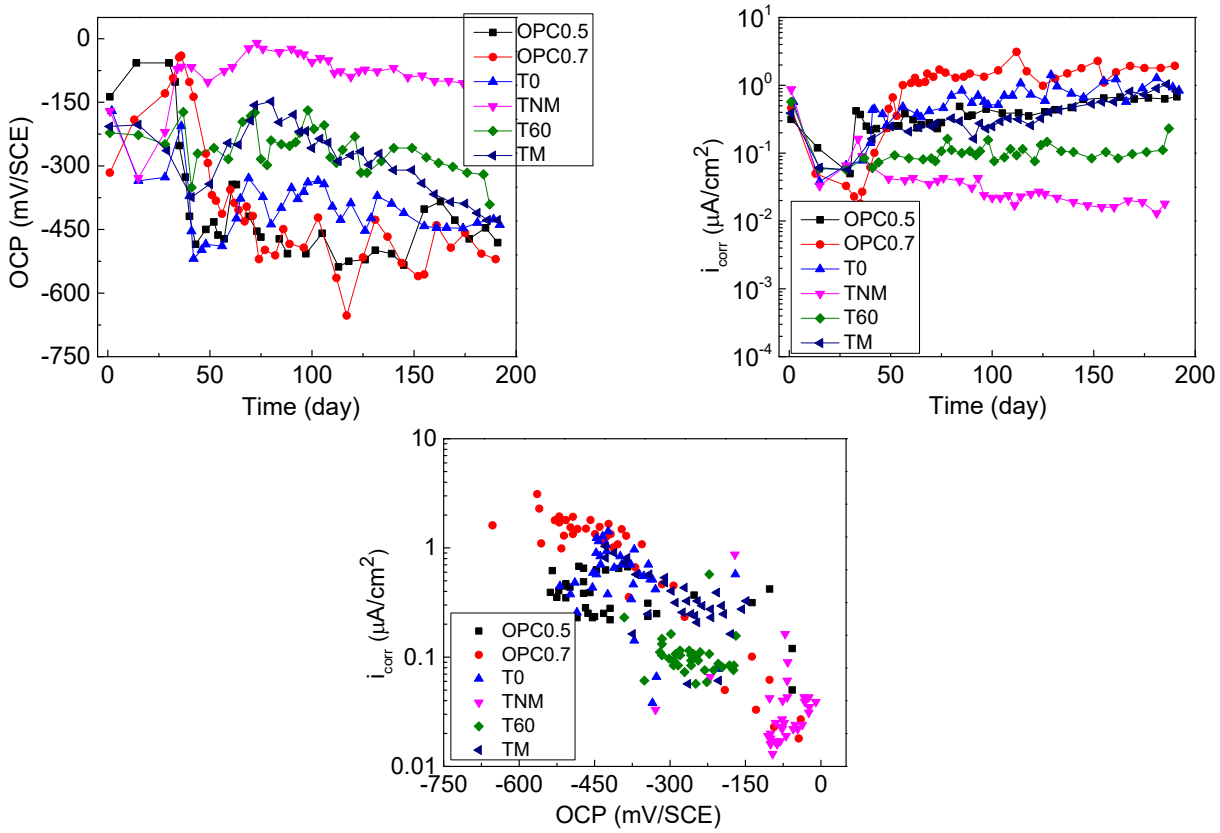

Figure 15. Corrosion potential and rate evolution with time and correlation between them.

Case 3: Velu Saraswathy, Ha-Won Song, "Electrochemical studies on the corrosion performance of steel embedded in activated fly ash blended concrete", Electrochimica Acta 51 (2006) 4601–4611 (Saraswathy and Song 2006).

Concrete specimens prepared with 10–40% of activated fly ash replacement were evaluated for their open circuit potential measurements, impedance measurements, linear polarization measurements, and the results were compared with those for OPC concrete without fly ash. All the studies confirmed that up to a critical level of 20–30% replacement; activated fly ash cement improved the corrosion–resistance properties of concrete. It was also confirmed that the chemical activation of fly ash yielded better results than the other methods of activation investigated in this study. Above 30% replacement level, the permeability of concrete was found to increase;

hence more chloride anions penetrated even at three cycles of exposure and the potential shifted towards more negative directions.

Cylindrical reinforced mortar (cement/sand=1:3, w/c=0.45) specimens of size 50 mm diameter and 50 mm height were cast in triplicate with OPC (control) and OPC replaced by fly ash (AFA: as–received fly ash; PFA: physically activated fly ash; TFA: thermally activated fly ash; CFA: chemically activated fly ash) at 10–40% replacement levels. All the triplicate specimens were cured in distilled water for 28 days. After 28 days the specimens were taken out, dried and immersed in 3% NaCl solutions for open circuit potential measurements. The potential of the embedded steel rebar was measured against a saturated calomel electrode (SCE) using a high impedance voltmeter. The concrete specimens were then subjected to alternate wetting (15 days) and drying (15 days) in 3% NaCl solution in order to accelerate corrosion. The potential readings were measured at 30 days intervals. The solution was changed once in 2 weeks in order to induce accelerated corrosion. Potential measurements were carried out for both OPC and fly ash blended systems at an ambient temperature of 30 + 1 °C.

Figure 16 shows the OCP evolution with time. It can be observed all OCP decreased slowly as a function of test duration.

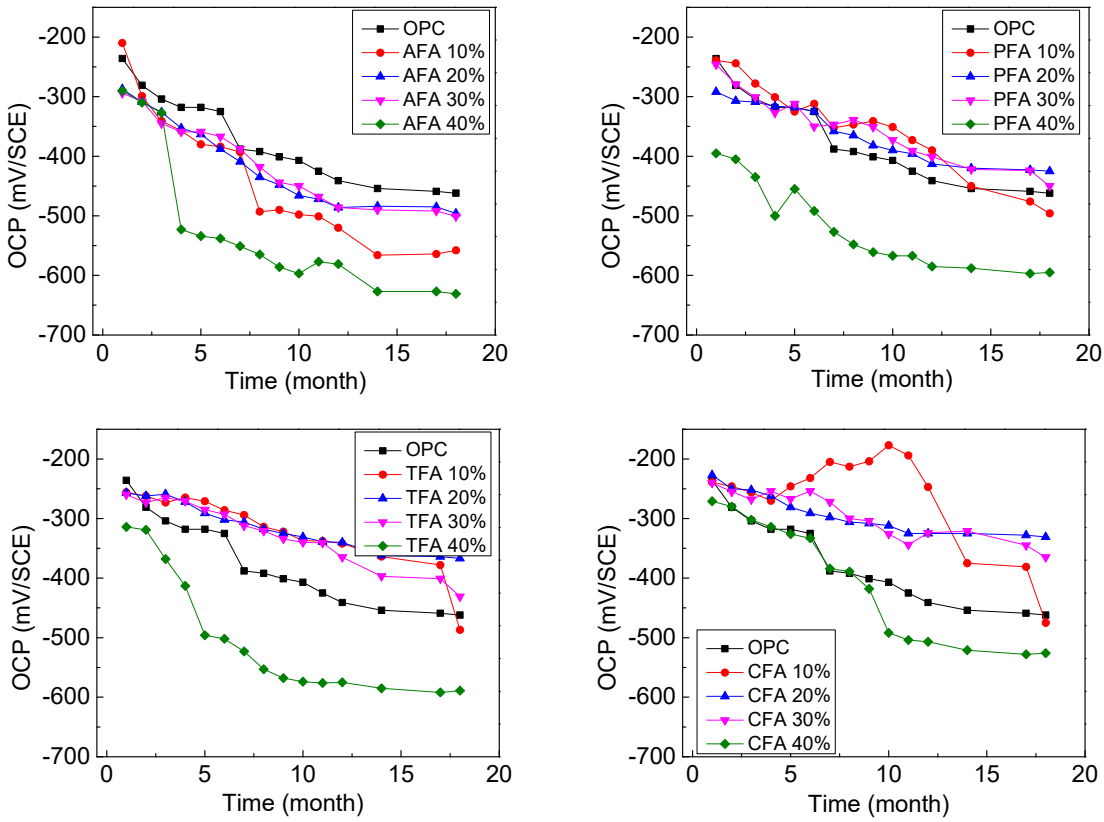

Figure 16. Corrosion potential evolution with time.

Figure 17 shows the correlations between the corrosion rate and the OCP for some specimens experiencing active corrosion stage (propagation stage). It can also be observed that a high corrosion rate is related to a more negative corrosion potential regardless of fly ash addition or treatment. It is noted there are four measurements for each mixture, which corresponds to the

four different percentage of addition including 10%, 20%, 30%, and 40% replacement. In general, with an increase in the addition, the corrosion rate increases. Take the AFA as an example, the corrosion rates increase from 4.35 μA/cm^2 to 15.4 μA/cm^2 as the addition increased from 10% to 40%.

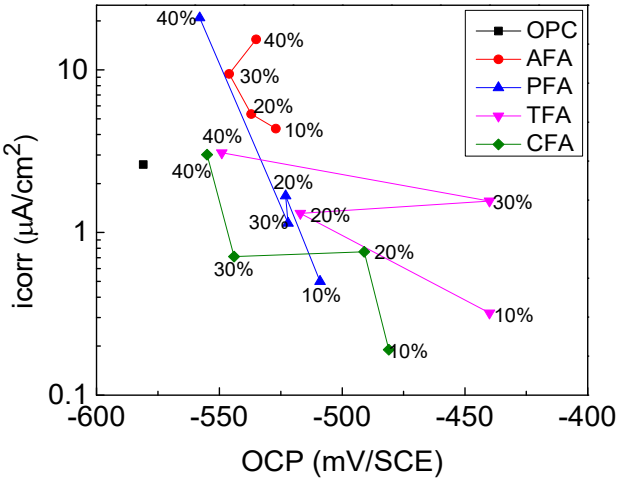

Figure 17. Correlation between corrosion potential and corrosion rate.

1.4.3 – Studies that included blast furnace slag cement

Case I: Brian B. Hope, Alan K.C. Ip, "Corrosion of steel in concrete made with slag cement", ACI Materials Journal 1987: 525–531. (Hope and Ip, 1987)

Test specimens were 114 × 300 × 400 mm reinforced concrete slabs. Three 13 mm smooth mild steel bars were embedded 250 mm in concrete and centered 56 mm from the top surface of each slab. The bar located at the center of the slab was used as a counter electrode, and the other two bars, placed 144 mm on each side of the center bar, were working electrodes. The active area of each bar is 102 cm^2. Three concrete mixes were used: concrete A was ordinary Portland cement, Concrete B with 75% cement and 25% slag; Concrete C with 50% cement and 50% slag. All specimen were firstly cured in water for around 35 days, then subjected to wetting-drying cycles to 193 days. At 270 days, the specimens were oven dried at 105 °C for 14 days, the specimens were then soaked in air-saturated water for the next 14 days and dried in laboratory air for the following 14 days.

Figure 18 shows the evolution of concrete resistivity, corrosion potential and corrosion rates for all three concrete specimens. It can be observed that as time passed the concrete resistivity increased. Particularly in the first 60 days, the resistivity increased rapidly. Concrete with slag show a high resistivity, and with an increase of the slag percentage, the concrete resistivity also increased. As for the corrosion, the corrosion potential suddenly decreased around 80 days, indicating active corrosion. However, the corrosion rate decreased all the time from the start. This is probably because of the increase in concrete resistivity.

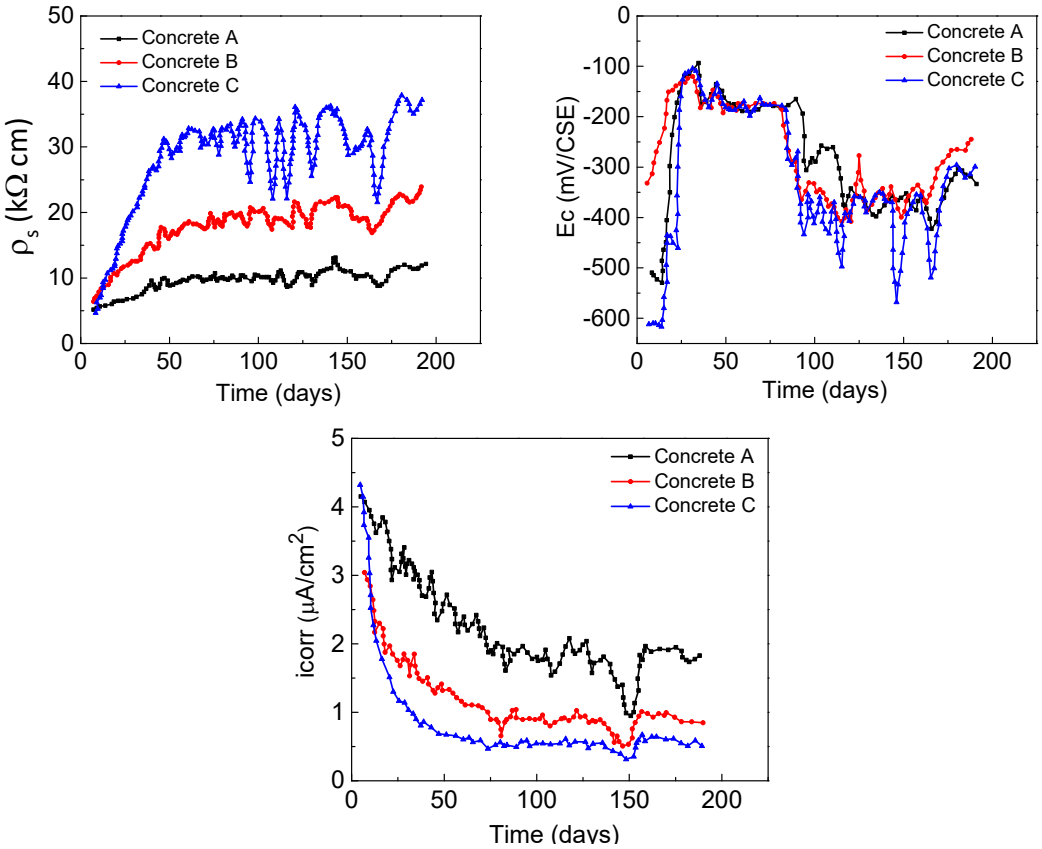

Figure 18. Evolution of concrete resistivity, corrosion potential, and corrosion rate over time.

Figure 19 shows the correlation between concrete resistivity and corrosion potential, corrosion rate before 270 days. It can be observed with an increase of concrete resistivity, the corrosion rate decreased almost in a linear trend for all three specimens. However, no correlation was observed between the concrete resistivity and the corrosion potential for specimens A and C. For specimen B, a trend can be observed, and the corrosion potential increased with an increase in the concrete resistivity. This is in agreement with observations from other researchers.

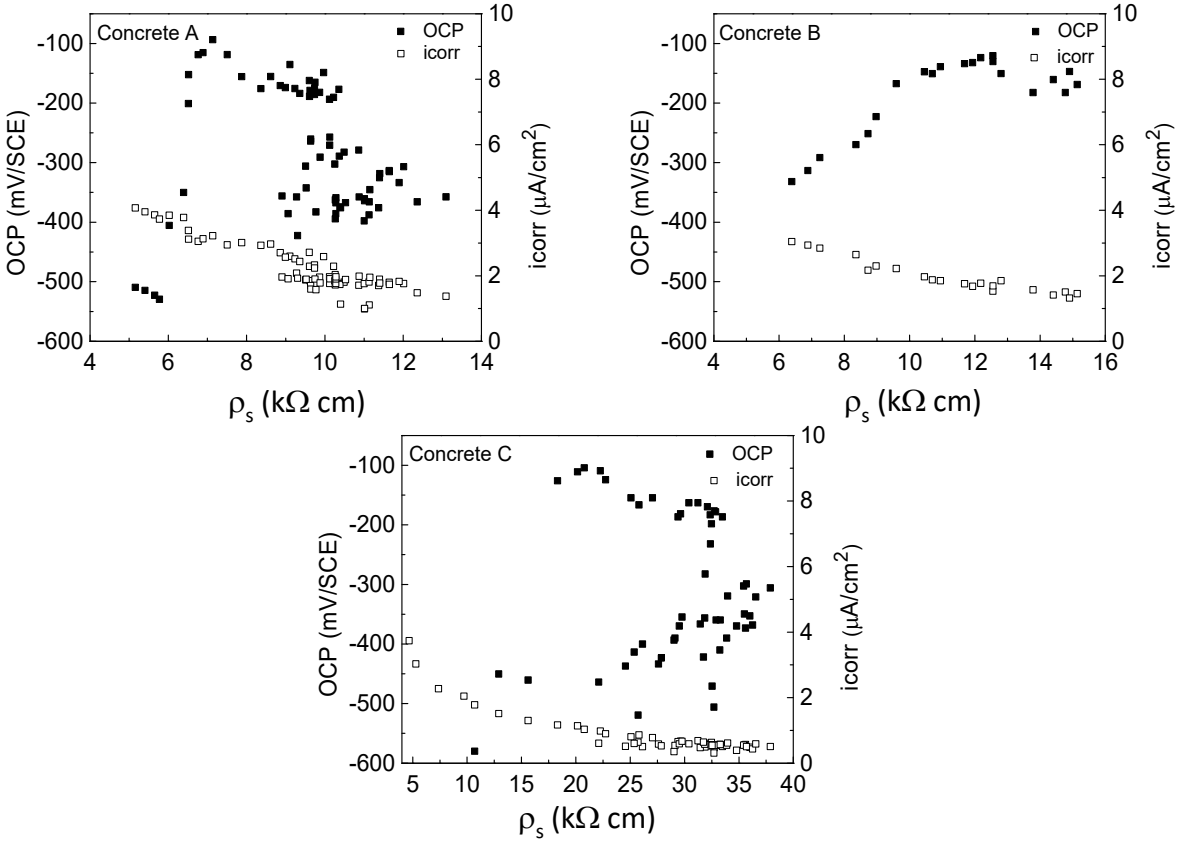

Figure 19. Correlations between corrosion potential, corrosion rate, and concrete resistivity from the beginning to 270 days.

Figure 20 shows the concrete resistivity, corrosion potential and corrosion rate evolution after 270 days. It can be observed that with an increase of time, the concrete resistivity decreased, the corrosion potential decreased, and the corrosion rate increased. As a matter of fact, all the specimens were undergoing active corrosion state after 270 days. The decrease in the concrete resistivity was attributed to the penetration of chloride. The increase in the corrosion rate is due to the penetration of oxygen.

Figure 21 shows the correlation between concrete resistivity, corrosion potential and corrosion rate when the specimens were corroding after 270 days. It can be observed that in the active corrosion stage, the corrosion rate decrease with an increase in the concrete resistivity. Correspondingly, the corrosion potential increased with an increase in the concrete resistivity.

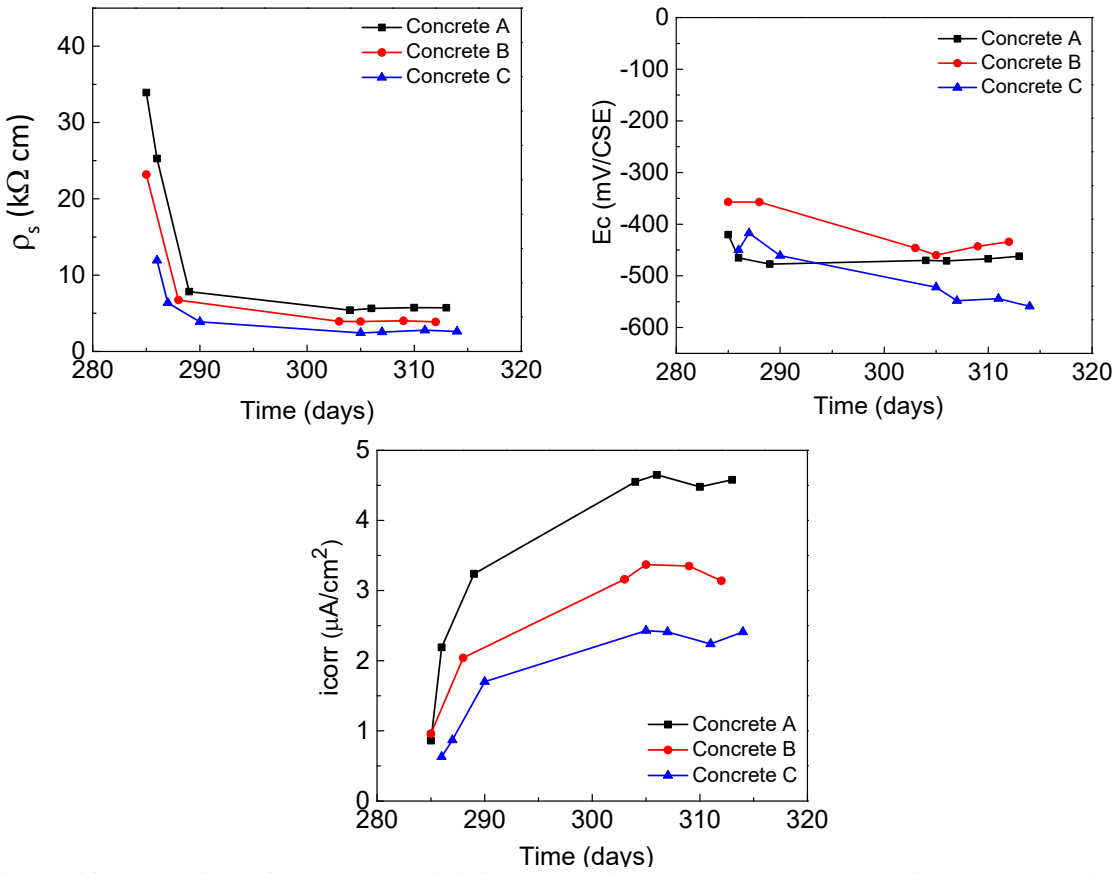

Figure 20. Evolution of concrete resistivity, corrosion potential, and corrosion rate over time.

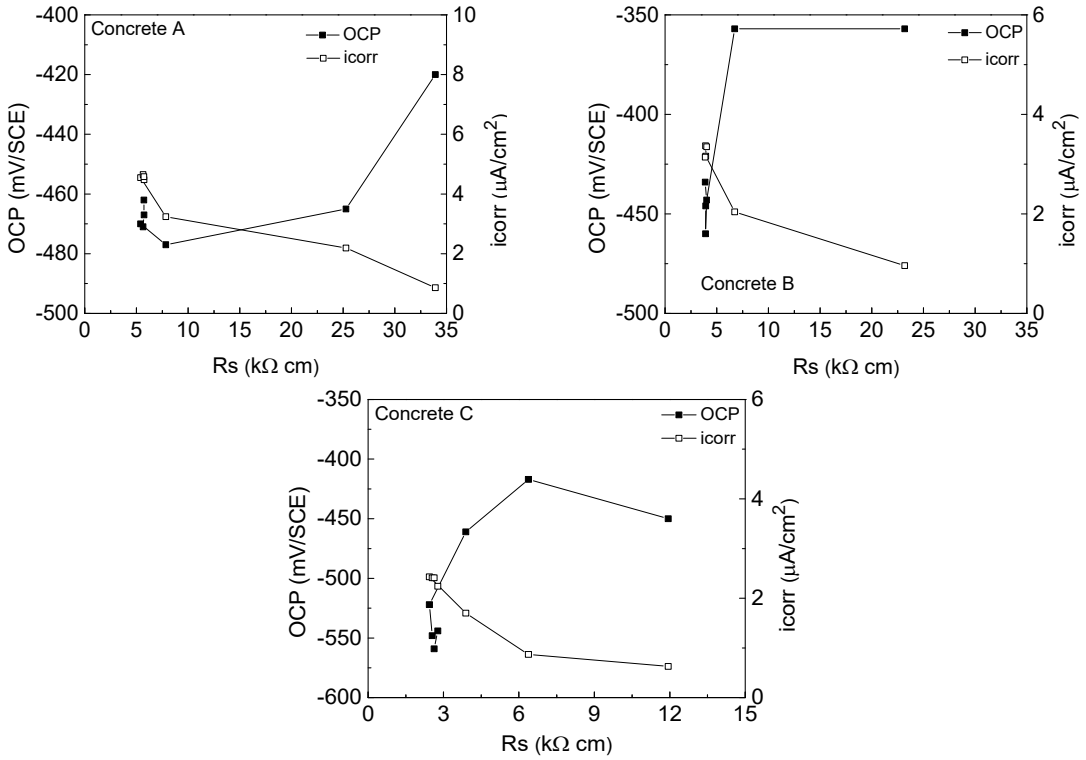

Figure 21. Correlations between corrosion potential, corrosion rate, and concrete resistivity after 270 days (active corrosion).

1.4.4 – Studies with fly ash, silica fume, and slag

Case I: Ran Huang, Jiangjhy Chang, Jiannkuo Wu, Correlation between corrosion potential and polarization resistance of rebar in concrete, Materials Letters 28 (1996) 445-450.(Huang, Chang, and Wu 1996)

Reinforced concrete cylinder specimen with a diameter of 50 mm and height of 80 mm were prepared. The steel bar has a diameter of 10 mm, and the concrete cover was 20 mm. The control specimen were prepared with type I Portland cement and siliceous sand in the weight ratio of 0.5 and the water/cement ratio was kept at 0.35, 0.45, and 0.55. In mixes, partial cement was replaced by 10 and 20% fly ash and 15 and 30% slag, respectively. All specimens were immersed in 3.5% NaCl solution for the electrochemical corrosion tests. Polarization resistance and open circuit potential were measured periodically.

Figure 22 shows the evolution of OCP with time for different specimens. Specimens with slag addition had a lower corrosion potential than specimens with fly ash regardless of the water to cement ratio. For specimens with w/c equals to 0.35 and 0.45, no general trend was observed over time for open circuit potential, and most of the specimens fluctuated around certain values. However, for specimens with w/c=0.55, a decrease in the OCP happened after 600 hours, which is attributed to corrosion initiation.

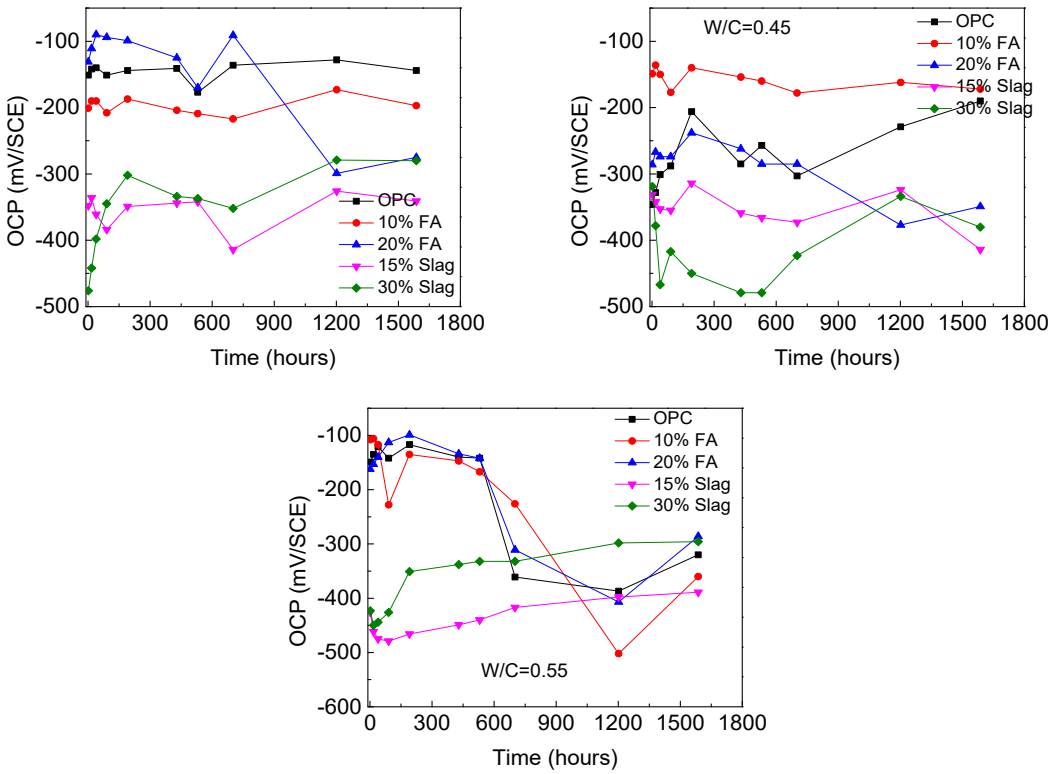

Figure 22. Evolution of OCP over time for different specimens (w/cm=0.35, 0.45, 0.55).

Figure 23 shows the evolution of polarization resistance with time. The polarization resistances of OPC specimens are higher than specimens mixed with fly ash or silica fume, particularly at the beginning of the test period. For specimens with w/c=0.55, the polarization resistances of specimens mixed with fly ash are higher than OPC specimens after 700 hours. But, the polarization resistance of the specimen mixed with silica fume is still lower than OPC specimens.

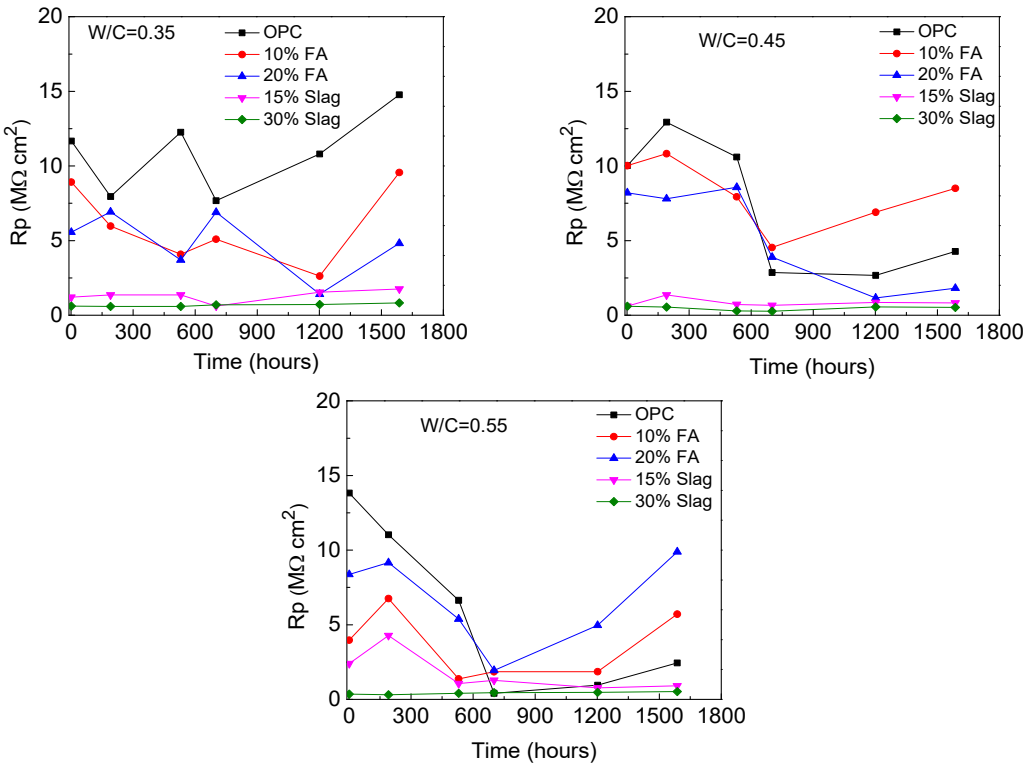

Figure 23. Evolution of polarization resistance over time for different specimens.

Figure 24 shows the correlation between OCP and polarization resistance for all specimens. It can be observed, a high polarization resistance corresponds to a more positive corrosion potential. This is more obvious for specimens with w/c=0.35 and 0.45.

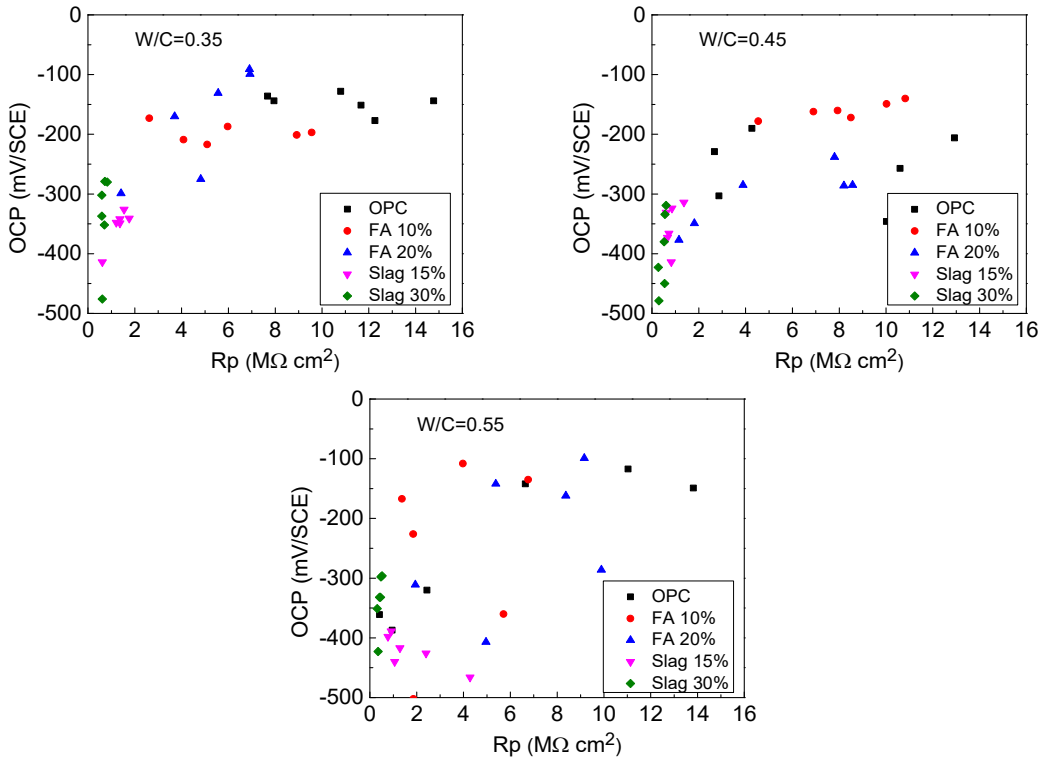

Figure 24. Correlation between OCP and polarization resistance.

The papers described above are a subset of those available in the literature, additional examples can be found in references (Romano, Brito, and Rodrigues 2013; Ahlström et al. 2016; Millard et al. 2001; Martínez and Andrade 2009; Polder, R.B., Bertolini 1983; Cabrera and Ghoddoussi 1994). Moreover, Gullikers (Gulikers 2005) points out that for microcells, the electrical resistivity of the electrolyte adjacent to the steel/concrete interface is of prime importance. This interfacial layer may have a different chemical composition and physical structure than that of the bulk concrete more remote. Consequently, the resistivity of the bulk concrete could be a poor indicator of the electrolytic resistivity at the steel-concrete interface. In the case of macrocells, the resistivity of the cover (that could approximate the bulk resistivity) would be as relevant as that of concrete at the steel reinforcement interface

1.5 – Note on corrosion propagation and time to cracking

Besides the experimental results described above, research efforts over the last few decades have also been focused on developing models that estimate the time to cracking. Most of these studies have focused on OPC concrete without admixtures; very few models have been done that include high-performance admixtures (for corroding reinforcing steel embedded in concrete). Jamali et al. (Jamali et al. 2013) reviewed empirical, analytical and numerical models that have been developed for modeling corrosion-induced concrete cover cracking due to reinforcing steel corrosion. Jamali stated that the parameters that need to be considered are corrosion rate, type of corrosion products, corrosion accommodating region, mechanical properties of materials and geometry. Jamali et al. (Jamali et al. 2013) states that when the corrosion morphology is due to localized corrosion (as per chloride-induced corrosion), the anodes and cathodes could be

separated and corrosion products form only locally. This changes the geometrical locations of these products (compared to taking place around the whole rebar diameter and a certain length) and thus affects when and where cracking occurs.

Torres–Acosta (Torres-Acosta and Sagüés 2004) and Busba (Busba and Sagüés 2013) included in their experiments and empirical model the effect of the anode–length and how the average penetration depth increased with cover/diameter (of rebar) increase for a constant c/L. It assumed that corrosion was taking place around the rebar perimeter.

Otieno et al. (M. Otieno, Beushausen, and Alexander 2012; M. B. Otieno, Alexander, and Beushausen 2010) did a review of the corrosion rates that have been used and include results of experiments with an incipient crack. Angst et al. (Ueli Angst et al. 2010), described the effect of reinforcement length (sample size) on the chloride threshold.

The paper from Jamali et al. (Jamali et al. 2013) describes that in some cases (as part of his literature search) where chloride-induced corrosion took place rust–stains or cracks were not visible; upon forensic examination, a significant cross-section loss was observed at the corroding site. Angst et al.(Ueli Angst et al. 2010) describes, as an example, a bridge deck with a damaged waterproofing membrane, where concrete is locally saturated with (often chloride–bearing) water and thus oxygen starvation is likely. In such cases, anodic iron dissolution might occur (once corrosion has initiated) without sufficient precipitation of corrosion products to form cracks (Broomfield 2007). This type of corrosion is commonly referred to as 'black rust'(Broomfield 2007) since the iron may remain dissolved in the concrete pore solution until the concrete is removed during visual inspection and thus access to oxygen is provided. Walsh and Sagüés (Walsh and Sagüés 2016) reported similar findings while performing forensic analysis of reinforced concrete pile that had been fully immersed for an extended period of time. As part of past research for FDOT (F. J. Presuel-Moreno and Moreno 2016), five rebar specimens were terminated after more than 16 years of exposure to sea water (wet/dry cycles). (The remaining samples are now more than 24 years and are part of this project.) Upon exposing the reinforcing steel, it showed a black/dark green corrosion product. Similar findings were observed on single rebar specimens embedded in mortar which were subjected to accelerated chloride transport to initiate corrosion (Francisco Presuel-Moreno 2015).

Angst et al. (U Angst et al. 2012) describes that for a purely chloride–induced (pitting) corrosion, the usually assumed model (i.e., corrosion taking place around the whole rebar) appears not to be suitable to describe the occurring processes for several reasons. First, iron dissolution only takes place locally rather than uniformly around and along the entire rebar. Second, the corrosion products are much more soluble and precipitation is unlikely, in particular near the corroding spot (due to the presence of chlorides which enhance solubility). Finally, initiation of chloride-induced corrosion is often associated with local weaknesses in the steel/concrete interface, viz. higher local porosity, which would – for the case of precipitation – additionally prevent the formation of expansive pressure. Angst (U Angst et al. 2012) reports documented cases in which corrosion was initiated by chlorides. There were little or no signs of corrosion stains at the surface during inspections. Significant cross-section loss was found upon terminating the specimens.

Additionally, Walsh and Sagüés (Walsh and Sagüés 2016) and Sanchez and Sagüés (Sánchez and Sagüés 2017) reported a halo effect (cathodic prevention similar to what is observed for pitting corrosion of stainless steel (Budiansky, Hudson, and Scully 2004)) of a corroding site on the surrounding steel, such that the next corroding site was found a certain distance from the initial anode. In partially-immersed bridges exposed to a marine environment, the chloride ions penetrated from the surface toward the reinforcement. Thus, the side of the rebar facing the chloride exposed concrete surface reached the chloride threshold first and then corrode. The initial corrosion site(s) can be as small as a small pit (e.g., <1 mm diameter). Once corrosion has initiated, it is likely that the corroding site(s) would exert some cathodic prevention on the surrounding steel area (and the throwing power would depend on the concrete resistivity and moisture content) such that the next corroding site would be located some distance from the initial corroding site.

It is not clear how the above-described processes affect what has been observed in Florida substructures. Besides the corrosion products being more soluble in the presence of chlorides, high moisture might also enhance how far these corrosion products can travel thru the concrete microstructure (e.g., at tidal and submerged region elevations). On the other hand, once chlorides exceed a certain concentration (significantly larger than the threshold) corrosion could occur around the whole rebar and with a considerable anode length, which then could proceed as often modeled and cause cracking and spalling.

Angst et al. (U Angst et al. 2012) stated in their paper that it is not trivial to determine if corrosion has initiated if there are no visual signs of distress. Alternative assessment tools might need to be developed.

1.6 – Summary and conclusions

In this review, corrosion data from the literature was extracted and analyzed. Emphasis was focused on the corrosion parameters that could assist in the study of the propagation stage like corrosion potential, corrosion rate or polarization resistance, and concrete resistivity (or concrete solution resistance). Their evolution of these parameters with time and the correlations between these parameters were studied. Specimens included slab, prism, and cylinders. Mortar or concrete mixed with ordinary Portland cement and high-performance admixtures like fly ash, silica fume, blast furnace slag were all included. Most of the specimens were immersed in a saline solution or subjected to cyclic wetting-drying cycles to accelerate the chloride transportation. The test duration range from a few days to 1000 days dependent on the specimen and experimental design.

After analysis of the results, it is found that before the initiation of corrosion (at the first stage), there are no obvious correlations between the corrosion rate, concrete resistivity, and corrosion potential. Concrete resistivity depends on its chemical compositions and microstructures, which is associated with the hydration process. Hydration of concrete may take a few years depending on its composition (with or without the addition of high-performance admixtures), during which the resistivity increases over time. Moisture content can affect concrete resistivity significantly. Corrosion potential is also affected by a number of factors, which include not only the concrete properties but also the surface and environmental (exposure) conditions. Before initiation of corrosion, the corrosion rate is reported to be very small, which is lower than 0.1 $\mu A/cm^2$. This small current density strongly depends on factors such as properties of the passive film, concrete cover, as well as exposure conditions. In sum, these factors affect the measurements of concrete

resistivity, corrosion rate, and corrosion potential in the first stage more than during the second stage. But even during the propagation stage, factors such as the moisture content and concrete composition will dictate the concrete resistivity, and to some degree, affect the corrosion rate of active steel.

After corrosion initiation, which usually takes from a few to many years (propagation stage), the hydration process of concrete cover is close to complete and its dielectric properties become stabilized. At the same time, some portion of the passive film is destroyed after corrosion has initiated. If the concrete structures are exposed to the marine environment or subjected to chloride attack from de-icing salts, then initially the corrosion of steel is localized and focused at some isolated sites. The localized corrosion sites work as the anode, while the non-corroding rebar is the cathode. The surrounding concrete between the anodic sites and the cathodic sites will serve as a medium for corrosion current to flow. If the concrete is wet, with no cementitious admixtures (like fly ash, slag, etc.), more porous (i.e., higher w/cm) and attacked by chloride, then the concrete resistivity is low, resulting in a higher corrosion current and more negative corrosion potential. In this scenario, the correlations between corrosion potential, corrosion rate, and concrete resistivity gradually become clear and obvious, particularly when the concrete contains only OPC.

The addition of high-performance concrete admixtures such as fly ash, silica fume, and slag cement, on the one hand, changes the hydration process and chemical composition, and on the other hand, reduces the porosity of concrete cover over time. It is believed that this not only delays the initiation of corrosion but also influences the propagation stage (reduced corrosion rate due to poorer macrocell). However, based on the literature review, it is found that there are limited corrosion-related data (corrosion potential, corrosion rate, and concrete resistivity) collected during the corrosion propagation stage, particularly after the addition of high-performance admixtures. Although there are a few studies showing corrosion data in the second stage, either they measured the corrosion potential/rate, or they measured the concrete resistivity. Very few studies showed all three measurements and their correlation after addition of high-performance concrete admixtures.

In addition, some of the variations observed in the above-reviewed papers can be attributed to factors affecting the corrosion/resistivity relationship; for example, the material and exposure conditions should carefully be chosen. A standardized geometry and method could be used for testing the E, i_{corr}, resistivity relationship so that the experimental data obtained in different laboratories and conditions can be compared. Hornbostel and Geiker (Hornbostel et al. 2013) suggested that an extensive field survey of the E, i_{corr}, resistivity relationship should be undertaken to identify any possible deviations between laboratory studies and reality.

The following chapters will describe the experiments, results, forensic analysis, discussion and conclusions for the research efforts carried as part of this project.

Chapter 2 – Experimental Methods and Methodology

This chapter describes the concrete compositions and the specimens geometry. The samples are reinforced concrete specimens that were either prepared as part of previous projects (labeled older specimens in the scope and previous tasks) or the specimens were prepared as part of this project. The older specimens are described first. This chapter also describes the methodology used to accelerate chloride transport via electromigration. Once corrosion has been taking place for sometime a modest anodic current was applied to selected rebars as to accelerate corrosion. The procedure implemented is also presented here. Finally, the electrochemical measurements, performed to monitor the reinforcing steel, are also described.

2.1 – Older specimens

2.1.1 – SDS (simulated deck slab specimens): single-rebar and four-rebar concrete specimens

Concrete specimens with a w/cm ratio of 0.41 were prepared with 390 kg/m^3 of cementitious material(F. Presuel-Moreno, Liu, and Suarez 2010). Table 9 presents the concrete compositions for the different mixes. The specimens were 30 × 30 × 15 cm. The embedded reinforcement was ϕ = 16 mm rebars (i.e., #5 rebars). There were samples with one rebar and samples with four rebars. The concrete cover was 5 cm for specimens with one rebar. For the specimens with 4 rebars, the concrete cover for the top two rebars was 5 cm, and for the other two rebars (transverse to the other two) the concrete cover was about 6.6 cm. Figure 25 shows a schematic of specimens with a single and four rebars

Table 9. Details of concrete mixes prepared in 2007

ID	Cement (kg/m^3)	FA (kg/m^3)	SF (kg/m^3)	Water (kg/m^3)	Fine agg. SSD (kg/m^3)	Coarse agg. SSD (kg/m^3)
1B, 1C, 1D, 2B	390	–	–	159.9	734	996
1F, 1G, 1H, 2D	312	78	–	159.9	734	996
3B	280.8	78	31.2	159.9	734	996

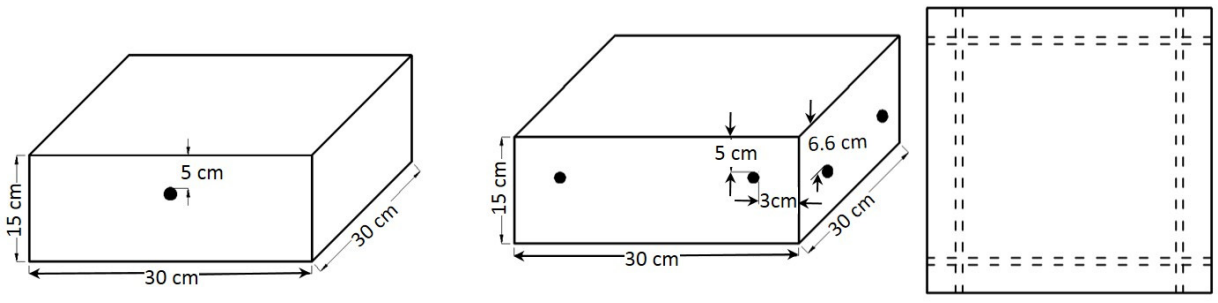

Figure 25. Diagrams showing the reinforced concrete blocks: one-rebar specimen (left); four-rebar specimen (center and right).

Table 10 presents the group names given to the samples and how many were prepared and used to study the corrosion propagation. Groups 1B, 1C, 1D and 2B were prepared with ordinary Portland cement (OPC) only, and Groups 1F, 1G, 1H and 2D were prepared with OPC and Fly Ash (FA), FA as 20% cementitious replacement. Group 3B specimens were prepared with OPC, FA (20%) and Silica Fume (SF) 8%.

The early curing of the samples was as follows: Specimens from groups 1C, 1F and 3B were exposed to a high moisture room for about 1 year, these samples were then exposed to a laboratory environment (70°F and approx. 65 to 70 RH). Specimens in groups 1B, 1D, 1G, and 1H were exposed for 60 days in the high moisture room followed by 60 days' exposure to laboratory environmental conditions. These specimens were then exposed outdoors to cyclic ponding with seawater (1 week with seawater and 1 week without seawater) for 3 to 6 months. A solution reservoir was installed for the ponding. A plastic plate was placed on top of the solution reservoir, which minimized evaporation and prevented rain from reaching the ponding area. The specimens were then brought back to the lab and remained under lab exposure for one to three years, prior to accelerated chloride transport exposure (this procedure is described in a subsequent section).

Two rebar specimens were prepared with the concrete mix containing 20% FA as described above. This geometry is named modified Tombstone specimen. The dimensions for the two rebar specimens are 61 × 25.4 × 17.8 cm (24 × 10 × 7 in). Five specimens were prepared with two #5 (1.6 cm diameter) rebar segment bars parallel and embedded along the long axis with a spacing of seven inches in between and displaced from the center to obtain four different concrete covers. The four concrete covers were: 8.9 cm, 7.6 cm, 4.4 cm, and 2.5 cm. Two of these five specimens were selected for this project. Figure 26 shows a picture of one of the two rebar specimens.

Table 10. Description of prepared specimens.

ID	Mix design	Number of rebars	Number of specimens
1B, 1C	OPC	single rebar	3
1D	OPC	four rebars	2
1F, 1G	OPC+FA	single rebar	4
1H	OPC+FA	four rebars	2
2B	OPC	single rebar	2
2D	OPC+FA	single rebar	1
3B	OPC+FA+SF	single rebar	4

Figure 26. Two-rebar specimens

2.1.2 – Single-rebar mortar specimens

The mortar specimens were 7.5 cm tall, 12.5 cm wide and 31.5 cm long (direction of the rebar). Specimens not subjected to electromigration had a 25.4 cm long solution reservoir, those subjected to electromigration had solution reservoirs that ranged from 10 cm to 1.5 cm long. A #3 (0.95 cm diameter) rebar was centered along the 12.5 cm x 7.5 cm face. The mortar used in the specimens is derived from a Florida Department of Transportation (FDOT) Class V concrete mix design. Mix design 1 (MD1) is reported in Table 11. The mortar cover was 0.8 cm for MD1 specimens. The samples were prepared during spring 2006(Tanner 2006), some were subjected to ponding with 10% NaCl solution shortly after. A number of samples were stored in a high humidity chamber for several years and solution reservoirs were installed in 2014. Chloride transport was accelerated on these selected samples and the rebar was used as one of the electrodes. Finally, a solution reservoir was installed in 2017 on three specimens (approx. 18 cm long) and ponding was started but chloride transport was not accelerated. Electrochemical characterization took place regularly over the past 400 to 500 days.

Table 11. Mortar mix design component and mass

Concrete group	Cement (kg)	FA (kg)	Water (kg)	Fine agg. SSD (kg)	w/c	s/c
MD1	14	3.36	6.6	48	0.38	2.76
MD2	18	–	6.8	50	0.38	2.76

2.1.3 – Five-rebar specimens exposed outdoors.

Figure 27 shows the dimensions of the 5 rebar specimens. Prior to outdoor exposure testing (shortly after casting), the specimens were inverted (as–cast face down); and a polycarbonate bath was mounted on what became the top surface (see Figure 27). The exposure took place outdoors most of the time, but early on the specimens were exposed indoors for a couple of years. A one week wet — one–week dry ponding cycle was instituted in January 1995 using fresh natural sea water. The typical conductivity of seawater measured at the FAU site is ~ 40

mS/cm. A rectangular plastic plate was placed on top of the specimens to prevent rainfall intrusion and minimize evaporation during the rainy/dry seasons. As shown in Figure 27, each of the bottom bars was electrically connected to one of the top bars so that a macrocell resulted between the two. Six specimens were selected for electromigration. A smaller solution reservoir was installed on the selected five rebar specimens by a placing two polycarbonate pieces so that the new reservoir length is 10 cm. Appendix B contains tables describing the concrete mix compositions for the specimens.

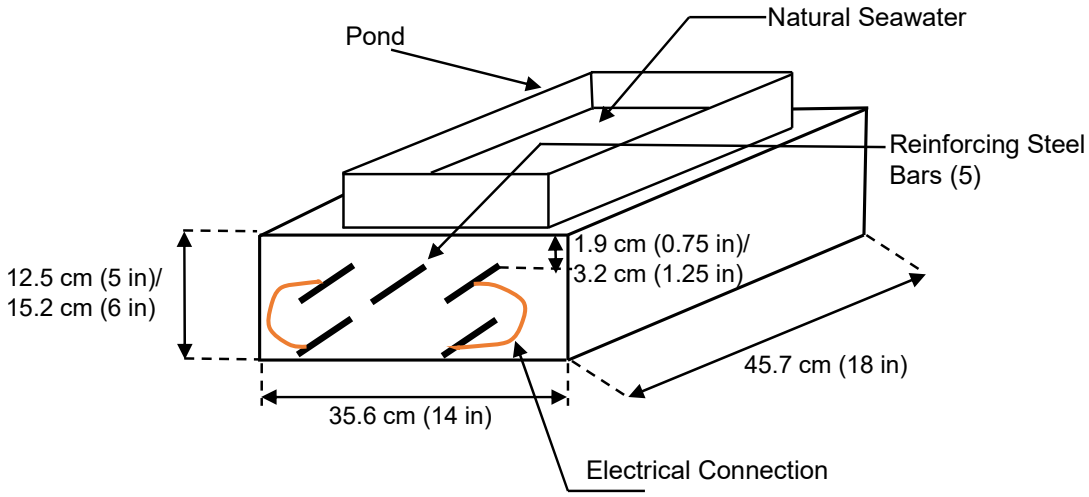

Figure 27. Five-rebar specimen diagram

2.2 – Specimens prepared 2016

Four different type of reinforced concrete samples and concrete cylinders were prepared during spring 2016. Two batches per concrete mix design were cast to accommodate the preparation of the concrete volume needed for reinforced concrete specimens and concrete cylinders (these cylinders are being used as part of a parallel project). These mixes are named SL and FA, see Table 12. Two other mixes were prepared during summer 2016 (see Table 12), but only single rebar specimens and three-rebar specimens were prepared, the number of specimens was reduced, and hence only one batch per mix was prepared. Three concrete mixes were prepared with a w/cm ratio of 0.41 and one mix was prepared with a w/cm of 0.37. Table 12 shows the details of the concrete composition. The SL specimens were prepared with blast furnace slag (50% cement replacement) on 4/4/2016, FA specimens with Fly Ash (20% cement replacement) were prepared on 4/18/2016. Mix T1 contains both FA and blast furnace slag, and mix T2 contains both FA and silica fume. Concrete mixes T1 and T2 were prepared on August 19, 2016. Details of each concrete mix can be found in Appendix 2.

Table 12. Concrete mix detail for specimens prepared Spring and Summer 2016

Mix	Cast Date	Cementitious Content	Cement Content	20% FA	8%SF	50% Slag	Fine agg.	Coarse agg.	w/cm ratio
		(kg/m^3)	(kg/m^3)	(kg/m^3)	(kg/m^3)	(kg/m^3)	(kg/m^3)	(kg/m^3)	
SL	4/4/2016	390	195		0	195	782	1009	0.41
FA	4/18/2016	390	312	78	0	0	967	833	0.41
T1	8/19/2016	390	117.5	78.3	0	195.18	761	1009	0.41
T2	8/19/2016	390	289	70	31	0	790	1046	0.37

Rebar segments were cut to size. The rebars were wire brushed. Prior to casting, the reinforcement was degreased by cleaning it with hexane. For mixes SL and FA, four types of specimens were prepared that included two tombstone specimens per composition and two modified tombstone specimens cast with six rebars. Figure 28(a) shows the mold of a modified tombstone sample with six rebars (#3 diameter) prior to pouring concrete. The concrete cover was one inch. The specimen dimension for the six-rebar specimens was 61 × 25.4 × 17.8 cm (24 × 10 × 7 in). Twelve specimens were prepared in 30.5 × 30.5 × 7.6 cm (12 × 12 × 3 in) blocks containing three #4 rebars each, which were equally spaced with 2.5 cm (1 inch) concrete cover measured from the mold bottom surface (this became the top surface during exposure). Figure 28(c) shows six molds for the samples with three rebars. Figure 28 (b) shows three molds for samples with dimensions of 30.5 × 10.1 × 6.9 cm (12 × 4 × 2.7 in) containing one rebar. Eleven single-rebar specimens were prepared per mix with a concrete cover of 0.75 cm (0.3 in) with #3 rebars. Two ternary blends were prepared on August 19, 2016. T1 contains supplementary cementitious materials of 50% slag and 20% FA (cement replacement), whereas T2 contains supplementary cementitious materials of 20% FA and 8% silica fume. During the casting that took place on August 19, 2016, four three-rebar specimens and five (T1) or six (T2) single-rebar specimens were prepared per concrete mix.

For single-rebar samples, each rebar was drilled and tapped on one end and a stainless steel screw installed before casting the concrete. This step was done to provide an electrical contact. The three-rebar samples were drilled (but not all tapped) and fitted with stainless steel screws, nuts, and washers, but this step was done after the samples arrived at the FAU marine materials lab, for sample and environment preparations.

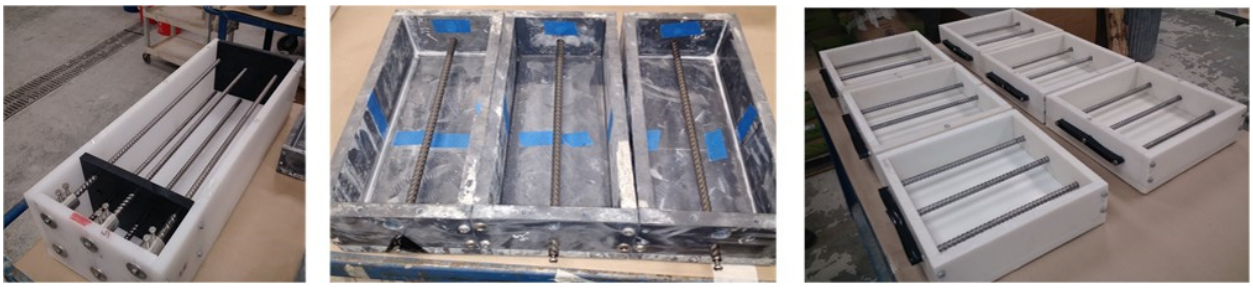

(a) (b) (c)

Figure 28. Molds with reinforcement prior to casting: (a) modified tombstone specimen (6 rebars); (b) single rebar-samples; (c) three-rebar samples

Stainless steel (or TiMMO) mesh was embedded on the top surface during casting on all specimens. This surface became the bottom surface during the experiment. The mesh was used as one of the electrodes while applying electromigration so as to accelerate the chloride transport. The length of the meshes varied from 2.5 cm to 15 cm. The reason for the different mesh length was to attempt to have different anode lengths for testing (once corrosion of the rebar had initiated). The specimens were prepared at the FDOT State Materials Office. On some mixes, the slump was slightly lower than targeted, possibly due to modest moisture loss of the aggregates, as the aggregates were stored over the weekend. After one day, the molds were

removed and transferred to the fog room for curing. Compression strength was performed at 60 days of age, Table 13 shows the results of this testing.

Table 13. Compressive strength

		Compressive Strength (psi)			
Mix ID	Cast ID	Specimen 1	Specimen 2	Specimen 3	Avg Comp
Slag M1	2016–04–003	9453	9691	9441	9528.3
Slag M2	2016–04–002	8866	9169	9069	9034.7
FA Mix1	2016–04–017	6385	5959	6212	6185.3
FA Mix2	2016–04–018	5381	5060	5031	5157.3
T1	2016–08–009	4240	4448	4335	4340
T2	2016–08–010	3720	3689	3522	3640

2.3 – Specimen setup preparation for electromigration

After casting, the samples were kept in a high humidity chamber located at FDOT–SMO for about a month. At the end of May 2016 for SL and FA mixes and towards mid–October for ternary blends, these samples were transported to FAU SeaTech campus for the next phase of the experiment. These samples were also kept in a high humidity chamber while at SeaTech while awaiting solution reservoir installation. The samples then were moved to the laboratory environment (65% RH and 21°C) to install the solution reservoir for ponding. The electrical connection was completed. The six rebar samples were stored outdoors once they reached FAU, the initial curing was in a fog room at FDOT–SMO.

A plastic reservoir was attached on the top surface (this was the mold surface at casting) using marine adhesive on the single and three rebar specimens. The reservoir installation took place at least 40 days after casting. A reservoir was also installed on the six rebar specimens. The reservoir was filled with NaCl solution (10% by weight). Different reservoir sizes were installed to investigate the effect of different corroding lengths. Each reservoir was fixed and centered along the rebar length on the top surface of the concrete samples. For the 3-rebar samples, it was ensured that the installed reservoir covered the 3 rebars. The ponding length varied from 2.5 cm to 17.5 cm in length.

Figure 29 (a) shows a picture of four of the single rebar samples and Figure 29 (b) shows three of the 3 rebar samples after placing the solution reservoirs, but prior to filling it with the solution. The samples were stored in high humidity 3 to 7 days prior to the next step. Figure 29 (c) shows three out of four modified tombstone specimens with six rebars, prior to installing the solution reservoir. The solution reservoir was installed on each of these four samples.

(a) (b) (c)

Figure 29. Specimens with reservoirs installed (a) single-rebar specimens; (b) three-rebar specimens; (c) Modified tombstone specimens at SeaTech before testing.

Table 14 shows the initial chloride amounts determined using FDOT method. Electrodes (stainless steel wire mesh or TiMMO mesh) with similar sizes that those embedded were placed on the top surface inside the solution reservoir.

Table 14. Initial chloride concentration

Sample description	Chloride	
	ppm	lb/yd^3
Slag Mix 2	34.08	0.13
Slag Mix 1	37.38	0.14
Fly Ash Mix 1	29.63	0.109
Fly Ash Mix 2	36	0.126
T1 Mix	24.5	0.09
T2 Mix	43.6	0.16

2.4 – Electromigration on newer samples

Most of the single rebar and three rebar specimens were placed in transparent plastic bins. Each specimen was partially submerged. The solution used was $Ca(OH)_2$, and approximately one cm of the concrete specimen was immersed. A white plastic mesh (acrylic perforated) was placed underneath each sample. This step was done to minimize leaching from the concrete.

A power supply was used to set a potential hold between the top and bottom mesh. An electric field then drives the chlorides in the solution above each rebar via electromigration into the concrete and towards the embedded rebar(s). The electrode placed in the NaCl solution was connected to the negative terminal of the power supply. The embedded mesh in each specimen was connected to the positive terminal of the power supply. In some cases, an external TiMMO mesh was placed underneath the sample. An acrylic mesh was also placed in the solution reservoir to avoid direct contact between the titanium wire mesh and the concrete surface. Figure 30 shows selected specimens while being subjected to electromigration.

Each sample was labeled as indicated in Table 15, Table 16, and Table 17. Each of these tables also includes the sample name/ID, the length of the reservoir, when the electromigration began and when it ended. Table 15 and 16 gives a description of single rebar samples made with slag and fly ash, respectively. Table 17 lists all the 3 rebar samples per their mix type and mesh dimensions (both 04/04/16–SL mix and 04/18/16–FA mix). Table 15, Table 16 and Table 17 also include a column which shows the calculated Ampere–hour applied. A similar labeling was used for specimens prepared with ternary blends. Table 18 and Table 19 show the labels for the samples prepared with ternary concrete compositions. Several electromigration periods applied within the start and the end date on any given specimen.

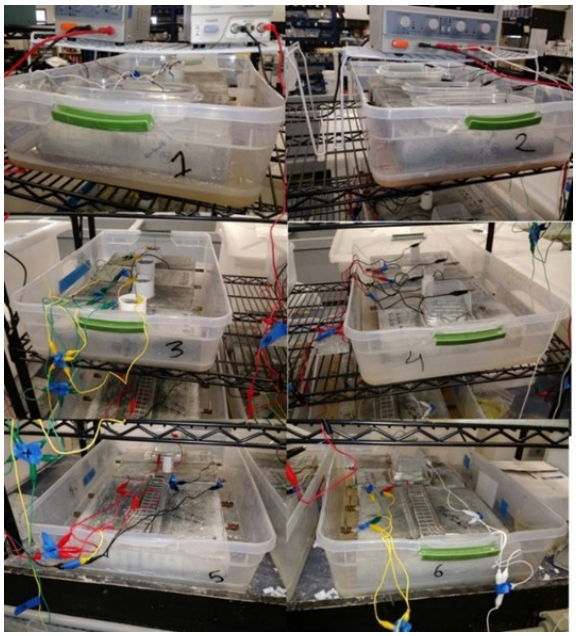

Figure 30. Selected samples during chloride migration process.

Table 15. Single-rebar samples made with slag replacement.

Cast date 4/4/2016		Migration Time Started	Migration Ending Date	Total Ampere Hour
Sample Number	Reservoir Length (cm)			
SL-1	17.5	07/29/16	9/5/2016	1.701
SL-2	17.5	07/29/16	1/4/2017	1.470
SL-3	17.5	07/26/16	8/15/2016	3.162
SL-4	2.5	07/26/16	1/10/2017	3.660
SL-5	2.5	07/26/16	1/4/2017	3.701
SL-6	5	07/26/16	1/4/2017	4.016
SL-7	5	07/26/16	1/4/2017	2.482
SL-8	5	07/26/16	1/4/2017	2.351
SL-9	10	07/26/16	1/4/2017	4.282
SL-10	10	07/26/16	1/4/2017	2.369
SL-11	10	07/26/16	12/9/2016	3.438

Table 16. Single-rebar samples made with fly ash replacement

4/18/2016		Migration Time Started	Migration Ending Date	Total Ampere Hour
Sample Number	Reservoir Length (cm)			
FA-1	5	07/26/16	1/4/2017	4.069
FA-2	5	07/26/16	1/4/2017	3.015
FA-3	5	07/26/16	8/15/2016	1.718
FA-4	7.5	07/26/16	8/15/2016	5.889
FA-5	7.5	07/26/16	8/15/2016	3.524
FA-6	7.5	07/26/16	9/5/2016	3.729
FA-7	17.5	07/26/16	11/28/2016	8.145
FA-8	17.5	07/26/16	1/4/2017	6.942
FA-9	17.5	07/26/16	12/9/2016	6.676
FA-10	2.5	07/26/16	12/9/2016	2.742
FA-11	2.5	07/26/16	12/9/2016	3.531

Table 17. Three-rebar samples: reservoir length and ampere-hour applied

Sample Number	Batch Date	Mesh Length	Migration Status	Total Ampere Hour
1X	4/4/2016	5	Stopped	2.151
2X	4/4/2016	2.5	Stopped	3.053
3X	4/4/2016	10	Stopped	0.781
4X	4/4/2016	15	Stopped	3.283
5X	4/18/2016	2.5	Stopped	1.493
6X	4/4/2016	10	Stopped	0.297
7X	4/18/2016	5	Stopped	3.262
8X	4/4/2016	10	Stopped	2.050
9X	4/4/2016	3	Stopped	5.095
10X	4/18/2016	2.5	Stopped	3.262
11X	4/18/2016	2.5	Stopped	0.758
12X	4/18/2016	5	Stopped	0.758
13X	4/18/2016	10	Stopped	2.269
14X	4/18/2016	15	Stopped	2.304
15X	4/4/2016	10	Stopped	1.760
16X	4/4/2016	5	Stopped	0.551
17X	4/4/2016	5	Stopped	0.569
18X	4/18/2016	15	Stopped	1.484
19X	4/4/2016	2.5	Stopped	0.171
20X	4/18/2016	10	Stopped	3.320
21X	4/18/2016	10	Stopped	2.410
22X	4/4/2016	15	Stopped	1.581
23X	4/18/2016	5	Stopped	1.407
24X	4/18/2016	15	Stopped	1.598

Table 18. Single-rebar samples made with T1 or T2 mixes

Sample name	Ponding Length in (cm)	Migration Started	Migration Ended	Ampere hour
T1(6)	15	11/18/2016	12/9/2016	0.56
T1(7)	5	11/18/2016	1/4/2017	0.665
T1(8)	15	11/18/2016	12/9/2016	0.565
T1(9)	10	12/16/2016	1/4/2017	0.612
T1(10)	5	11/18/2016	1/4/2017	0.665
T2(1)	5	11/18/2016	12/10/2016	0.578
T2(2)	15	11/18/2016	1/4/2017	0.654
T2(3)	5	11/18/2016	1/4/2017	0.654
T2(4)	10	12/16/2016	1/4/2017	0.536
T2(5)	5	11/18/2016	1/4/2017	0.654
T2(11)	15	11/18/2016	12/9/2016	0.771

Table 19. Three-rebar samples made with T1 or T2 mixes.

Sample name	Ponding Length (cm)	Migration Started	Migration Stopped	Ampere Hour
T1(25X)	5	10/31/2016	12/9/2016	0.40
T1(26X)	2.5	10/31/2016	11/11/2016	0.81
T1(27X)	10	10/31/2016	11/11/2016	0.81
T1(28X)	5	10/31/2016	11/11/2016	0.81
T2(29X)	10	10/31/2016	12/9/2016	0.51
T2(30X)	2.5	10/31/2016	12/9/2016	0.30
T2(31X)	5	11/1/2016	12/9/2016	0.46
T2(32X)	5	10/31/2016	11/11/2016	0.81

The application of electromigration started on 07/29/16 to some of the samples prepared in April/2016. Due to the number of samples and the limited number of power supplies, the samples subjected to electromigration alternated. For this part of the experiment forty–six concrete blocks were subjected to the accelerated chloride transport, for SL and FA specimens. This was followed by applying electromigration to the T1 samples and the T2 samples (19 additional specimens).

Initially, all the single SL and FA rebar specimens were subjected to electromigration along with specimens 1X and 2X (the latter two are three rebar samples). Electromigration took place on the other SL and FA three-rebar samples at a later date. A given potential was applied for several days at one time, the delta potential across a 100 ohms' resistor was used to assess the amount of current applied. Periodically the system was turned off and the rebar potential was monitored with respect to a saturated calomel reference electrode throughout the disconnected period at regular intervals. Although the rebars were not connected, an ionic current produced by the applied electric field polarizes them. After monitoring the rebar potential (typically up to 2

hours) for some time with the system disconnected, the applied potential was resumed if the last rebar potential measured suggested that corrosion had not initiated. The electromigration process was continued until the specimen showed an off-rebar potential that can be considered as the initiation of corrosion in that embedded rebar (a value of –0.150 Vsce or more negative was assumed to be indicative of corrosion initiation).

As indicated above the samples were energized at alternate times. Initially, the applied potential was 9 V. It was reduced to 3 V after 7 days when a potential greater than +2V was found when measuring rebar potential vs. a saturated calomel electrode while the electric field was still on. A test similar to a depolarization test was performed periodically, i.e., the rebar potential readings were taken with the power supply on, a few seconds after turning the power supply off and rebar off potentials after one hour and two–hour intervals. It was then determined either to keep the electromigration off or to restore the applied potential (i.e., electromigration back on). After selected disconnections, the system remained turned off for two days or longer and then LPR and EIS tests performed. In some instances the system was left off for a longer period of time, the rebar potential measured and if it had shifted to values more positive that –0.15 Vsce, then electromigration was restarted.

Samples prepared with ternary blends were also subjected to electromigration. Table 18 and Table 19 indicate the assigned labels and when electromigration started.

2.5 – Electromigration on modified tombstone specimens

During the April 2016 concrete casting, two modified tombstone specimens were cast on each day (four total modified–tombstone specimens). Each specimen has six #4 rebars. Two specimens contain SL mix and two were prepared with FA mix. The samples are 24 in × 10 in × 7 in. The concrete cover along the wide side (10 inches) on the rebars is 1 inch. The samples were placed outdoors while awaiting set–up preparation for electromigration. A solution reservoir was installed on each specimen. For these specimens, a similar arrangement than that just described for electromigration approach (for single and three rebar specimens) was implemented during the summer/2016. The major difference is that rather than using a power supply, 9V batteries were used to provide the applied potential. The batteries were replaced periodically (typically once a week) once the battery potential was less than 2 V. A mesh was placed in the solution reservoir (connected to the negative terminal) and the embedded electrode on the bottom side of each specimen was connected to the positive terminal. The batteries were placed inside a pelican box that minimized moisture ingress.

Figure 31. Electromigration being applied to a specimen with six rebars.

A solution reservoir was installed on one of the wide sides of the selected six rebar specimens, the reservoir was filled with 10% NaCl. This specimen face became the top side, but it was the mold bottom during casting. Figure 31 shows one of these specimens. A TiMMO mesh was placed on the reservoir and a stainless steel mesh (or TiMMO mesh) was placed below the specimen (the mesh had similar dimensions than the mesh in the solution reservoir). The electromigration began mid–Summer 2016 (8/6/2016) and was suspended during Summer 2017 (7/25/2017).

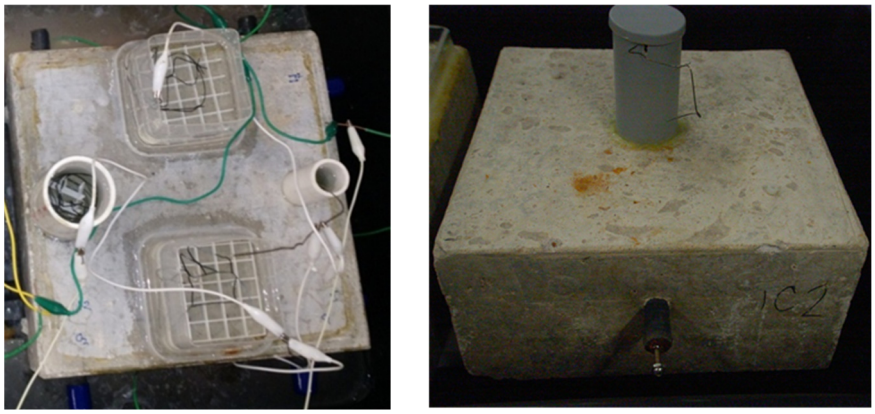

Figure 32. Pictures showing the two different specimen types.

2.6 – Electromigration on older specimens

2.6.1 – Galvanostatic approach

This section describes the accelerated chloride transport on the older single rebar specimens. Specimens 1C (1C1 and 1C2), and 1F (1F1 and 1F2) were cured in a fog room for 800 and 700 days, respectively, and then exposed to the laboratory environment for 1 year. 1B1, 2D1, 1G1

and 1G2 specimens were cured in the fog room for 60 days, then exposed to 75% RH for 700 days, and then to lab conditions for one year. Specimens 1B1, 1G1 and 1G2 were exposed to seawater ponding for 300 (1B1) days or 100 days while outdoors and part of the time exposed indoors at 75% RH exposure, then exposed to laboratory conditions. After the above–described exposure periods (November 2010), it was then decided to install a smaller solution reservoir (5 cm diameter cylinder) filled with 15% NaCl. See the picture on the right in Figure 32. The specimens were then transferred to a high humidity environment. The rebar on each specimen was anodically polarized with a galvanostat (max current applied 125 μA) to accelerate the chloride transport, and a titanium mixed metal oxide mesh was used as the counter electrode. The polarization took place for 400 days. The applied electric field might have caused some of the chlorides to reach not just the top side of the rebar but also below. Since the whole rebar was used as the working electrode the chloride transport likely extended beyond the solution reservoir.

2.6.2 – Electromigration approach

Specimens 1D1, 1D2, 1H1 and 1H2 were cured in the fog room for 60 days, then exposed to 75% RH for 700 days, and then to lab conditions for approximately four years. Specimens 1DA, 1DB, 1H1 and 1H2 were exposed to seawater ponding for 300 (1D) or 100 (1H) days while outdoors and the latter exposure time indoors at 75% RH exposure. Specimens 3BX and 3BY were cured in the fog room for 360 days, and then exposed to laboratory conditions for 3 years. Specimens 2B1, 2B2, 3B3 and 3B4 were cured in the fog room for 60 days, then for 80 days in the laboratory humidity, followed by 220 days under 75% RH. Specimens 2B1, 2B2, 3B3 and 3B4 were then exposed to laboratory conditions for 2 years.

During spring 2016, solution reservoirs were installed on all specimens described in the above paragraph. Figure 33 shows in the picture on the left the location and size of the reservoirs installed on specimens with four rebars: two 10 cm square reservoirs, one 5 cm diameter and one 2.5 cm diameter reservoir on each sample with four rebars. A solution with 10% NaCl (by weight) was poured in the reservoir. Chloride transport was then accelerated via an electromigration cell approach. A steel mesh of similar dimensions to each of the reservoir footprints was placed below the corresponding rebar of each concrete specimen. The specimens were placed in trays and raised from the bottom using plastic supports. Each tray was filled with calcium hydroxide solution. The $Ca(OH)_2$ solution reached the bottom of each specimen (~1 cm of the concrete specimen was immersed), so as to provide good contact and to minimize leaching from the concrete. A 100–ohm resistor was placed in series to each sample to measure the delta potential with the power supply on (so as to assess the current being applied). Initially, 15 V potential difference between the top and bottom mesh was applied using a power supply. The applied potential was reduced to 10 V after 5 days, after noticing a quite noble potential of the rebar vs. a saturated calomel reference electrode while the applied potential was 15 V. Table 20 shows the dates in which electromigration started and the applied potential and duration. Periodically, rebar potential measurements vs. a saturated calomel electrode were taken with the system on, a few seconds after shut–off the applied potential, and after one- and two-hour intervals (similar to a depolarization test). After inspecting the two-hours off rebar potential, the applied potential was resumed if the rebar potential was more positive than –0.15 Vsce.

The electromigration process was applied first on 1H1, 1H2, 3B3, 3B4, 3BX, 3BY and was continued for about a month. The power supply was turned off periodically, sometimes the samples were disconnected for two days and then LPR and EIS measurements were performed. Specimens 1DA, 1DB, 2B1, and 2B2 were subjected to electromigration subsequently. For label notation of the four rebar samples, the square ponds were denoted as SQ1 and SQ2 (10 cm side) and the 2.5 cm cylindrical pond was denoted as O1 (2.5 cm diameter) and the 5 cm diameter cylindrical as O2. Samples 3BX and 3B4 have 10 cm square solution reservoir. Samples 2B1, 2B2, 3BY, and 3B3 have 5 cm diameter solution reservoirs.

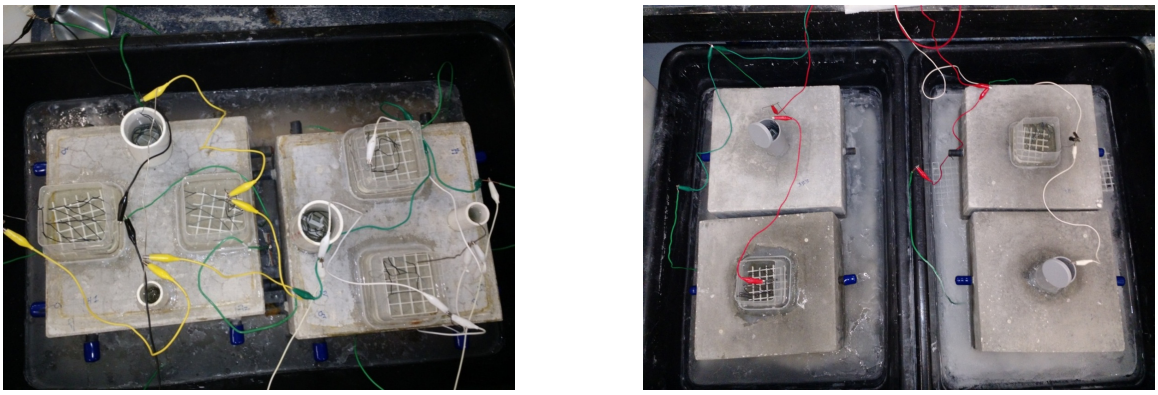

(a) (b)

Figure 33. Samples during electromigration process: (a) 1H1 and 1H2; (b) 3B3, 3B4, 3BX, 3BY

After the electromigration was suspended, the rebar potential, solution resistance (Rs), and the polarization resistance of each rebar were periodically monitored.

Table 20. Samples exposed to electromigration

Sample name	Migration Start Day	Migration End Day	Total Migration Time in (Days)	Approximated Voltage–hour	Approximated Ampere–hour
1H1O1	2/29/2016	3/28/2016	26 (15V for 12 days, 10V for 14 days)	7680	9.062
1H1O2	2/29/2016	3/28/2016	26 (15V for 12 days, 10V for 14 days)	7680	9.062
1H1SQ1	2/29/2016	3/28/2016	26 (15V for 12 days, 10V for 14 days)	7680	9.062
1H1SQ2	2/29/2016	3/28/2016	26 (15V for 12 days, 10V for 14 days)	7680	9.062
1H2 O1	2/29/2016	3/28/2016	26 (15V for 12 days, 10V 14 for days)	7680	8.350
1H2 O2	2/29/2016	3/28/2016	26 (15V for 12 days, 10V for 14 days)	7680	8.350
1H2 SQ1	2/29/2016	3/28/2016	26 (15V for 12 days, 10V for 14 days)	7680	9.321
1H2 SQ2	2/29/2016	3/28/2016	26 (15V for 12 days, 10V for 14 days)	7680	8.350
3B3	2/29/2016	Continues (up to 11/28/16)	75 (15V for 12 days, 10V for 14 days, 3V for 49 days)	11208	8.153
3BX	2/29/2016	3/28/2016	26 (15V for 12 days, 10V for 14 days)	7680	7.091
3B4	2/29/2016	Continues (up to 11/28/16)	75 (15V for 12 days, 10V for 14 days, 3v for 49 days)	11208	7.664
3BY	2/29/2016	3/28/2016	26 (15V for 12 days, 10V for 14 days)	7680	7.664
1DAO1	4/13/2016	4/15/2016	2 (10V applied) days	480	1.430
1DAO2	4/13/2016	5/13/2016	9 (10V applied) days	2160	6.462
1DASQ1	4/13/2016	4/15/2016	2 (10V applied) days	480	1.430
1DASQ2	4/13/2016	4/15/2016	2 (10V applied) days	480	1.430
1DBO1	4/13/2016	Continues (up to 12/2/16)	37 (10V applied 17 days, 3V 20 days)	5808	8.067
1DBO2	4/13/2016	Continues (up to 12/2/16)	37 (10V applied 17 days, 3V 20 days)	5520	8.067
1DBSQ1	4/13/2016	11/11/16	37 (10V applied 17 days, 3V 20 days)	5808	7.328
1DBSQ2	4/13/2016	Continues (up to 11/28/16)	37 (10V applied 17 days, 3V 20 days)	5808	8.067
2B1	7/14/16	08/30/16	32(15V for 14 days,10V for 3 days,3V for 15 days)	6840	1.869
2B2	7/14/16	08/30/16	32(15V for 14 days,10V for 3 days,3V for 15 days)	6840	1.715

2.6.3 – Electromigration on selected outdoor old specimens

Selected specimens that have been exposed outdoors were selected for accelerated chloride transport. For these specimens, a similar arrangement than that just described for the electromigration approach was implemented. The major difference is that rather than using power supplies, 9V batteries were used to provide the applied potential holds. The batteries were replaced periodically (typically once a week). The electromigration application started early-mid October 2016 and ended on July 25, 2017. Two different types of specimens were exposed outdoors, two rebar specimens (see geometry in Figure 34.a) and 5 rebar specimens (see geometry in Figure 34.b).

The five rebar specimens selected for accelerated chloride migration were originally prepared in 1994 with various compositions. Six samples were selected; Table 21 shows the sample identification and the concrete main admixture (see appendix B for concrete mix detail). Silica fume slurry was used and part of the mass counted toward the water.

Table 21. Five-rebar specimens selected for electromigration

Specimen ID	Admixture
AO5	OPC only
FA1–7	20% FA
FA2–3	35% FA
FA3–3	50% FA
SF1–2	6% SF
SF3–1	27% SF

FA – Fly Ash, SF – Silica Fume (Note silica fume slurry was used)

(a) (b)

Figure 34. Electromigration applied to a specimen with (a) two rebars and (b) five rebars

A solution reservoir was installed on one of the wide sides of the selected two rebar specimens, the reservoir was filled with 10% NaCl. This specimen surface became the top side. Figure 34 (a) shows one of these specimens. A TiMMO mesh was placed on the reservoir and a stainless steel mesh (or TiMMO mesh) was placed below the specimen (similar dimensions that the solution reservoir). The electromigration started to be applied mid–October 2016 and was ended on

7/25/2017. Figure 34 (b) shows the set–up implemented for the five rebar specimens. A TiMMO mesh was placed on the solution reservoir, the solution, in this case, is seawater (periodic refilling is done due to evaporation). A second mesh was placed below each specimen and extends the width of each specimen.

2.7 Applied current to selected samples to accelerate corrosion

Some of the samples (after electromigration had been suspended for more than 100 days on the single rebar and 3 rebar specimens prepared in 2016) were selected for a modest anodic polarization via an applied current (between embedded rebar and an electrode in the reservoir). This anodic polarization tends to accelerate any ongoing corrosion. Starting on 2/28/17, some of the single rebar samples were selected to undergo accelerated corrosion using a galvanostatic pulse (i.e., applying a small constant anodic current up to a maximum of 125 μA).

Samples were selected by comparing the rebar potential and R_c values for those specimens with the same reservoir length. SL and FA samples had more than one sample for a given concrete reservoir size. A comparison of rebar potential and R_c values were used to select the samples for which it was to be applied. The samples were selected based on a criterion (in most instances the specimen with the most negative rebar open circuit potential and smallest R_c values for a given reservoir size sample of the same concrete mixture was selected; alternatively, the sample with the most negative rebar potential was selected if the difference in R_c was small). Selected samples were transferred to a high humidity chamber before connection. In parallel, a calculation was done to determine the magnitude of the current to be applied according to reservoir size (rebar surface below the reservoir). The initially applied current was calculated by assuming that half of the rebar area under the reservoir was corroding. Plausible corroding rebar length is affected by the rebar area directly under the chloride reservoir installed on each sample (See Table 22). It is speculated that the rebar under the smallest size reservoir should have smallest corroding area (the assumption is that the whole area or a similar fraction of the area is corroding proportional to the reservoir size). It was considered that only the top side of the rebar area is corroding. The reason behind this assumption is that it would take additional time to develop corrosion on the bottom side of the rebar (the side that is facing the opposite direction from the chloride reservoir). However, it is also possible that not the whole top side area of the rebar under the reservoir is corroding.

Another parameter investigated was the rebar size. The recently prepared samples and the selected 2008/2009 samples had different rebar diameters. There were #3, #4 and #5 rebar sizes among the selected samples. The amount of current that was initially applied considered both rebar size and section of the rebar length under the solution reservoir. The estimated applied current for each sample according to rebar size (rebar #) and reservoir size is shown in Table 23.

Before the samples were connected, the open circuit potential (rebar potential) and R_c were recorded for comparison later. While applying a constant current, the negative terminal was connected to the TiMMO mesh in the solution reservoir and the positive terminal to the working electrode (i.e., the rebar). This was done to polarize the rebars anodically.

For the new samples, galvanostats were used (by in-house galvanostats powered by 9V batteries). A 15 kΩ resistor was used for monitoring the applied current by measuring the voltage across the resistor for all of the samples. Three versions of the device exist with ranges of 0–2.5 µA, 2.6–5 µA, and 6–125 µA. Initially, all the selected samples were connected to devices with the largest current range.

For six of the 2008/2009 samples (1H1O1, 1H1SQ1, 1H2O2, 3BX, 3B4, 2B2) a different galvanostat was used. The galvanostat had a 100Ω resistor in series, connected to it for measuring the delta voltage across the resistor. Among the three available current ranges (0–1.2 mA, 0–12 mA, and 0–120 mA) the lowest range was used.

Two voltmeters were used: one was used to measure the rebar on potential in the sample and the other voltmeter was used to measure the delta voltage across the resistor for that selected sample. This process was performed periodically during the accelerated corrosion process. Both types of galvanostats have a variable resistor that allows adjusting the applied current. The applied current was sometimes adjusted downwards. In some cases when too much polarization was observed, a lower range galvanostat was used.

Table 22. Rebar area size in cm^2

Rebar Size	Radius in cm	2.5 cm long	5 cm long	10 cm long	17.5 cm
Number 5 Rebar	0.79	6.23	12.47	24.93	43.64
Number 4 Rebar	0.63	4.99	9.97	19.95	34.91
Number 3 rebar	0.47	3.74	7.48	14.96	26.19

Table 23. Target current applied according to rebar size and reservoir length

	Rebar diameter	2.5 cm	5 cm	10 cm	17.5 cm
Assuming 5 µA/cm^2	# 5 rebar	31.17	62.34	124.68	218.12
	# 4 rebar	24.94	49.87	99.75	174.55
	# 3 rebar	18.7	37.4	74.81	130.95

Although current was applied according to the assumed corroding area, however, some rebars appear to have a smaller corroding area than anticipated. Thus, the on-rebar potential went to quite positive values after a few days of anodic polarization. The applied current was adjusted downward for samples that experienced this phenomenon. In some instances, this was implemented by changing to a galvanostat with a smaller current range (e.g., from a galvanostat with 2.6 to 5 µA to a galvanostat with 0 to 2.5 µA range). In general, the applied current effect on the on-rebar potential was targeted to be at most 100–200 mV more positive than the open circuit potential of the rebar before applying the anodic polarization. As indicated above this was not always the case. If the on-rebar potential went to a very positive value, the applied current was changed using the adjustable switch (variable resistor) to keep the applied voltage across the resistor and on-rebar potential within the target value.

As a galvanostat with a smaller range was used on single rebar samples needing a lower applied current, a larger range galvanostat became available which was used to connect it to one of the 3 rebar samples. Here, for each selected 3-rebar sample, only one rebar (the rebar that had the lowest OCP and smaller R_c value) was selected for the experiment. The current was applied only to one of the three rebars. The reservoir size was also taken into account (SL or FA samples). A similar connection procedure was followed for the selected rebar within a three rebar–sample as that described for single rebar samples. The other two rebars were not connected and as described above during the electromigration process section these not–connected rebars experienced ionic polarization due to the applied current as the solution reservoir covers the 3 rebars (i.e., it was possible that part of the ionic current reached the other two rebars and polarized them).

The rebar condition evolution with respect to rebar potential, R_s and R_c, were periodically measured. Prior to measuring LPR, EIS and Galvanostatic pulse, the samples were disconnected for at least two days; the selected specimens were then connected again. In a few instances, the solution was removed for a few days to improve oxygen availability in the concrete at the rebar depth and promote corrosion. Solution removal also took place on the rest of the indoor samples. The solution was then added to the reservoir and the accelerated corrosion procedure was then restarted. In some instances, the samples remained disconnected for several weeks with the solution in the reservoir. The anodic polarization was suspended in January 2018 but the electrochemical monitoring continued.

2.8 Electrochemical measurements

The rebar potential was measured periodically during the corrosion propagation stage using a saturated calomel electrode. This same type of electrode was used to measure the rebar potential during the electromigration period and also to measure the rebar potential of the samples selected for modest anodic polarization. The values are shown in the results section on plots that show Rs and R_c values were measured at least two days after turning off the system (i.e., disconnected).

Three types of readings were performed. Initially, only EIS and LPR tests were conducted. The EIS was performed from 10 kHz to 1 Hz, and the magnitude of the impedance chosen was 54 Hz; this value was assumed to represent the solution resistance (Rs). The linear polarization test was from 10 mV below the open circuit potential to 1 mV above open circuit potential. However, after approximately 6 months, the linear polarization test was performed from the open circuit potential to 8 mV below it. The scan rate chosen was either 0.1 mV/s or 0.05 mV/s.

The rebar potential, EIS and LPR tests were performed within the period of time that the electromigration was applied (but after the system was off for at least two days) and after suspending electromigration. This latter period of time is called here the corrosion propagation period and assumes that corrosion was initiated during the electromigration or soon after it was suspended.

Galvanostatic pulse (GP) tests were performed on most lab specimens starting on April 2017. This test method provided an alternative way of measuring R_s and R_c values. The measured values were later labeled R_sGp and R_cGP. The GP test was performed on the same day when LPR and EIS tests were done on any given sample. The galvanostatic pulse applied was 10

microamperes. The first set of measurements was made for 140 seconds. The duration of the GP was increased to 300 seconds during the second set, as it was observed that at 140 seconds the slope of the curve is still changing (according to theory constant slope is needed for determining R_c). Subsequent tests were performed for 200 seconds as a compromise. The GP test measures the open circuit potential for a few seconds first. Then the pulse is applied and the rebar potential as a function of time was measured. The R_sGP was calculated by using the rebar potential prior to the GP and using the first potential reading with the current pulse (i.e., the initial on–potential). The R_cGP was calculated by calculating the difference between the initial on–potential and the rebar potential value measured at 200 seconds. The I_{corr}GP was calculated using the R_c values and a B constant of 26.1 mV.

2.8.1 – Monitoring of corrosion propagation on indoor lab specimens

After the electromigration was suspended, the rebar potential, solution resistance and the polarization resistance of each rebar were periodically monitored every month. In the results section R_c, R_s, and E_{corr} vs. time will be shown for selected specimens (for both before and after suspending electromigration).

The corrosion propagation process is monitored by:

1) Measuring the open circuit potentials of the reinforcement against a saturated calomel reference electrode using a high impedance voltmeter, initially twice a month, and then at least once a month. Later it was measured when the electrochemical tests were performed.
2) Linear polarization (LPR) measurements were carried out at least once a month. From LPR test the Rpapp and E_{corr} measurements were collected.
3) R_s (solution resistance) values were measured via EIS (Electrochemical Impedance Spectroscopy), prior to the LPR test. The solution resistance was taken as the magnitude of the impedance measured at 54.51 Hz.
4) R_c (corrected polarization resistance) was calculated by subtracting Rs from the calculated Rpapp.
5) R_s and R_c from Galvanostatic pulse measurements were measured starting on April 2017.

In the results chapter, R_cLPR refers to the corrected polarization resistance obtained with LPR/EIS, and R_cGP refers to the polarization resistance measured using the galvanostatic pulse test. Similar labels were developed for R_sLPR and R_sGP.

2.8.2 – Outdoor electrochemical monitoring

The rebar potential of the >24–year (five rebars) samples was periodically monitored vs. a saturated calomel electrode. These measurements were suspended, and instead, the readings from a Gecor8 used starting February of 2017. A Gecor8 was used to monitor the samples starting in February of 2017. Additional measurements were performed, for a total of 8 times including Feb 2017. The measurements were performed 2/17, 3/17, 6/17, 8/17, 10/17, 1/18, 3/18 and 5/18. The devices measured the corrosion rates with a confinement arrangement and reports both isolated and non–isolated corrosion current density values. The device also reports the rebar potential vs. a copper sulfate electrode, the solution resistance, and the resistivity with the probe and rebar arrangement. The user enters the concrete cover, and the rebar size. After reviewing the first two sets of values and performing a visual inspection, selected samples were terminated. In the case

that only one rebar was active, that section of the specimen was cut off and a new reservoir was installed in the remaining section for additional exposure.

The Gecor8 was also used in a few instances to measure the corrosion rate of selected MD samples and single rebar samples with a 5 cm concrete cover. The solution reservoir was large enough to accommodate the probe on MD samples. The solution reservoir was momentarily removed from single rebar specimens with 5 cm cover and after the measurements reinstalled. Three of these samples were terminated, and prior to removing the rebar, one more set of readings was performed with the Gecor8. These measurements were not performed on terminated MD specimens.

The corrosion rate, rebar potential, and concrete resistivity were measured using a commercial corrosion meter Gecor 8[†] (NDT James Instruments Inc., U.S.). Since all concrete specimens were exposed to seawater, the corrosion rate and resistivity were measured by using sensor B (submerged condition) that was placed on the top of concrete and parallel to the steel bars (the solution level that covered a portion of the probe).

2.9 – Chloride measurement and forensic study

Selected specimens from both indoor laboratory specimens and outdoor specimens were terminated.

Outdoor samples: In April 2017 (after 23 years of exposure testing), the corrosion test was stopped on five concrete blocks. Rebars from two additional samples were terminated during November 2017. A total of 15 top–row rebars were removed.

The chloride penetration through the concrete was measured. First, a 3.8 cm nominal diameter concrete core was obtained between rebars on selected specimens. The concrete core was sliced using a thin lapidary diamond blade. Ten slices were obtained from the exposed surface. Layer 1 was 2.0 mm, layers 2 and 3: 3.0 mm, layers 4 to 8: 4.0 mm, and the last two layers 4.5 mm each. The slices were ground into powder. The chloride concentration of the concrete powders was determined using the Florida Department of Transportation (FDOT) titration method(FM5-516 2009)

In addition to the chloride concentration at different depths, the chloride concentration on the top of the steel bar was also measured. The concrete specimen was opened to expose the steel rebar with a diamond saw (prior to these cuts, two transversal cuts along the rebar length were performed). The concrete powder was collected by milling the grooves of the concrete above the rebar at locations without corrosion products (i.e., the concrete rebar trace). Thus, the chloride measured will be the chloride concentration near the steel bar surface. The chloride concentration determination was also performed using FDOT method(FM5-516 2009) or a modified approach that used a smaller amount of concrete powder when necessary. The FDOT method measures the total chlorides. The steel bars of the terminated specimens were removed and the rust product removed chemical cleaning and then by sandblasting. The cross-section loss (using a caliper) and the length of the corrosion sites were determined.

[†] Trade `Name.

Samples 1DA (four rebar specimen), 1F1, 1B1 and 2D2 with 5 cm concrete cover were selected for forensic analysis. Samples SL1, SL2, FA9, FA10, T1–X, and T2–X were terminated. Rebars A and B from specimens 16X were removed and inspected. Samples MD–NP35, MD1–NP37, MD1–NP38, MD1–B (10 cm long reservoir), MD1–H (3 cm reservoir) were terminated.

2.9.1 – Visual inspection upon terminating specimens

A chisel was used to separate the top–cover concrete from the bottom section of the specimen. Upon exposing the corroding rebar, pictures were taken that documented the extent of the corrosion products. Pictures were taken also of the concrete above the rebar trace. The rebar was separated using a mallet and the bottom surface of the rebar was then photographed.

In cases in which the mortar or concrete showed cracks, additional pictures were taken to document the crack pattern.

2.9.2 – Reinforcement cleaning

Most rebars were wire brushed first to remove any excess corrosion products. Then the rebars were cleaned as per ASTM G 1–03(ASTM G01-03 2017). This was achieved by repeatedly conducting a procedure of immersion in a cleaning solution (93.5 wt% HCl + 0.7 wt% Sb_2O_3 + 4.7 wt% $SnCl_2$), rinsed with water, mass measured and then repeated until a constant mass was reached. In some cases, the corrosion products persisted and in that case, the rebar was sandblasted.

2.9.3 – Visual inspection after cleaning reinforcement

Pictures were taken after cleaning the rebars. In some cases, a macro lens was used to get a better view of the corroded surface.

Chapter 3 – Results: Laboratory Samples

3.1 – Older samples

3.1.1 – Concrete samples with single rebar

Eight of the single rebar older samples were subjected to electromigration (for approx. 400 days) by using the rebar as one of the electrodes. The rebar evolution was monitored via LPR and EIS for over 2300 days (i.e., current monitoring time in days including electromigration period is ~2700 days). Figure 35 and Figure 36 shows how the rebar potential, solution resistance (R_s) and corrected polarization resistance (R_c, see experimental chapter) evolved with time for rebars embedded in samples 1F1 and 1B1, respectively. In the plots in Figure 35 and Figure 36, R_s and R_c values are shown on a linear scale. The Rs values over time varied as observed in Figure 35 and Figure 36. Rs values measured on 1F1 specimen remained close to 0.9 kΩ over the reported period, whereas the Rs values measured on 1B1 specimen oscillated and ranged within values close to 4 kΩ and as little as 0.5 kΩ. Appendix C contains the plots for the other six samples. Figure 37 and Figure 38 shows how the R_c changed as a function of time, but now these plots show the R_c values in log10 scale. Figure 37 shows the R_c values for the rebars in 1B1, 2D2, 1C1 and 1C2 samples. Figure 38 shows the R_c values for the rebars in 1F1, 1F2, 1G1 and 1G2 specimens. The R_c value on any given rebar did not remain constant over time but oscillated. The changes in R_c values can in part be explained by changes in the moisture content on the concrete. Three samples were selected for forensic analysis from these 8 samples and it is described in the forensic analysis chapter. These were chosen from those with the lower R_c values, particularly in more recent measurements.

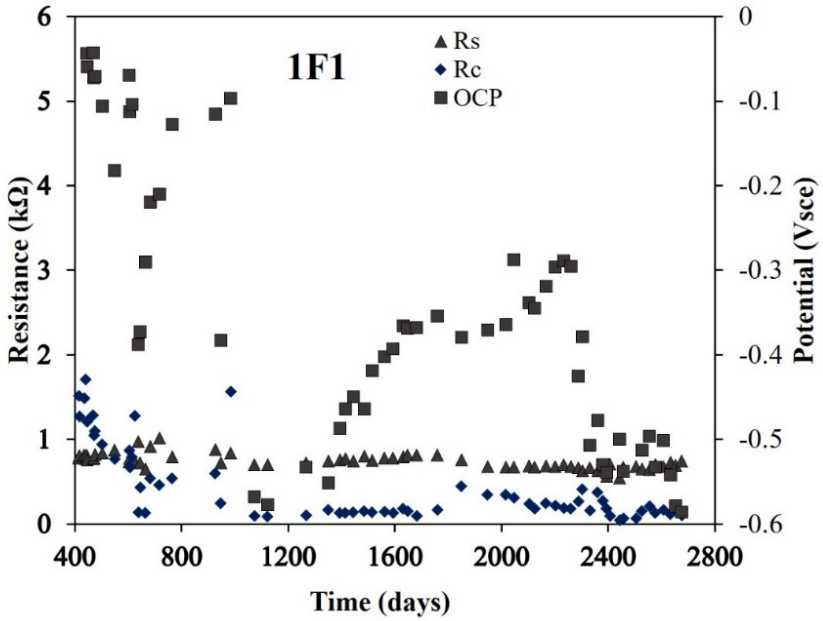

Figure 35. Rebar potentials, R_s,, and R_c vs. time for rebar in 1F1 specimen.

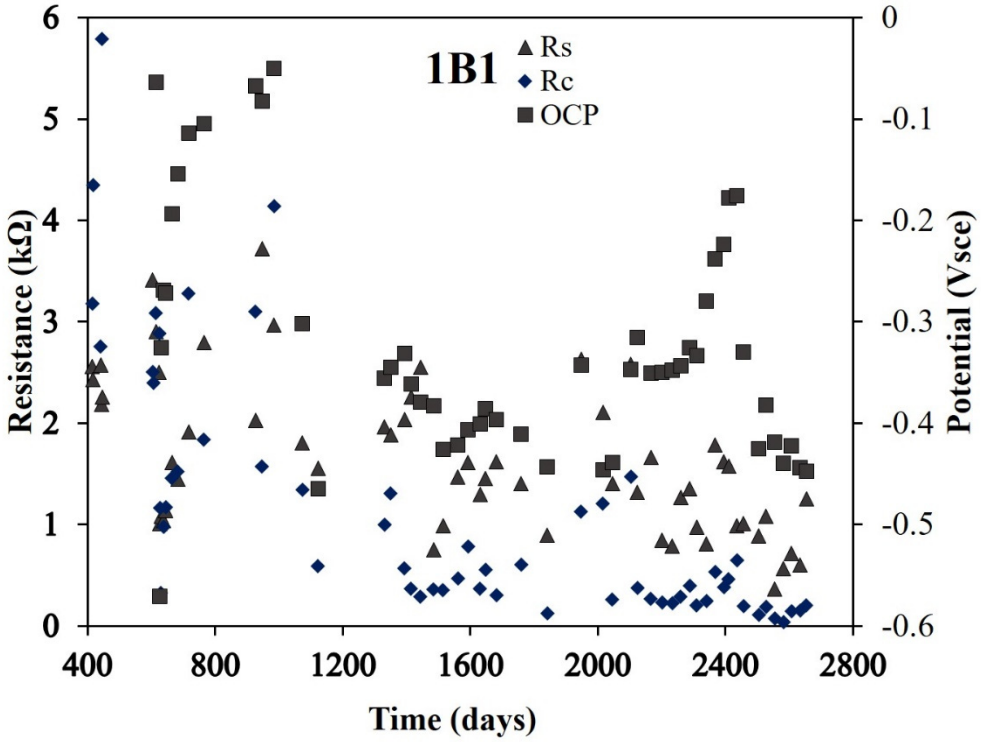

Figure 36. Rebar potentials, R_s, and R_c vs. time for rebar in 1B1 specimen.

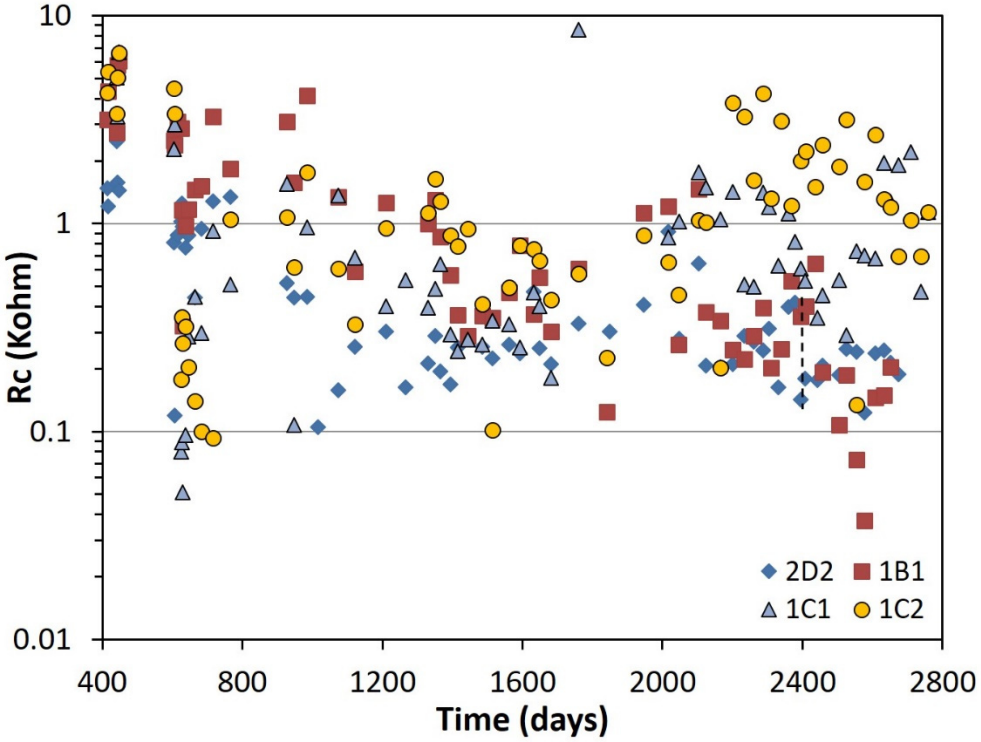

Figure 37. R_c vs. time measured on rebars of specimens with OPC only.

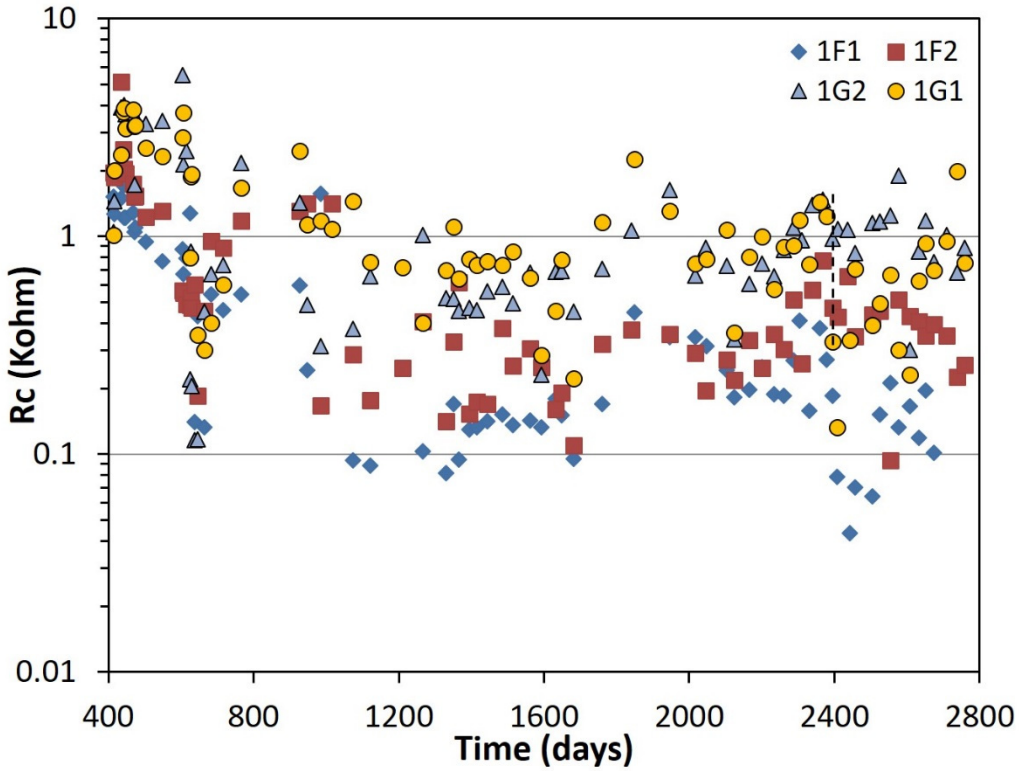

Figure 38. R_c vs. time measured on rebars on specimens with OPC+FA

Specimens 1F1, 1B1 and 2D2 were terminated; these specimens exhibited the smaller R_c values as shown in Figure 37 and Figure 38. For the remaining specimens, the R_c values shown suggest that the rebar embedded in specimen 1F2 was corroding at a faster rate than the rebars in specimens 1G1 and 1G2. The rebar in specimen 1C1 was corroding at a faster rate than the rebar in specimen 1C2, by comparing R_c values. Table 24 shows the average I_{corr} for these specimens. The average I_{corr} was calculated from R_cLPR and R_cGP values measured over the last 400 days. The average I_{corr} values in the table indicate that the three terminated samples had an average I_{corr} greater than 100 μA and that the average Icorr from GP and LPR were comparable. The average I_{corr} of the last three readings from both GP and LPR methods for the not terminated samples was sometimes comparable. For example, let's observe the 1C1 rebar average I_{corr} values: a more notable difference is observed on some of the other rebars. In general, the I_{corr} values calculated from R_cLPR are greater than the I_{corr} values obtained from R_cGP values. The exception in Table 24 is for the I_{corr} corresponding to rebar 1G2 (when comparing I_{corr} average over the last 3 readings). For some samples, a large difference was observed when comparing the average I_{corr} over the last 400 days vs. the average I_{corr} for the last 3 readings. For some samples, for example, in 1F2 and 1G2 an increase in average I_{corr} was observed from recent readings using EIS/LPR but not for average I_{corr} values performed using GP method. It is not clear why this occurred.

Table 24. Comparison of R_s and I_{corr} using both LPR and GP tests.

	One year GP		Average last 3	One year EIS/LPR		Average last 3
	Ave R_s (kΩ)	Ave I_{corr} (μA)	I_{corr} (μA)	Ave R_s (kΩ)	Ave I_{corr} (μA)	I_{corr} (μA)
1C1	2.9	66.4	17.8	2.4	16.3	17.08
1C2	4.4	33.8	37.0	3.1	36.8	32.16
1B1	1.1	260.9	355.2	1.0	313.2	156.32
2D2	1.0	126.3	122.8	0.8	122.3	121.09
1F1	0.8	173.8	150.7	0.7	150.6	188.36
1F2	1.0	48.7	49.0	0.9	49.9	71.54
1G1	2.2	32.7	28.6	2.0	29.0	21.49
1G2	3.8	22.5	22.8	3.4	21.2	31.89

3.1.2 – Mortar samples with single rebar

Table 25 presents the average value for Rs, two average I_{corr} values measured over at least the last 300 days using the GP method on MD1 specimens. (Five of these samples were terminated, and this is also indicated in the table by an asterisk.) The label Ave I_{corr} in the table refers to averaging each I_{corr} value after each R_c value was converted to I_{corr}; the column on the right refers to average I_{corr} obtained by first averaging R_c and then the average R_c was used to calculate I_{corr}.

The I_{corr} was also measured on three samples that were subjected to chlorides in 2006 with no polarization (indicated with NP in the specimen ID). These samples had likely been corroding for several years, but showed no signs of cracks or corrosion stains. Recall that there was no solution on it for 4 years. NaCl solution was added in the reservoir as part of this project. The smallest average I_{corr} for these rebars (from R_c average) was 650 μA for MD1-NP38, whereas MD1-NP37 showed an average I_{corr} of 1,193 μA. These three samples were forensically analyzed.

Sample MD1-B had a 10-cm solution reservoir and was subjected to accelerated chloride migration as part of this project. The average I_{corr} was smaller (one third to one fourth of the average I_{corr}GP measured on MD1-NP corroding samples. The sample MD1-H had a solution of 1.5-cm when the electromigration took place; it was later changed to a 3-cm solution reservoir, and for the last 300 days, a larger solution reservoir was installed (similar in size to the reservoir used on MD1-NP samples). A small crack was observed before terminating this sample. MD1-A sample also has a 10-cm solution reservoir, but the average corrosion current was 88 μA, i.e., about one third of that observed on MD1-B (299 μA). The embedded rebar was used as one of the electrodes on MD1 samples subjected to electromigration. This table shows that MD1-NP specimens showed the largest average I_{corr} values from all the measurements performed in this project. A large solution reservoir was installed about 300 days ago on the two samples (MD1-NoCorr specimens), with the smallest average I_{corr} (< 30 μA) and no electromigration was applied to these specimens.

Table 25. R_s and average I_{corr} obtained from GP readings.

		Ave 300 days	300 days	300 d–Ave R_c
		R_s (kΩ)	Ave I_{corr} (μA)	I_{corr} (μA)
	MD1–NP35*	0.15	903	810
	MD1–NP37*	0.12	1740	1193
	MD1–NP38*	0.19	886	652
10 cm	MD1–A	1.74	94	88.7
	MD1–B*	0.42	357	299
1.5 to 20 cm	MD1–H*	1.17	139	114
	MD1–NoCorr–1	2.06	25.8	25.1
	MD1–NoCorr–2	1.8	14.3	13.9
1.5 to 20 cm	MD1–F	0.56	103	78
	MD1–G	0.67	163	139
	MD1–J	1.6	55.6	54.2

Terminated Sample indicated by *

3.2 – Four– and single-rebar older samples subjected to electromigration in 2016

Day zero on the plots shown in this section indicate the day that the solution was added to the reservoir. The monitoring period for the various rebars in the samples then ranged from several years (e.g., more than seven years for samples 1F1, 1B1 described above) to two years (2 years+ for 1D, 1H, 3B samples) and are expressed as the number of days in the plots. OCP in the plots refers to the rebar potential measured.

This section presents typical plots of rebar potential vs. time and R_s, R_c vs. time on the same plots for specimens subjected to high moisture during the corrosion propagation stage. The rebar potential was measured against a saturated calomel electrode. The plots are grouped based on the solution reservoir size.

3.2.1 – Specimens cast with ordinary Portland cement

The samples that contain only OPC will be described first. The measurements were performed assuming one cm^2 area of steel since the corroding area is not known. Note: the rebar potential of the mature samples (prepared in 2008/9) prior to energizing were typical of that reported for not corroding steel on most specimens (except 3 rebars of specimen 1DA). The blue vertical lines indicate the approximate start point and duration of each electromigration period. The gray bars indicate the approximate start and duration of each anodic current pulse (used to modestly

accelerate the corrosion of the reinforcement). The vertical black dotted lines enclose the period in which electromigration occurred.

Figure 39 and Figure 40 show the evolution of the rebar potential and the measured R_s and R_c values on rebars 1DAO1 and 1DBO1. These are the rebars under a 2.5 cm diameter solution reservoir. The rebar identified as 1DAO1 showed an initial potential value that was more negative than –0.4 Vsce, whereas initially, the rebar potential for 1DBO1 was around –0.02 Vsce. The potential of 1DBO1 remained close to this value during the electromigration period and the 100 days that followed. The 1DBO1 rebar potential then shifted to more negative values ranging between –0.25 and –0.3Vsce. The R_c values measured on 1DAO1 rebar were smaller than 0.3 kΩs. The R_c calculated from the measurements after subtracting R_s were significantly smaller on 1DAO1 rebar compared to the R_c calculated on 1DBO1 rebar. After the potential drop was observed on 1DBO1 rebar, the R_c value decreased in magnitude but later oscillated to values similar to those measured during the electromigration period.

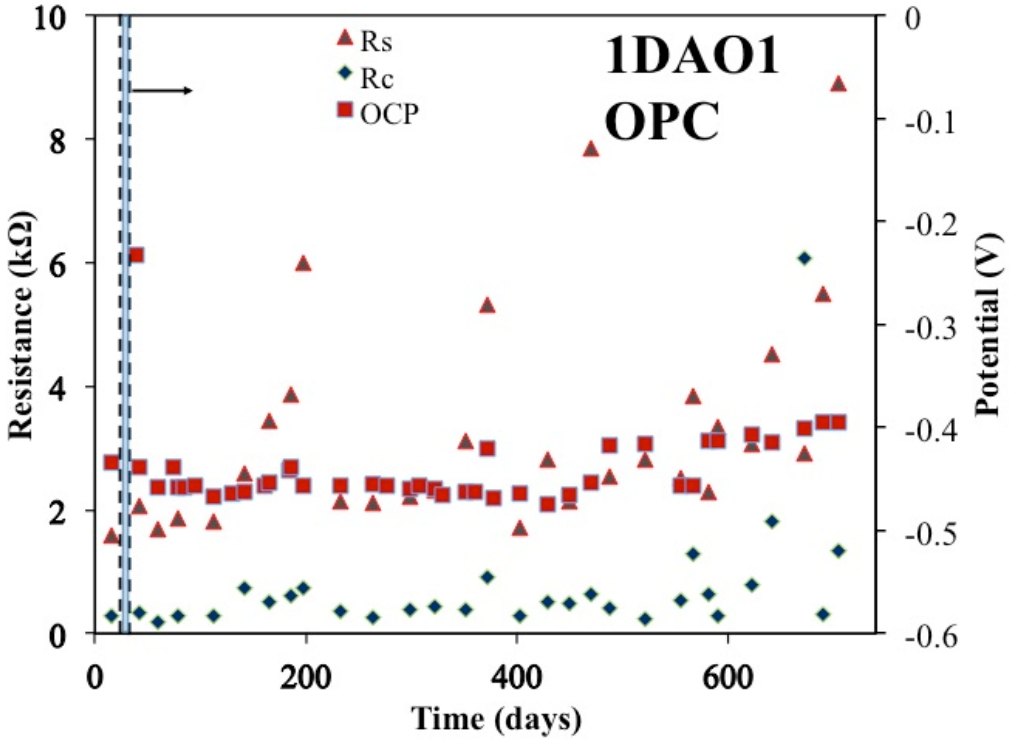

Figure 39. Rebar potentials, R_s, and R_c values measured on rebar 1DAO1

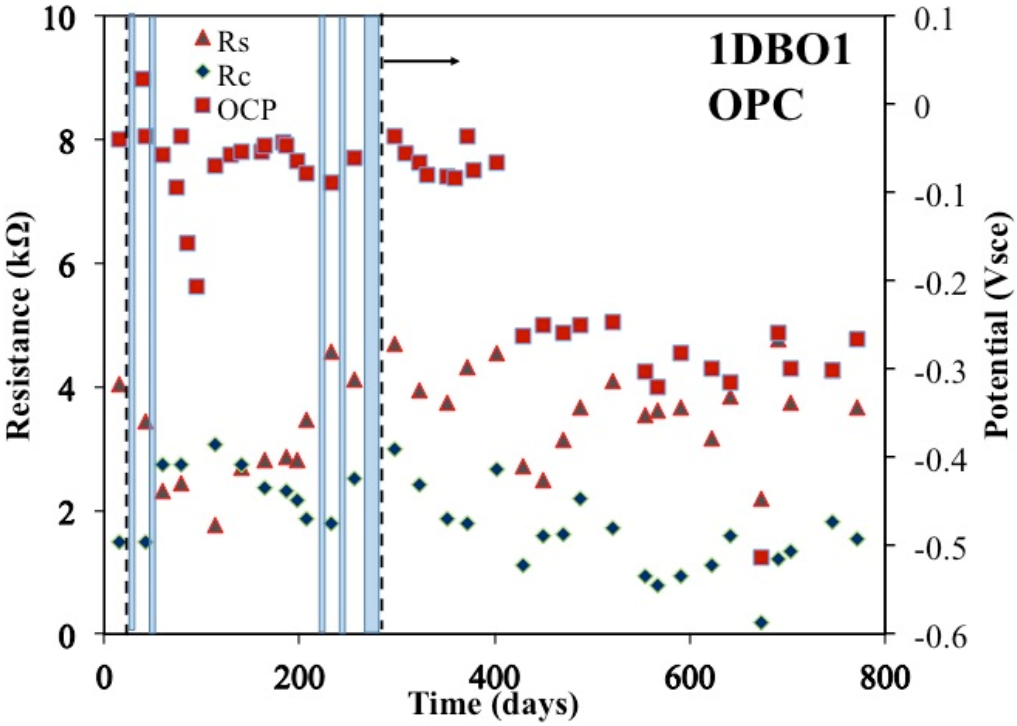

Figure 40. Rebar potentials, R_s, and R_c values measured on rebar 1DBO1

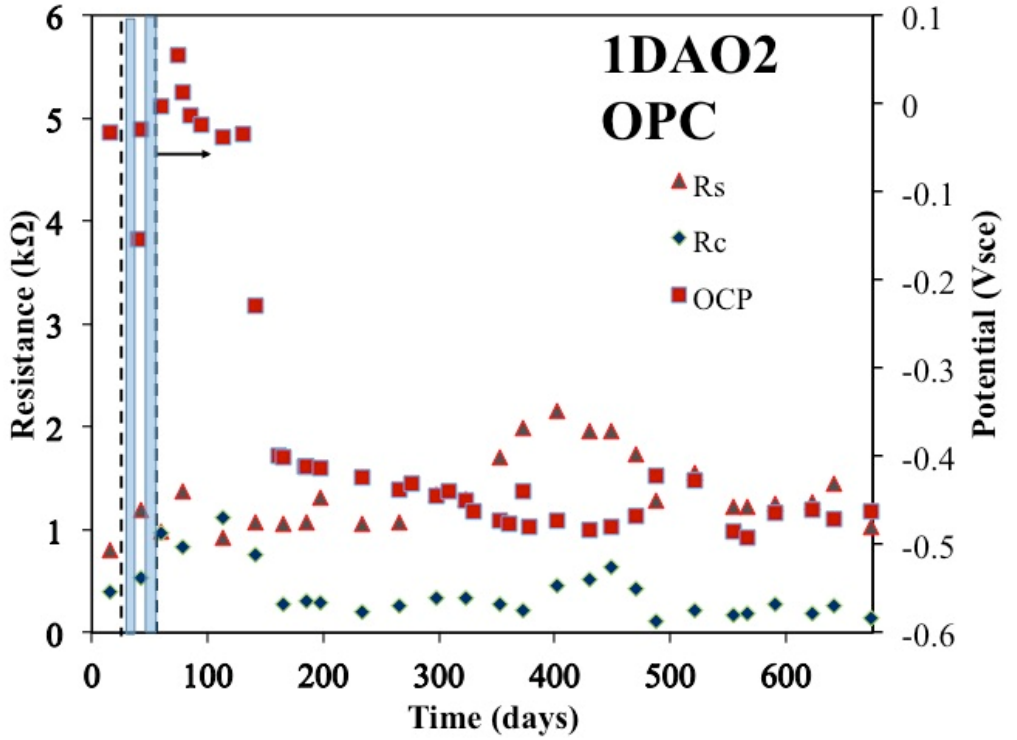

Figure 41. Rebar potentials, R_s, and R_c values measured on rebar 1DAO2

Figure 41 and Figure 42 show the electrochemical measurements performed on the rebars with a solution reservoir 5 cm diameter on 1D specimens. These figures show that a potential drop was observed on both 1DAO2 and 1DBO2 rebars following the electromigration period. The R_c also decreased significantly once the rebar potential was more negative than –0.3 Vsce. The R_s on both was on average around 1 kΩ.

Figure 43 and Figure 44 shows plots of the electrochemical characterization performed on 1DASQ1 rebar and on 1DASQ2 rebar, respectively. Both rebars have 10 cm solution reservoir. The rebar potential measured combined with the R_c values recorded on both rebars suggest that corrosion was taking place. Figure 45 and Figure 46 show that a potential transient and corresponding decrease in R_c values was observed on the rebars 1DBSQ1 and 1DBSQ2, respectively. The current E_{corr} value is around –0.4 Vsce on both rebars.

The instances in which electromigration took place are represented by blue bars and enclosed within vertical dash lines. These bars are not to scale and just provide an approximate duration and when the electromigration was applied. The total ampere–hour that each rebar received is indicated in Table 20.

Figure 47 and Figure 48 show that samples 2B1 and 2B2 appear to have a different transient. These samples were not previously exposed to chlorides, whereas 1DA and 1DB specimens had been exposed to chlorides during their first year. The ampere–hour that was calculated after the electromigration suggest that chlorides might not have penetrated to the rebar surface on the rebar embedded in specimen 2B1 (based on the observed rebar potential values). It is interesting to note that the R_c values and corrosion potential did experience a drop in magnitude as those that took place on rebars embedded in 1DA and 1DB specimens (described herein). The chloride concentration might not have been large enough to sustain active corrosion as the potential drifted to more positive values as time passed. Moreover, the additional exposure time was not long enough as to reach the threshold concentration by diffusion within the monitored period.

The ionic current produces polarization of the reinforcing steel which in some cases allow corrosion to initiate at a lower threshold, but if the site is small and no additional chlorides reach the rebar surface so as to keep the corroding site active, it is possible that the rebar becomes passive again. This is suspected to have taken place on the rebar embedded in specimen 2B1.

The external current that was applied to accelerate the corrosion on selected samples might have acted as anodic protection in some cases (either because of corrosion products build up or by anodic protection). The applied current may have generated a layer built up (corrosion products and other reactants), which when present slows corrosion rate. Consequently, upon removal of the applied current, it can take a long time to re–activate the specimen (particularly if the corroding site was small and if a high enough chloride concentration was not surrounding the rebar).

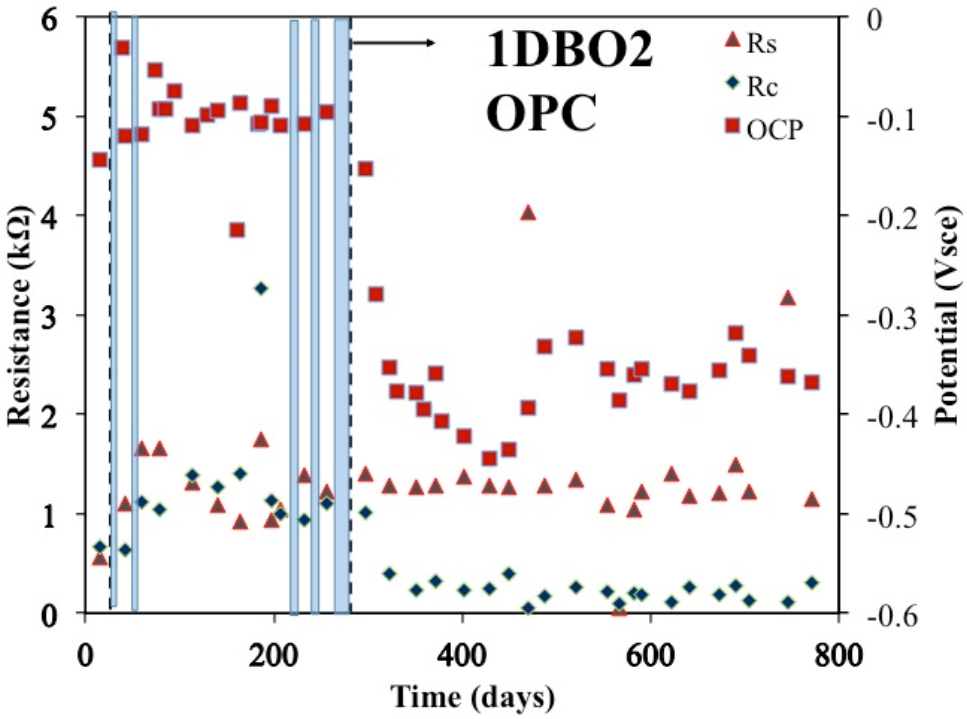

Figure 42. Rebar potentials, R_s, and R_c values measured on rebar 1DBO2

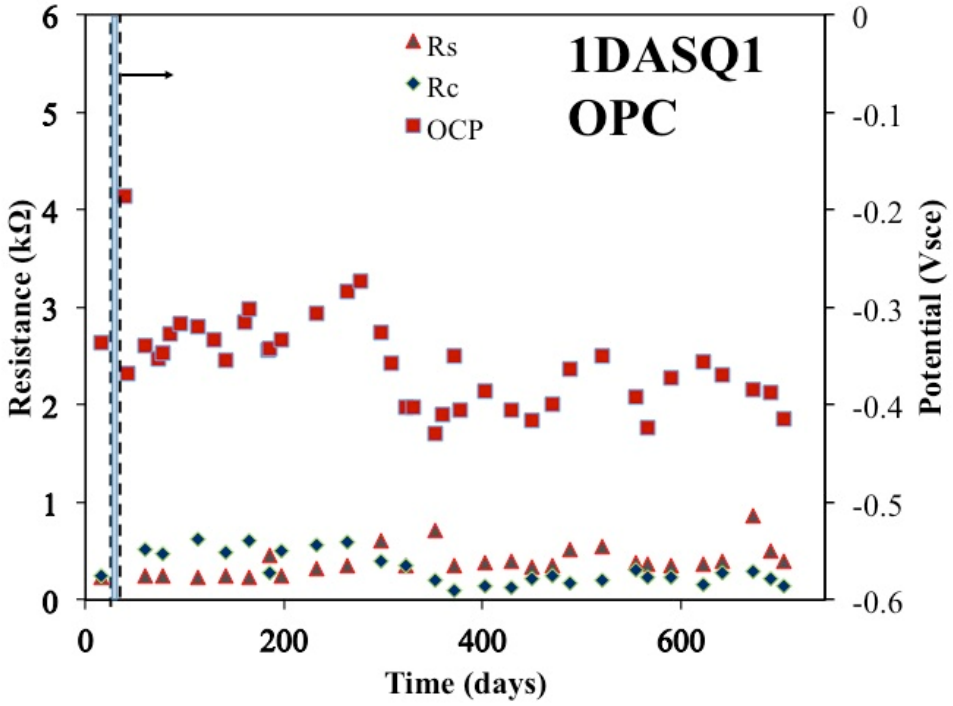

Figure 43. Rebar potentials, R_s, and R_c values measured on rebar 1DASQ1

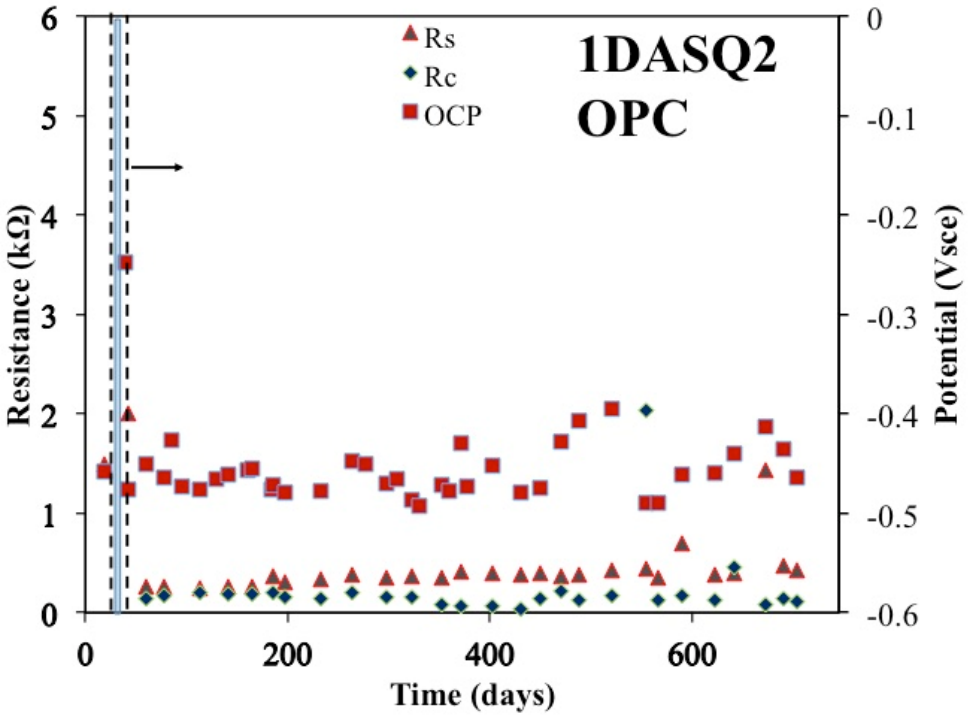

Figure 44. Rebar potentials, R_s, and R_c values measured on rebar 1DASQ2

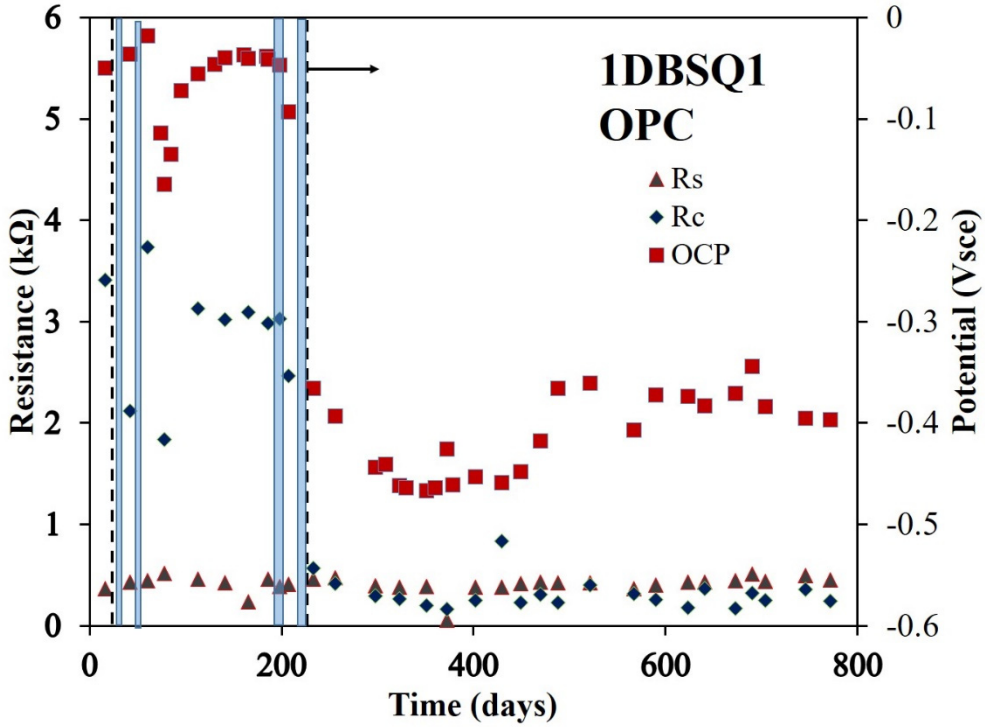

Figure 45. Rebar potentials, R_s, and R_c values measured on rebar 1DBSQ1

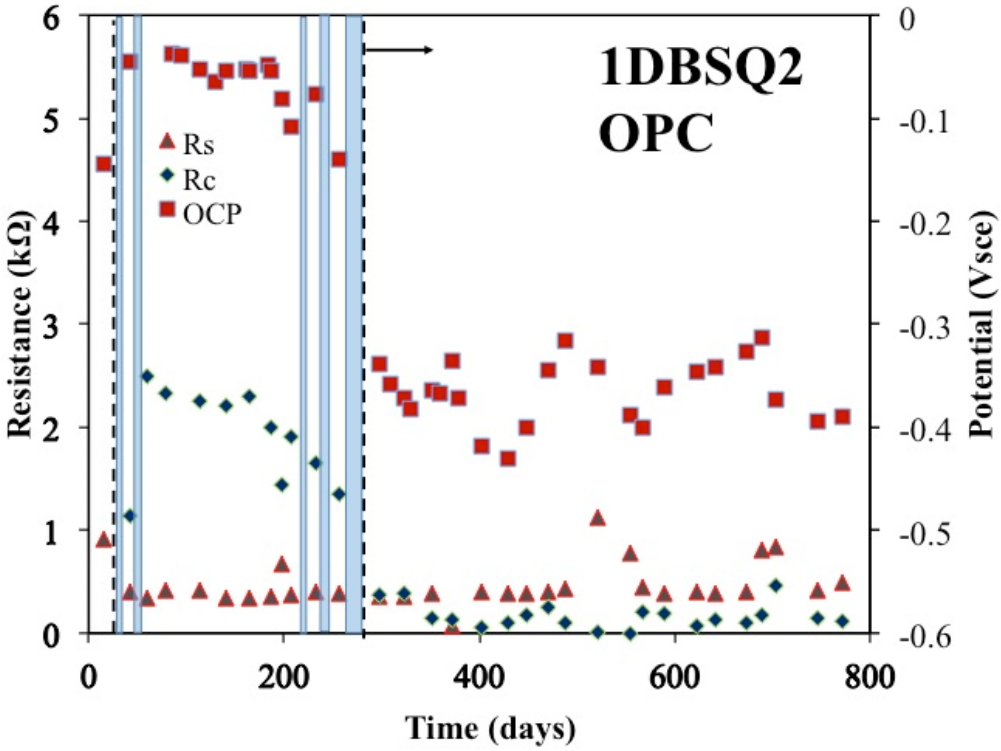

Figure 46. Rebar potentials, R_s, and R_c values measured on rebar 1DBSQ2

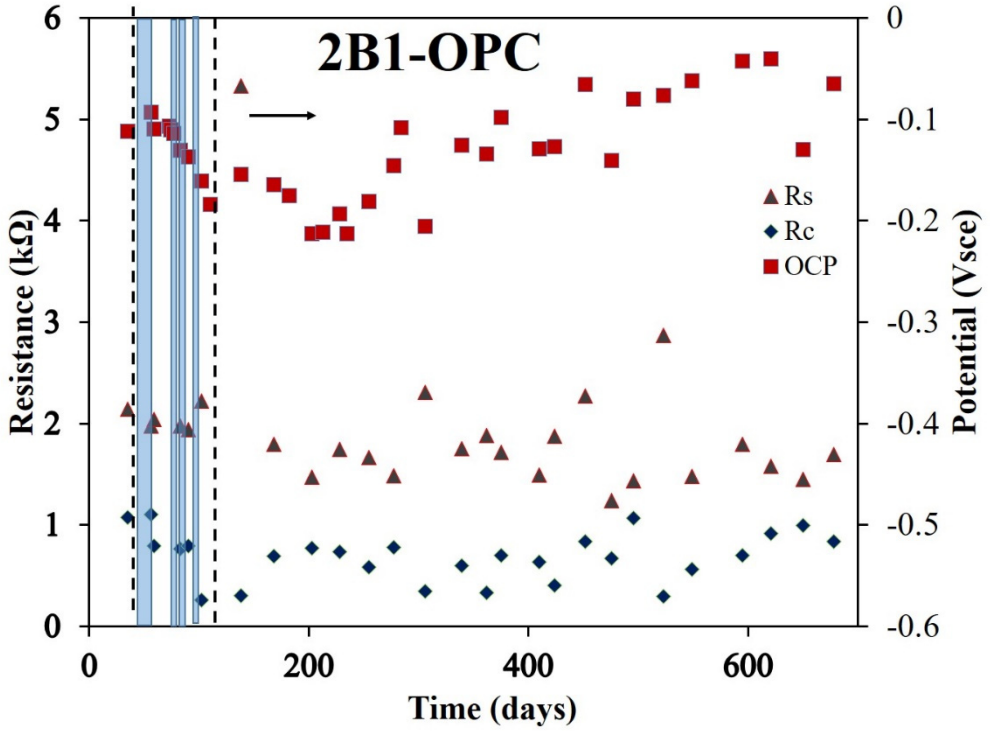

Figure 47. Rebar potentials, R_s and R_c, values measured on rebar 2B1

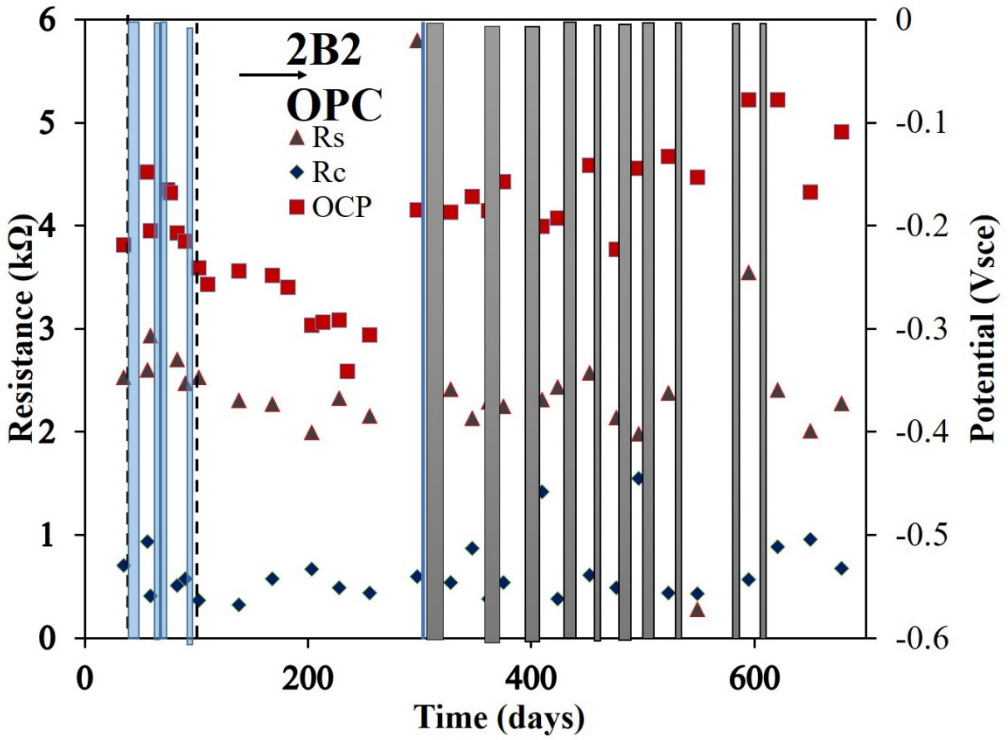

Figure 48. Rebar potentials, R_s, and R_c values measured on rebar 2B2

3.2.2 – Four-rebar specimens cast with 20% fly ash

Seven out of eight rebars in 1H specimens were subjected to only two periods of electromigration. Rebar 1H2SQ1 was subjected to a third electromigration period around day 370. The integrated ampere–hour values are shown in Table 20.

Similar to what was described above for 1D specimens, two rebars had 2.5 cm diameter solution reservoirs installed above them. These rebars are named 1H1O1 and 1H2O1. The solution resistance measured on rebar 1H2O1 was twice that measured on 1H1O1 rebar, see Figure 49 and Figure 50. In a similar manner, larger R_c values were measured on rebar 1H2O1 when compared to R_c values measured on rebar 1H1O1. For most of the period (after the electromigration) the rebar potential of both samples showed values around –0.3 Vsce. The two most recent rebar potential readings on specimen 1H1O1 were close to –0.5 Vsce, but the R_c and Rs did not change much compared to previous measurements.

Figure 51 and Figure 52 shows the measurements that were done on rebars 1H1O2 and 1H2O2 (5 cm diameter reservoir installed above them). A transient from passive potential to active potential was recorded shortly after the electromigration was removed. The R_s values measured on 1H1O2 ranged between 1 to 2 kΩ and typically was larger than the R_s measured on rebar 1H2O2. The R_c values measured on 1H1O2 were somewhat smaller than the R_c measured on 1H2O2. The rebar potential for both samples was around –0.3 Vsce.

Figures 53 to Figure 56 show the electrochemical monitoring of specimens with 10 cm square reservoirs (1H1SQ1, 1H1SQ2, 1H2SQ1, and 1H2SQ2) installed above them. The transition to more negative potential did not take place at the same time on these rebars. There was usually a delay that ranged from 30 days to several months. A significant reduction in the magnitude of R_c was observed when the potential drop occurred. Sample 1H1SQ1 was subjected to modest applied current around day 380. Rebar 1H1SQ1 was the rebar with the smaller R_c values (prior, during and after applying the modest anodic current). Rebars that were selected for applied current during the propagation period likely had a higher corrosion rate with the current on. The R_c, E_{corr} values that are shown took place at least two days after the current was removed.

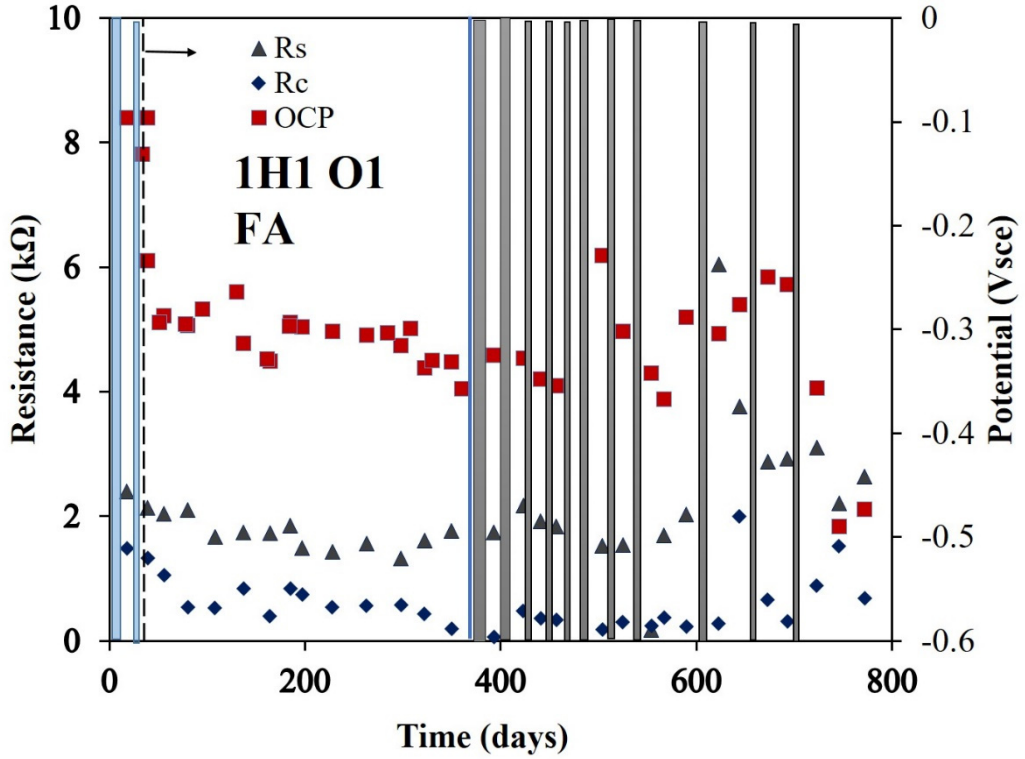

Figure 49. Rebar potentials, R_s, and R_c values measured on rebar 1H1O1 (2.5-cm reservoir)

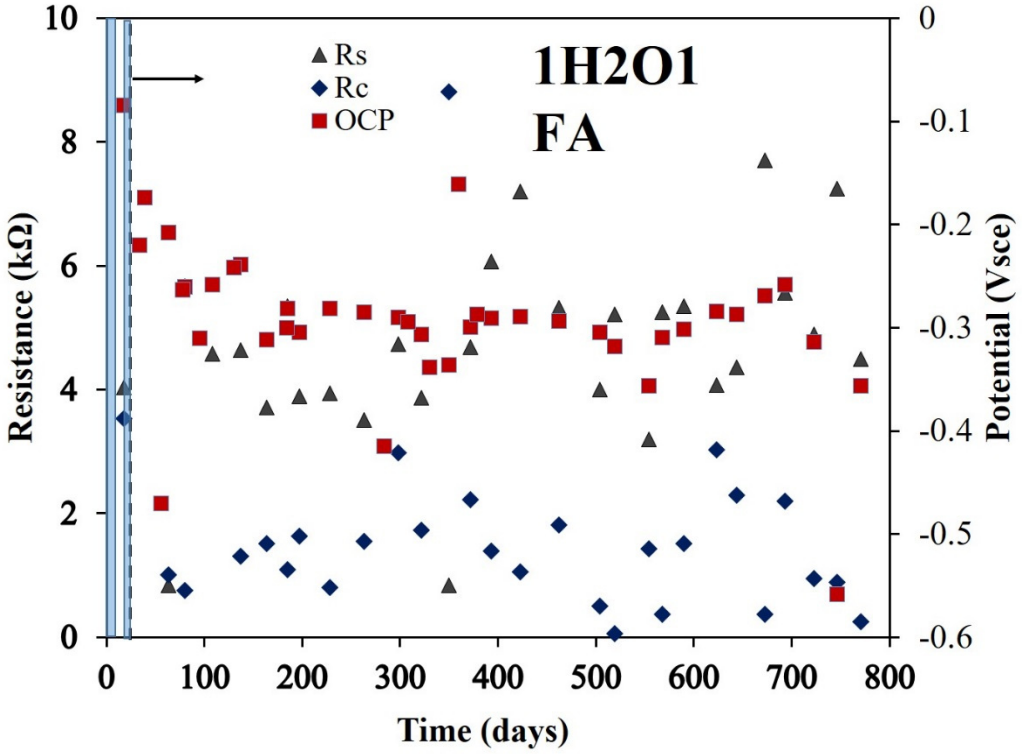

Figure 50. Rebar potentials, R_s, and R_c values measured on rebar 1H2O1 (2.5-cm reservoir)

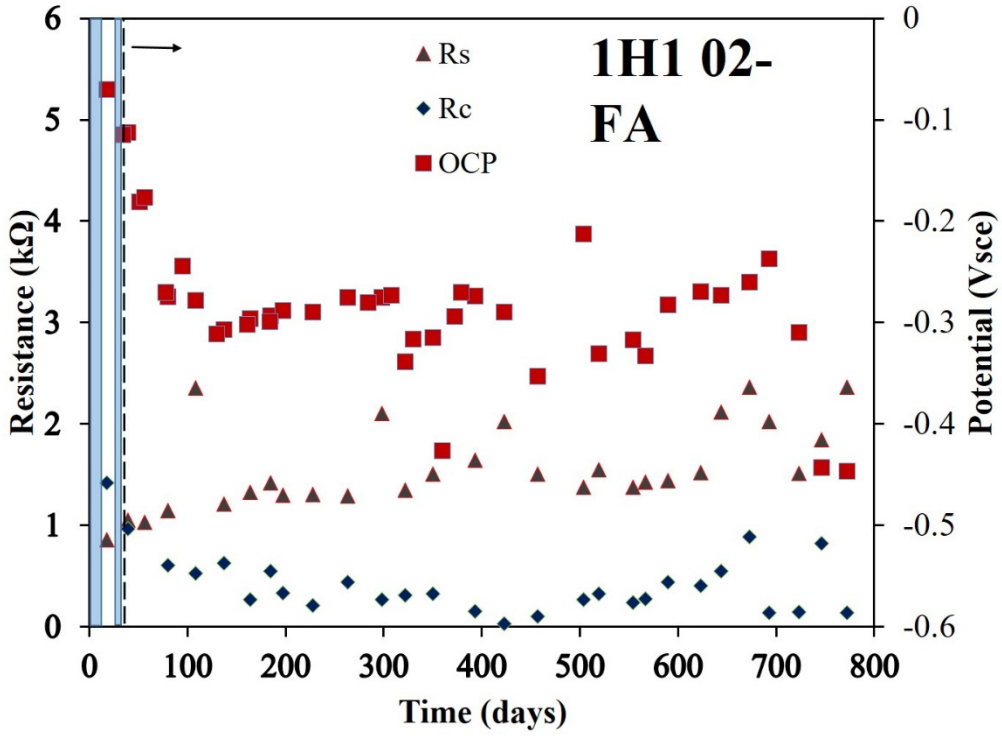

Figure 51. Rebar potentials, R_s, and R_c values measured on rebar 1H1O2 (5-cm reservoir)

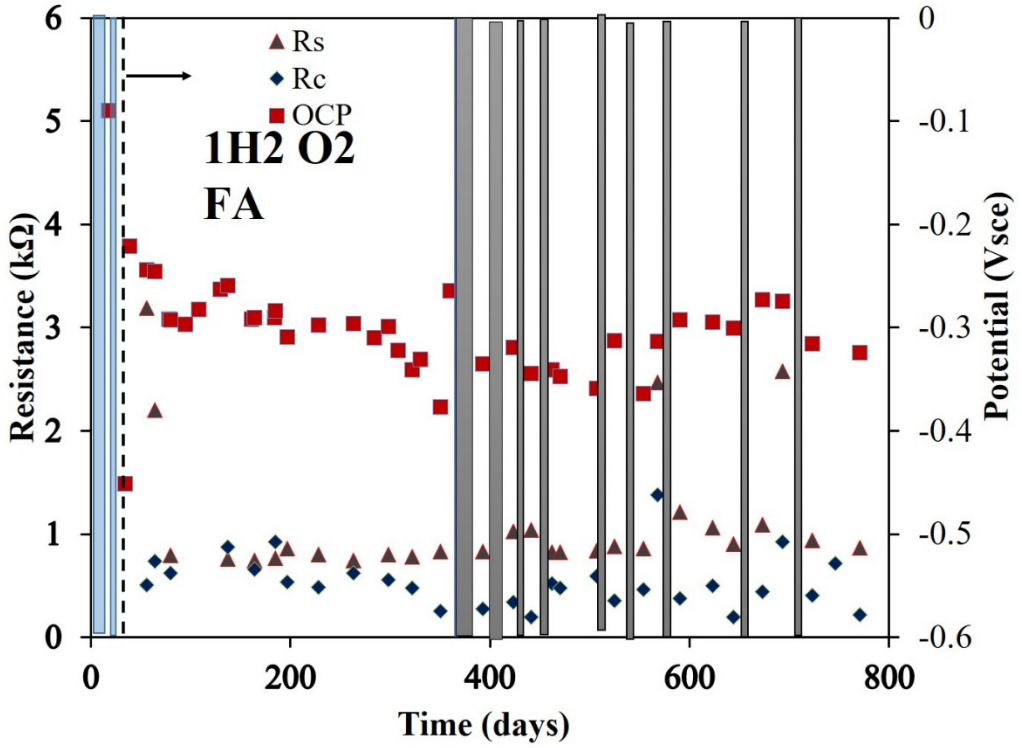

Figure 52. Rebar potentials, R_s, and R_c values measured on rebar 1H2O2 (5-cm reservoir)

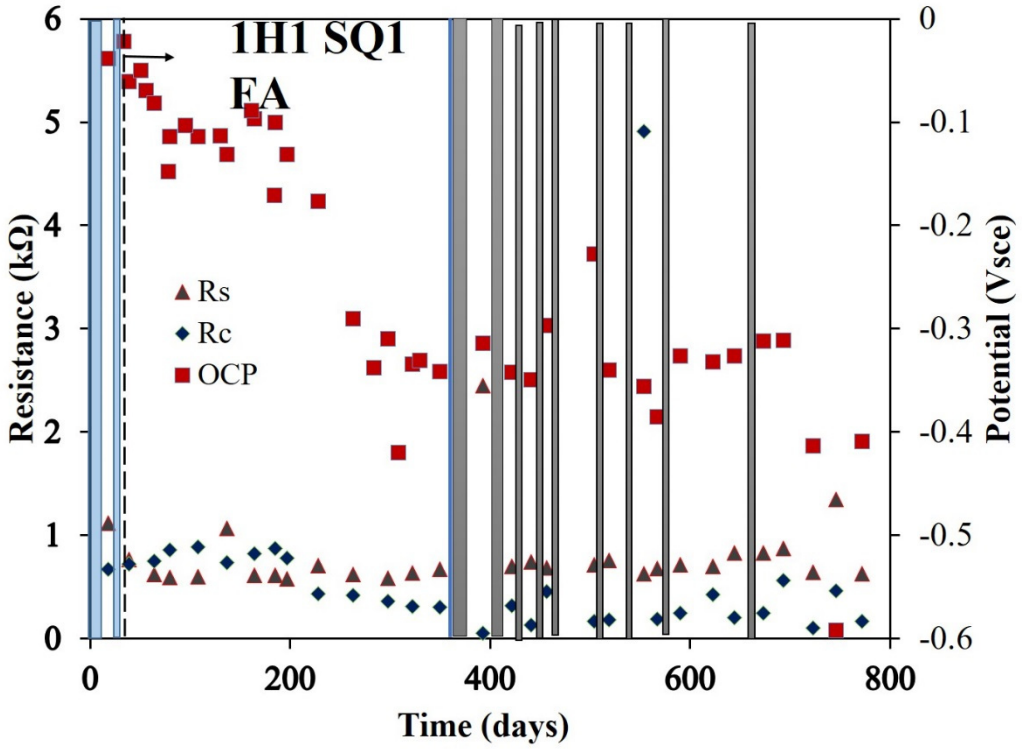

Figure 53. Rebar potentials, R_s, and R_c, values measured on rebar 1H1SQ1 (10-cm reservoir)

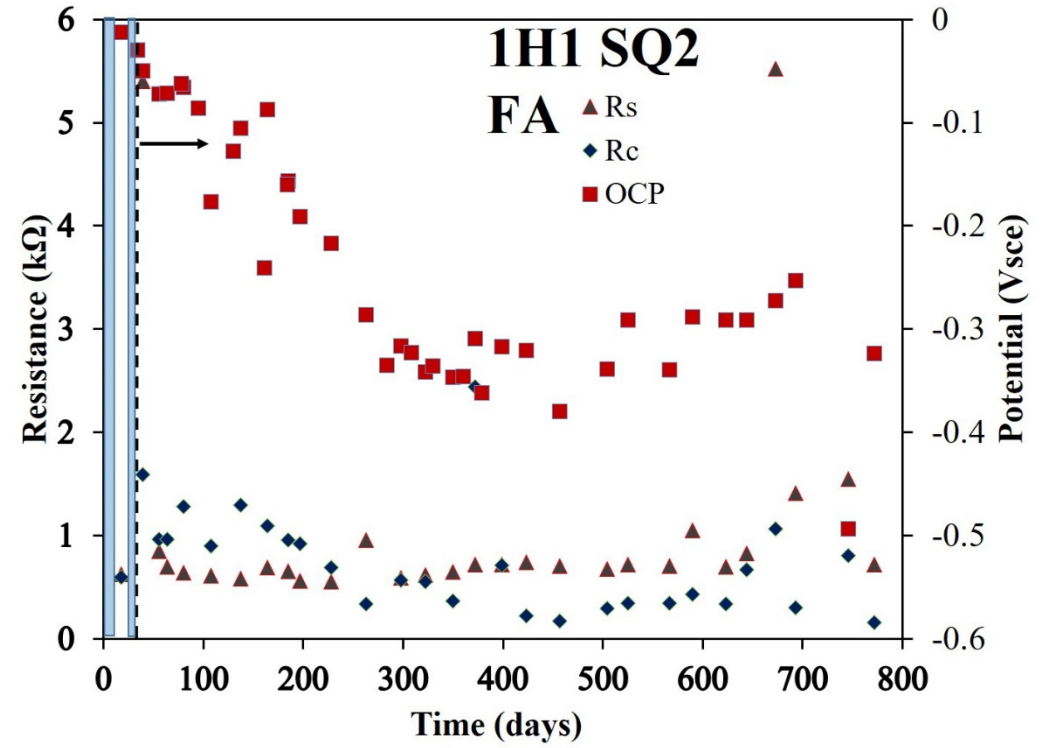

Figure 54. Rebar potentials, R_s, and R_c values measured on rebar 1H1SQ2 (10-cm reservoir)

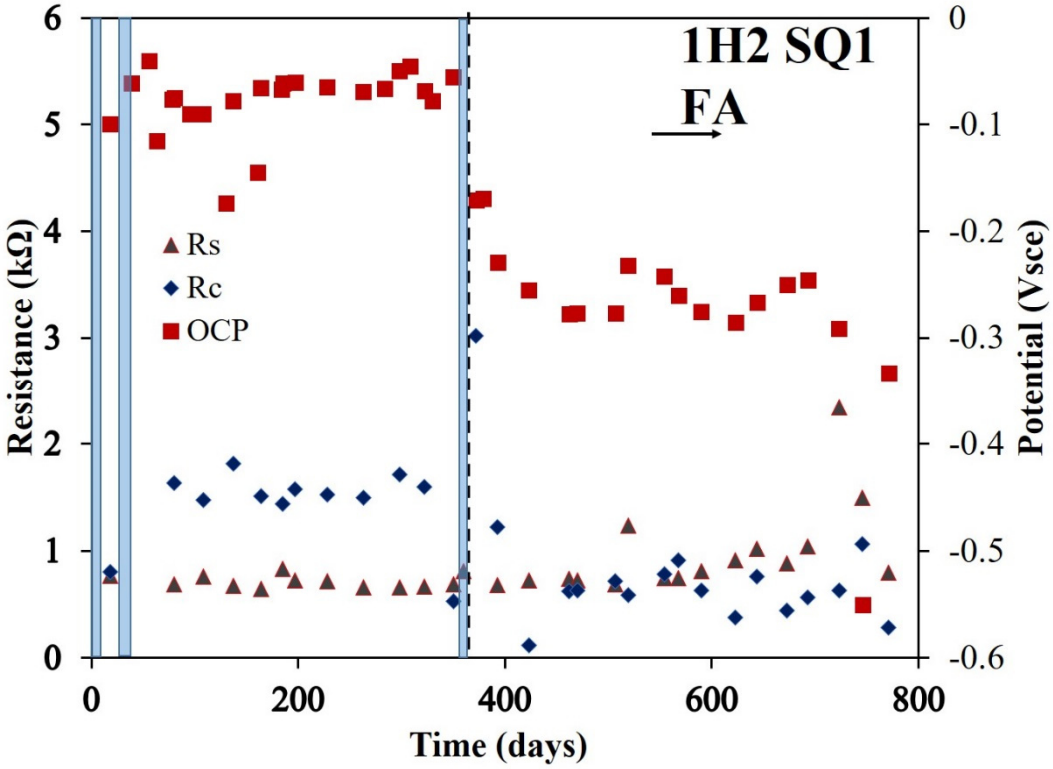

Figure 55. Rebar potentials, R_s, and R_c values measured on rebar 1H2SQ1 (10-cm reservoir)

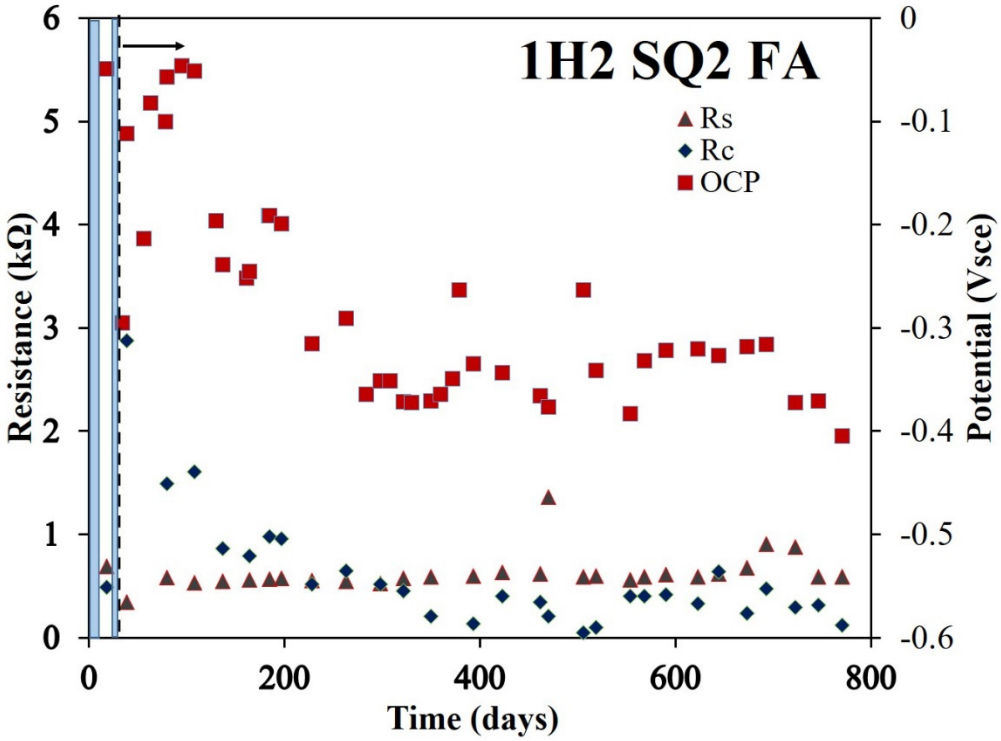

Figure 56. Rebar potentials, R_s, and R_c values measured on rebar 1H2SQ2 (10-cm reservoir)

3.2.3 – Specimens with fly ash and silica fume

Four specimens with single rebar and concrete composition of 20% FA and 8% SF were available. Specimens 3BX and 3B4 have a 10 cm solution reservoir above the rebar. Based on the rebar potential and the R_c values, the rebars in both specimens are believed to be active. Specimens 3BY and 3B3 have a 5 cm solution reservoir. Figure 57, Figure 58, Figure 59 and Figure 60 show the rebar potential, R_c and R_s measured on the rebars embedded on samples 3BX, 3B4, 3B3, and 3BY respectively. The transition to active corrosion appeared to have taken place on the rebar embedded in specimen 3BY. The rebar potential showed a gradual shift towards more positive values starting on day 150, but the R_c values remained the same over this period of time (a more modest and gradual increase in R_c was observed). The rebar in specimen 3B3 might not have become active when observing the rebar potential vs. time, and the R_c values are somewhat larger than the R_c values observed on specimen 3BY.

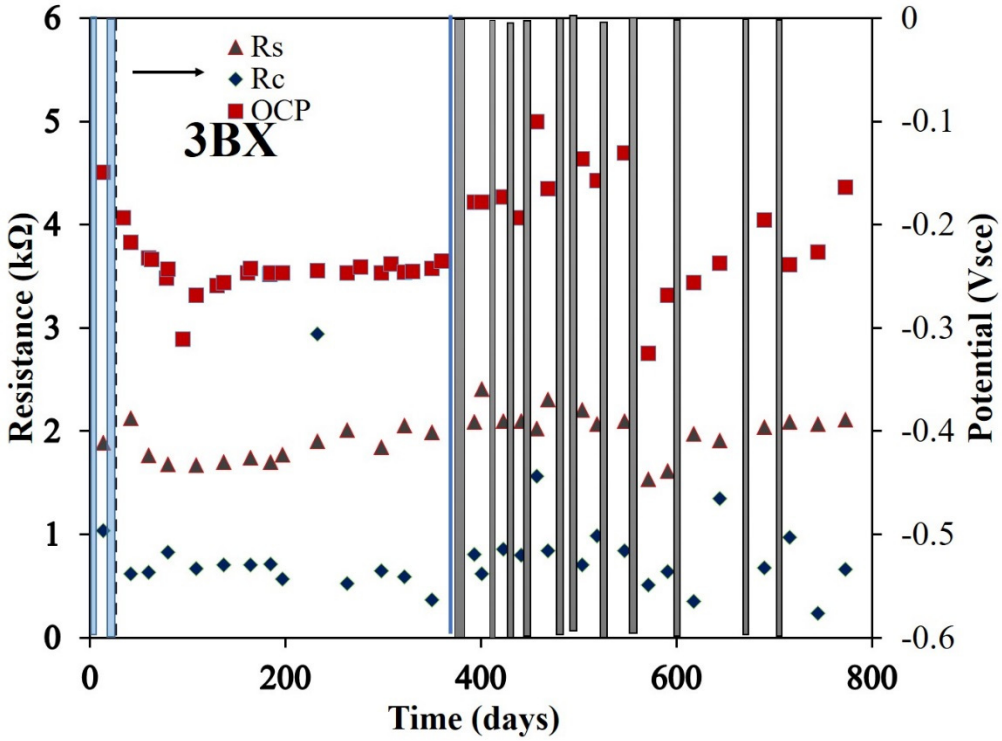

Figure 57. Rebar potentials, R_s, and R_c values measured on rebar 3BX (10-cm reservoir)

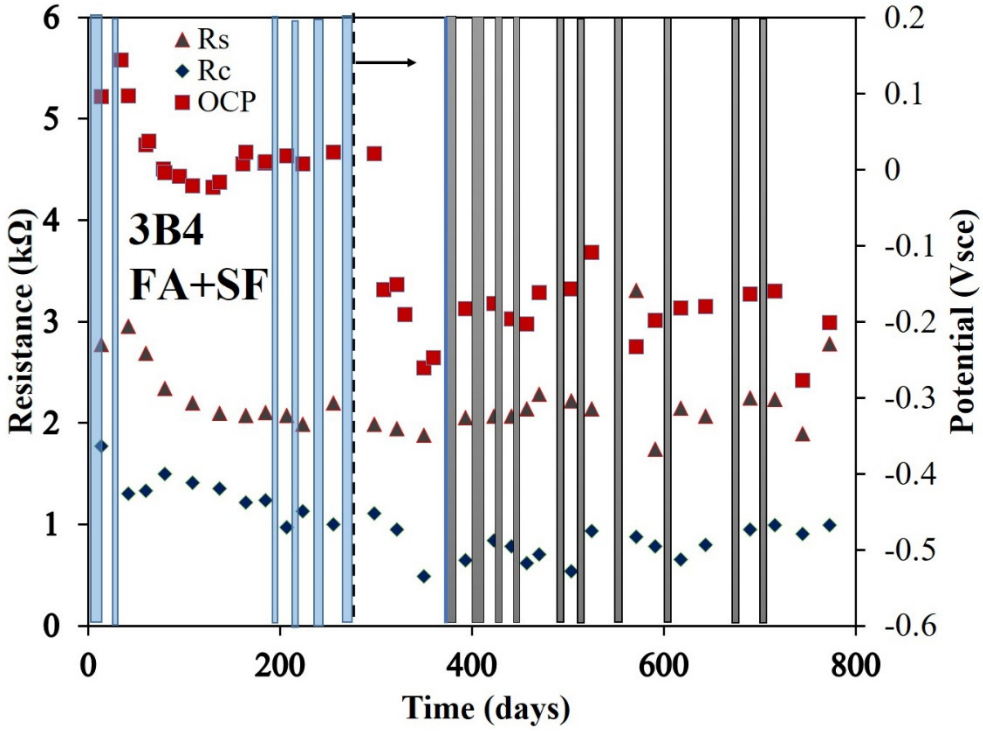

Figure 58. Rebar potentials, R_s, and R_c values measured on rebar 3B4 (10-cm reservoir)

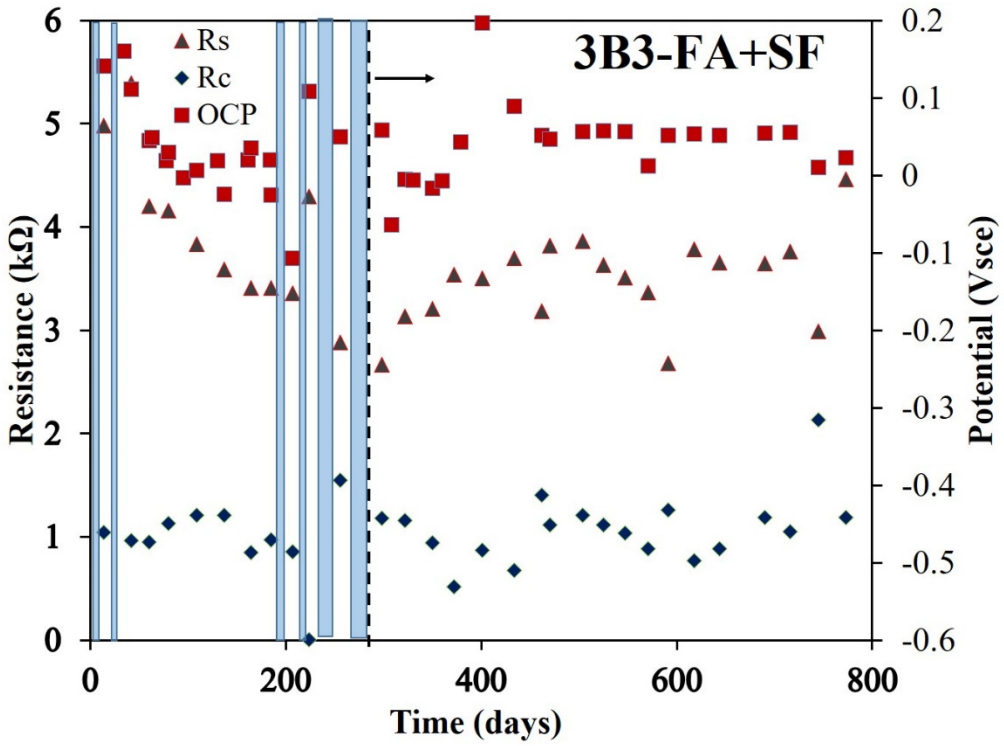

Figure 59. Rebar potentials, R_s, and R_c values measured on rebar 3B3 (5-cm reservoir)

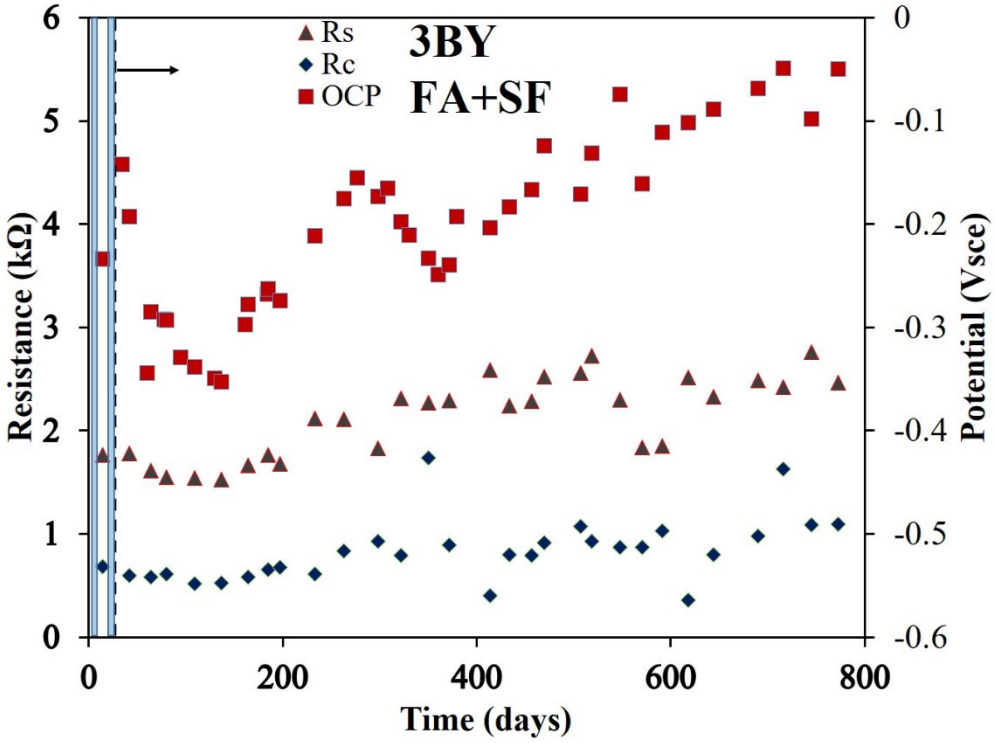

Figure 60. Rebar potentials, R_s, and R_c values measured on rebar 3BY (5-cm reservoir)

3.2.4 – R_s and average I_{corr} – single-rebar specimens with 5-cm cover

Table 26 shows the average Rs, average I_{corr} measured over 400 days and the average I_{corr} of three recent measurements (from GP measurements). Single rebar specimens with 5 cm concrete cover have an average Rs value that ranged from 0.8 kΩ to 4.4 kΩ. There appears to be a wide range for rebars embedded in OPC; the average Rs considering all OPC samples ranged from 1.0 kΩ to 4.4 kΩ. Whereas the average Rs for rebars in specimens with FA, Rs ranged from 0.8 kΩ to 3.8 kΩ. Finally, for rebars embedded in samples with FA+SF, the Rs ranged from 2.7 kΩ to 3.9 kΩ (this last set had reservoirs of two different sizes). From Table 25, it can be observed that in most samples the average corrosion current measured over the last 400 days was larger than the average corrosion current of the three most recent readings.

The average I_{corr}GP over the last 400 days was 66.4 μA for the rebar on specimen 1C1 and 33.8 μA for the rebar on specimen 1C2, whereas the I_{corr}GP average for the three most recent readings was 17.8 μA for the rebar in specimen 1C1 and 37 μA for the rebar in specimen 1C2. For some rebars, there was not much change when comparing overall average I_{corr} vs. the three recent readings I_{corr} average. As an example see values corresponding to rebars on specimens 2B1 and 1F2.

Table 26. R_s and average I_{corr} obtained from GP readings – 5-cm cover specimens

	400 days		3 Recent
ID	Ave R_s (kohms)	Ave I_{corr} µA	I_{corr} µA
1C1	2.9	66.4	17.8
1C2	4.4	33.8	37.0
1B1*	1.1	260.9	355.2
2D2*	1.0	126.3	122.8
2B1	1.9	17.4	16.0
2B2	2.6	24.0	19.0
1F1*	0.8	173.8	150.7
1F2	1.0	48.7	49.0
1G1	2.2	32.7	28.6
1G2	3.8	22.5	22.8
3B3	3.9	12.0	10.4
3BX	2.4	23.5	23.0
3B4	2.5	21.0	21.4
3BY	2.7	13.1	11.8
Max	4.4	260.9	355.2
Min	0.8	12.0	10.4

3.2.5 – R_s and average I_{corr} – four-rebar specimens with 5-cm cover

Table 27 (1D specimens) and Table 28 (1H specimens) presents one year averaged values for R_s, R_c and I_{corr}, and the I_{corr} obtained from the averaged R_cGP. For several rebars, these two values are quite different. The average I_{corr} is the sum of all I_{corr} values divided by the number of measurements. Table 27 shows the average values obtained on rebars embedded in 1D specimens. Rebar 1DASQ2 had the largest average Icorr. Specimen 1DA showed a crack that likely originated from the 1DASQ2 rebar. (See the forensic analysis chapter.) Table 28 shows R_s, R_c and I_{corr} obtained from R_cGP on rebars embedded on 1H specimens. The largest average I_{corr} was observed on rebar 1H1SQ1, followed by rebar 1H1O2, whereas the larger I_{corr} using the average R_c was observed on rebar 1H1O1. In some cases, the two I_{corr} values were comparable, whereas in others, the average I_{corr} was larger than the I_{corr} obtained form average R_c. The latter indicates that on those samples the R_c oscillated over a wide range.

Table 27. Average: R_s, R_c, and I_{corr} obtained from GP readings – 1D Specimens

Reservoir	Rebar Id	R_s(kΩ)	R_c(kΩ)	I_{corr} µA	I_{corr} using ave R_c, µA
2.5 cm	1DAO1	4.67	0.40	68.8	65.1
	1DBO1	4.73	1.59	19.9	16.4
5 cm	1DAO2	4.95	0.21	141.2	126.5
	1DBO2	1.52	0.22	137.3	116.3
10 cm	1DASQ1	0.52	0.29	93.4	88.6
	1DASQ2	0.61	0.15	294.6	178.6
	1DBSQ1	1.09	0.32	88.2	82.1
	1DBSQ2	0.56	0.28	99.5	92.3

Table 28. Average: R_s, R_c, and I_{corr} obtained from GP readings – 1H Specimens

	Rebar Id	R_s(kΩ)	R_c(kΩ)	I_{corr} µA	I_{corr} using Ave, R_c, µA
2.5 cm	1H1O1	2.26	0.54	49.9	48.8
	1H2O1	6.16	1.36	30.5	19.2
5 cm	1H1O2	2.09	0.69	62.7	38.0
	1H2O2	2.05	0.70	38.7	37.4
10 cm	1H1SQ1	0.91	0.74	77.0	35.1
	1H1SQ2	4.41	0.60	54.8	43.4
	1H2SQ1	1.22	1.37	40.2	19.0
	1H2SQ2	0.78	0.59	46.4	44.6

3.3 – Single-rebar and three-rebar specimens prepared in 2016

3.3.1 – SL single-rebar specimens.

Figure 61 shows the R_c, R_s and rebar potentials measured on specimen SL1. The rebar in specimen SL1 experienced a potential drop after the electromigration was suspended. R_c experienced a modest decrease and remained at a relatively low value over the monitored period. The rebar potential oscillated (starting on day 180) and tended to drift toward more positive values. Figure 62 shows the R_s, R_c and rebar potential measured on specimen SL2. The rebar in SL2 was subjected to additional electromigration periods (compared to SL1). On day 200 the rebar potential decreased and remained at values of –0.25V or more negative. The R_c experienced a modest decrease. During the electromigration, both R_c and Rs appear to increase monotonically. The rebar in sample SL2 was subjected to a small anodic current so as to accelerate corrosion starting on day 280, but it was suspended by day 570. The Rs appear to remain the same during the later corrosion monitoring period. The rebar potential in specimen SL2 fluctuate somewhat but remained more negative than –0.25 Vsce. The R_c also fluctuated some but were below 1 kΩ during the propagation stage, i.e., after suspending the electromigration. Appendix D contains the figures for the other SL specimens as well as corresponding similar plots for FA specimens. Appendix E contains the figures for the T1 and T2 specimens and Appendix F contains the figures for the monitoring of the 3-rebar specimens.

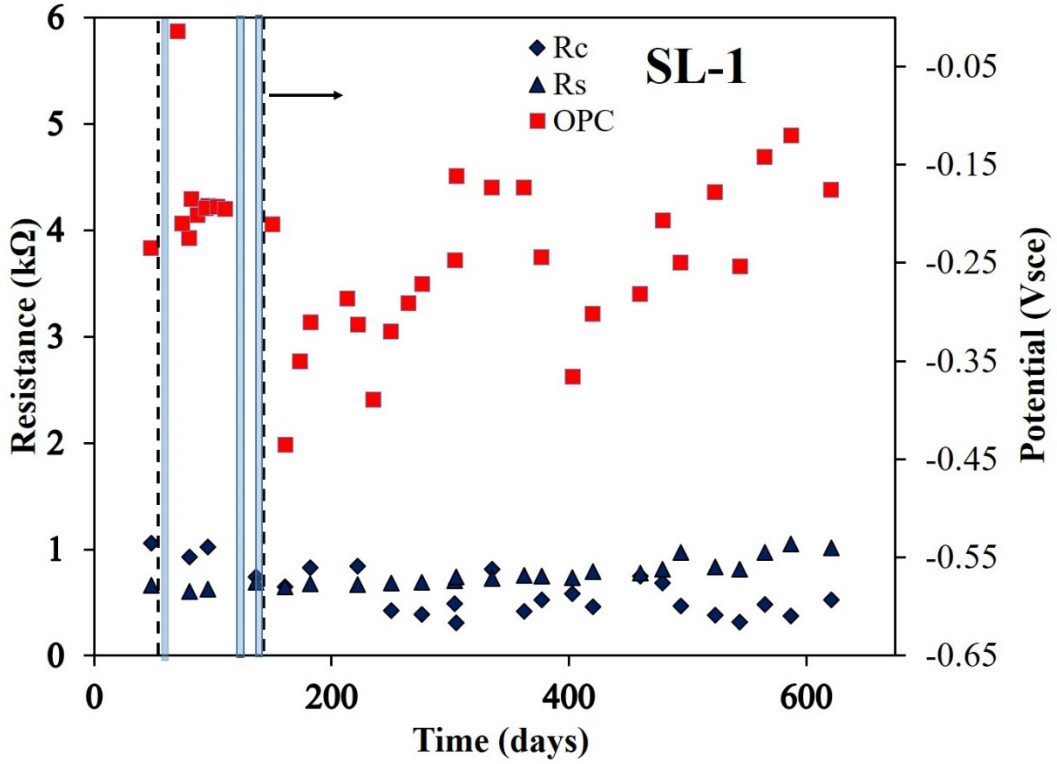

Figure 61. Rebar potentials, R_s, and R_c values measured on rebar embedded in SL-1 specimen

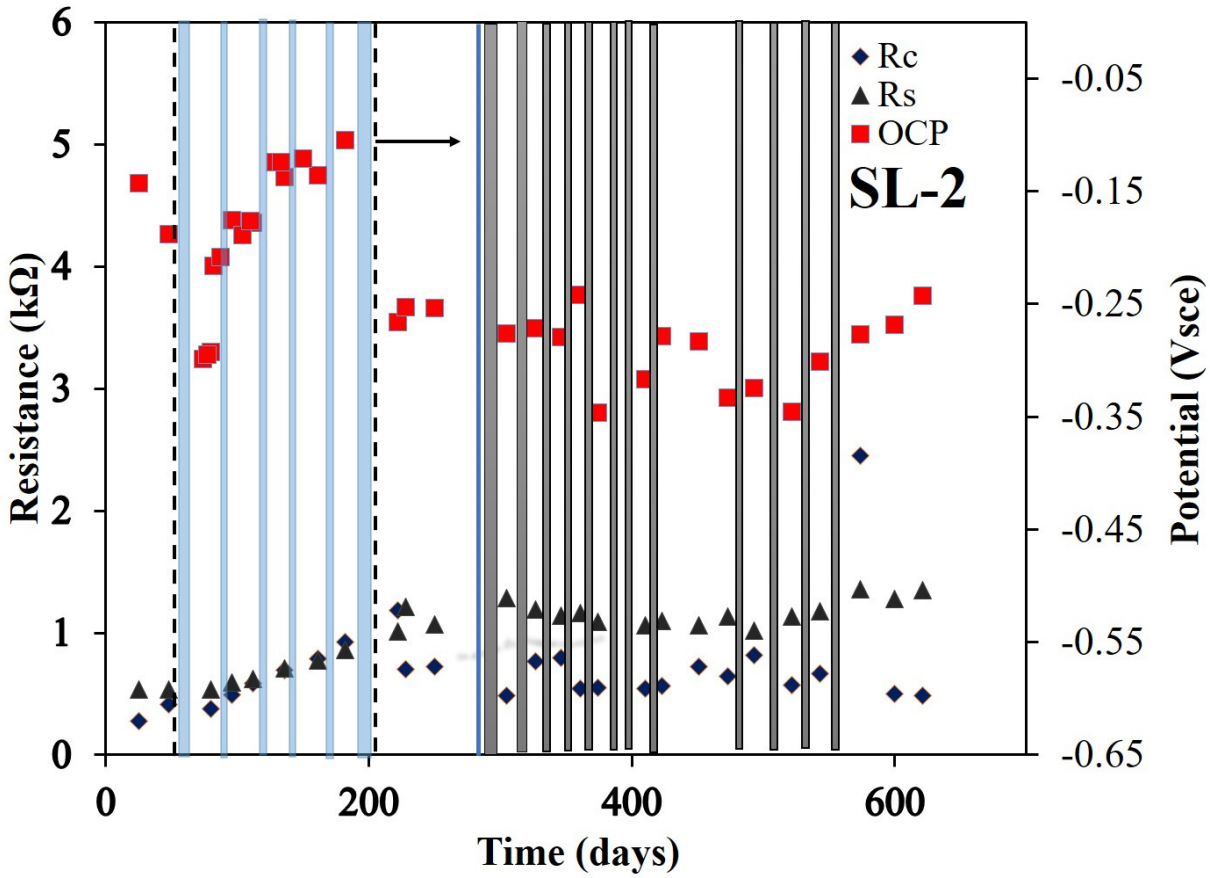

Figure 62. Rebar potentials, R_s, and R_c values measured on rebar embedded in SL-2 specimen

Table 29 shows the average R_s values obtained with the GP method, the average R_c values obtained with GP, and the I_{corr} obtained using the average R_cGP, the Icorr calculated using the average R_cLPR, average I_{corr} three recent R_cLPR measurements and the ratio between the I_{corr}GP and I_{corr}LPR. The measurements taken between March 2017 to May 2018 were included to calculate these averages. For I_{corr}LPR the average I_{corr} over the last 3 measurements is also included. Finally, the rightmost column shows the ratio between the average I_{corr}LPR/average I_{corr}GP.

The rebar with the largest average I_{corr}LPR was the rebar embedded in sample SL1, but the rebar with the largest average I_{corr}GP was the rebar in specimen SL2. The rebar in sample SL3 has the third largest average I_{corr}GP. These three SL samples have the longer solution reservoir. The rebars with the lowest average I_{corr}GP were the samples with the smaller solution reservoir.

Table 29. Average: R_s, R_c and I_{corr} obtained from LPR and GP readings – SL specimens

	Average values from GP			GP	LPR and EIS	LPR	Ratio
	R_s kΩ	R_c kΩ	Ave I_{corr} using each I_{corr} (μA)	Ave I_{corr} using Average R_c GP (μA)	Ave I_{corr} using Average R_c LPR (μA)	I_{corr} last 3 (μA)	
SL-1	0.99	1.30	20.54	20.09	51.72	56.7	2.57
SL-2	1.44	1.02	25.92	25.66	33.89	22.7	1.32
SL-3	1.79	1.48	19.11	17.66	34.92	50.8	1.98
SL-4	17.24	5.27	6.71	4.96	4.13	2.64	0.83
SL-5	19.24	5.29	7.44	4.94	1.77	8.37	0.36
SL-6	6.55	3.35	7.95	7.80	6.33	15.93	0.81
SL-7	5.98	2.42	12.08	10.80	12.05	7.14	1.12
SL-8	6.51	1.70	17.20	15.35	7.72	7.48	0.50
SL-9	2.29	2.41	11.74	10.82	12.58	43.2	1.16
SL-10	2.04	1.84	14.88	14.17	28.87	21.8	2.04
SL-11	1.77	1.94	14.34	13.47	31.41	29.0	2.33

3.3.2 – FA single-rebar specimens.

General observations are based on R_c and E_{corr} magnitude. The rebar in the FA1 specimen was likely not corroding as indicated by the most recent rebar potential reading of –0.14 Vsce and an R_c > 6 kΩ. For the rebar in FA2, based on most recent E_{corr}, corrosion could be taking place, but an R_c >3 kΩ suggest that corrosion propagation was taking place at a very low corrosion rate (or small site) or that no corrosion was taking place. For the rebar in FA3, the most recent Ecorr suggests that corrosion was not taking place even though E_{corr} reached values as negative as –0.45 Vsce at an earlier date. The R_c value is now close to 3 kΩ, but previously it was as small as 0.75 kΩ.

The rebar in FA5 experienced a drop in rebar potential, but the measured R_c was not much different than before removing the electromigration. Initial R_c was about 3 kΩ, with most R_c values < 2 kΩ. The most recent R_c values ranged between 0.6 and 0.85 kΩ. The rebar potential decreased after the last electromigration period and remained there even when the current was applied, but starting on day 500, the rebar potential tended to increase; the recent E_{corr} was –0.328 V. The rebar in specimen FA6 experienced a rebar potential drop upon removing electromigration, then remained at E_{corr} of –0.45 V or more negative. The most recent E_{corr} was –0.32 V; recent Rc values showed an increase.

The R_c values measured on FA7 suggest that corrosion had been initiated. However, the most recent R_c value was greater than 2 kΩ. FA7 is an example of a rebar that experienced a potential transient shortly after removing the electromigration. The rebar potential moved towards more negative potential values. The R_c value also decreased significantly. The R_c values have oscillated over the last 500 days. Interestingly, the Rs increased with time until reaching 200

days of age, and then it remained around the same value. Rebar in sample FA8 showed a potential drop upon removing the electromigration. A small anodic current shifted the rebar potential to values close to –0.25 Vsce. The R_c oscillated some and the last few readings were smaller than 0.85 kΩ. The rebar in FA9 also experienced a potential drop shortly after removing the electromigration. However, the reduction in R_c was slower. After day 400 the E drifted toward more positive values reaching a rebar potential of 0.25. The rebar in samples FA10 showed a potential drop at around 180 days after removing the electromigration. The R_c value, however, initially experienced a drop, but later oscillated, with the last reading being ~3.8 kΩ. The rebar in FA11 did not experience a potential drop nor a decrease in R_c values.

It is important to mention that in all plots the rebar potential and other readings are influenced by the portion of the rebar not directly below the reservoir as well as any rebar outside of the concrete. In some cases, the moisture was so high that the portion of rebar outside of the concrete showed corrosion. The latter likely affected the rebar potential and the R_c readings.

Table 30. Average: R_s, R_c, and I_{corr} obtained from LPR and GP readings – FA specimens

	Average values from GP		GP	GP	LPR and EIS	LPR	
	R_s (kΩ)	R_c (kΩ)	I_{corr} (μA)	Ave I_{corr} (μA) using AveR_c	Ave I_{corr} (μA) using AveRc	I_{corr} last 3 (μA)	Ratio of Ave $I_{corr}LRPR_c$/ $I_{corr}GPR_c$
FA-1	6.23	4.96	5.38	5.27	6.77	7.66	1.29
FA-2	6.28	4.82	5.51	5.41	7.19	13.90	1.33
FA-3	2.96	1.74	19.56	14.97	20.36	14.67	1.36
FA-4	2.09	1.13	24.76	23.19	31.48	29.66	1.36
FA-5	2.38	1.60	16.58	16.28	20.03	38.42	1.23
FA-6	1.86	1.23	23.82	21.21	41.83	20.40	1.97
FA-7	1.87	1.59	16.85	16.42	16.28	11.66	0.99
FA-8	1.47	3.26	8.09	8.01	16.19	37.29	2.02
FA-9	1.81	1.75	15.52	14.95	18.97	24.54	1.27
FA-10	10.00	4.05	7.36	6.45	6.96	5.67	1.08
FA-11	20.84	10.50	3.28	2.49	2.85	3.85	1.15

Table 30 shows for FA single rebar the average R_s values obtained with the GP method, the average R_c values obtained with GP, and the I_{corr} obtained using the average R_cGP and the I_{corr} calculated using the average R_cLPR. The measurements taken March 2017 to May 2018 were included. The table includes the Icorr that is obtained by using each I_{corr} value rather than the average R_c value. For I_{corr} LPR the average I_{corr} over the last 3 measurements are also included. Finally, the rightmost column shows the ratio between the average I_{corr} LPR/average I_{corr} GP. The samples with the smaller (FA10 and FA11) reservoir had the largest R_s and smaller I_{corr}, the Icorr LPR values were 8 to 15 times greater than those measured with I_{corr} GP. Samples FA1 and FA2 had the next largest Rs, and the average Icorr GP and Icorr LPR were comparable. However, for

FA2 the average Icorr LPR of the last 3 readings was about twice the Icorr LPR using the readings over the last 400 days. The rebar with the largest average Icorr GP was FA4, but the one with the largest average Icorr LPR was FA6. The average Icorr LPR using the last 3 readings were comparable to the overall average Icorr GP.

3.3.3 – T1 and T2 single-rebar specimens.

Table 31 presents the average R_s, R_c, and Icorr from measurements taken over the last 400 days on T1 and T2 specimens. The values based on EIS/LPR and GP tests are both shown. In general, the average Icorr LPR tended to be larger than the Icorr GP regardless of the solution reservoir or if the samples was a T1 or a T2 sample. The average Rs tended to be slightly larger from readings taken using the GP tests. It is not clear what Icorr value Indicates that corrosion has initiated. Two samples were selected for forensic analysis based on the smaller average R_c value from each mix, samples T2–4, and T1–6. Sample T2–4 upon opening did not show corrosion within the rebar embedded in the concrete. The rebar of sample T1–6 showed no corrosion under the solution reservoir, but a small corroding site close to the concrete edge (see forensic analysis chapter). Both rebars showed some corrosion on the rebar surface that extended outside of the concrete.

Table 31. Average: R_s, R_c, and I_{corr} obtained from LPR and GP readings – T1 and T2 specimens

			LPR/EIS			GP
Sample	R_s kΩ	R_c kΩ	I_{corr} (μA)	R_s kΩ	R_c kΩ	Icorr (μA)
T2–1	6.3	2.4	12.0	7.3	3.7	7.6
T2–2	3.3	1.5	18.4	3.6	3.3	8.4
T2–3	7.1	2.6	12.2	8.1	5.1	5.4
T2–4	4.0	1.5	19.1	4.3	3.2	8.8
T2–5	6.8	3.3	8.5	7.6	6.6	4.0
T1–6	2.1	0.6	50.8	2.4	0.9	28.2
T1–7	5.1	2.1	15.1	5.9	4.3	6.2
T1–8	2.2	0.8	34.0	2.3	1.5	18.2
T1–9	2.6	0.9	33.8	2.9	1.7	16.3
T1–10	5.9	2.6	10.4	6.9	4.6	5.8
T2–11	3.3	2.1	13.1	3.7	5.3	5.0

3.3.4 – Comparing I_{corr} measured on three-rebar specimens.

The summary in Table 32 presents the average R_s, average R_c and average I_{corr} measured using the GP method on three-rebar specimens. Each row shows the values for rebars A, B and C. Table 33 presents a similar summary for average R_s, average R_c and average I_{corr}, obtained from EIS/LPR tests. Table 33 also includes the average rebar potential measured over the last 400 days. The average Icorr from EIS/LPR was larger than the average Icorr from GP for most rebars regardless of the solution reservoir length or the mix composition. When grouping the values of SL rebars in Table 32, the average Icorr of the nine rebars with a 2.5-cm reservoir was 15.7 μA,

for those with 5-cm reservoir length it was 15.4 μA, for those with 10-cm reservoir length it was 9.3 μA, and for those with a 15 cm solution reservoir it was 18 μA. However, if the maximum average Icorr within each group is evaluated, then the max Icorr was 23.9 μA for rebar 9X–A (2.5 cm), 28.3 μA for rebar 17X–A (5 cm), 16.6 μA for rebar 6X–A (10 cm) and 43.7 μA for rebar 4X–C (15-cm reservoir length). Table 33 shows similar trends for the Icorr values measured via LPR/EIS testing. The maximum average Icorr was measured on 17X–A rebar (89.5 μA, 5-cm reservoir), this value is 3.1 times the average Icorr measured via GP. The second largest average Icorr was measured on rebar 4X–C with an average Icorr of 82.5 μA, and it's 3 times larger than the values measured using the GP method. The ratio between Icorr values for 3-rebar specimens is shown in Table 34. It can be observed that the ratio was almost 1 to 1 in some cases, and in a few instances, the average Icorr from GP (e.g., 7X–A) was slightly larger than the Icorr from LPR/EIS. The average current for FA 3-rebar specimens are also shown in Table 32 (GP) and Table 33 (LPR/EIS) similar trends are observed, the maximum current measured using the GP method was 24.5 μA (14X–A) via GP and using LPR/EIS it was 65.1 μA (24X–B) both have a 15 cm long solution reservoir. The average I_{corr} are also shown for the T1 3-rebar and T2 3-rebar specimens, with the maximum and average I_{corr} values being somewhat smaller than those observed on SL and FA specimens.

Based on the rebar potential, there is one specimen that appears to have a more negative value within a given solution reservoir length. The sample with the more negative potential typically has a larger average Icorr (and corresponding lower average R_c). In most instances, the average Icorr from GP measurements is significantly smaller than the average I_{corr} calculated using EIS/LPR tests.

A wide range of Rs values was observed for samples of the same mix and same solution reservoir length. For example for samples with 5-cm long reservoir, the Rs between the concrete surface and rebar 17X–B was 0.82 kΩ, whereas the Rs was 2.1 kΩ for rebar 1X–A. This in part could be explained by the difference in duration of the electromigration, and that the humidity could vary from container to container (humidity chamber). It could also be influenced by the concrete heterogeneity.

The average rebar potential shown in Table 33, suggests that most rebars are in an active state, albeit with different degrees of activity taking place. There are a number of samples that have a rebar potential more positive than –0.2 Vsce (or –0.27 Vcse), which under atmospheric conditions would suggest only a small probability of active corrosion. A good number of rebars have rebar potential ranging between –0.2 and –0.3 Vsce, a third set has values that range between –0.3 and –0.4 Vsce and a fourth group has rebar potential values more negative than –0.4 Vsce. Reinforced concrete undergoing corrosion exposed to atmospheric conditions would suggest that the more negative the potential the more active the corrosion is. However, in our experiment, the moisture content (relative humidity in the chamber) was in some cases close to 100% RH, and hence with time, oxygen mass control limitations might have developed at the rebar depth. This might be what took place on instances in which the rebar potential was more negative than –0.5 Vsce. For the three rebar specimens, the coupling with the region not directly under the solution reservoir might have different rather than similar coupling interactions such as what took place on the single rebar specimens. The volume of concrete under high moisture conditions was likely quite different. An indirect measure of the different moisture was obtained

by comparing the Rs values measured on single rebar specimens vs. three rebar specimens for samples with the same solution reservoir length.

Table 32. Average: R_s, R_c, and I_{corr} obtained from GP readings – three-rebar specimens

		GP								
Reservoir Length	Sample	Rebar A			Rebar B			Rebar C		
		R_s	R_c	I_{corr}	R_s	R_c	I_{corr}	R_s	R_c	I_{corr}
2.5	2X–SL	2.45	1.68	12.8	2.07	2.04	13.0	2.39	2.65	10.1
2.5	19X	1.58	1.15	22.9	2.21	2.63	10.2	1.73	2.44	11.5
3	9X	2.04	1.35	23.9	1.95	1.53	19.4	2.18	1.72	17.4
5	1X	2.10	2.06	13.5	1.88	2.97	9.1	2.00	1.99	13.8
5	16X	1.59	2.81	9.3	1.38	8.85	11.8	1.40	2.86	9.8
5	17X	0.87	1.06	28.3	0.82	1.48	18.9	0.94	1.15	23.8
10	3X	1.07	3.89	6.8	0.89	3.52	7.5	1.03	3.81	6.9
10	6X	0.91	1.59	16.6	0.78	3.19	8.2	0.91	1.99	13.9
10	8X	1.15	3.24	8.2	0.90	3.31	7.9	1.07	3.95	6.7
10	15X	0.91	2.93	9.7	0.83	2.67	10.1	0.96	2.99	9.0
15	4X	0.80	1.69	15.8	0.73	1.25	22.9	0.74	0.63	43.7
15	22X–SL	1.05	2.81	10.0	0.96	3.49	7.5	1.07	3.26	8.1
2.5	5X–FA	2.79	4.20	6.3	2.14	4.04	6.5	2.69	4.17	6.3
2.5	10X	2.42	4.90	5.4	1.82	3.96	6.7	2.05	3.70	7.3
2.5	11X	2.04	2.39	16.3	1.82	3.31	8.9	2.17	3.20	9.1
5	7X	2.60	3.04	12.9	2.13	3.08	8.6	2.30	3.36	7.8
5	12X	1.07	1.53	19.4	1.04	1.79	15.2	1.15	1.70	17.3
5	23X	1.29	2.59	11.2	1.20	2.23	11.8	1.23	2.24	11.8
10	13X	1.45	2.07	17.2	1.34	2.05	14.3	1.67	3.08	10.0
10	20X	1.54	3.81	8.1	1.42	2.80	10.5	1.81	2.64	11.5
10	21X	0.99	1.90	18.0	0.92	1.65	19.4	0.98	1.66	18.8
15	14X	0.67	1.14	24.5	0.70	1.62	17.2	0.70	1.76	15.2
15	18X	0.90	3.36	8.1	0.89	3.80	7.1	0.98	3.99	6.8
15	24X–FA	0.69	2.00	13.6	0.65	1.44	19.2	0.71	1.79	15.4
2.5	26X–T1	3.11	1.89	16.2	2.67	1.82	17.4	2.93	2.25	13.1
5	25X	2.21	1.36	19.5	2.02	1.48	17.9	2.12	1.39	20.5
5	28X	2.10	0.39	6.9	2.46	3.37	7.8	2.73	3.64	7.4
10	27X–T1	1.71	1.37	19.7	1.75	1.34	20.8	1.93	1.27	22.0
2.5	30X–T2	4.28	3.52	7.6	3.92	4.45	5.9	4.45	3.95	6.8
5	31X	3.54	2.94	9.3	3.31	2.38	12.0	3.55	4.73	5.5
5	32X	3.49	2.55	11.7	3.18	2.57	11.3	3.43	2.35	12.8
10	29X–T2	2.55	1.57	17.3	2.42	3.09	8.5	2.57	3.86	6.8

Note: R_s and R_c units in kΩ, I_{corr} in μA

Table 33. Average: R_s, R_c, and I_{corr} obtained from EIS/LPR readings – three-rebar specimens

LPR												
Sample	Rebar A				Rebar B				Rebar C			
	R_s	R_c	I_{corr}	OCP	R_s	R_c	I_{corr}	OCP	R_s	R_c	I_{corr}	OCP
2X	1.55	1.54	17.0	–0.296	1.39	1.70	15.3	–0.374	1.66	2.01	13.0	–0.290
19X	1.39	0.47	55.1	–0.416	1.35	0.73	35.7	–0.348	1.47	0.71	36.6	–0.324
9X	1.68	0.80	32.4	–0.411	1.63	0.79	33.1	–0.412	1.77	1.07	24.4	–0.383
1X	1.55	0.93	28.0	–0.373	1.47	1.06	24.6	–0.274	1.51	1.00	26.1	–0.308
16X	1.22	1.13	23.1	–0.279	1.09	0.80	32.5	–0.375	1.22	1.21	21.7	–0.256
17X	0.80	0.29	89.1	–0.486	0.75	0.38	69.6	–0.480	0.81	0.47	55.4	–0.411
3X	0.81	1.57	16.6	–0.164	0.69	1.02	25.7	–0.168	0.81	1.75	14.9	–0.210
6X	0.81	0.48	54.4	–0.459	0.69	0.60	43.8	–0.340	0.84	0.42	62.0	–0.435
8X	0.87	1.09	24.0	–0.224	0.76	1.06	24.6	–0.221	0.84	1.45	18.1	–0.265
15X	0.71	0.58	44.9	–0.252	0.70	0.54	48.8	–0.265	0.77	0.59	44.2	–0.294
4X	0.64	0.54	48.0	–0.296	0.58	0.43	61.3	–0.349	0.61	0.32	82.5	–0.434
22X	0.84	0.96	27.3	–0.212	0.78	0.80	32.8	–0.239	0.84	0.87	29.9	–0.208
5X	2.15	2.07	12.6	–0.205	1.67	1.88	13.9	–0.195	2.05	2.20	11.9	–0.219
10X	1.86	1.71	15.3	–0.222	1.43	1.22	21.4	–0.232	1.69	1.71	15.3	–0.269
11X	1.70	0.86	30.5	–0.328	1.57	0.94	27.8	–0.293	1.83	1.02	25.5	–0.299
7X	1.68	2.21	11.8	–0.284	1.35	2.26	11.6	–0.284	1.52	2.23	11.7	–0.260
12X	0.92	0.43	60.8	–0.455	0.89	0.44	59.0	–0.365	0.98	0.46	56.3	–0.379
23X	1.12	0.60	43.8	–0.357	1.04	0.55	47.4	–0.371	1.06	0.77	33.8	–0.369
13X	1.08	0.79	33.2	–0.270	0.98	0.78	33.5	–0.323	1.14	1.21	21.6	–0.299
20X	1.05	1.26	20.8	–0.255	0.96	1.02	25.7	–0.303	1.10	1.34	19.4	–0.318
21X	0.84	0.53	49.7	–0.377	0.79	0.79	32.9	–0.417	0.82	0.53	49.3	–0.453
14X	0.55	0.62	41.9	–0.501	0.58	0.93	28.2	–0.531	0.59	0.71	37.0	–0.383
18X	0.72	0.68	38.2	–0.273	0.71	0.67	38.8	–0.233	0.81	0.67	38.7	–0.230
24X	0.60	0.53	49.7	–0.434	0.60	0.40	65.1	–0.416	0.63	0.53	49.0	–0.421
26X	2.44	1.11	23.42	–0.46	2.15	0.95	27.62	–0.37	2.35	1.07	24.47	–0.29
25X	1.94	0.75	34.63	–0.48	1.86	0.71	36.56	–0.46	1.91	0.77	34.05	–0.43
28X	2.21	1.82	14.37	–0.21	2.10	1.47	17.79	–0.18	2.28	2.05	12.71	–0.21
27X	1.50	0.66	39.56	–0.51	1.54	0.66	39.67	–0.5	1.74	0.76	34.36	–0.47
30X	3.85	1.74	15.04	–0.28	3.54	2.18	11.95	–0.27	4.14	2.05	12.73	–0.29
31X	3.15	1.34	19.5	–0.34	2.95	1.31	19.92	–0.31	3.03	2.44	10.68	–0.29
32X	3.10	1.25	20.81	–0.45	2.89	1.38	18.97	–0.46	3.06	1.45	17.97	–0.47
29X	2.29	0.87	29.86	–0.47	2.19	1.26	20.7	–0.31	2.26	1.55	16.82	–0.25

Note: R_s and R_c units in kΩ, I_{corr} in μA

Table 34. Ratios R_sEIS/R_sGP and I_{corr}LPR/I_{corr}GP – three-rebar specimens

Sample	Ratio of R_sEIS/R_sGP			Ratio I_{corr} LPR/GP		
	Rebar A	Rebar B	Rebar C	Rebar A	Rebar B	Rebar C
2X	0.63	0.67	0.69	1.33	1.18	1.29
19X	0.88	0.61	0.85	2.40	3.51	3.18
9X	0.82	0.84	0.81	1.36	1.71	1.40
1X	0.74	0.78	0.76	2.07	2.70	1.89
16X	0.77	0.79	0.87	2.48	2.75	2.21
17X	0.91	0.92	0.86	3.14	3.68	2.33
3X	0.76	0.77	0.79	2.46	3.45	2.17
6X	0.89	0.88	0.93	3.27	5.34	4.45
8X	0.76	0.85	0.79	2.94	3.11	2.68
15X	0.78	0.83	0.81	4.65	4.81	4.91
4X	0.80	0.80	0.82	3.03	2.68	1.89
22X	0.80	0.80	0.79	2.74	4.36	3.71
5X	0.77	0.78	0.76	2.02	2.13	1.89
10X	0.77	0.78	0.83	2.85	3.21	2.09
11X	0.83	0.87	0.84	1.87	3.13	2.80
7X	0.65	0.63	0.66	0.91	1.35	1.50
12X	0.86	0.85	0.85	3.14	3.87	3.26
23X	0.87	0.87	0.87	3.90	4.01	2.86
13X	0.74	0.73	0.68	1.93	2.34	2.15
20X	0.68	0.68	0.60	2.56	2.44	1.69
21X	0.85	0.85	0.84	2.76	1.70	2.62
14X	0.82	0.83	0.84	1.71	1.64	2.44
18X	0.80	0.80	0.83	4.72	5.44	5.68
24X	0.87	0.92	0.88	3.64	3.39	3.19
26X	0.79	0.81	0.80	1.45	1.59	1.87
25X	0.88	0.92	0.90	1.78	2.04	1.66
28X	1.05	0.85	0.83	2.07	2.28	1.73
27X	0.88	0.88	0.90	2.01	1.91	1.56
30X	0.90	0.90	0.93	1.98	2.03	1.86
31X	0.89	0.89	0.85	2.11	1.66	1.93
32X	0.89	0.91	0.89	1.78	1.68	1.40
29X	0.90	0.90	0.88	1.73	2.43	2.48

3.4 – Tombstone specimens (SL and FA)

Figure 63 shows the potential evolution for the two SL tombstone specimens and Figure 64 shows the potential evolution for the two FA specimens. Figure 65 shows the delta V measured across the resistor between the middle and left or right rebar for each of the SL specimens; a similar plot is shown in Figure 66 for the FA specimens. The shown values suggest that a transition from initially negative values toward more positive values was observed on all samples, then a plateau with a small oscillation was observed. The interconnected rebar potential values for SL samples are between 0 mVsce and –140 mVsce. On FA specimens the interconnected rebar potential values during recent readings are between +20 mVsce and –114 mVsce. This suggests that corrosion is not taking place.

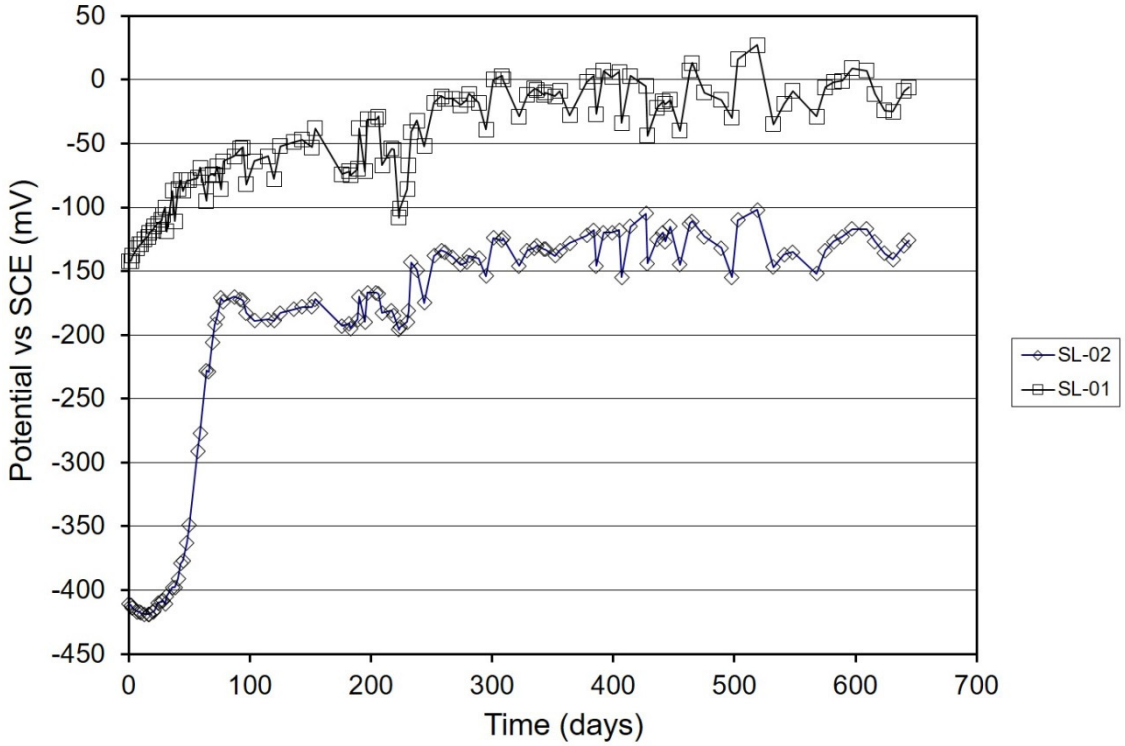

Figure 63. Rebar potential evolution on SL tombstone specimens

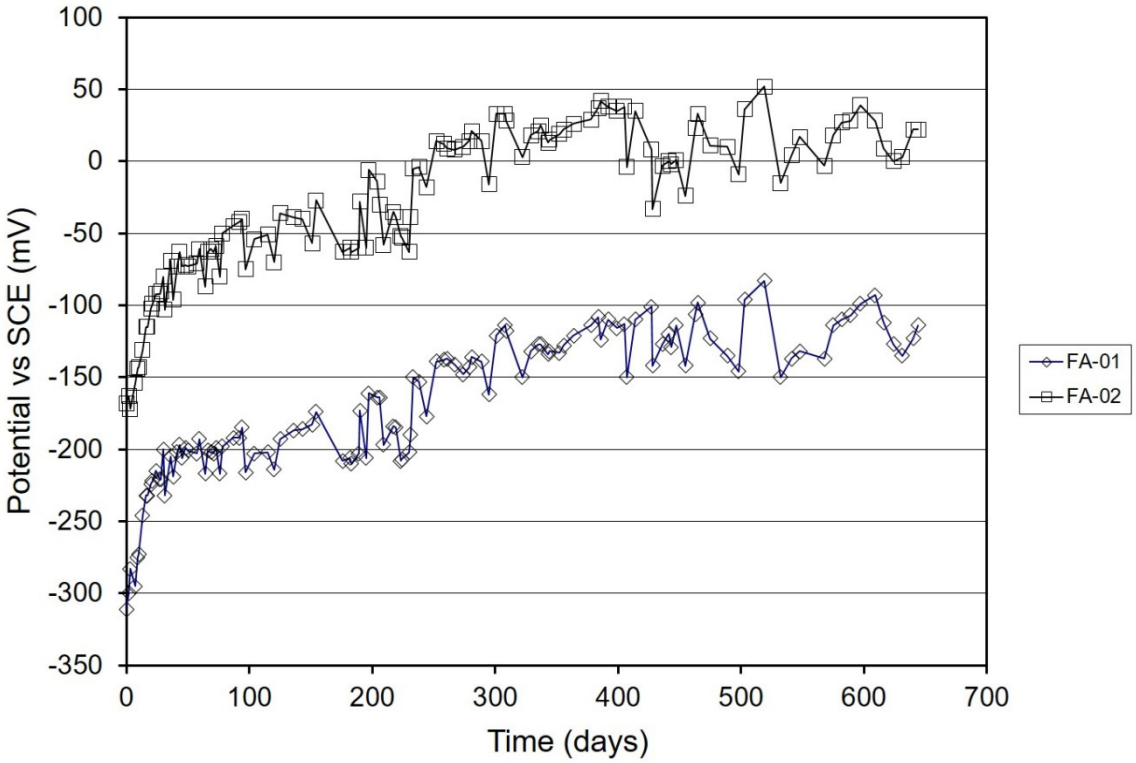

Figure 64. Rebar potential evolution on FA tombstone specimens

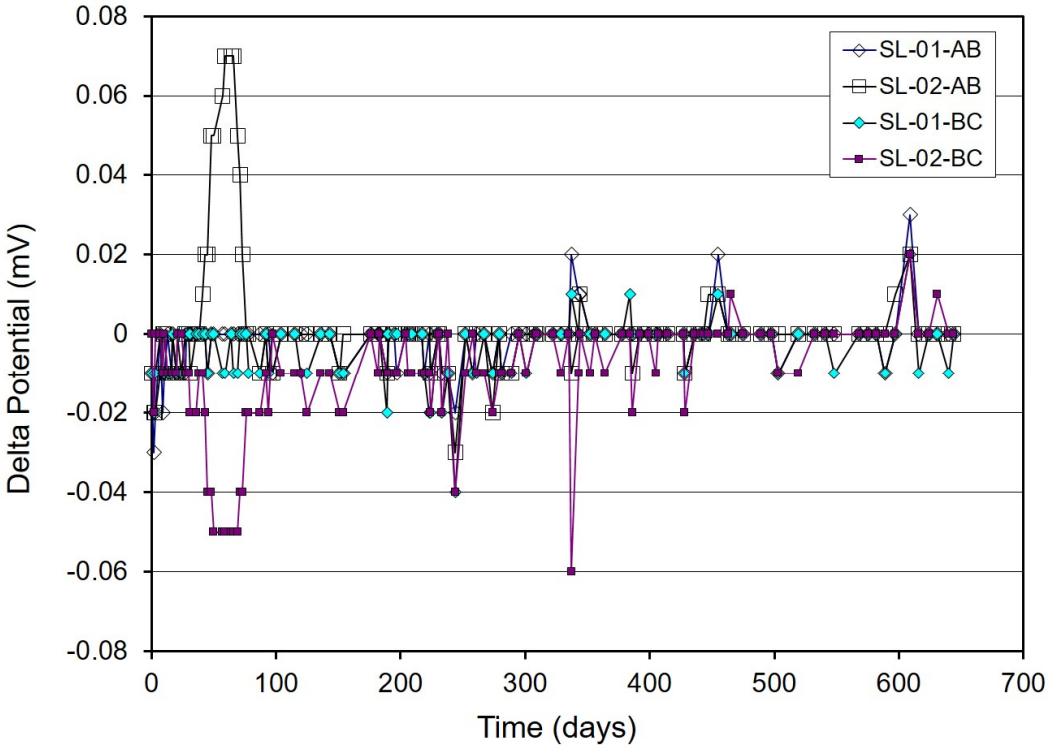

Figure 65. Delta potential measured across resistors on SL specimens

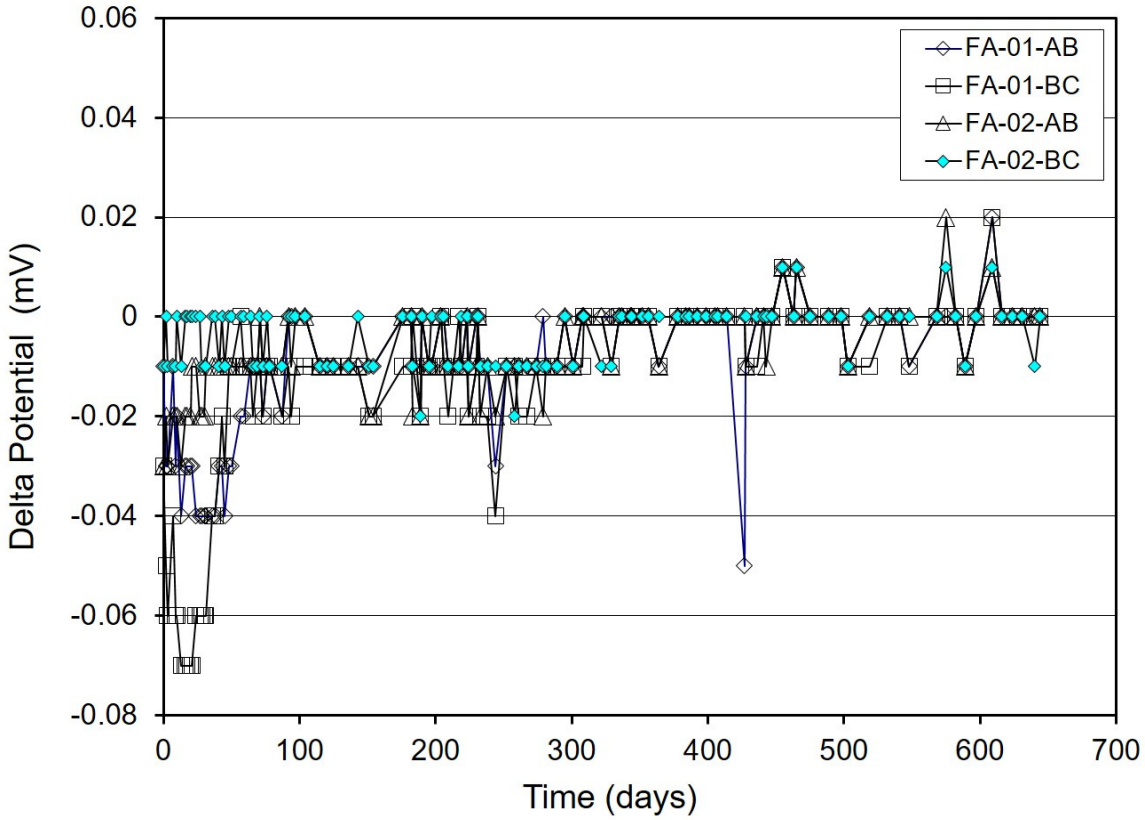

Figure 66. Delta potential measured across resistors on FA specimens

3.5 – Gecor 8 measurements on selected lab specimens (indoors)

The corrosion rate was measured using the Gecor 8 on several MD specimens with a solution reservoir large enough to accommodate probe B of the instrument. Probe B is a rectangular probe that was used when the reinforced concrete was immersed (in this case ponded). Additionally, it was used in January 2018 as well as prior to terminating some of the single rebar specimens with a 5 cm concrete cover. The corrosion rate was also measured with the Gecor 8 and the probe B. For the latter samples, which were tested in January 2018, the solution reservoir was removed and then re–installed. Figure 67 shows a plot that presents the rebar corrosion potential vs. corrosion rate and Figure 68 shows a plot that presents the resistivity vs. corrosion rate. At a given potential there is a range of i_{corr} values that were observed: for example at –0.250 Vcse, the corrosion rate ranged between 0.3 and 2 μA/cm^2. This could be in part due to the fact that electromigration (i.e., chloride transport) was localized on some of these samples, and hence the corroding area might be smaller than the area confined by probe B. All rebars had an i_{corr} greater than 0.3 μA/cm^2. This suggests that active corrosion is taking place on all samples or an electrochemical reaction is taking place at a measurable rate. Figure 68 suggests that there is a better correlation between the resistivity and the corrosion rate, i.e., there is not as much scatter. Although, in this case, one device measured both parameters.

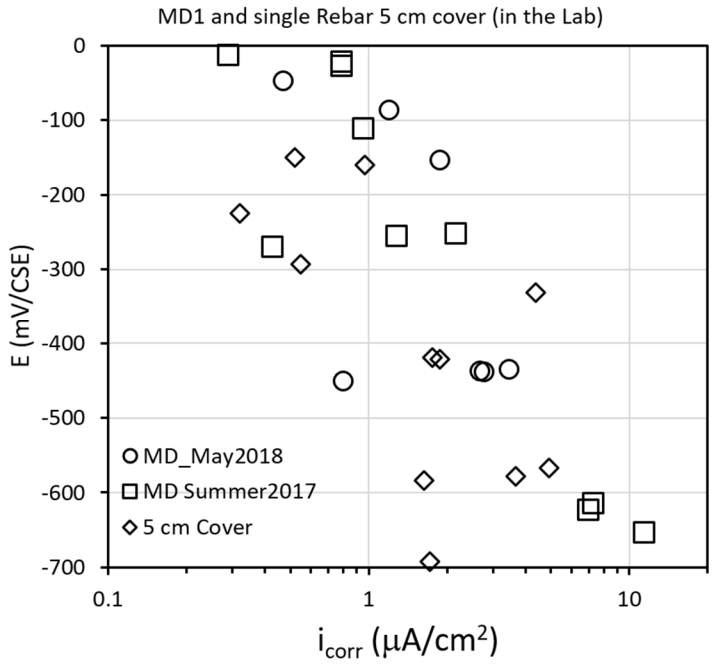

Figure 67. E_{corr} vs. i_{corr} measured on MD and 5-cm concrete cover specimens

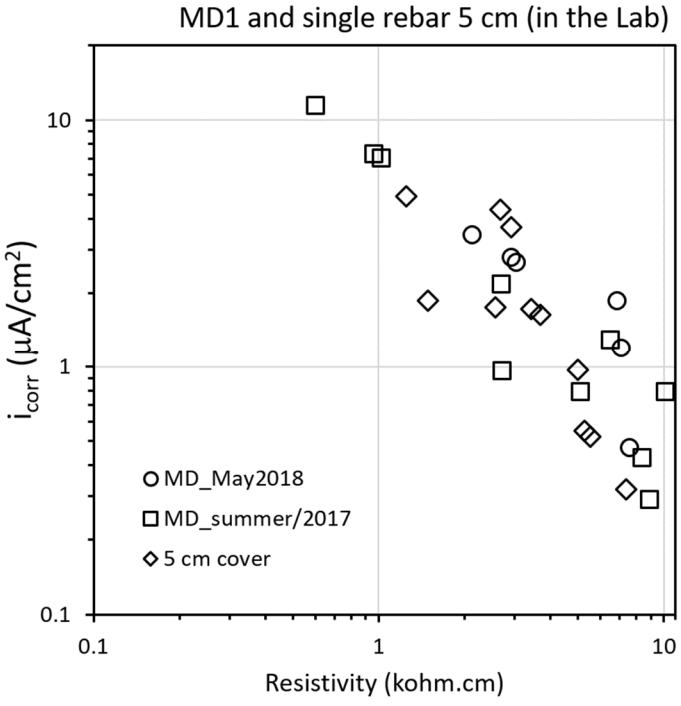

Figure 68. i_{corr} vs. resistivity measured on MD and 5-cm concrete cover specimens

3.6 – Gecor 8 measurements on selected specimens exposed outdoors

Figure 69 shows the rebar potential and i_{corr} measured on samples exposed outdoors that were subjected to electromigration. These measurements were performed on the modified tombstone specimens (6 rebar specimens or 2 rebar specimens) several months after stopping the electromigration. Probe B of the Gecor 8 was used, and in most cases, a wet sponge was used in between the probe and the concrete. The reservoirs were removed to accommodate the length of probe B. The electrochemical measurements were performed both on the top row and bottom row of rebars. The top row of the 6 rebar–specimens have a cover of 3 cm (1.25 inch) and the bottom row has a cover of approximately 14 cm (5.5 inches). For the second–row rebars, part of the applied current during the test might have been diverted to the rebar(s) on the top row. The two rebar specimens were measured on the side with a cover of 5 cm (2 inches), but migration took place on the side with a cover of 7.5 cm (3 in.). Regarding the corrosion current values shown in Figure 69, there are several cases in which the value was negligible and it has been plotted as 0.01 μA/cm^2 values. A second group corresponds to values that ranged between 0.03 and 0.07 μA/cm^2. These correspond to second–row rebars, for which corrosion might just be initiating. There is another cluster of corrosion rate values that ranged between 0.3 and 2 μA/cm^2 with rebar corrosion potentials that ranged between –200 mVcse and –350 mVcse. Six rebars were from the top row of SL and FA modified tombstone specimens and the other five rebars corresponded to the bottom row. About two cm of each sample was immersed in water and thus the moisture content on the concrete bottom portion might be higher than the top section.

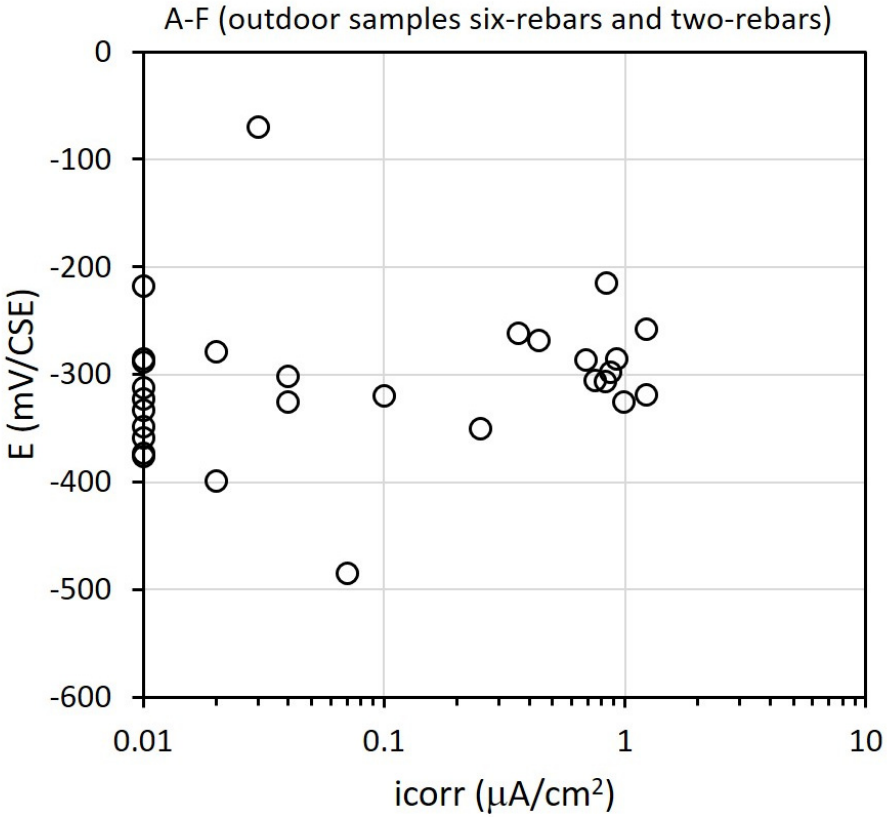

Figure 69. E_{corr} vs. i_{corr} measured on modified tombstone specimens exposed outdoors

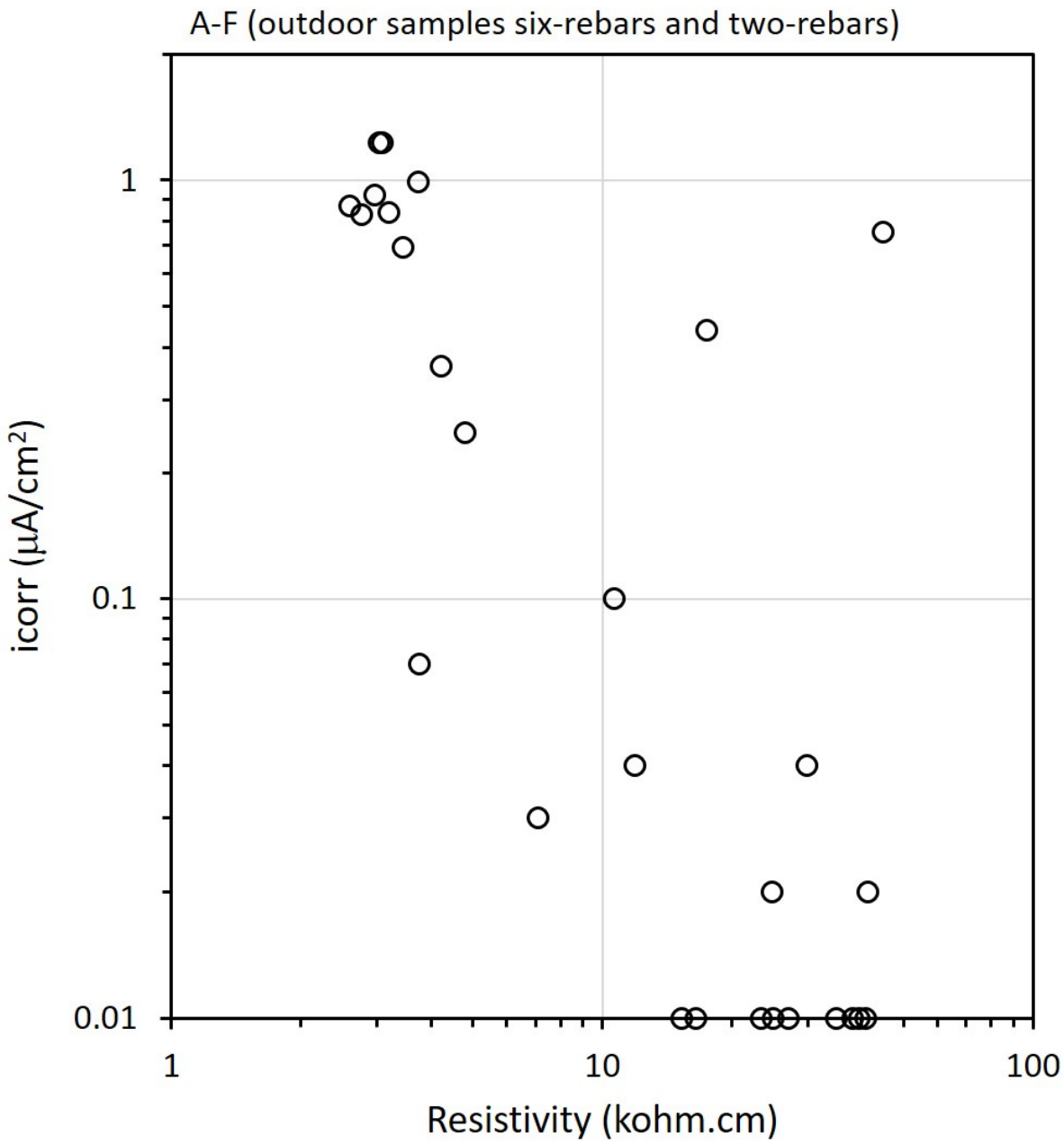

Figure 70. Resistivity vs. i_{corr} measured on modified tombstone specimens exposed outdoors

Figure 70 shows resistivity vs. i_{corr} measured using the Gecor 8 on rebars embedded on the modified tombstone specimens stored outdoors. Twelve of the rebars that had a corrosion rate greater than 0.3 µA/cm^2, ten of these rebars had resistivity values that ranged between 2 and 5 kΩ.cm and the other two had resistivity values greater than 10 kΩ.cm. The rebars with corrosion rates between 0.02 µA/cm^2 and 0.1 µA/cm^2 had resistivity values that ranged between 4 and 50 kΩ.cm. The rebars that have a negligible corrosion rate had resistivity values that ranged between 15 and 40 kΩ.cm.

3.7 – Calculated mass loss

The values shown in Table 35 present the calculated mass loss estimated from R_c values obtained after EIS/LPR measurements on 5 cm concrete cover specimens subjected to electromigration for 400 days and monitored for approx. 2200 days after that. The mass values were calculated by using Faraday law and R_cLPR values to estimate corrosion current. Then these corrosion current values are converted to charge and integrated to calculate the estimated mass loss. 1F1, 1B1 and 2D2 were samples terminated. The actual mass loss on these three rebars was smaller than predicted by Faraday's law.

Table 35. Estimated mass loss using Faraday law and R_cLPR values (up to 5/30/18)

	Mass grams		Mass grams
1B1	3.7	1F1	8.6
1C1	2.8	1F2	5.0
1C2	2.9	1G2	2.4
2D2	5.3	1G1	2.3

Chapter 4 – Results of Outdoor Samples

4.1 – Five-rebar specimens

The rebar corrosion potential vs. time for specimens that have been exposed outdoors to seawater for over 24 years have been reported in the past(F Presuel-Moreno et al. 2013) (previous research up to 18 years). A set of updated plots for samples available at the beginning of the current project are included in appendix H. The rebar potential shown on the appendix plots are vs. saturated calomel electrode, whereas rebar potential on the plots shown below is vs. copper sulfate electrode. Starting in February of 2017 measurements were performed with the Gecor 8 as described in the experimental section. This chapter describes how the corrosion rate, rebar corrosion potential, and resistivity correlated and changed over time. Eight sets of measurements were performed, the results of these measurements are presented below. The plots shown in the next few figures merged all readings as one series.

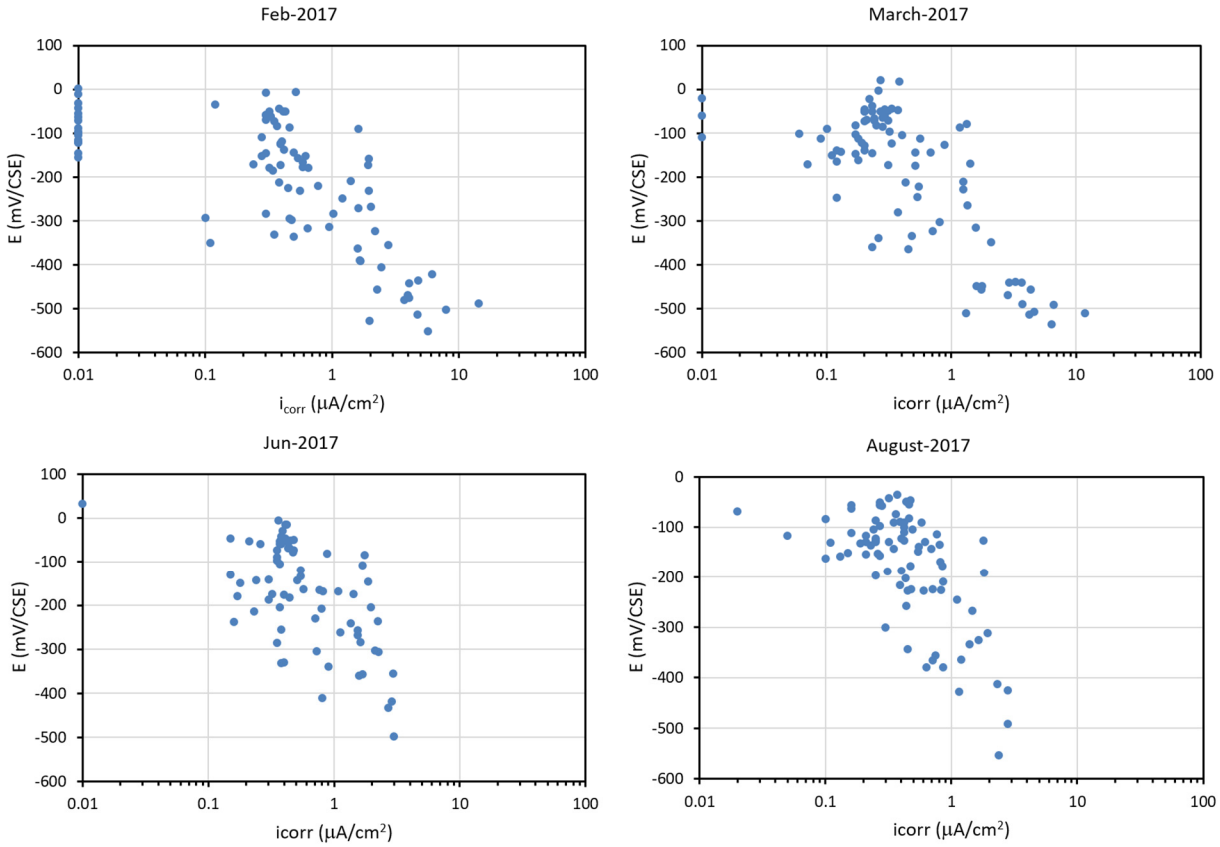

Figure 71. Rebar potential vs. corrosion current density measured on five-rebar samples.

Figure 71 shows four plots of i_{corr} vs. rebar potential measured with the Gecor8. There were several rebars that had a corrosion rate that was either 0.01 or smaller (reported as zero by the device) during the readings performed in February and March 2017. The values reported by the device as zero were plotted as 0.01 µA/cm^2, to visualize them in the log10 scale. These rebars had potential values that ranged between 10 mVcse and –160 mVcse. The number of rebars with such small corrosion current decreased from February to March 2017. It is possible that this is due to warmer temperatures in March. Interestingly, there were also a number of rebars that had

similar rebar potential but that show corrosion current density values that were greater than 0.1 μA/cm^2. There are several rebars that had potentials more negative than –400 mVcse and these typically had the largest corrosion current density. A number of these rebars with potentials more negative than –400 mV were terminated after March 2017, and hence they no longer appear on the plots corresponding to the months of June and August 2017. During the June readings, there was only one rebar with an i_{corr} of 0.01 μA/cm^2. The rest of the rebars had a corrosion rate that ranges between 0.1 and 3 μA/cm^2. Figure 72 shows the evolution of the rebar corrosion current density for tests performed in October 2017, January, March and May 2018. The potential values of the rebar spread over the same range, but the corrosion current density tended to shift toward larger values on the more recent two sets of readings. It is important to note that there is quite a bit of scattering on all the plots shown in Figure 72.

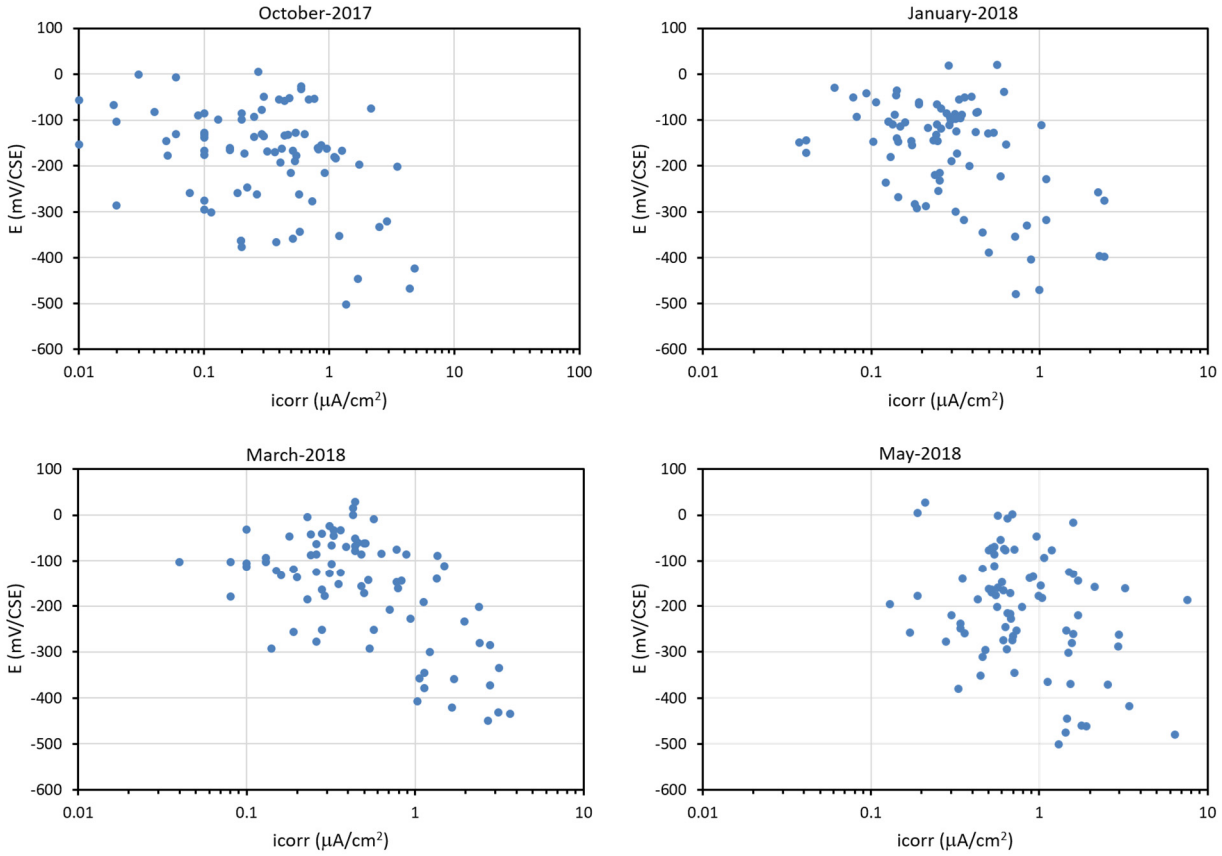

Figure 72. Rebar potential vs. corrosion current density measured between October 17 and May 18

Figure 73, Figure 74, Figure 75 and Figure 76 show plots of i_{corr} vs. resistivity measured on 5-rebar specimens. Only the rebars on the top row were measured. Figure 73 shows the data for the readings performed February and March 2017. There appears to be a good correlation for corroding rebars between the resistivity and i_{corr}. There were a number of rebars that had negligible i_{corr} with resistivity values that ranged between 5 and 45 kΩ.cm. Both sets of data appear to have a good correlation when only corroding rebars are included.

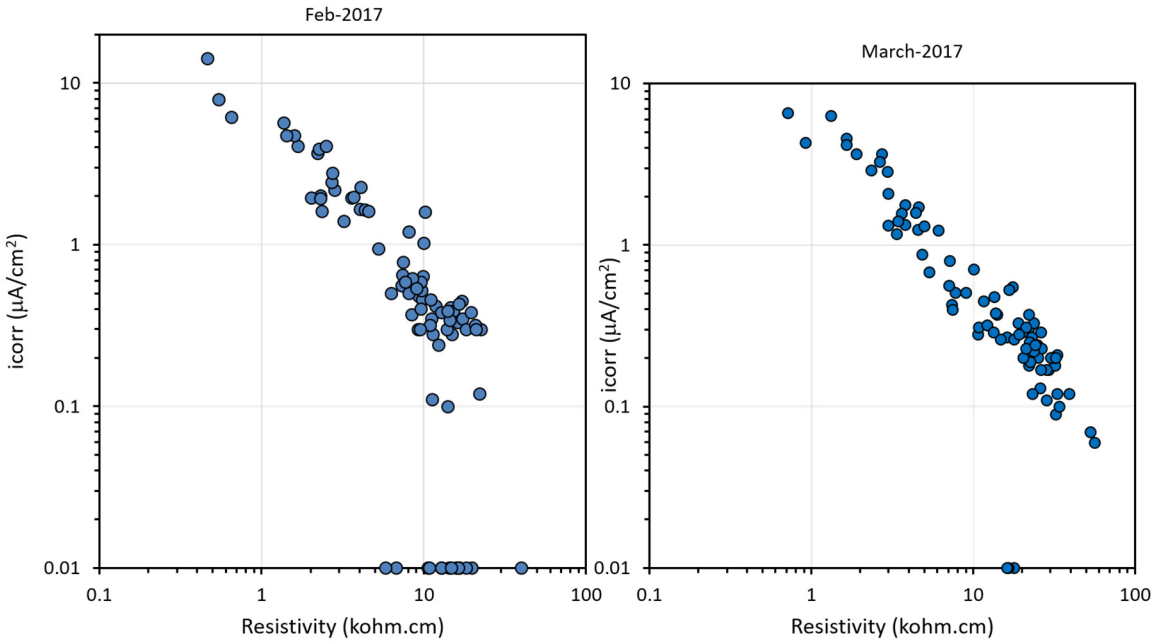

Figure 73. Rebar corrosion rate vs. resistivity measured in February and March 2017

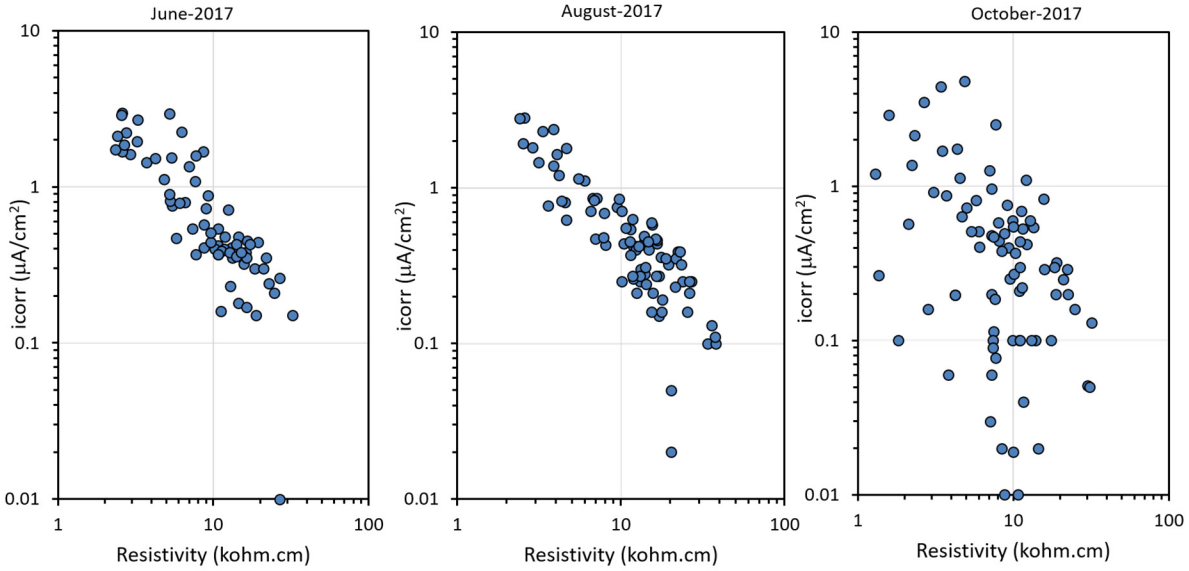

Figure 74. Rebar corrosion rate vs. resistivity measured between June and October 2017.

Figure 74 shows the data set for readings performed in June, August, and October of 2017. As time progressed there appears to be an increase in the scatter, particularly for the set of readings done during October 2017 (although this set includes 12 rebars for samples that were subjected to electromigration (on a 10 cm wide strip, i.e., the smaller length of the solution, reservoir and electromigration was applied from mid–June 2016 to early October 2017). No readings were taken with the Gecor 8 on these samples while under electromigration. The polycarbonate strips

(that allow for a smaller reservoir) were removed shortly before the measurements with the Gecor 8 were performed. During the measurements in June, the resistivity ranged between 2 and 30 kΩ.cm and the i_{corr} values ranged between 0.1 and 3 μA/cm^2. By August the resistivity range did not change, but the i_{corr} now ranged from 0.02 to 3 μA/cm^2. The low end of the resistivity range decreased on the readings taken in October, but the scatter in corrosion rate was significantly increased. Due to the storms that took place during Fall of 2017 the seawater in the reservoir was not replaced as regularly as during the spring and summer months.

Figure 75 shows the last three sets of readings. The set of values taken during January 2017 were affected by a cold front (i.e., morning temperature ranged between 55F and 65F), i.e., a somewhat lower temperature. This is reflected in the data showing larger resistivity values. The resistivity in a few samples reached values larger than 100 kΩ.cm. The readings performed in March had a lower range of resistivity values and a few more rebars had a higher corrosion rate than what was observed on the two previous sets of readings. By May 2018 the resistivity measured ranged between 1 and 30 kΩ.cm and the corrosion rate ranged between 0.1 and 8 μA/cm^2.

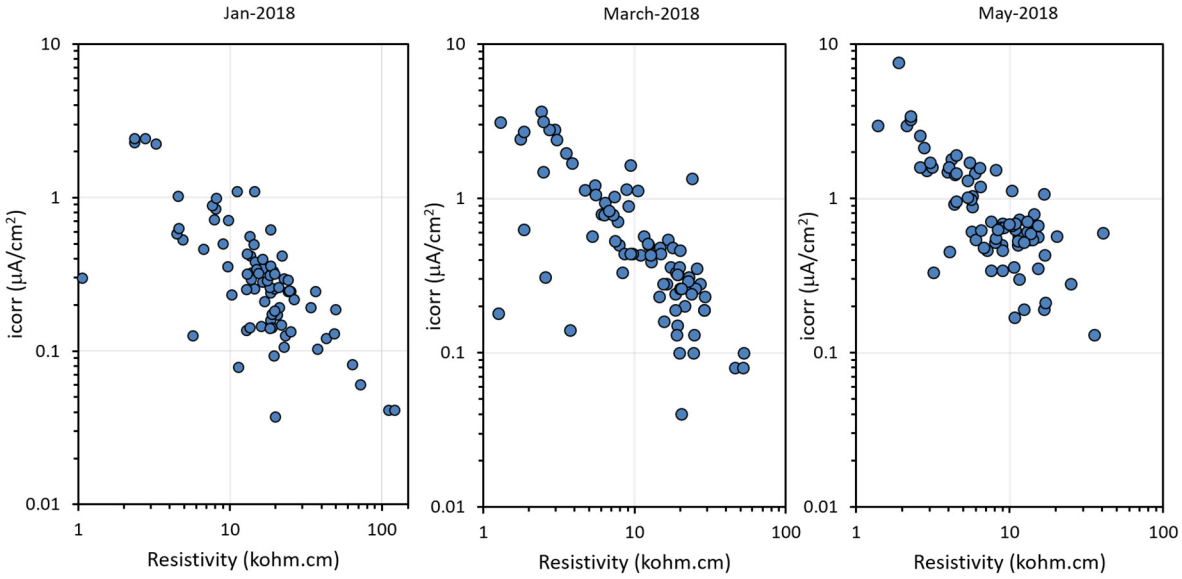

Figure 75. Rebar corrosion rate vs. resistivity measured between January and May 2018.

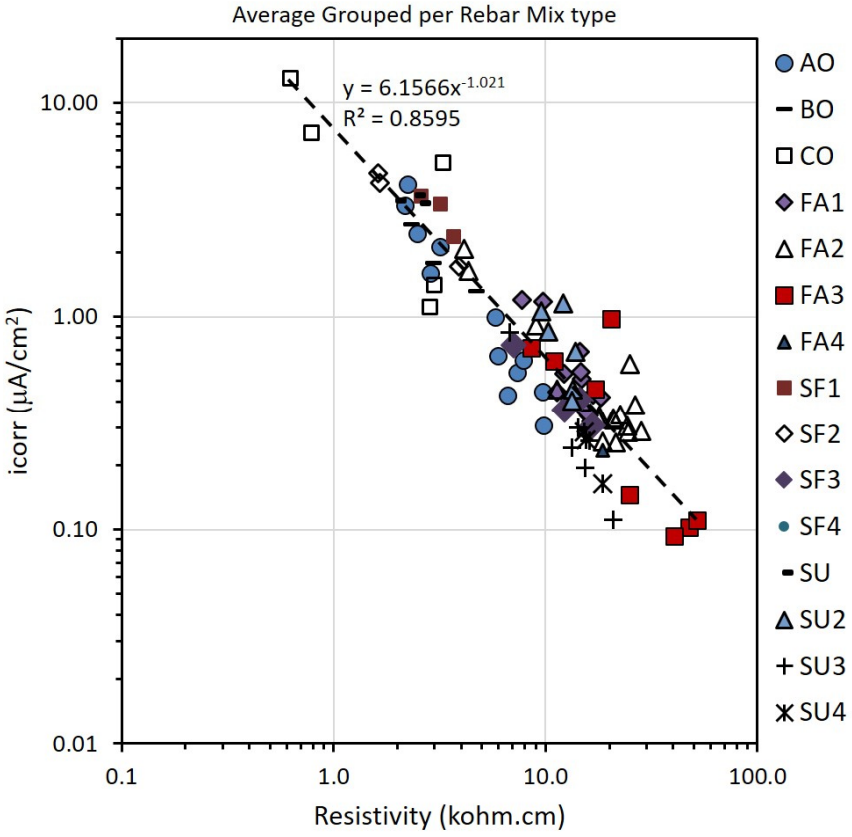

Figure 76. Average i_{corr} vs. average resistivity grouped per mix type

Figure 76 shows the average of the resistivity and average i_{corr} measured on a given rebar, but the data was grouped per concrete mix. It presents the average corrosion rate vs. average resistivity measured on each rebar from the outdoor specimens. The plot also includes the average values for the rebars that were terminated. It includes the values for five mixes not mentioned before; no documentation was found identifying the composition of these specimens. It appears that rebars embedded in BO mix are similar to either AO or CO, based on where their resistivity and i_{corr} values are located in the plot. The data for SU samples appear to be close to the data for SF1 and some of the AO values. SU2, SU3 and SU4 rebars appear to have a resistivity that is comparable to the resistivity of FA samples and those with higher amounts of SF. The spread/scatter of the resistivity vs. i_{corr} observed in previous plots is not as large in this plot. Rebars with average current densities larger than 1 were from mixes CO (5), AO (6), BO (3), SF1 (3), SF2 (3), SU (3), SU2 (2), FA1 (2), FA2 (2). It is important to note that a good number of samples were terminated at 17 years of age, but no corrosion rate was measured then. The trend line shown in Figure 76 was calculated by grouping all the different series shown in the Figure. The R^2 was 0.86 which can be considered a quite good fit. As it has been mentioned before both values were measured with the same device.

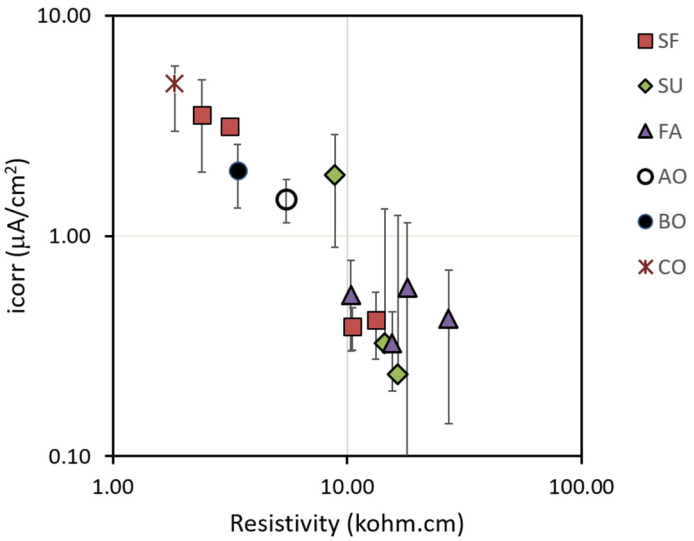

Figure 77. i_{corr} vs. resistivity averaged per mix.

Figure 77 shows the average resistivity and average i_{corr} of all rebars embedded in a given type of concrete. There are four symbols for FA and four symbols for SF, one per mix. The composition for SU3 and SU4 mixes (the two green diamonds farther to the right) are not known but based on average resistivity and average i_{corr} it appears to have Fly Ash, and or a high amount of SF. Most samples were selected for forensic analysis only after showing cracks on the concrete surface (two samples recently developed small cracks that have not been terminated). It will be interesting to continue periodic monitoring and possibly to open selected specimens that have an i_{corr} that is greater than 0.8 $\mu A/cm^2$, but that still does not show cracks. Samples with cracks tended to have smaller resistivity values because the solution in the reservoir filled the crack (recall that the solution filling the reservoir is seawater and that the concrete also contains chlorides built up over the years).

Table 36, Table 37 and Table 38 present the average for rebars A, B, and C and list the different concrete samples prepared for which there were rebars remaining.

Table 36. Average i_{corr}, E_{corr}, R_s and ρ measured on A rebars – 24–yr-old specimens.

Rebar A		TIME AVERAGE							
		i_{corr} AVG	STD	E_{corr} AVG	STD	Rs AVG	STD	ρ	STD
SF3–3	1B	0.35	0.26	–50.8	–51.17	2.4	0.57	14.4	3.43
SF4–2	4B	0.51	0.32	–197.2	–65.72	1.2	0.45	7.1	2.68
SF2–3	5B	1.72	0.07	–419.5	–40.31	0.7	0.03	3.9	0.18
SF3–1	6B	0.74	0.36	–206.0	–47.54	1.2	0.79	7.0	4.76
SF4–1	8B	0.29	0.17	–30.6	–42.94	2.0	0.39	12.0	2.34
SU3–1	10B	0.11	0.05	–76.0	–53.02	3.5	1.04	20.8	6.25
SU3–2	11B	0.30	0.20	–199.5	–67.50	2.4	0.91	14.3	5.43
SU4–1	12B	0.26	0.21	–159.4	–63.55	2.6	1.49	15.5	9.00
SU–2	14B	3.49	0.83	–458.5	–24.75	0.3	0.08	2.0	0.47
FA1–2	17B	1.19	1.02	–320.5	–43.49	1.3	0.42	7.8	2.49
FA1–4	19B	0.51	0.42	–115.7	–72.19	2.5	1.01	14.8	6.09
FA1–5	20B	0.34	0.17	–57.5	–17.97	2.9	0.66	16.0	5.69
FA1–6	21B	0.36	0.10	–64.1	–18.73	2.6	0.91	15.5	5.47
BO–2	27B	2.68	1.75	–344.6	–93.36	0.4	0.19	2.3	1.11
AO7	38B	4.17	3.24	–479.5	–111.11	0.4	0.26	2.2	1.56
AO6	39B	0.31	0.13	–62.4	–18.08	1.6	0.69	9.8	4.15
AO5	40B	1.60	0.64	–252.9	–62.39	0.6	0.11	2.9	0.79
A04	41B	0.45	0.23	–137.2	–72.20	1.6	0.68	9.7	4.11
SF1–2	44B	2.39	0.38	–417.1	–38.79	0.6	0.14	3.7	0.86
SU2–2	49B	1.15	0.54	–278.1	–131.03	2.0	0.86	12.1	5.15
SU2–1	50B	0.85	0.51	–190.4	–74.48	1.7	1.06	10.3	6.35
FA2–7	51B	0.40	0.22	–196.3	–47.62	2.5	1.10	14.9	6.63
FA2–6	52B	0.33	0.11	–202.9	–74.50	2.9	1.48	17.7	8.86
FA3–6	54B	0.72	0.40	–390.9	–70.89	1.4	0.55	8.6	3.31
FA3–4	56B	0.46	0.60	–293.7	–78.99	2.9	1.66	17.1	9.98
FA3–3	57B	0.10	0.06	–127.3	–88.17	7.9	6.21	47.6	36.99
FA1–7	59B	0.68	0.42	–124.3	–62.25	2.4	2.14	14.6	12.64
CO2	61B	13.01	1.77	–499.0	–15.56	0.1	0.01	0.5	0.05
FA2–5	63B	0.33	0.07	–155.3	–36.45	3.5	0.60	21.2	3.59
CO4	64B	1.11	0.51	–107.5	–20.46	0.5	0.18	3.3	1.07
FA2–4	65B	0.38	0.59	–127.9	–63.16	4.4	3.28	26.4	19.66
FA2–2	67B	0.29	0.14	–82.8	–50.43	4.2	0.91	28.2	6.14
FA2–3	68B	0.26	0.11	–164.3	–48.31	3.6	2.28	21.5	13.64
FA4–3	73B	0.24	0.06	–137.0	–21.21	3.1	0.88	18.6	5.30

Table 37. Average i_{corr}, E_{corr}, R_s and ρ measured on B rebars – 24–yr-old specimens

Rebar B		TIME AVERAGE							
		i_{corr} AVG	STD	E_{corr} AVG	STD	Rs AVG	STD	ρ	STD
SF3–3	1B	0.37	0.22	–19.0	–47.84	2.0	0.50	12.3	3.00
SF4–2	4B	0.44	0.11	–119.2	–36.66	1.6	0.44	9.8	2.67
SF2–3	5B	4.67	0.09	–510.5	–3.54	0.3	0.00	1.6	0.04
SF3–1	6B	0.87	0.52	–260.8	–39.64	1.4	0.82	8.3	4.92
SF4–1	8B	0.30	0.16	–48.6	–37.97	2.0	1.00	12.0	6.03
SU3–1	10B	0.19	0.08	–119.2	–70.42	2.6	0.97	15.3	5.81
SU3–2	11B	0.24	0.12	–194.9	–63.08	2.2	0.78	13.3	4.66
SU4–1	12B	0.16	0.14	–128.3	–58.44	3.1	1.42	18.6	8.47
SU–2	14B	3.70	0.01	–485.0	–7.07	0.4	0.06	2.5	0.36
FA1–2	17B	0.44	0.29	–130.4	–38.01	1.9	0.57	11.3	3.40
FA1–4	19B	0.30	0.15	–87.2	–42.67	3.9	3.63	15.7	3.50
FA1–5	20B	0.42	0.08	–50.8	–11.91	2.5	0.56	14.7	3.35
FA1–6	21B	0.40	0.12	–80.2	–28.51	2.4	0.54	14.4	3.11
BO–2	27B	1.76	0.84	–230.0	–97.74	0.5	0.22	2.9	1.33
AO7	38B	3.32	1.24	–459.5	–75.66	0.4	0.13	2.2	0.75
AO6	39B	0.43	0.34	–137.5	–42.59	1.1	0.58	6.6	3.46
AO5	40B	2.45	0.41	–305.8	–35.25	0.4	0.08	2.5	0.44
A04	41B	0.55	0.21	–154.9	–30.69	1.2	0.35	7.3	2.12
SF1–2	44B	3.39	2.22	–416.9	–107.97	0.6	0.20	3.2	1.21
SU2–2	49B	0.69	0.40	–228.3	–89.57	2.3	0.58	13.8	3.51
SU2–1	50B	0.45	0.36	–122.6	–68.32	2.2	0.81	13.5	4.86
FA2–7	51B	0.33	0.21	–137.8	–58.77	3.5	0.94	20.8	5.66
FA2–6	52B	0.34	0.12	–175.4	–29.85	3.0	1.17	17.9	7.02
FA3–6	54B	0.09	0.05	–124.3	–38.26	6.7	1.50	40.4	9.02
FA3–4	56B	0.62	0.47	–374.8	–50.45	1.8	0.89	10.9	5.33
FA3–3	57B	0.11	0.07	–87.5	–78.69	8.6	6.82	51.8	40.72
FA1–7	59B	0.55	0.32	–78.1	–41.12	2.4	1.87	14.7	11.20
CO2	61B	7.27	0.96	–497.0	–8.49	0.1	0.02	0.6	0.12
FA2–5	63B	0.91	0.48	–353.2	–53.40	1.5	0.46	9.1	2.76
CO4	64B	1.41	0.41	–112.5	–26.64	0.5	0.14	2.9	0.83
FA2–4	65B	0.31	0.16	–155.2	–46.15	4.1	2.71	24.4	16.26
FA2–2	67B	0.35	0.21	–109.6	–49.30	3.8	0.80	22.5	4.83
FA2–3	68B	0.60	0.52	–130.4	–39.18	4.3	2.65	25.0	13.81
FA4–3	73B	0.42	0.06	–287.5	–10.61	2.1	0.35	12.5	2.11

Table 38. Average i_{corr}, E_{corr}, R_s and ρ measured on C rebars – 24–yr-old specimens

Rebar C		TIME AVERAGE							
		i_{corr} AVG	STD	E_{corr} AVG	STD	R_s AVG	STD	ρ	STD
SF3–3	1B	0.31	0.22	–9.4	–27.41	2.8	0.92	16.7	5.54
SF4–2	4B	0.38	0.11	–98.9	–40.37	1.8	0.44	10.7	2.65
SF2–3	5B	4.21	0.77	–438.0	–2.83	0.3	0.06	1.7	0.33
SF3–1	6B	1.19	0.61	–296.2	–26.68	1.1	0.62	6.8	3.70
SF4–1	8B	0.39	0.28	–27.4	–43.32	2.0	1.10	11.7	6.58
SU3–1	10B	0.26	0.21	–196.5	–78.79	2.7	1.07	16.2	6.40
SU3–2	11B	0.85	0.39	–390.1	–39.69	1.1	0.44	6.8	2.66
SU4–1	12B	0.29	0.19	–160.4	–51.61	2.5	1.07	15.2	6.45
SU–2	14B	3.39	0.77	–469.5	–0.71	0.4	0.08	2.6	0.49
FA1–2	17B	0.54	0.28	–111.2	–38.78	2.0	0.76	12.2	4.54
FA1–4	19B	0.32	0.19	–106.1	–49.04	2.7	0.70	16.4	4.20
FA1–5	20B	0.43	0.08	–47.3	–6.96	2.8	0.57	16.7	3.48
FA1–6	21B	0.42	0.14	–67.2	–21.03	3.1	0.70	18.3	4.23
BO–2	27B	1.31	0.95	–260.0	–79.32	0.8	0.29	4.7	1.71
AO7	38B	1.00	0.40	–293.6	–114.71	1.0	0.31	5.8	1.87
AO6	39B	0.62	0.29	–176.2	–30.60	1.3	0.60	7.9	3.59
AO5	40B	2.12	0.61	–211.1	–31.29	0.5	0.11	3.2	0.67
A04	41B	0.65	0.55	–242.8	–119.88	1.0	0.17	5.9	1.04
SF1–2	44B	3.67	0.57	–441.0	–2.83	0.4	0.01	2.6	0.11
SU2–2	49B	1.06	0.68	–284.5	–60.28	1.6	0.71	9.6	4.23
SU2–1	50B	0.40	0.19	–100.1	–68.56	2.2	0.96	13.3	5.78
FA2–7	51B	2.08	1.11	–399.8	–65.14	0.7	0.40	4.1	2.41
FA2–6	52B								
FA3–6	54B	0.15	0.10	–197.3	–69.89	4.2	2.33	24.9	13.96
FA3–4	56B								
FA3–3	57B	0.97	1.25	–304.3	–189.46	3.4	2.93	20.3	17.47
FA1–7	59B	1.17	0.70	–78.2	–45.29	1.6	1.22	9.7	7.36
CO2	61B	5.26	1.31	–439.5	–24.75	0.1	0.03	0.8	0.19
FA2–5	63B	0.26	0.12	–92.1	–43.72	3.1	0.76	18.5	4.55
CO4	64B	1.39	0.53	–149.4	–29.19	0.5	0.20	3.0	1.19
FA2–4	65B	1.64	0.47	–519.0	–12.73	0.7	0.15	4.3	0.90
FA2–2	67B	0.29	0.06	–109.9	–53.73	4.1	0.89	24.6	5.36
FA2–3	68B	0.46	0.20	–252.3	–23.32	1.9	0.96	11.3	5.75
FA4–3	73B								

4.2 – Chloride profiles

This section presents selected chloride concentration profiles obtained from slicing the cores from samples chosen for chloride analysis. Results are also presented for chloride concentration just above the rebar trace. The chloride concentration shown is the average concentration from triplicate measurements per slice or the average of two measurements for the concentrations corresponding to locations above the rebar trace. The buildup effect due to rebar presence has been reported before by Sagues [26], Hartt [27], and Presuel [28] from modeling and experimental results. The rebar interrupts the pathway for chloride transport. The rebar is impervious to the passage of chlorides, which in turn, causes the chloride concentration to build up faster in the region adjacent to the rebar closest to the exposed surface. Figure 78 shows the chloride concentration profiles for concrete blocks with different mix design. Chloride concentrations corresponding to concrete locations just above the rebar trace are around 8.0 kg/m^3, which is represented by the solid fill, a single point in the figure. It can be observed that with an increase of the depth, the chloride concentration decreases. It is noted that the concrete cover thickness is around 20 mm.

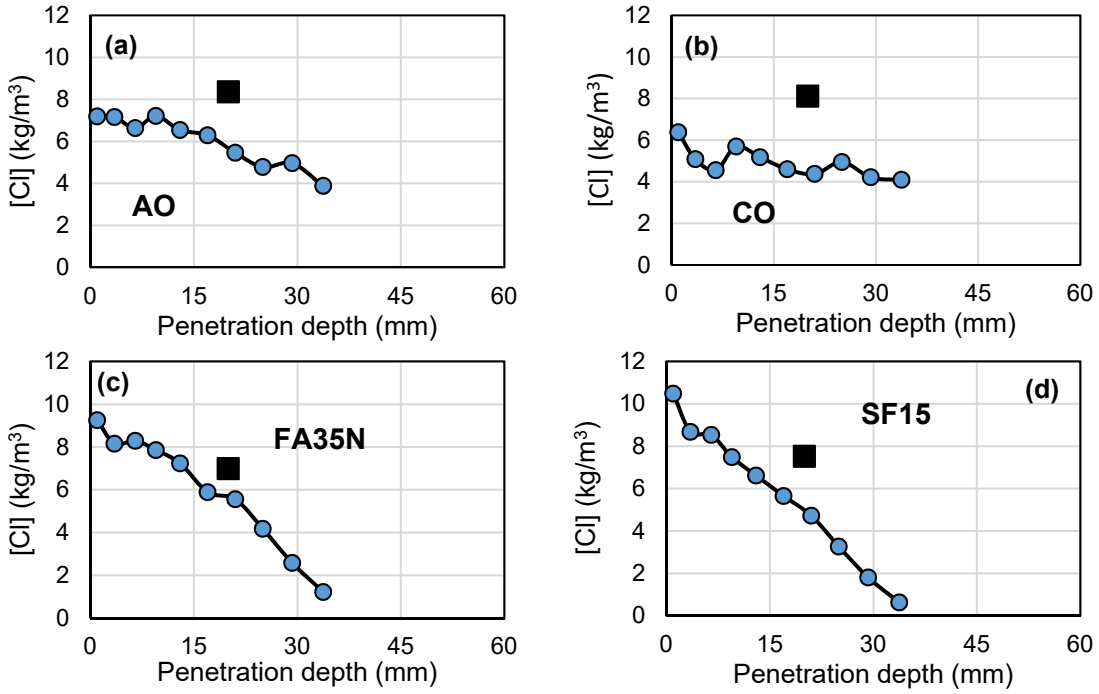

Figure 78. Chloride transport as a function of concrete depth for specimens with different admixtures.

Table 39 compares the diffusivity of concrete specimens with different admixtures at different ages. For the AO specimen, the coefficient of diffusion is around 3.48×10^{-12} m^2/s after 3 years of exposure test. It reduced to 1.5×10^{-12} m^2/s after 15 years and 1.62×10^{-12} m^2/s after 23 years of exposure test, respectively. The decrease in the coefficient of diffusion is due to the slow hydration of cement in the concrete. As for concrete with calcium nitrite CO, the Dapp was not measured at 3.3 years, and it is close to the values of AO after 15 years and 23 years of exposure. For concrete with fly ash FA35N, the D_{app} is 0.74×10^{-12} m^2/s after 3.3 years of exposure and

reduced to 0.29×10^{-12} m^2/s after 15 years, and then increased to 0.60×10^{-12} m^2/s after 23 years. Compared with AO specimen, the lower D_{app} for the specimen with fly ash is due to the relatively contact microstructure from the pozzolanic reaction of fly ash. For specimens with silica fume SF15, the Dapp is around 2.29×10^{-12} m^2/s after 3.3 years, and decreased to 0.24×10^{-12} m^2/s after 15 years and increased slightly to 0.39×10^{-12} m^2/s after 23 years.

Table 39. Comparison of the coefficient of diffusion (D) for different concrete blocks

Time (year)	D_{app} ($m^2/s \times 10^{-12}$)			
	AO	CO	FA35N	SF15
3.3	3.48	NA	0.74	2.29
>15	1.5	1.4	0.29	0.24
>23	1.62	1.32	0.60	0.39

Chapter 5 – Forensic Analysis

Two types of reinforced concrete samples were considered for forensic analysis. The first type includes five-rebar samples exposed outdoors to ambient conditions (with the solution reservoir filled with seawater during the wet cycle). Several of the outdoor five-rebar samples showed cracks in the concrete; this typically occurred above one of the rebars on the top row. From the lab indoor-exposed samples, only two reinforced concrete samples and five of the single-rebar mortar samples showed cracks. In the case of the reinforced concrete samples, the crack appears to have originated from a corrosion site that was not right below the solution reservoir, whereas those in the mortar samples was initiated by corrosion of the rebar right below the solution reservoir. Selected pictures of the crack from the top and on the side when available, are presented in this chapter for the latter types of samples for both concrete and mortar specimens.

In this chapter, the surface conditions of the rebars upon opening and after cleaning the rebars are presented. In most cases, the portion of the rebar with the most corrosion is presented, but for selected samples, a picture of the whole rebar upon opening and after cleaning is shown. The top side of the rebar is the surface of the rebar right below the solution reservoir. In most instances, only the top side of the rebar is presented, because the bottom side did not experience corrosion. For cases in which corrosion occurred on both sides, pictures with views of both sides are included. The rebars from samples exposed outdoors for over 24 years to seawater wet/dry cycles are presented first. Another section describes the forensic analysis of rebars removed from lab samples exposed indoors. This chapter includes observations of one four-rebar sample, three single-rebar samples with 5-cm concrete covers, six single-rebar samples with 8 mm concrete covers, and two rebars from a three-rebar specimen. Finally, single-rebar mortar samples are presented. The mortar cover was-8 mm.

5.1 – Samples with cracks (5-cm concrete cover)

Figure 79 shows the crack that extended to the concrete surface on the side on the four-rebar specimen 1DA. The rebar (1DASQ2) had a 10-cm solution reservoir installed during spring 2016, but this particular specimen had been exposed to chlorides for approximately six months a few months after the concrete was prepared in 2008. Upon exposing the rebar, it was verified that corrosion took place not just below the solution reservoir but also away from it. Figure 80 shows the two surfaces upon doing an intermediate cut. The red lines are slightly offset from the crack to highlight the crack location.

Figure 79. Specimen 1DA showing the crack that extended to the surface (left side) which depicts the crack extended to the concrete surface on the side.

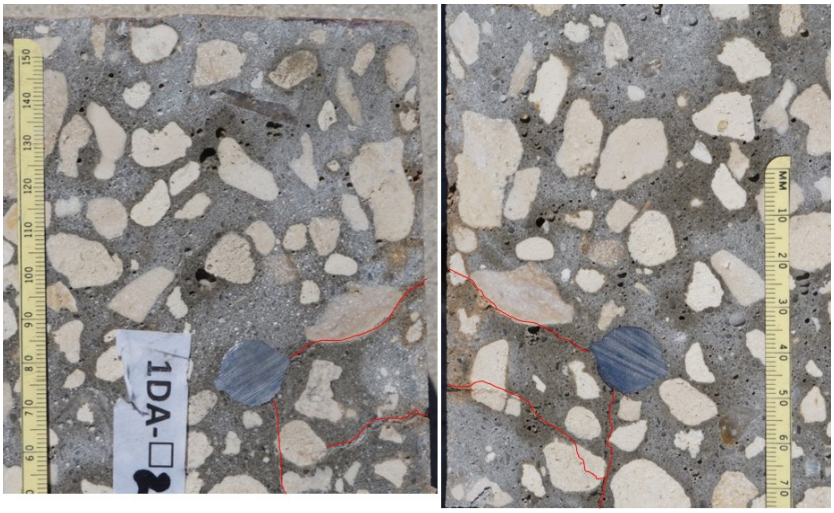

Figure 80. View of crack inside the concrete upon cutting the specimen for 1DASQ2. The red lines highlight an offset to the crack location.

Figure 81 shows sample 1B1 before removing the rebar, the figure has on the first row a picture of the top view that shows a crack and the bottom picture has a side view indicating that the crack reached a side surface where the rebar exits the concrete.

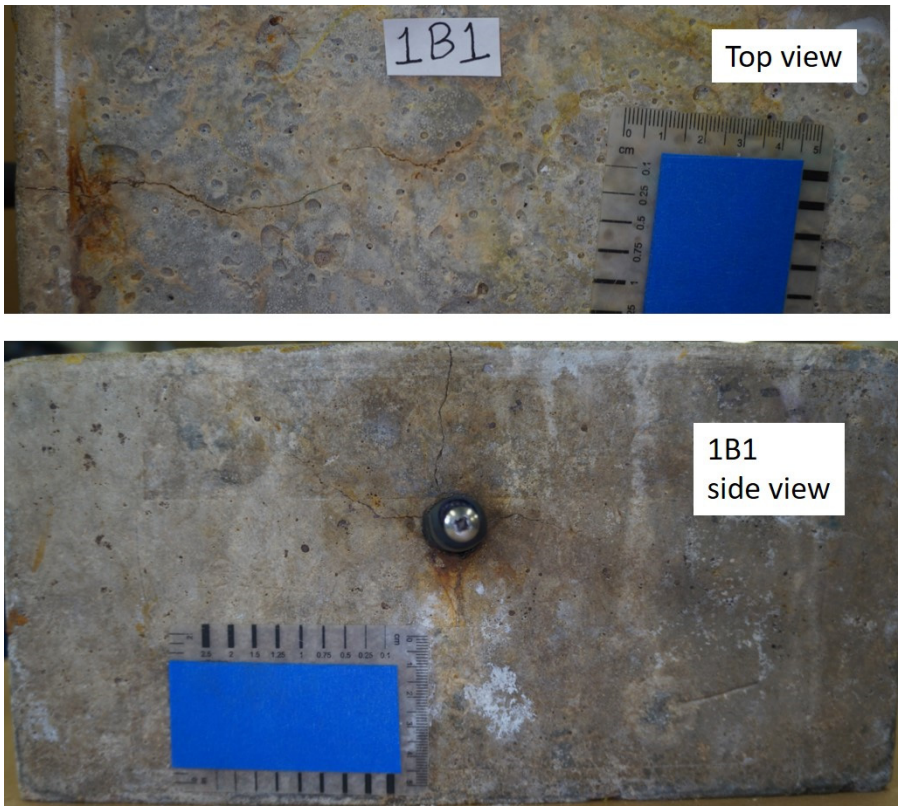

Figure 81. Top view and side view for specimen 1B1 (sides that show the crack)

Figure 82 shows two pictures of the top view for MD1–NP specimens NP35 (left) and NP38 (right). The pictures were taken before removing the rebars. The picture for NP35 shows several rust spots stains and a crack, whereas the picture on the right for NP38 shows only one red rust spot.

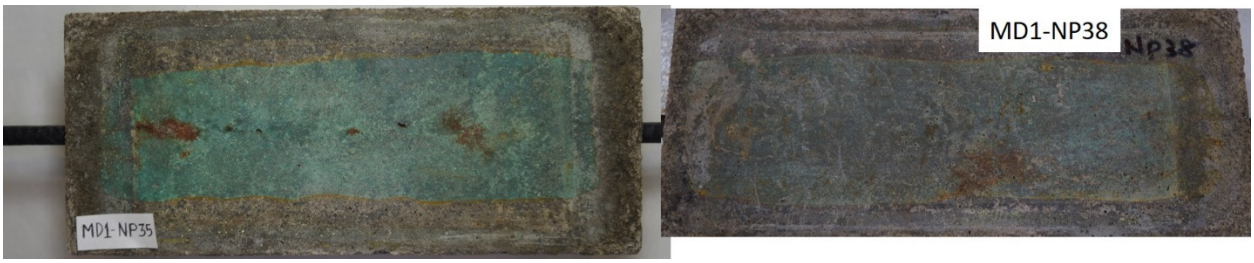

Figure 82. Top view of specimen MD1–NP35 and MD1–NP38

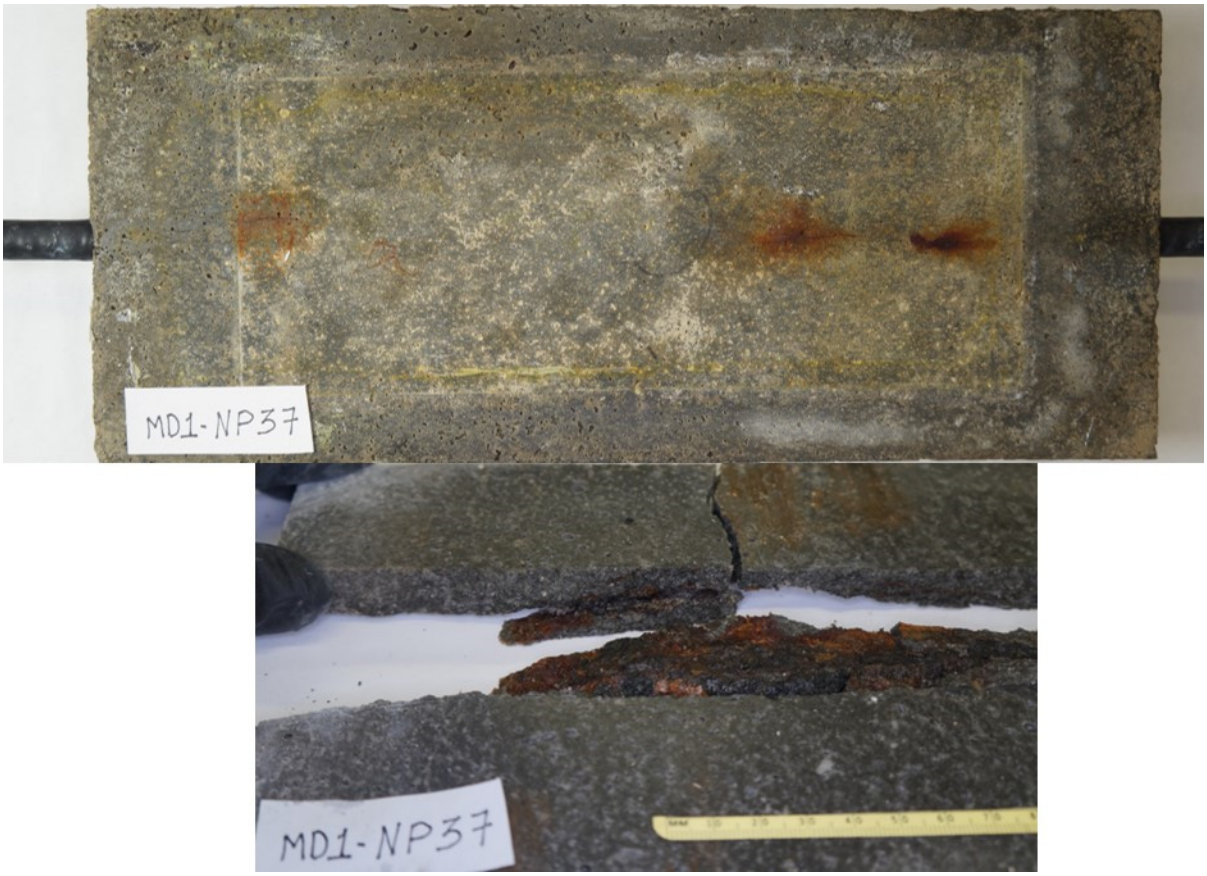

Figure 83. Top view (top) and upon opening (below) MD1–NP37.

Figure 83 shows the top view of MD1–NP37 and also a picture of the mortar above the rebar, where the corrosion products that travelled along the crack are visible. Figure 83 shows a picture of the top view for specimen MD1–NP37 with a crack that displays three red–rust stains. It indicates that the corrosion products moved along the crack length. Figure 84 presents a similar picture for specimen MD1–B, this specimen had a square 10 cm solution reservoir, the rust stained most of the reservoir footprint, and a crack is also visible from the top view. The picture on the bottom in Figure 84 shows the mortar above the rebar with the corrosion products still a dark green/black color. It also shows that the corrosion products moved into the mortar and caused a crack. Finally, Figure 85 shows the top view and cross-section view of the mortar upon opening specimen MD1–H. This specimen initially had a 1 cm long reservoir, but it was later changed to a 3 cm long solution reservoir. As part of this project, a larger solution reservoir was installed so that Gecor 8 readings with probe B were possible. The bottom picture shows the rebar trace and how far the corrosion spot was. The picture of the other mortar piece shows the crack moved from the rebar surface towards the mortar surface (reservoir side). MD1–B and MD1–H specimens were subjected to electromigration for several months, likely beyond the point in which corrosion had initiated. These samples then were exposed to lab conditions for over 3 years before cracks appear on the surface. Companion specimens that have not been terminated do not show corrosion spots on either the mortar surface or cracks, but the corrosion rate measurements indicate that corrosion is on–going.

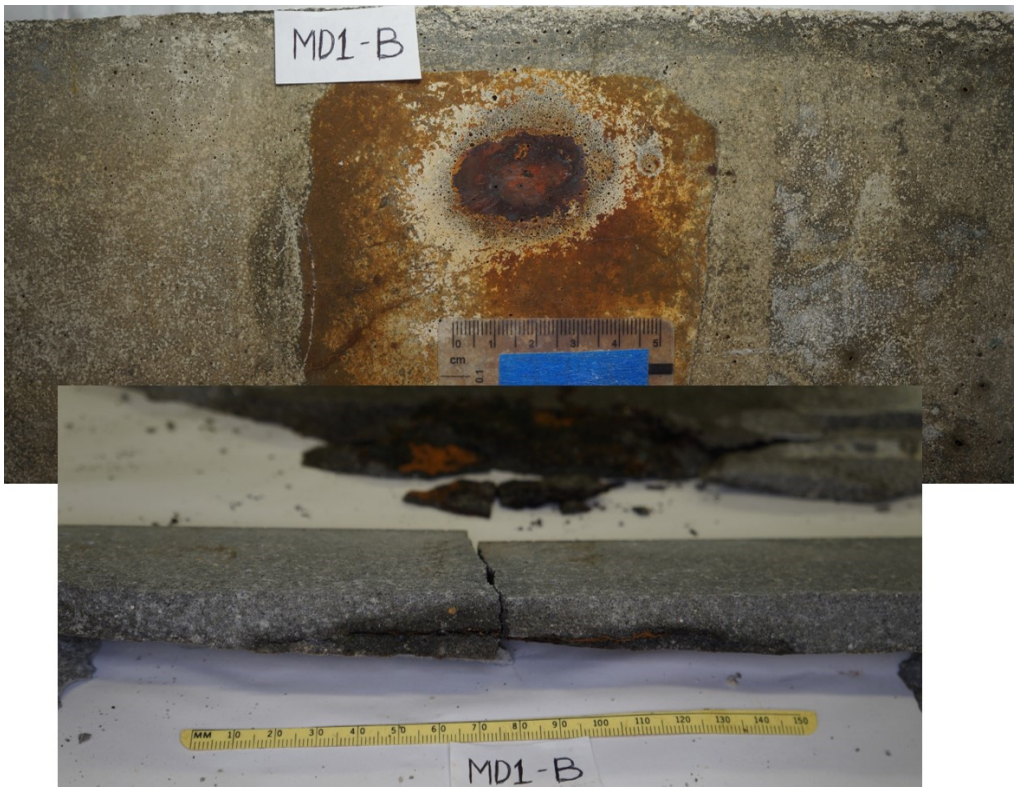

Figure 84. Top view and cross-sectional view upon opening MD1–B

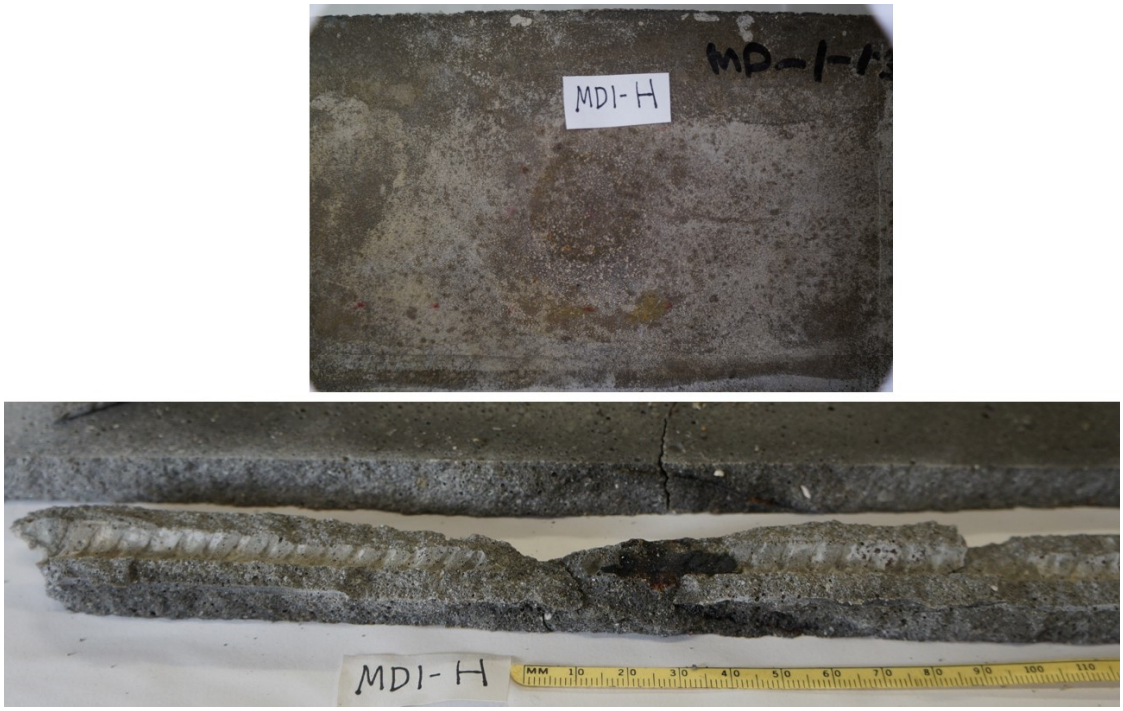

Figure 85. Top view and a cross-sectional view for specimen MD1–H

5.2 – Selected comparison for AO terminated rebars

Figure 86 shows pictures of rebar AO7–A before and after cleaning it. It can be observed that after removing the corrosion products a good amount of cross-section loss had occurred on this rebar. Figure 87 shows pictures of rebar AO7–B before and after cleaning and on a third row two pictures showing close–ups of the regions that had the most corrosion. It can be observed that although there was cross-section loss on rebar AO7–B, the cross-section loss was not as significant as what was observed on rebarAO7–A.

Figure 86. Before and after cleaning rebar AO7–A (close–up)

Figure 87. Before and after cleaning rebar AO7–B (full size and two close–ups after cleaning)

Figure 88 shows pictures of rebar AO4–C before and after cleaning. The rebar orientation shown on the top picture indicates that the rebar edge pointed up during exposure, the top side had the most corrosion, the picture after cleaning shows the rebar rotated a few degrees (compared to the rebar view before cleaning) so that the corroded area after cleaning can be better observed. This picture after cleaning suggests that there are two regions with major cross-section loss.

Figure 88. Before and after cleaning rebar AO4–C (close–up)

5.3 – FA rebars

Below are figures that compare the rebar surface condition upon opening and after cleaning the rebar for the four FA rebars that were terminated. For cases where the concrete had a crack above the rebar, a picture of the crack is included if available. Figure 89 shows pictures of rebar FA1–2–A before and after cleaning the rebar. A small corrosion spot is observed on the left and a large corrosion spot with significant cross-section loss observed on the right. Figure 90 shows a hair crack and a small spall that took place above the rebar along the corrosion site.

Figure 89. Before and after cleaning rebar FA1–2–A

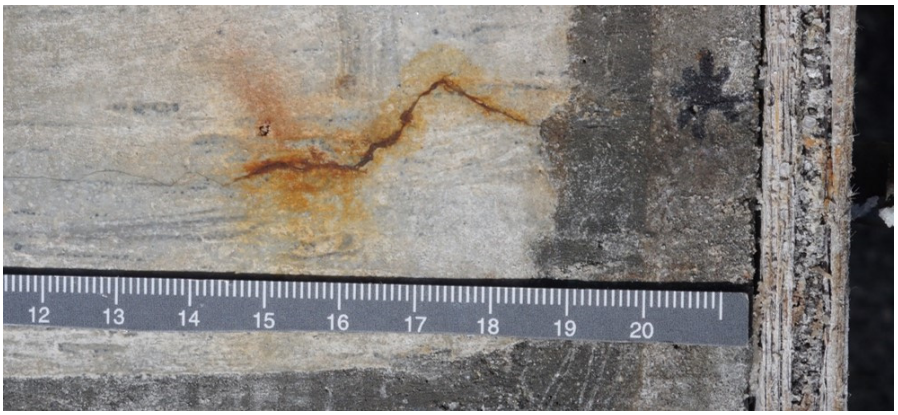

Figure 90. Crack observed on the concrete surface above rebar FA1–2–A

Figure 91 shows rebar C for a rebar embedded in specimen FA2–4. Figure 91 shows the rebar upon exposing it to the environment and the bottom picture shows the rebar condition after cleaning it. There is a large corrosion spot visible upon exposing the rebar, the picture after cleaning the rebar indicates that there was a significant amount of cross section. The surface of the concrete before opening showed a thin crack. See Figure 92 shows a hair crack that was visible on the concrete surface.

Figure 91. Before and after cleaning rebar FA2–4C

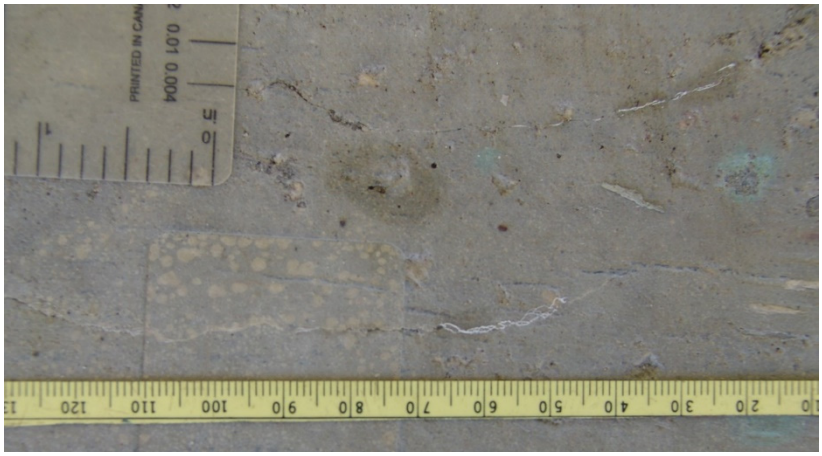

Figure 92. Crack observed on the concrete surface above rebar FA2–4C

Figure 93 shows rebar B embedded in specimen FA4–3–B. The top picture shows a number of reddish corrosion spots, suggesting that corrosion was not on–going at those locations. Although harder to see from the picture before cleaning (top row), there were several darker spots. The sites with red rust might be no corroding or now corroding at a low corrosion rate. The picture after cleaning suggests that in some regions there has been a modest reduction of the cross-section. Figure 93 shows in a third row a couple of close–up pictures for the regions with the most cross-section loss. Figure 94 shows rebar FA4–3C, the corrosion spot, which in this case, was almost 7 cm long, and the cross-section loss was not as significant as what was observed on rebar FA2–4–C, but more significant than that seen on rebar FA4–3–B.

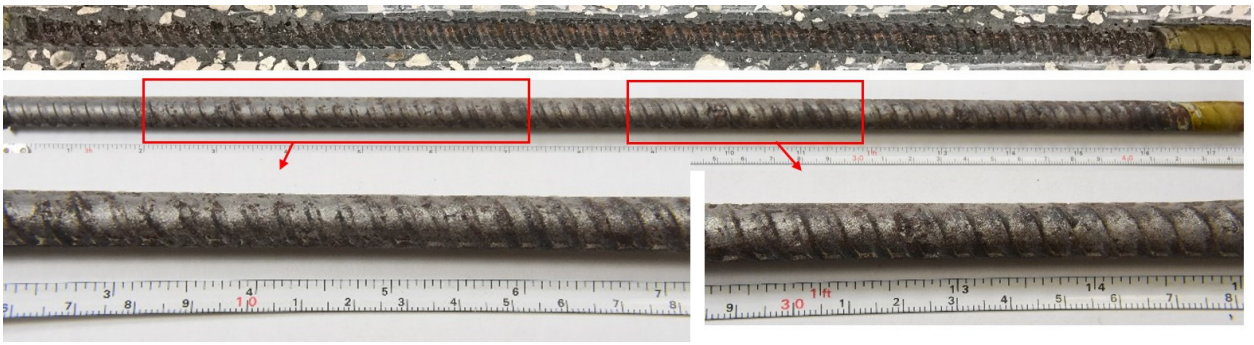

Figure 93. Before and after cleaning rebar FA4–3–B

Figure 94. Before and after cleaning rebar FA4–3C

No crack was observed above rebar FA4–3–B, and a short think crack was visible above FA4–3–C (See Figure 95).

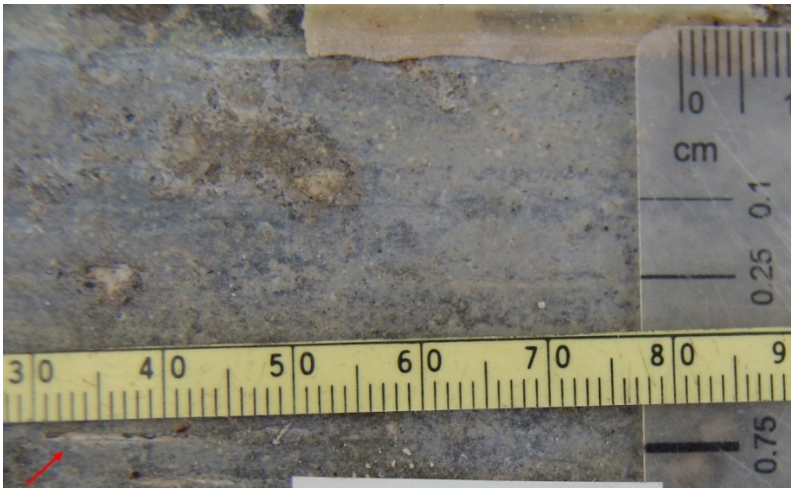

Figure 95. Crack observed on the concrete surface above rebar FA4–3–C

5.4 – SF rebars

Figure 96 shows the corrosion extent that took place on rebar SF1–2–C. In this case, the diamond blade hit the rebar and it can be observed in the top pictures. In the center is a view of the rebar after cleaning with the same orientation before cleaning. The picture in the third row shows another picture after cleaning the rebar. The rebar has the axes rotated such that a better view of the cross-section loss is observed. Figure 97 shows a picture of the crack that was visible at the surface of the concrete above the corroding spot. It can be seen that the crack width is small.

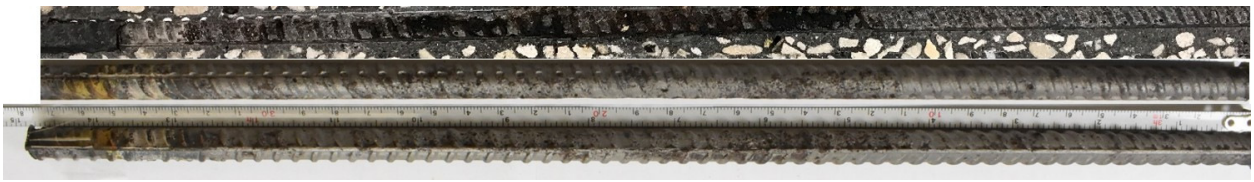

Figure 96. Before and after cleaning Rebar SF1–2–C

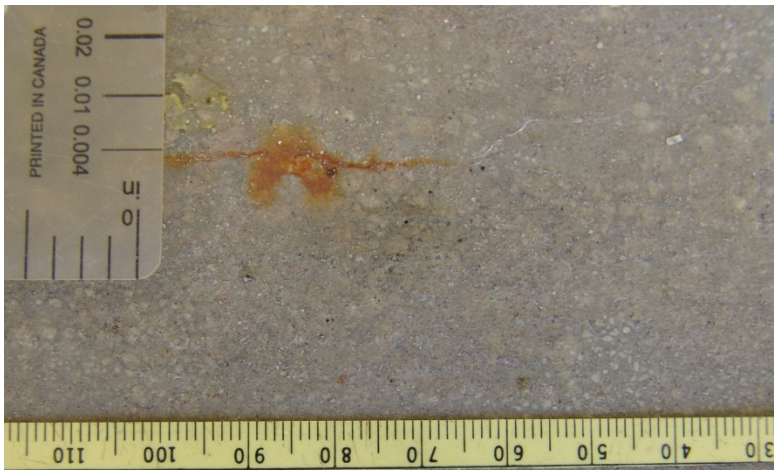

Figure 97. Crack observed on the concrete surface above rebar SF1–2–C

The next three figures show the exposed rebars embedded in specimen SF2–3;the three rebars were removed. Two cracks were observed in these specimens (see Figure 98). It is not clear if the corrosion product from rebar SF2–3–A (Figure 99), or the corrosion products from rebar SF2–3–B (Figure 100) caused the transverse crack. The corrosion spots prior to cleaning are about the same length on all rebars in this specimen. Figure 101 shows that slightly more cross section loss was observed on SF2–3–C. The pictures shown in here and in the previous section are evidence that a significant amount of cross-section loss after corrosion that has been propagating (on–going) for several years can occur. The cross-section loss and consequent corrosion products can then cause cracks in the concrete samples cast with FA or SF.

Figure 98. Cracks observed on the concrete surface on specimen SF2–3

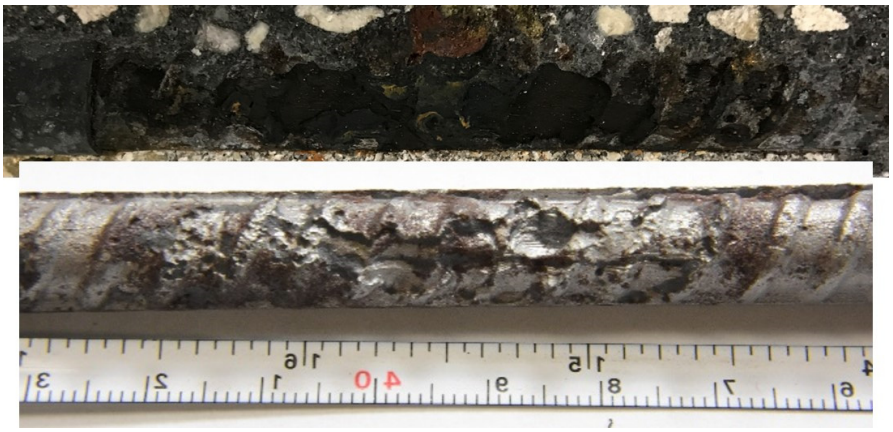

Figure 99. Before and after cleaning rebar SF2–3–A

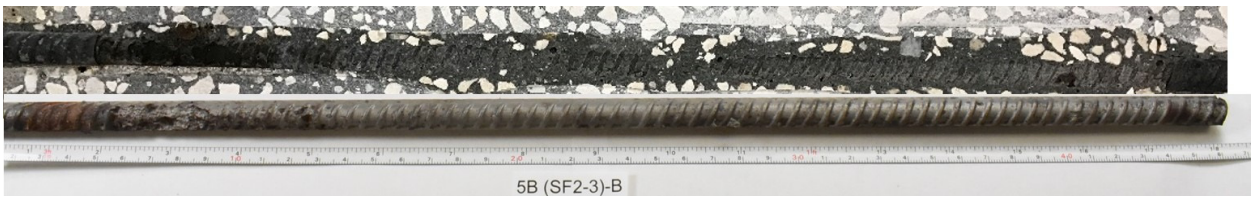

Figure 100. Before and after cleaning rebar SF2–3B

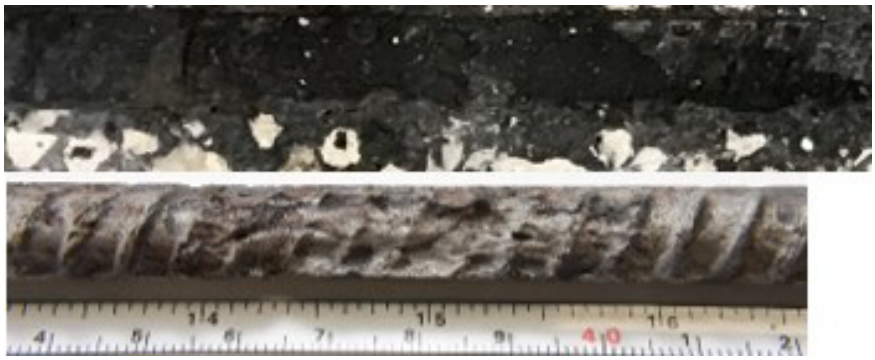

Figure 101. Before and after cleaning rebar SF2–3–C

The CO and SU samples are not included in this section. These rebars displayed cross-section loss, but the concrete did not contain supplementary cementitious materials. Close–up pictures after cleaning are included in Appendix I for the rebars removed from the CO and SU terminated samples.

5.5 – Single-rebar specimens with 5-cm concrete cover

The figures in this section describe the three specimens terminated that have a single rebar. A solution reservoir was installed centered and it was a 5 cm cylinder. The corrosion products in one of the rebars caused cracks that were visible on the top and side views. Figure 102 shows the top view indicating that corrosion occurred on one side, outside of the area of the rebar below the solution reservoir. Figure 103 shows that a significant amount of corrosion occurred on the bottom side of the rebar. This specimen was subjected to electromigration for about 400 days

(not all the time on), and then recently a modest corrosion anodic current was applied as to accelerate corrosion. The long electromigration period and the fact that the top side of the rebar being under the troweled surface might have allowed corrosion to initiate on the bottom side. A shrinkage wrap that was present since casting might have allowed for corrosion to initiate in the form of crevice corrosion.

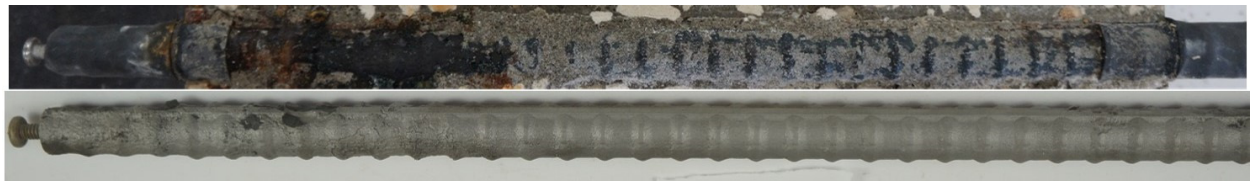

Figure 102. Before and after cleaning rebar 1B1, top view.

Figure 103. Before and after cleaning rebar 1B1, bottom view

Figure 104 and Figure 105 show the top view and bottom view respectively, of the rebar embedded in specimen 1F1. Figure 104 shows a dark region at the rebar center, and upon cleaning a few small corrosion spots were observed (pitting corrosion). On the left side of the picture, the rebar shows corrosion spots and suggests that crevice corrosion took place under the shrinkage wrap. The calculated (using R_c and Faraday law) mass loss was significantly larger than that amount of mass lost shown here.

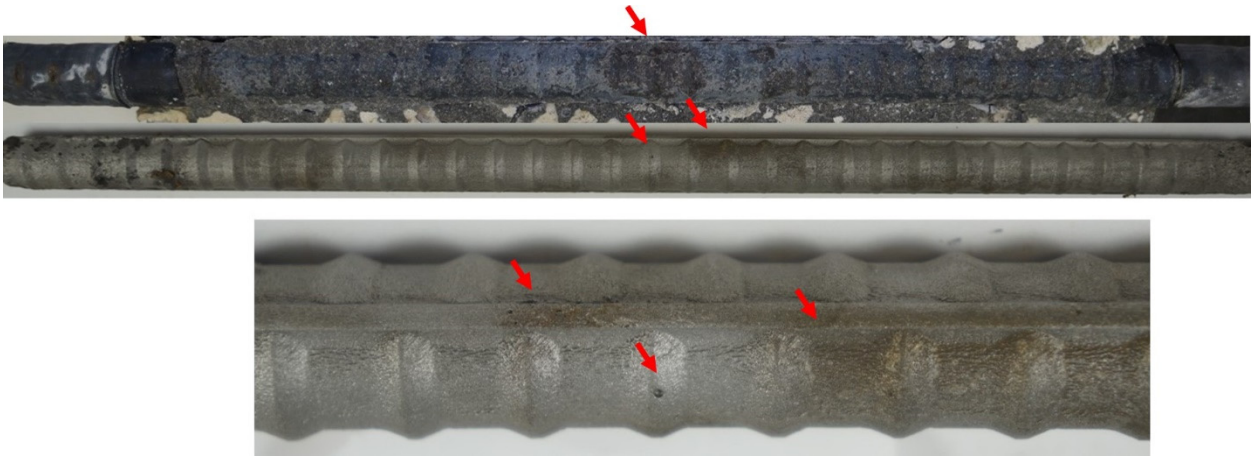

Figure 104. Before and after cleaning rebar 1F1, top side

The pictures in Figure 105 show several red rust spots on the bottom side of Rebar 1F1. However, upon cleaning the rebar, it appears that these were quite shallow corroding sites.

Figure 105. Before and after cleaning rebar 1F1, bottom side

Figure 106 and Figure 107 shows the corrosion that took place on the rebar embedded in specimen 2D2. Figure 106 shows the top side of the rebar before and after cleaning. No corrosion was observed below the solution reservoir. On the rebar ends, it appears that some crevice corrosion took place. Figure 107 shows that corrosion took place on the bottom side extending from underneath the shrinkage wrap to almost the middle of the rebar. A modest amount of cross-section loss was observed upon cleaning the rebar.

Figure 106. Before and after cleaning rebar 2D2, top side

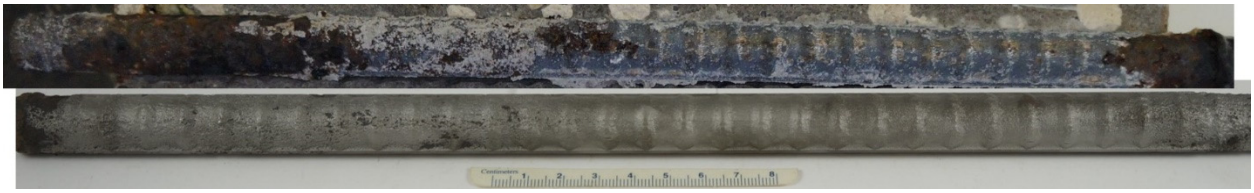

Figure 107. Before and after cleaning rebar 2D2, bottom side.

5.6 – Forensic analysis of rebars embedded in mortar specimens

Figure 108 shows the corrosion spot shortly after removing the rebar and after cleaning from sample MD1-B. This rebar had 10 cm solution reservoir. The section shows that the corrosion spot was about 10 cm long. A significant cross section loss is visible after cleaning the rebar.

Figure 108. Before and after cleaning rebar in MD1-B

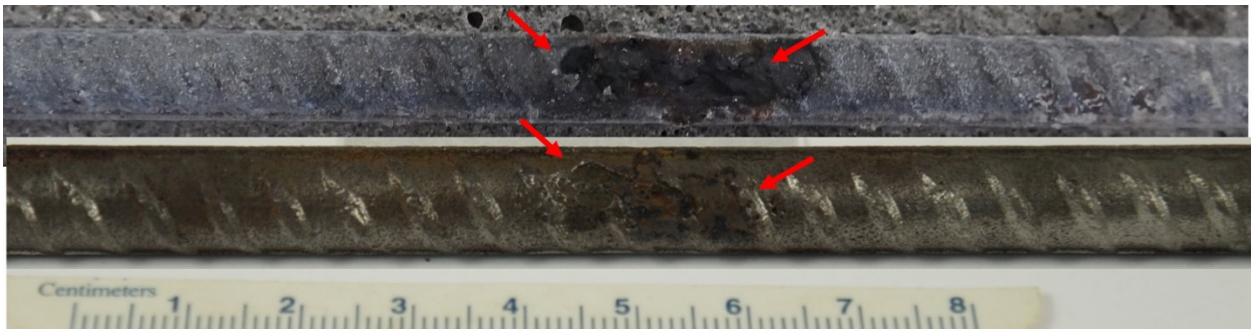

Figure 109. Before and after cleaning rebar in MD1-H.

Figure 109 shows the rebar removed from specimen MD1-H; this specimen initially had a 1.5-cm long reservoir, but later it was changed to a 3-cm diameter, and as part of this project, a large reservoir was installed. The corrosion spot appears to be a little longer than 2 cm upon opening, but after cleaning, the rebar the corrosion spot was close to 1.5 cm long. The depth of the corrosion spot was significant in this case. Figure 110, Figure 111, and Figure 112 show the rebars removed from specimens MD1-NP35, MD1-NP37, and MD1-NP38, respectively. Only the sections with the most corrosion are shown here. The three rebars had significant cross-section loss and long corrosion spots. Corrosion sites of about the same length were observed on MD1-35 (Figure 110) and MD1-37 (Figure 111). Two corrosion spots were observed on the rebar removed from specimen MD1-38 (Figure 112).

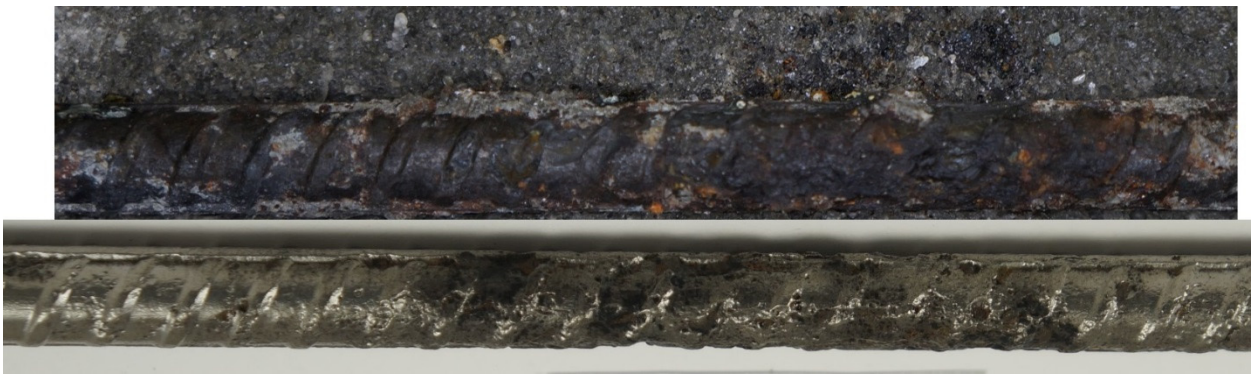

Figure 110. Before and after cleaning rebar in MD1-NP35

Figure 111. Before and after cleaning rebar in MD1-NP37.

Figure 112. Before and after cleaning rebar in MD1-NP38.

5.7 – Forensic analysis of four-rebar specimen 1DA

Figure 113 and Figure 114 show the top and bottom respectively of rebar 1DAO1 before and after cleaning the rebar. No corrosion is observed in the center segments that were below the solution reservoir. Corrosion took place at the edge of the shrinkage wrap (see right side before cleaning). Figure 115 shows that corrosion did take place below the solution reservoir on rebar 1DAO2 (5 cm solution reservoir) and also some distance from the solution reservoir (see the spot on the left piece before cleaning). Moderate cross-section loss was observed at both locations.

Figure 113. Before and after cleaning rebar 1DAO1, top side

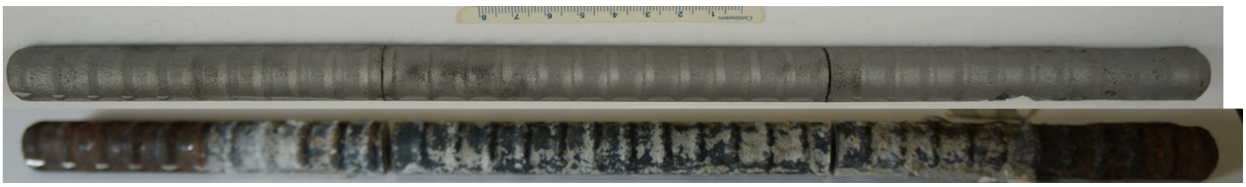

Figure 114. Before and after cleaning rebar 1DAO1, bottom side

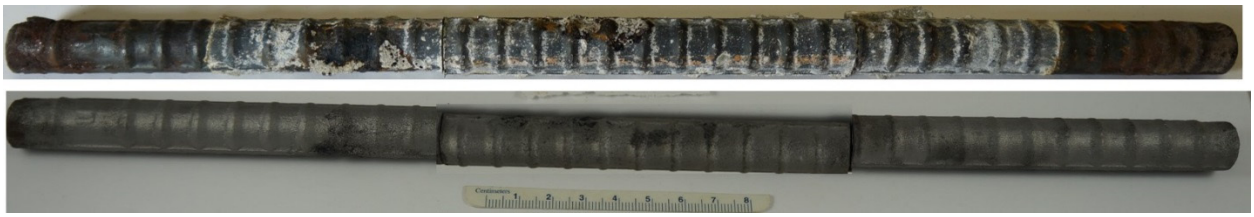

Figure 115. Before and after cleaning rebar 1DAO2, top side

Figure 116 shows the top view of rebar 1DASQ1. A small corrosion spot was observed centered under the solution reservoir (in this case the solution reservoir was 10 cm) and another site on the left section also under the solution reservoir; the latter had a deeper cross section loss. The right side of the rebar is not shown and it did not show corrosion. Figure 117 shows the top view of rebar 1DASQ2, indicating that there was no significant corrosion under the reservoir. Figure 118 shows the bottom view of rebar 1DASQ2, a large spot is observed on the left side of the rebar, the cross-section loss was significant and it caused the crack that is shown in Figure 79 and Figure 80.

Figure 116. Before and after cleaning rebar 1DASQ1, top side

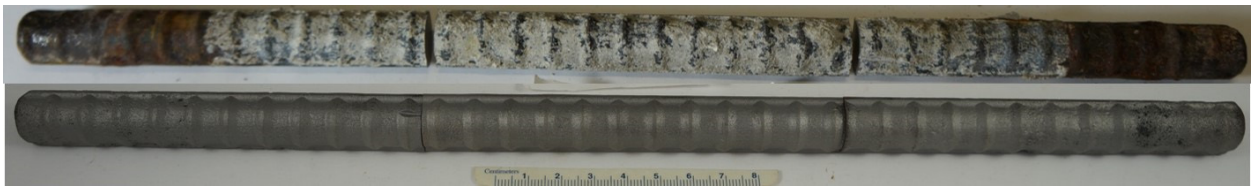

Figure 117. Before and after cleaning rebar 1DASQ2, top side

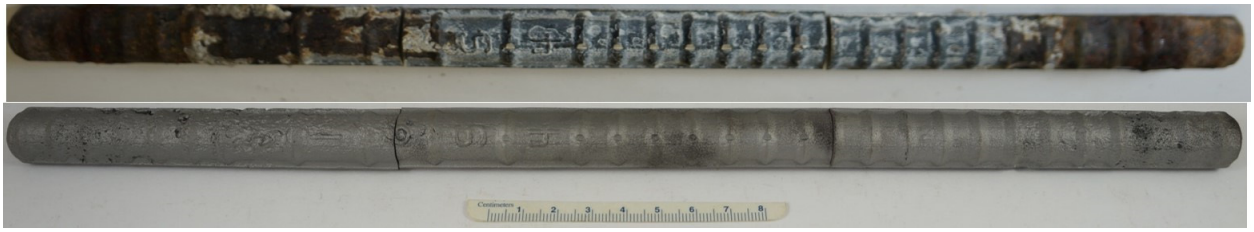

Figure 118. Before and after cleaning rebar 1DASQ2, bottom side

5.8 – Single-rebar reinforced concrete samples

Figure 119 shows that only a small corrosion spot was present on the rebar embedded in specimen SL1. A modest amount of corrosion is observed in the region after cleaning. The length of the corroding spot is about 3 to 4 mm. Figure 120 shows that there were two corrosion spots on the top surface of the rebar embedded in specimen SL2. The corroding sites were somewhat deeper on this rebar than the rebar on specimen SL1. The solution reservoir was about 15 cm long, thus it appears that corrosion has initiated and propagated on a small fraction of the surface subjected to electromigration.

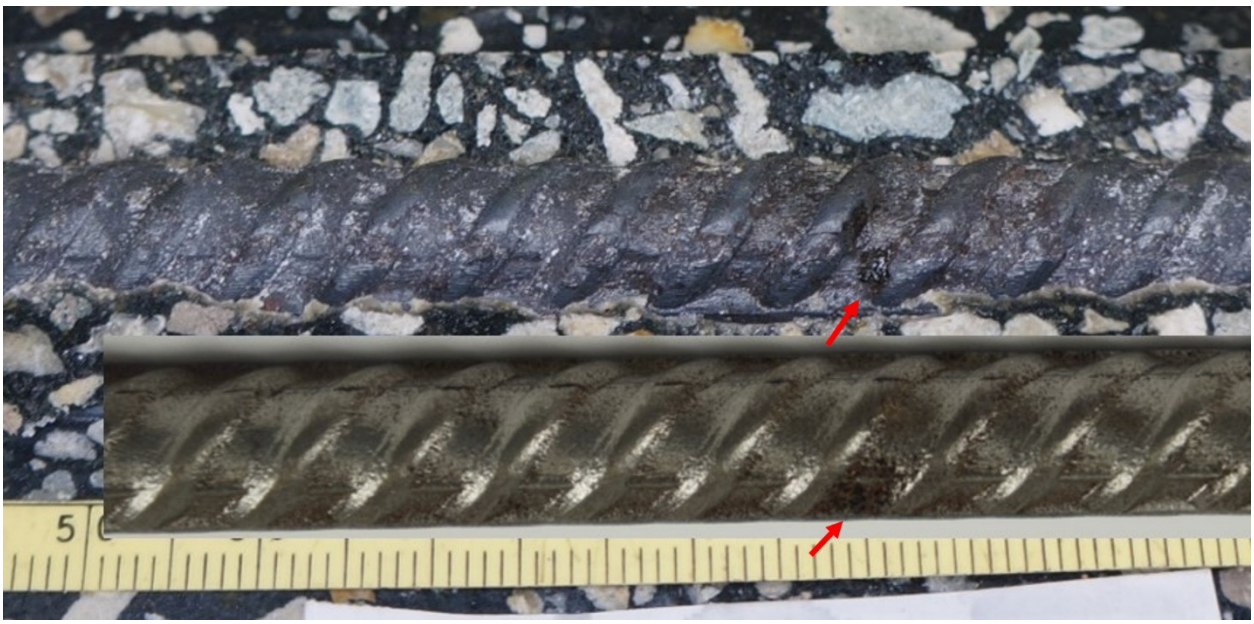

Figure 119. Before and after cleaning rebar in specimen SL1

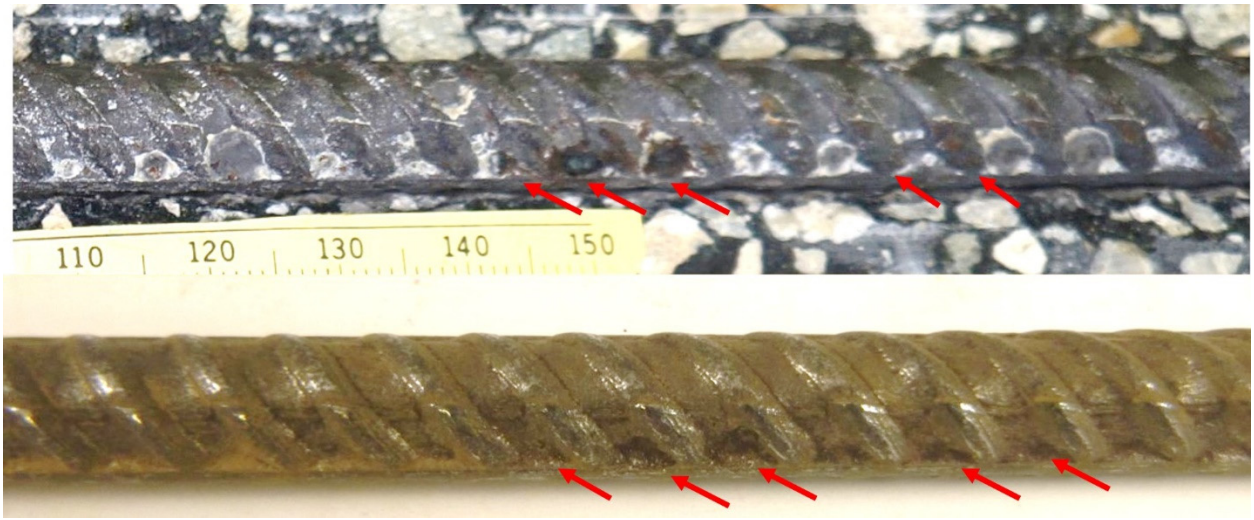

Figure 120. Before and after cleaning rebar in specimen SL2

Figure 121 and Figure 122 shows the rebar surface before and after cleaning on rebars embedded in specimens FA8 and FA9, respectively. Figure 121 shows a small corroding site before

cleaning on the rebar embedded on specimen FA8; the cross-section loss is visible but not significant. Figure 122 shows that three corrosion spots developed on the rebar embedded in sample FA9. The smallest spot is a little hard to see on the picture after cleaning due to the angle of the picture (an arrow indicates the location). The larger corroding spots show a modest but significant cross-section loss; the rebar in specimens FA9 was subjected to anodic current to accelerate corrosion for a short period of time. Both of these rebars had a solution reservoir of about 15 cm long, hence just a small fraction of the area corroded. The opposite side of both rebars showed no corrosion.

Figure 121. Before and after cleaning rebar in specimen FA8

Figure 122. Before and after cleaning rebar in specimen FA9

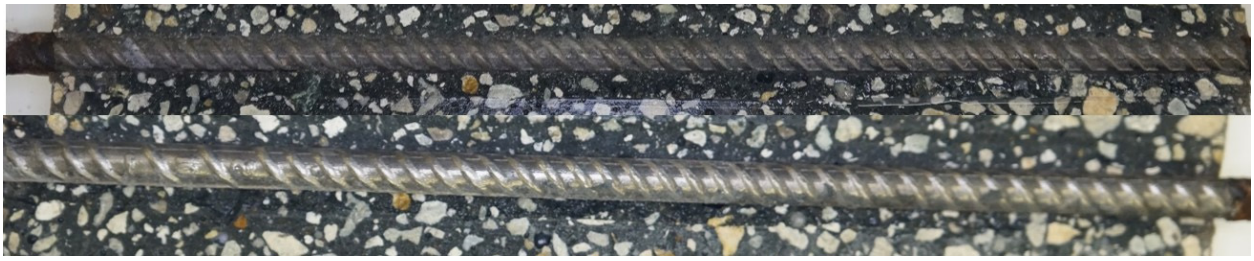

Figure 123. Rebar embedded in T1 specimen: top and bottom, no corrosion on either side.

Figure 123 shows the surface condition of the rebar before cleaning the top and the bottom sides of the rebar embedded in sample T1. In this case, the picture on the second row shows the bottom side of the rebar. No corrosion was observed within the region under the reservoir or the section within the concrete. However, surface corrosion took place on the rebar extending outside of the concrete. It is not clear why the potential and the R_c magnitude suggested some activity on the rebar. No corrosion was observed on the T2 terminated sample on the top side, a

small corrosion spot was observed close to the concrete edge outside of the region under the reservoir. Corrosion was observed on the rebar extending outside the concrete. The surface extending outside of all other T1 and T2 samples was wire brushed and then covered with shrinkage wrap. Sample 16X was terminated and it is not clear if corrosion was taking place before exposing the rebar. Figure 124 and Figure 125 show the surface before and after cleaning for rebars A and B embedded in specimens 16X. The red rust spots might have developed upon exposing the rebar to the laboratory environment. Upon cleaning both show that there was no cross-section loss.

Figure 124. Before and after cleaning rebar 16X–A

Figure 125. Before and after cleaning rebar 16X–B

Chapter 6 – Discussion

6.1 – Accelerated chloride transport

Electromigration test is typically used to measure the chloride non–steady-state migration coefficient. A modified electromigration method was implemented here to accelerate the chloride transport. The electromigration drove the chlorides into the concrete. For samples for which electromigration was applied in 2016, the rebar was not used as one of the electrodes. The chlorides penetrated and were based on E_{corr} and R_c values, corrosion of the embedded rebar was initiated. In some cases, there was a delay from when electromigration was suspended and when a significant rebar potential drop occurred. The accelerated chloride transport works well to initiate rebar corrosion embedded in high–performance concrete.

6.2 – Corrosion monitoring

Monitoring of corrosion evolution via EIS, LPR and GP tests were successful in assessing changes in rebar potential, R_c and R_s. During the corrosion propagation, the values sometimes oscillated. In a few instances, the rebar potential and corresponding R_c value drifted towards more positive potential and larger R_c, respectively. This event suggests that the corroding site tended to re-passivate or that with time the non-corroding region was able to polarize the rebar to more positive values.

Similarities on the corrosion current magnitude for samples with very different solution reservoirs might be influenced by the actual corroding site size, with the sites on samples with different reservoir lengths having similar corroding sizes. (This speculation needs to be verified as part of a future project: the caveat is that the terminated samples won't be available for additional corrosion site growth).

6.3 – Rebar potential

The rebars of samples exposed outdoors for more than 24 years which contain supplementary cementitious materials experienced interesting rebar potentials vs. time. (Actually, even outdoor samples with OPC and OPC+CN had similar transient but these took place earlier.) The rebar potential was quite noble (positive) for several years (with values as positive as +100 mVsce and as negative as –50 mVsce). After 12 to 15 years on some samples, a modest (moderate) potential decay started to occur (in some samples this took place earlier or later), reaching a new plateau (See appendix 8). In some cases, the rebar potential oscillated during the period of the gradual potential decay. The oscillation either stopped or continued, with values returning to the new nobler values (about 100 to 150 mV more negative than earlier on). The rebar potential on some samples at a later time experienced a significant potential drop and continue to decay or plateau to values more negative than –200 mVsce, and reaching values as negative as –500 mVsce. Samples that experience the latter transition were terminated soon after as part of the previous research effort. Other rebars experienced this transition before the current project started and, in a few cases, the corrosion propagation caused large cracks (one sample each for mixes AO, SU, CO, and SF1), but on others, just a hair crack was observed and rust stains were visible on some as shown in the forensic analysis chapter. The gradual potential decay describe above could be indicative of incipient corrosion or that corrosion sites are small and the non–corroding rebar dominating the measured rebar potential. Measurements with a commercial device suggest that

some electrochemical reactions are taking place. It would be interesting to terminate some of the remaining samples that have rebars potential that have not experienced the transition to significantly more negative potentials, whereas for other allow corrosion to propagate till cracks or rust stains are visible.

The rebar potential trend just described was not observed in the new samples subjected to electromigration. Electromigration was applied to accelerate the chloride migration into the concrete so as to initiate the rebar corrosion. Different types of rebar potential transients were observed. The transient in some cases might be influenced by concrete composition, length (size) of the reservoir, total ampere-hour applied, and other factors as moisture content and RH surrounding the samples. A couple of cases are explored here.

6.4 – Effect of moisture on the monitoring measurements.

A high humidity environment was implemented on most specimens stored indoors. However, some of the 30 cm × 30 cm × 15 cm tall samples (single and four-rebar specimens) were not kept at as high humidity as some of the more recently prepared samples.

For the samples prepared in 2016, a portion of rebar extended outside the concrete as it was not covered with shrinkage wrap. This rebar section sometimes corroded under the high humidity environment, as in some cases the moisture was quite high: droplets were found on the rebar. In some cases, the solution that filled the reservoir spilled outside reaching the rebar, not within the concrete. It is possible that this might have polarized the rebar potential measured and also the Rc values measured. It was decided to cover the rebar section extending outside of the concrete with shrinkage wrap. The electrochemical measurements after this were more consistent when comparing consecutive readings.

6.5 – Cracks

Corrosion did initiate on specimens prepared with concrete containing supplementary cementitious materials. If the propagation stage is long it appears that the corrosion products that build up were able in a few cases to produce cracks. A few outdoor samples with FA and with SF displayed cracks. Only one sample with SF showed cracks that spalled the concrete (see Figure 98).

The mortar samples with fly ash and low w/cm also experienced cracks after re-wetting the concrete for about a year.

6.6 – Distribution of residual cross-sectional area

The rebars removed from outdoor samples were cleaned and then the distribution of the cross-section loss measured. A similar procedure was done on rebars removed from terminated indoor exposed samples. The results from the samples tested outdoor are presented first. A caliper was used to estimate the diameter change as a function of rebar length and also the diameter of the no corroding region and from these values the residual area was calculated. Figure 126 shows the distribution of residual cross-sectional area for two rebars embedded in specimen AO7 (38B) and

one steel bar for AO4 (41B). Localized corrosion is present on the surface, and it is present at two separated sites for AO7–b, one site for 38B–a, and two almost overlapping sites for AO4–C. The two localized corrosion sites on 38B–b have a length of 50 mm, the corrosion site is around 150 mm long for specimen 38B–a, and the corrosion sites have a combined length of 75 mm. The average corrosion mass loss ranges from 1.02% to 6.1%, and the pitting factors are 1.34, 1.12 and 2.99.

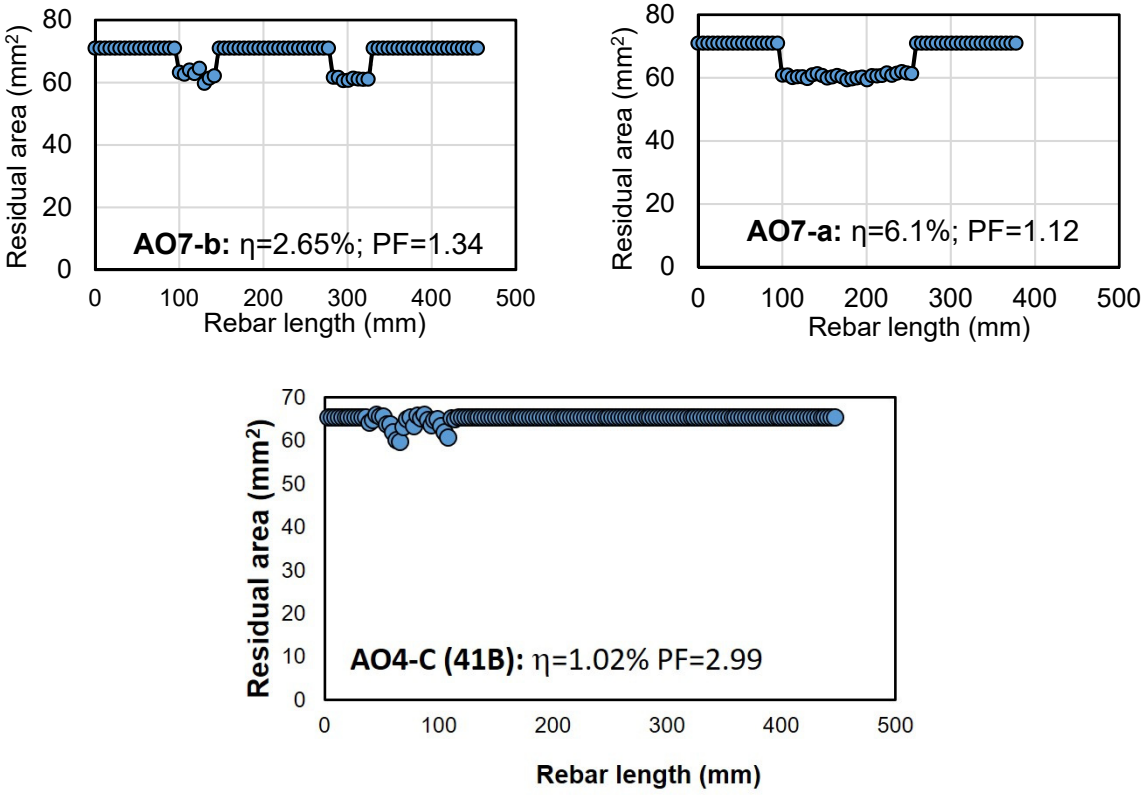

Figure 126. Distribution of residual cross-sectional area along the length for rebars in OPC specimens.

For steel bars embedded in specimen CO2 (61B), the distribution of the residual cross-sectional areas for all three bars are shown in Figure 127. Significant localized corrosion is observed, and the average mass loss ranges from 4.04% to 9.86% with pitting factors varying from 1.56 to 2.06, respectively. Compared with rebars embedded in OPC specimen, the length of the corrosion sites is much longer, from 80 mm to 180 mm. For steel bar 61B–b, the corrosion–induced area loss is almost 50% (35 mm^2 over 70 mm^2) at the most severe cross-section.

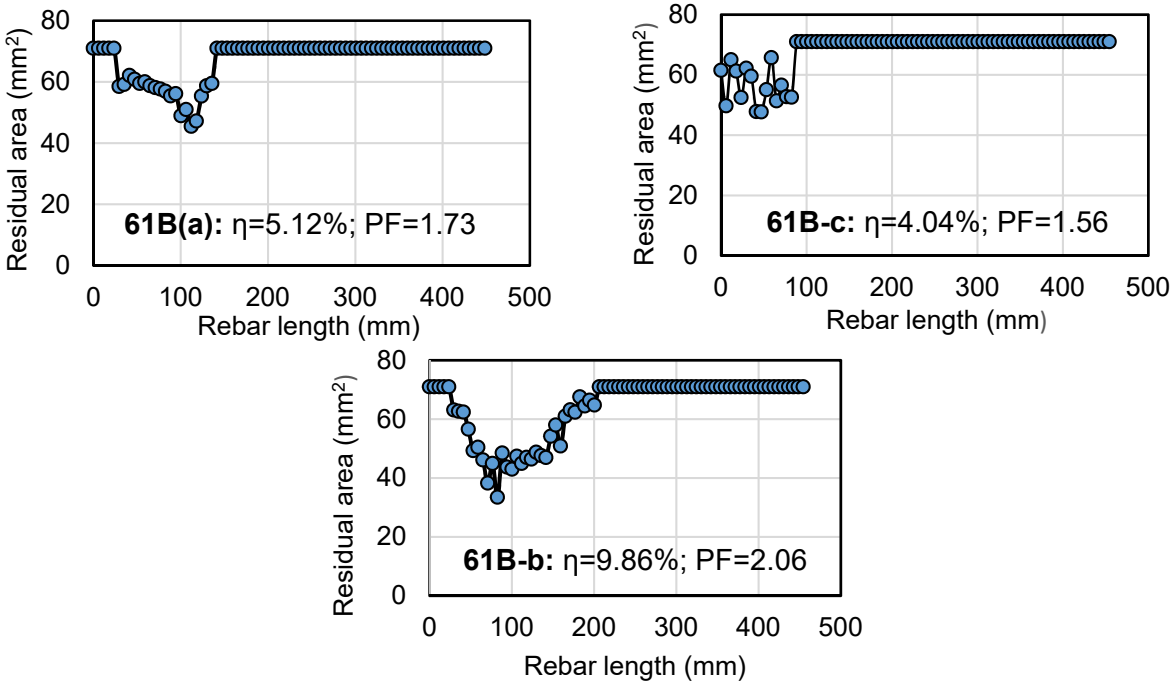

Figure 127. Distribution of residual cross-sectional area along the length for rebars in CO specimen.

The distribution of residual cross-sectional areas for rebars embedded in specimens with fly ash is shown in Figure 128. The average corrosion mass loss ranged between 1.19% and 2.7% and the pitting factor ranged between 1.14 and 2.19. Pitting corrosion happened only in a small area with a length of around 60 mm on two rebars (73B–c and 65B–C) and about 30 mm long on the rebar of specimen FA1–2 (17B). Compared with rebars in OPC specimen, the corrosion attack on FA specimen is less severe, but still enough to cause cracks. Figure 129 shows the distribution of residual cross-sectional area for steel bars embedded in concrete specimens with silica fume, similar to other rebars: corrosion concentrated on one area, with the length varying from 50 mm to 150 mm. The corrosion loss ranges from 1.66% to 4.24%, and the pitting factor is from 1.56 to 2.65. Figure 130 shows the distribution of residual cross-sectional area for steel bars embedded in mortar specimens with Fly Ash. The rebars shown in here had a pitting factor that ranged between 1.57 and 1.86, with the average corrosion mass loss ranging between 0.93 (small solution reservoir) and 2.87 (10 cm solution reservoir).

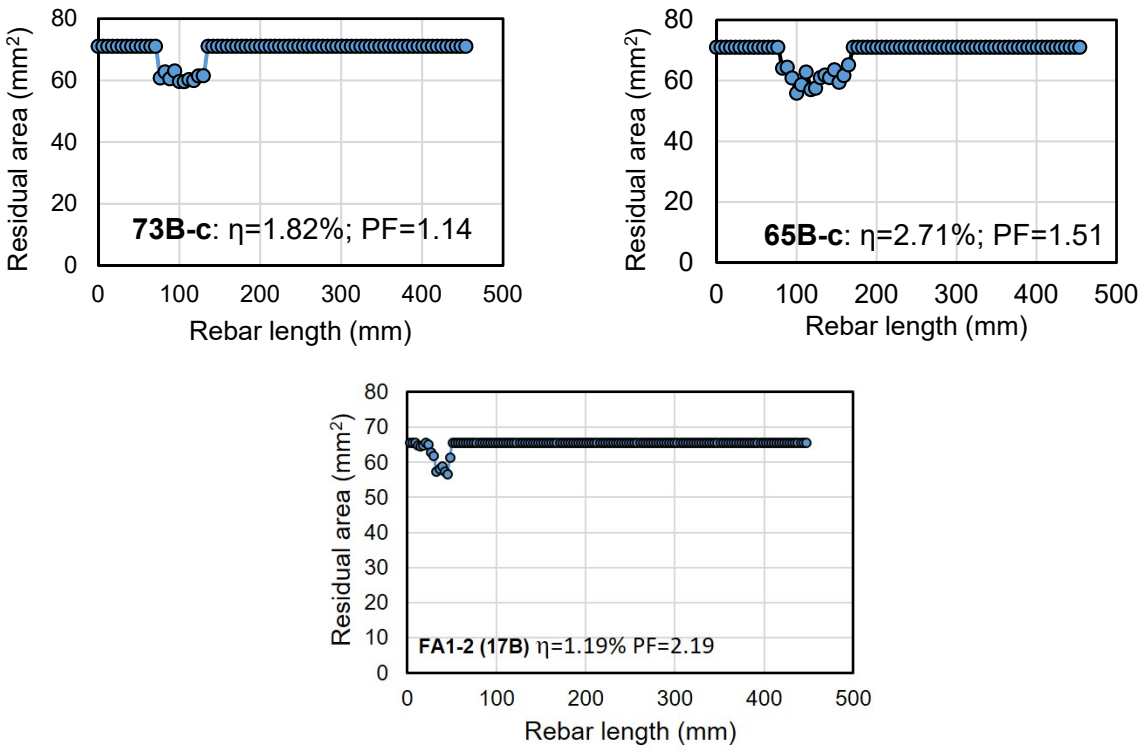

Figure 128. Distribution of residual cross-sectional area along the length for rebars in FA specimens.

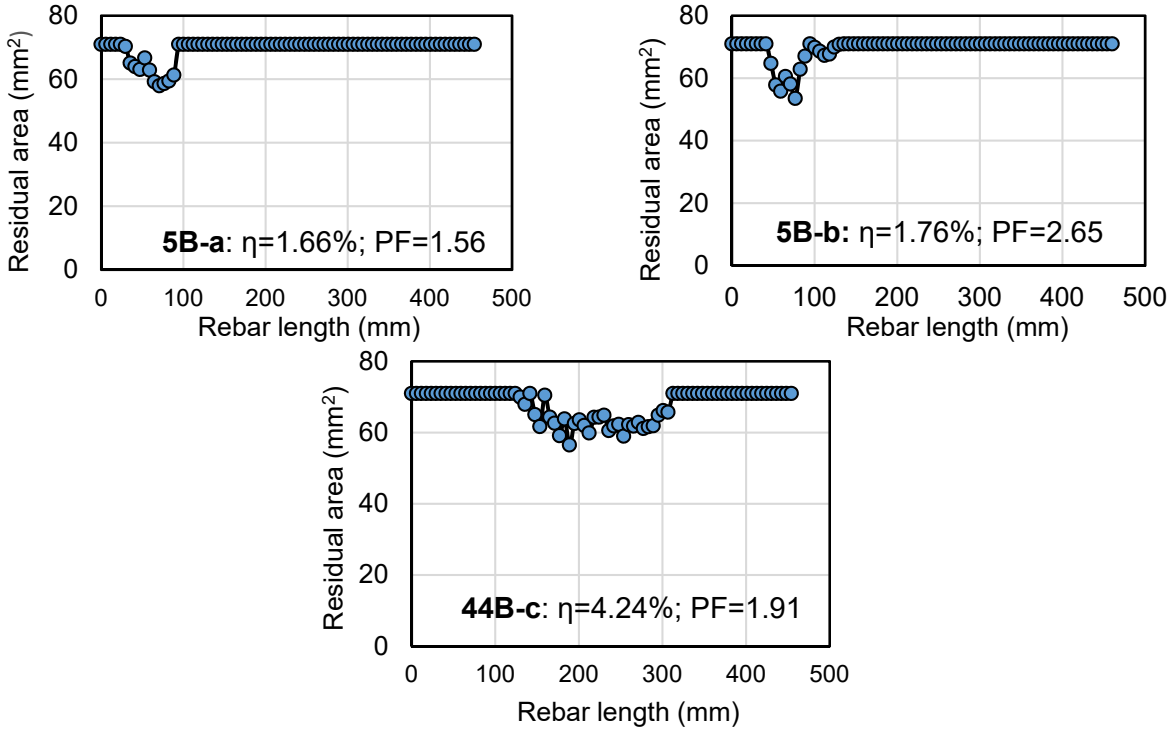

Figure 129. Distribution of residual cross-sectional area along the length for rebars in SF specimens.

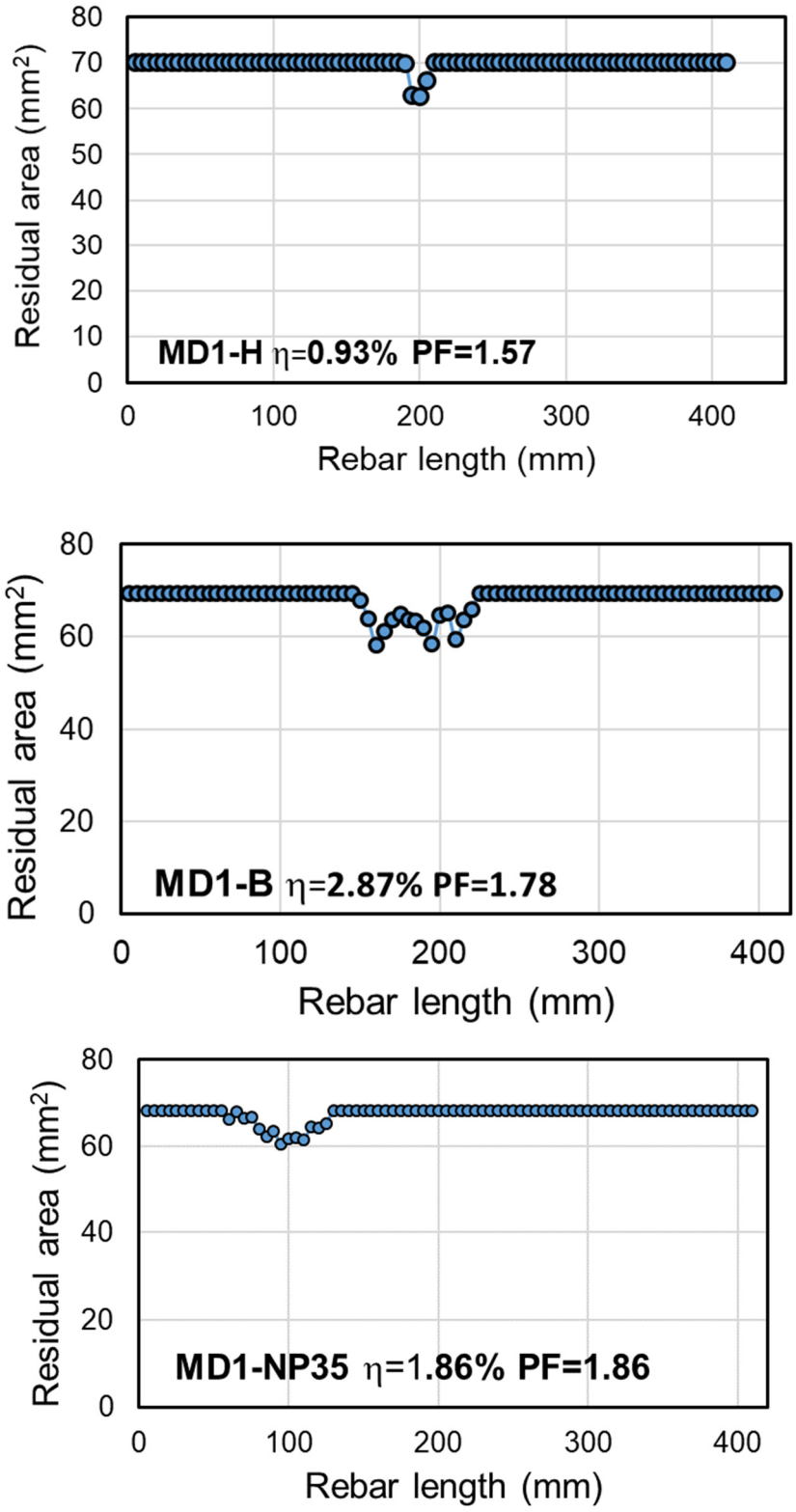

Figure 130 Distribution of residual cross-sectional area along the length of rebars in MD specimens

The average corrosion–induced mass loss of steel bars was also determined by using the equation shown here

$$\eta=(m_0–m)/m_0 \times 100\% \quad (1)$$

where m_0 is the rebar mass before corrosion which was obtained from uncorroded steel bars, m is the rebar mass after exposure test. The distribution of the residual area was used to integrate and estimate the mass of the rebar after cleaning (i.e., mass after exposure test). For samples that had i_{corr} measurements with the Gecor8 and that had a measurable average corrosion–induced mass percent loss. A plot was prepared with this data and is shown in Figure 131. The plot shows two series: empty circles correspond to values measured on rebars obtained from outdoor samples and the filled circles with the rebars removed from indoor exposed samples. It appears that there is some scatter, this might be in part due to the fact that indoor lab specimens were terminated closely after identifying the crack, whereas for outdoor samples corrosion might have been taken place for months to years after (long corrosion propagation) with some causing cracks on the surface of the concrete.

Figure 131 shows a plot of the corrosion rate vs. percent averaged corrosion mass loss (η) and Figure 132 shows a plot of the resistivity vs. η for rebars that after cleaning showed a significant mass loss. The plots on each of these figures have two series and for each series, the corresponding trend line is shown. The empty circle symbol series corresponds to values obtained on rebar removed from samples exposed outdoors to wet/dry cycles with seawater; the filled circle series corresponds to the values measured on rebars removed from indoors samples. The corrosion rate and resistivity are values measured using the Gecor 8. The data suggests a correlation exists but with some scatter. From Figure 131 it can be observed that the rebars removed from laboratory samples appear to have a smaller average mass loss with corrosion rates greater than 1 $\mu A/cm^2$; this could be in part due to smaller solution reservoir (on some of these specimens) and a shorter propagation period. The outdoors samples showed a larger average mass loss suggesting that corrosion had propagated for a longer time.

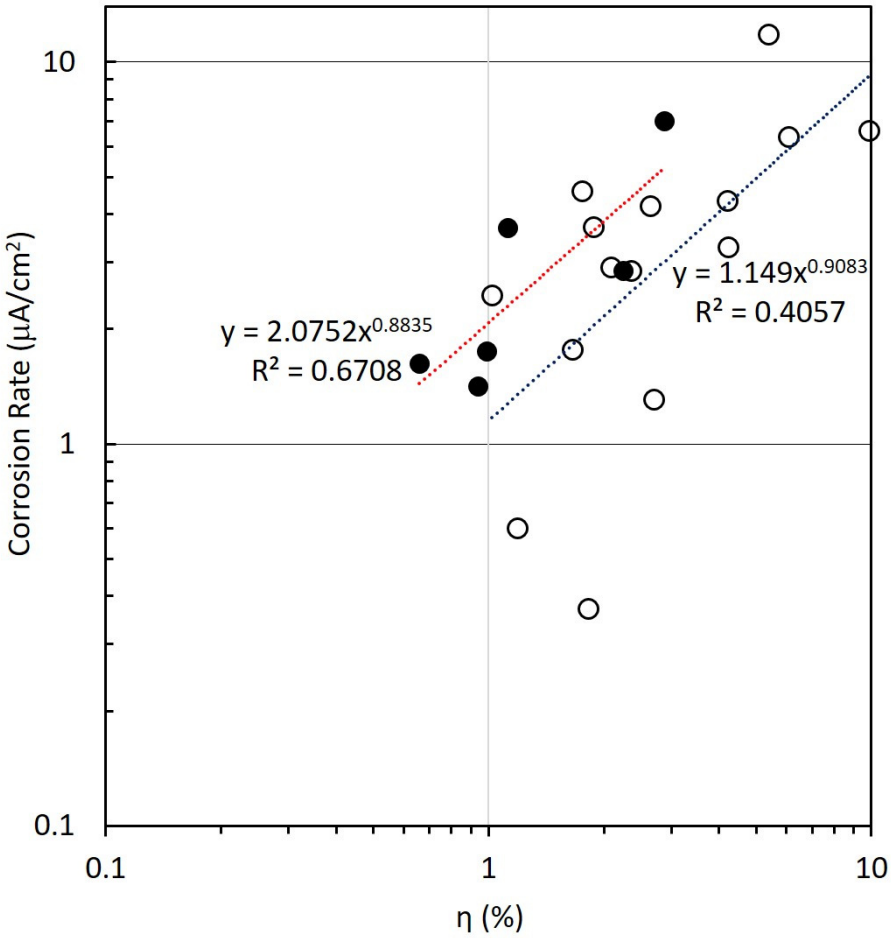

Figure 131. Corrosion rate vs. η

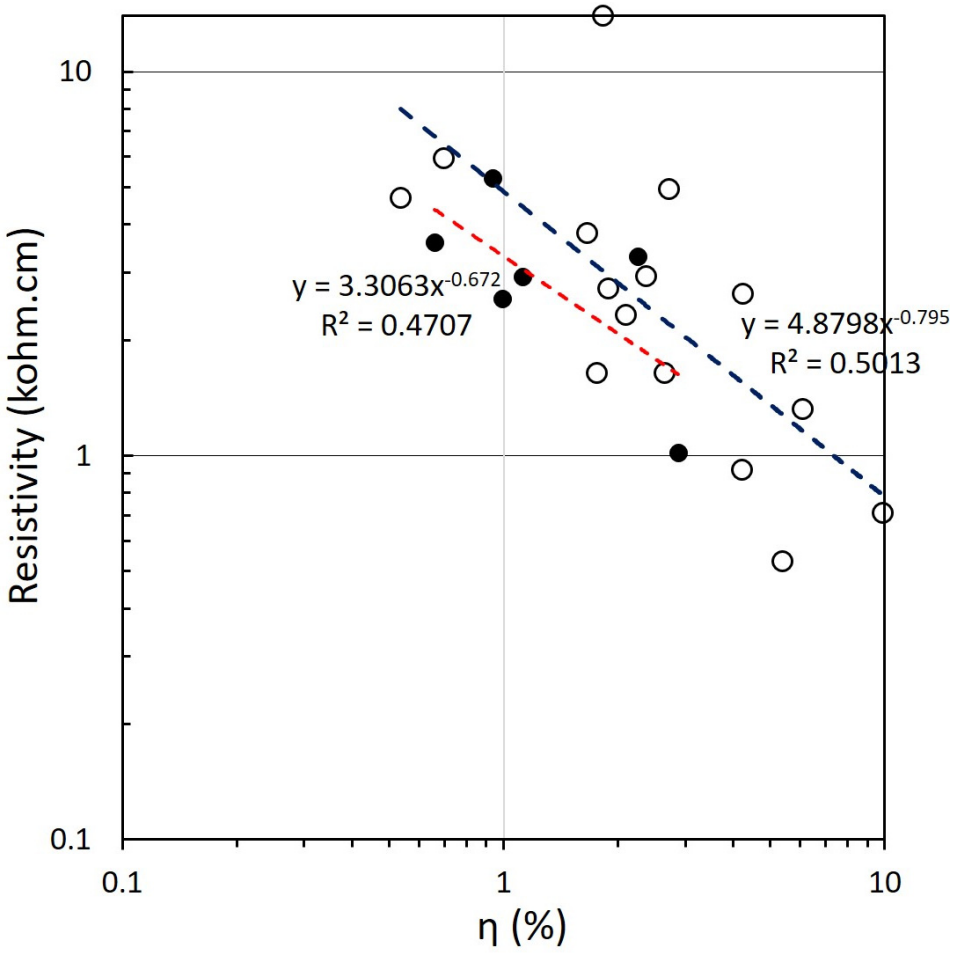

Figure 132. Resistivity vs. η

Chapter 7 – Conclusions

Accelerated chloride transport was successfully implemented on various types of samples. Corrosion was initiated on most embedded rebars after subjecting the samples to accelerated chloride transport. The chlorides penetrated and based on E_{corr} and R_c values, corrosion of the embedded rebar was initiated. In some cases, there was a delay from when electromigration was suspended and when the rebar potential drop occurred. The accelerated chloride transport worked well to accelerate the corrosion initiation of rebars embedded in high-performance concrete.

7.1 – Summary of monitoring lab samples

Linear polarization resistance, galvanostatic pulse, solution resistance, and rebar potential were periodically measured on the lab samples. The corrosion current was calculated from the R_c values calculated after the measurements. A small number had corrosion currents greater than 40 μA. The samples with the largest corrosion current were selected to be terminated as well as some of the samples prepared in 2016 that had the more negative corrosion potential and larger corrosion current.

The corrosion current measured in most instances was larger on rebars of specimens with no supplementary cementitious materials when compared to the corrosion current measured on rebars in specimens with fly ash or fly ash and silica fume. See Table 26, Table 27 and Table 28. In a few cases, the corrosion current values were comparable for cases with the same solution reservoir dimensions.

7.2 – Summary of outdoor samples

In this study, it was observed that based, on the corrosion rate, measured values of rebar potential > –0.2 Vcse did not always indicate a non-corroding reinforcement. The rebar potential of these samples shifted to more negative values. The corrosion rate in these cases was indicative of incipient corrosion. A rebar potential more positive than –0.2 Vcse was likely due to the corroding site being small, and when coupled with the non-corroding region, reached a couple potential of this magnitude. However, no sample was terminated that had a rebar potential > –0.2 Vcse and where the corrosion rate measurement indicated that corrosion was taking place. Terminated samples had rebars with both negative potential and high corrosion current density.

Regardless of concrete composition, corrosion was initiated on some of the rebars. A large number of rebars embedded in AO, CO, SF1, and FA4 became corroded. The AO and CO terminated samples showed significant cross-section loss and longer corrosion sites. It appears that if corrosion propagated long enough, cracks would eventually occur. It is important to note that the samples presented here had a thin concrete cover (< 2 cm) and that larger covers may substantially delay the time to crack.

7.3 – Summary of forensic analysis

Rebars removed from samples exposed outdoors for over 24 years (wet/dry seawater cycles) showed various degrees of corrosion activity. Corrosion was initiated on samples with FA and also on samples with SF, and in some cases, it caused cracks that were visible at the concrete

surface. A larger frequency of damage and more cross-section loss were observed on samples with no supplementary cementitious material (i.e., mixes AO cast with OPC and CO cast with OPC+CN).

Rebars removed from mature indoor samples also showed various degrees of corrosion. In some cases, the length of the corrosion spot was influenced by the solution reservoir size.

Corrosion was initiated on the bottom side of the rebar on specimens that had the reservoir on the troweled surface, on the two samples that showed surface cracks on the concrete above the rebar and on the side surface.

Rebars removed from mortar samples showed various degrees of cross-section loss. The samples exposed to electromigration show areas that ranged from 3 cm to 10 cm (similar to the reservoirs above them), whereas the samples not subjected to electromigration but where corrosion had propagated for several years show one or two corrosion spots with significant cross-section loss.

Rebars removed from recently prepared specimens had small corrosion spots and a more modest amount of cross-section loss.

The distribution of residual cross-section loss was measured on a number of specimens. This allowed calculating the average mass loss. The average mass loss was then correlated to the corrosion rate measured with the Gecor 8 and also vs. the resistivity measured with the Gecor 8. The data suggests a correlation exists but with some scatter. From Figure 131 it can be observed that the rebars removed from laboratory samples appear to have a smaller average mass loss with corrosion rates greater than 1 $\mu A/cm^2$; this could be in part due to smaller solution reservoir (on some of these specimens) and a shorter propagation period. The terminated outdoor samples showed a larger average mass loss with larger corrosion sites, suggesting that corrosion had propagated for a longer time.

References

Ahlström, J., J. Tidblad, B. Sederholm, and L. Wadsö. 2016. "Influence of Chloride and Moisture Content on Steel Rebar Corrosion in Concrete." *Materials and Corrosion* 67 (10): 1049–58. https://doi.org/10.1002/maco.201508799.

Ahmad, Shamsad. 2003. "Reinforcement Corrosion in Concrete Structures, Its Monitoring and Service Life Prediction - A Review." *Cement and Concrete Composites* 25 (4–5 SPEC): 459–71. https://doi.org/10.1016/S0958-9465(02)00086-0.

Ahmad, Shamsad, and Shamsad Ahmad. 2014. "An Experimental Study on Correlation between Concrete Resistivity and Reinforcement Corrosion Rate." *Anti-Corrosion Methods and Materials* 61 (3): 158–65. https://doi.org/10.1108/ACMM-07-2013-1285.

Angst, U, B Elsener, A Jamali, and B Adey. 2012. "Concrete Cover Cracking Owing to Reinforcement Corrosion – Theoretical Considerations and Practical Experience Dedicated to Professor Dr . Bernhard Elsener on the Occasion of His 60th Birthday." *Materials and Corrosion*, no. 12: 1069–77. https://doi.org/10.1002/maco.201206669.

Angst, Ueli, Bernhard Elsener, Claus K. Larsen, and Øystein Vennesland. 2010. "Considerations on the Effect of Sample Size for the Critical Chloride Content in Concrete." In *Proc. 2nd Int. Symp. on Service Life Design for Infrastructures*, 569–76. Delft: RILEM Publications S.A.R.L.

Angst, Ueli M., Bernhard Elsener, Claus K. Larsen, and Øystein Vennesland. 2011. "Chloride Induced Reinforcement Corrosion: Electrochemical Monitoring of Initiation Stage and Chloride Threshold Values." *Corrosion Science* 53 (4): 1451–64. https://doi.org/10.1016/j.corsci.2011.01.025.

ASTM C876-15. n.d. "Standard Test Method for Corrosion Potentials of Uncoated Reinforcing Steel in Concrete,." West Conshohocken, PA.

ASTM G01-03. 2017. "Standard Practice for Preparing, Cleaning, and Evaluating Corrosion Test Specimens." West Conshohocken, PA

Broomfield, John. 2007. "Corrosion of Steel in Concrete," 277.

Budiansky, N D, J L Hudson, and J R Scully. 2004. "Origins of Persistent Interaction among Localized Corrosion Sites on Stainless Steel." *Journal of The Electrochemical Society* 151 (4): B233–43. https://doi.org/10.1149/1.1666168.

Busba, Ezeddin, and Alberto A. Sagüés. 2013. "Critical Localised Corrosion Penetration of Steel Reinforcement for Concrete Cover Cracking." *Nace Corrosion 2013 Conference & Expo*, no. 2747: 1–14.

Cabrera, JG, and P Ghoddoussi. 1994. "The Influence of Fly Ash on the Resistivity and Rate of Corrosion of Reinforced Concrete." *Durability of Concrete: Proceedings of the Third CANMET-ACI International Conference*, 229–44.

Choi, Yoon Seok, Jung Gu Kim, and Kwang Myong Lee. 2006. "Corrosion Behavior of Steel Bar Embedded in Fly Ash Concrete." *Corrosion Science* 48 (7): 1733–45. https://doi.org/10.1016/j.corsci.2005.05.019.

Criado, M., I. Sobrados, J. M. Bastidas, and J. Sanz. 2016. "Corrosion Behaviour of Coated Steel Rebars in Carbonated and Chloride-Contaminated Alkali-Activated Fly Ash Mortar." *Progress in Organic Coatings* 99: 11–22. https://doi.org/10.1016/j.porgcoat.2016.04.040.

Elsener, B. 2005. "Corrosion Rate of Steel in Concrete-Measurements beyond the Tafel Law." *Corrosion Science* 47 (12): 3019–33. https://doi.org/10.1016/j.corsci.2005.06.021.

FM5-516. 2009. "Florida Method of Test For Determining Low-Levels of Chloride in Concrete

and Raw Materials." Tallahassee, FL, USA: Florida Department of Transportation, 2005.
Garcés, P., L. G. Andión, E. Zornoza, M. Bonilla, and J. Payá. 2010. "The Effect of Processed Fly Ashes on the Durability and the Corrosion of Steel Rebars Embedded in Cement-Modified Fly Ash Mortars." *Cement and Concrete Composites* 32 (3): 204–10. https://doi.org/10.1016/j.cemconcomp.2009.11.006.
Glass, G. K., and N. R. Buenfeld. 1997. "The Presentation of the Chloride Threshold Level for Corrosion of Steel in Concrete." *Corrosion Science* 39 (5): 1001–13. https://doi.org/10.1016/S0010-938X(97)00009-7.
González, J. A., J. M. Miranda, and S. Feliu. 2004. "Considerations on Reproducibility of Potential and Corrosion Rate Measurements in Reinforced Concrete." *Corrosion Science* 46 (10): 2467–85. https://doi.org/10.1016/j.corsci.2004.02.003.
Gu, Ping, and J J Beaudoin. 1998. "Obtaining Effective Half-Cell Potential Measurements in Reinforced Concrete Structures." *Construction Technology Update No.18*, 1–4.
Gulikers, J. 2005. "Theoretical Considerations on the Supposed Linear Relationship between Concrete Resistivity and Corrosion Rate of Steel Reinforcement." *Materials and Corrosion* 56 (6): 393–403. https://doi.org/10.1002/maco.200403841.
Hornbostel, K., C. K. Larsen, and M.R. Geiker. 2013. "Relationship between Concrete Resistivity and Corrosion Rate – A Literature Review." *Cement & Concrete Composites* 39.
Huang, Ran, Jiang Jhy Chang, and Jiann Kuo Wu. 1996. "Correlation between Corrosion Potential and Polarization Resistance of Rebar in Concrete." *Materials Letters* 28 (4–6): 445–50. https://doi.org/10.1016/0167-577X(96)00099-7.
Ip, Brian B Hope and Alan C. n.d. "Corrosion of Steel in Concrete Made With Slag Cement." *ACI Materials Journal* 84 (6). https://doi.org/10.14359/2470.
Jamali, Amin, Ueli Angst, Bryan Adey, and Bernhard Elsener. 2013. "Modeling of Corrosion-Induced Concrete Cover Cracking: A Critical Analysis." *Construction and Building Materials* 42: 225–37. https://doi.org/10.1016/j.conbuildmat.2013.01.019.
Kayali, O., and B. Zhu. 2005. "Chloride Induced Reinforcement Corrosion in Lightweight Aggregate High-Strength Fly Ash Concrete." *Construction and Building Materials* 19 (4): 327–36. https://doi.org/10.1016/j.conbuildmat.2004.07.003.
Law, D W, S G Millard, and J H Bungey. 1999. "The Use of Galvanostatic Pulse Measurements to Determine Corrosion Parameters." *Durability of Building Materials and Components* 8: 310–19.
Martínez, I., and C. Andrade. 2009. "Examples of Reinforcement Corrosion Monitoring by Embedded Sensors in Concrete Structures." *Cement and Concrete Composites* 31 (8): 545–54. https://doi.org/10.1016/j.cemconcomp.2009.05.007.
Millard, S. G., D. Law, J. H. Bungey, and J. Cairns. 2001. "Environmental Influences on Linear Polarisation Corrosion Rate Measurement in Reinforced Concrete." *NDT and E International* 34 (6): 409–17. https://doi.org/10.1016/S0963-8695(01)00008-1.
Miranda, J. M., A. Fernández-Jiménez, J. A. González, and A. Palomo. 2005. "Corrosion Resistance in Activated Fly Ash Mortars." *Cement and Concrete Research* 35 (6): 1210–17. https://doi.org/10.1016/j.cemconres.2004.07.030.
Montemor, M.F, a.M.P Simões, and M.M Salta. 2000. "Effect of Fly Ash on Concrete Reinforcement Corrosion Studied by EIS." *Cement and Concrete Composites* 22 (3): 175–85. https://doi.org/10.1016/S0958-9465(00)00003-2.
Monticelli, C., M. E. Natali, A. Balbo, C. Chiavari, F. Zanotto, S. Manzi, and M. C. Bignozzi. 2016a. "A Study on the Corrosion of Reinforcing Bars in Alkali-Activated Fly Ash Mortars

under Wet and Dry Exposures to Chloride Solutions." *Cement and Concrete Research* 87: 53–63. https://doi.org/10.1016/j.cemconres.2016.05.010.
Monticelli, C, M E Natali, A Balbo, C Chiavari, F Zanotto, S Manzi, and M C Bignozzi. 2016b. "Corrosion Behavior of Steel in Alkali-Activated Fly Ash Mortars in the Light of Their Microstructural, Mechanical and Chemical Characterization." *Cement and Concrete Research* 80 (C): 60–68. https://doi.org/10.1016/j.cemconres.2015.11.001.
Morris, W., A. Vico, M. Vazquez, and S. R. De Sanchez. 2002. "Corrosion of Reinforcing Steel Evaluated by Means of Concrete Resistivity Measurements." *Corrosion Science* 44 (1): 81–99. https://doi.org/10.1016/S0010-938X(01)00033-6.
Morris, W, A Vico, and M Vázquez. 2004. "Chloride Induced Corrosion of Reinforcing Steel Evaluated by Concrete Resistivity Measurements." *Electrochimica Acta* 49 (25): 4447–53. https://doi.org/10.1016/j.electacta.2004.05.001.
Newton, C J, and J M Sykes. 1988. "A Galvanostatic Pulse Technique for Investigation of Steel Corrosion in Concrete." *Corrosion Science* 28 (11): 1051–74. https://doi.org/https://doi.org/10.1016/0010-938X(88)90101-1.
Oelßner, W., F. Berthold, and U. Guth. 2006. "The IR Drop - Well-Known but Often Underestimated in Electrochemical Polarization Measurements and Corrosion Testing." *Materials and Corrosion* 57 (6): 455–66. https://doi.org/10.1002/maco.200603982.
Otieno, M., H. Beushausen, and M. Alexander. 2012. "Prediction of Corrosion Rate in Reinforced Concrete Structures - A Critical Review and Preliminary Results." *Materials and Corrosion* 63 (9): 777–90. https://doi.org/10.1002/maco.201106282.
Otieno, M.B., M.G. Alexander, and H.-D. Beushausen. 2010. "Corrosion in Cracked and Uncracked Concrete – Influence of Crack Width, Concrete Quality and Crack Reopening." *Magazine of Concrete Research* 62 (6): 393–404. https://doi.org/10.1680/macr.2010.62.6.393.
Polder, R.B., Bertolini, L. 1983. "Concrete Resistivity and Reinforcement Corrosion Rate as a Function of Temperature and Humidity of the Environment." TNO Report 273.
Presuel-Moreno, F., Y. Liu, and A. Suarez. 2010. "Characterization of New and Old Concrete Structures Using Surface Resistivity Measurements." Florida Department of Transportation Research Report BD-546-08, Florida Atlantic University; Boca Raton, FL:
Presuel-Moreno, F.J., and E.I. Moreno. 2016. "Effects of Fly Ash and Silica Fume on Time to Corrosion Initiation for Specimens Exposed Long Term to Seawater." *ACI SP-308*.
Presuel-Moreno, F, Y. Liu, Y.-Y. Wu, and W. Arias. 2013. "Analysis and Estimation of Service Life of Corrosion Prevention Materials Using Diffusion, Resistivity and Accelerated Curing for New Bridge Structures." Florida Department of Transportation Research Report BDK79-977-02 (Volume 1) Florida Atlantic University; Boca Raton, FL.
Presuel-Moreno, Francisco. 2015. "Corrosion Propagation of Carbon Steel Rebar With Different Concrete Covers and Concrete/Mortar Compositions." *CORROSION 2015*. Dallas, Texas: NACE International.
Romano, Pedro, Paulo S.D. Brito, and Luiz Rodrigues. 2013. "Monitoring of the Degradation of Concrete Structures in Environments Containing Chloride Ions." *Construction and Building Materials* 47: 827–32. https://doi.org/10.1016/j.conbuildmat.2013.05.042.
Sánchez, A N, and A A Sagüés. 2017. "Reinforced Concrete Corrosion Damage Forecast with Potential Dependent Threshold: Sensitivity to System Parameters." *CORROSION 2017*. New Orleans, Louisiana, USA: NACE International.
Saraswathy, Velu, and Ha Won Song. 2006. "Electrochemical Studies on the Corrosion

Performance of Steel Embedded in Activated Fly Ash Blended Concrete." *Electrochimica Acta* 51 (22): 4601–11. https://doi.org/10.1016/j.electacta.2006.01.005.
Stern, Milton, and A.L Geary. 1957. "Electrochemical Polarization." *Journal of The Electrochemical Society* 104 (9): 559. https://doi.org/10.1149/1.2428653.
Tanner, R. 2006. "Effect of Polarization on Steel Embedded in Simulated Piling Specimens Evaluated by Critical Chloride Threshold." Master Thesis, Florida Atlantic University, Boca Raton, FL.
Torres-Acosta, Andrés A., and Alberto A. Sagüés. 2004. "Concrete Cracking by Localized Steel Corrosion - Geometric Effects." *ACI Materials Journal* 101 (6): 501–7. https://doi.org/10.14359/13489.
Tuutti, K. 1982. "Corrosion of Steel in Concrete." Lund University.
Walsh, Michael T, and Alberto A Sagüés. 2016. "Steel Corrosion in Submerged Concrete Structures—Part 1: Field Observations and Corrosion Distribution Modeling." *CORROSION* 72 (4): 518–33. https://doi.org/10.5006/1945.
Yeau, Kyong Yun, and Eun Kyum Kim. 2005. "An Experimental Study on Corrosion Resistance of Concrete with Ground Granulate Blast-Furnace Slag." *Cement and Concrete Research* 35 (7): 1391–99. https://doi.org/10.1016/j.cemconres.2004.11.010.

Appendix A: List of Symbols and Abbreviations

Table 40. List of symbols and abbreviations

Symbols	Explanation
EIS	Electrochemical impedance spectroscopy
R	Concrete resistance (Ω or kΩ)
ρ	Concrete resistivity (Ωm or kΩ.cm)
OCP	Open circuit potential (mV or V vs. a reference electrode)
Cl_{TH}	Critical chloride concentration
i_{corr}	Corrosion rate in current density ($\mu A/cm^2$)
I_{corr}	Corrosion rate in current (μA) when corroding area is not known
R_s	Solution resistance/concrete resistance from EIS/other method
ρ_s	Resistivity measured between rebar and concrete surface (kΩ.cm)
R_sGP	Solution resistance measured using galvanostatic pulse
Rp	Polarization resistance (Ω or kΩ)
R_{ct}	Charge transfer resistance (Ω or kΩ)
Rp_{app}	Apparent polarization resistance not IR corrected
R_c	Rp_{app} – Rs – corrected polarization resistance (Ω or kΩ)
R_cGP	Rc measured using galvanostatic pulse test
Log	Logarithmic axis
LPR	Linear polarization resistance
GP	Galvanostatic pulse
WE	Working electrode (corroding steel bar)
CE	Counter electrode
RE	Reference electrode
w/c	Water to cement ratio
w/cm	Water to cementitious ratio
OPC	Ordinary Portland cement
c:a:w	Cement: aggregate: water
SC	Slag cement
SF	Silica fume
BFSC	Blast furnace slag cement
FA	Fly ash
SRPC	Sulfate Resistance Portland Cement
Pozz C	Pozzolanic Cement

Appendix B: Mix Designs

Table 41. Slag mix 1 prepared on 4/4/16

TRIAL BATCH -- DATA AND CALCULATIONS
(Saturated, Surface-dry Aggregates)

Specification					Date:	April 4, 2016	
Cement Content:	658	lbs			Project:	**FAU - Slag MIX1**	
W/CM (lbs/lbs):	**0.410**						
C. A. Gradation:	# 89				Weights by:		
Air Content (%):	1.5	to	5.0		Mixing By:		
Slump Range (in):	5	to	8		Design By:		
Fine Agg. SSD:	0.30	Lab =	0.00		Witness By:		
Coarse Agg. SSD:	4.60	Lab =	6.88				
Batch Size (ft^3):	6.0	C.F. =	0.2222				
Ratio of Fine Agg:	41.9 %	by volume					

MATERIAL	SOURCE	WT. PER YD^3 (LB)	SPECIFIC GRAVITY	VOL. PER YD^3 (CF)	WT. PER BATCH (LB)	ADJ. WT. PER BATCH (LB)	REMARKS
CEMENT	Cemex	329	3.15	1.67	73.1	73.1	
FLY ASH							
GGBF SLAG		329	2.86	1.84	73.1	73.1	
ULTRA FINE FA							
METAKAOLIN							
SILICA FUME							
WATER	Local	270	1.00	4.33	60.0	52.3	
FINE AGG.	GA-397	1318	2.63	8.03	292.9	292.0	
COARSE AGG.	87-090	1701	2.45	11.13	378.0	386.6	
AIR ENTRAINER	WR Grace Darex AEA	3.3 oz			21.7 ml	21.7 ml	3 oz.cwt
ADMIXTURE	WR Grace WRDA 60	39.5 oz			259.6 ml	259.6 ml	6 oz.cwt
ADMIXTURE	ADVACAST 600	29.6 oz			194.5 ml	194.5 ml	See Remarks
TOTAL				27.00			

Plastic Property			
Slump (in):	1	Slump By:	
Air (%)	4.20%	Air By:	
Mix Temp (°F):	66	Temp By:	
Unit Weight (lb/ft^3):	139.36	Unit Weight By:	
Workability:	good	Cylinders By:	
Initial Set (min):		Air Temp (°F):	70
Final Set (min):		Final Bleed:	
Remarks:	extra 50 mL of Advacast 600		

Moisture Calculations	
rock weight - wet(lb)	rock weight - dry (lb)
14.6	13.66

Table 42. Slag mix 2 prepared on 4/4/16

TRIAL BATCH -- DATA AND CALCULATIONS
(Saturated, Surface-dry Aggregates)

Specification				Date:	April 4, 2016	
Cement Content:	658	lbs		Project:	**FAU - Slag MIX2**	
W/CM (lbs/lbs):	**0.410**					
C. A. Gradation:	# 89			Weights by:		
Air Content (%):	1.5	to	5.0	Mixing By:		
Slump Range (in):	5	to	8	Design By:		
Fine Agg. SSD:	0.30	Lab =	0.00	Witness By:		
Coarse Agg. SSD:	4.60	Lab =	6.88			
Batch Size (ft^3):	6.0	C.F. =	0.2222			
Ratio of Fine Agg:	41.9 %	by volume				

MATERIAL	SOURCE	WT. PER YD^3 (LB)	SPECIFIC GRAVITY	VOL. PER YD^3 (CF)	WT. PER BATCH (LB)	ADJ. WT. PER BATCH (LB)	REMARKS
CEMENT	Cemex	329	3.15	1.67	73.1	73.1	
FLY ASH							
GGBF SLAG		329	2.86	1.84	73.1	73.1	
ULTRA FINE FA							
METAKAOLIN							
SILICA FUME							
WATER	Local	270	1.00	4.33	60.0	52.3	
FINE AGG.	GA-397	1318	2.63	8.03	292.9	292.0	
COARSE AGG.	87-090	1701	2.45	11.13	378.0	386.6	
AIR ENTRAINER	WR Grace Darex AEA	3.3 oz			21.7 ml	21.7 ml	3 oz.cwt
ADMIXTURE	WR Grace WRDA 60	39.5 oz			259.6 ml	259.6 ml	6 oz.cwt
ADMIXTURE	ADVACAST 600	29.6 oz			194.5 ml	194.5 ml	See Remarks
TOTAL				27.00			

Plastic Property

Slump (in):	0.75	Slump By:	
Air (%)	3.10%	Air By:	
Mix Temp (°F):	65	Temp By:	
Unit Weight (lb/ft^3):	141.28	Unit Weight By:	
Workability:	good	Cylinders By:	
Initial Set (min):		Air Temp (°F):	71
Final Set (min):		Final Bleed:	

Remarks: extra 75 mL of Advacast 600

Moisture Calculations	
rock weight - wet(lb)	rock weight - dry (lb)
14.6	13.66

Table 43. Fly ash mix 1 prepared on 4/18/16

TRIAL BATCH -- DATA AND CALCULATIONS
(Saturated, Surface-dry Aggregates)

Specification				Date:	April 18, 2016	
Cement Content:	658	lbs		Project:	**FAU - Fly Ash**	
W/CM (lbs/lbs):	**0.410**					
C. A. Gradation:	# 89			Weights by:		
Air Content (%):	1.5	to	5.0	Mixing By:		
Slump Range (in):	5	to	8	Design By:		
Fine Agg. SSD:	0.30	Lab =	0.00	Witness By:		
Coarse Agg. SSD:	4.60	Lab =	8.26			
Batch Size (ft^3):	6.0	C.F. =	0.2222			
Ratio of Fine Agg:	52.0 %	by volume				

MATERIAL	SOURCE	WT. PER YD^3 (LB)	SPECIFIC GRAVITY	VOL. PER YD^3 (CF)	WT. PER BATCH (LB)	ADJ. WT. PER BATCH (LB)	REMARKS
CEMENT	Cemex	526	3.15	2.68	116.9	116.9	
FLY ASH		132	2.43	0.87	29.3	29.3	
GGBF SLAG							
ULTRA FINE FA							
METAKAOLIN							
SILICA FUME							
WATER	Local	270	1.00	4.33	60.0	49.7	
FINE AGG.	GA-397	1631	2.63	9.94	362.4	361.4	
COARSE AGG.	87-090	1404	2.45	9.18	312.0	323.4	
AIR ENTRAINER	WR Grace Darex AEA	3.3 oz			21.7 ml	21.7 ml	3 oz.cwt
ADMIXTURE	WR Grace WRDA 60	39.5 oz			259.6 ml	259.6 ml	6 oz.cwt
ADMIXTURE	ADVACAST 600	29.6 oz			194.5 ml	194.5 ml	See Remarks
TOTAL				27.00			

Plastic Property			
Slump (in):	1.75	Slump By:	
Air (%)	8.50%	Air By:	
Mix Temp (°F):	65	Temp By:	
Unit Weight (lb/ft^3):	135.8	Unit Weight By:	
Workability:		Cylinders By:	
Initial Set (min):		Air Temp (°F):	
Final Set (min):		Final Bleed:	
Remarks:			

Moisture Calculations	
rock weight - wet(lb)	rock weight - dry (lb)
18.34	16.94

Table 44. Fly ash mix 2 prepared on 4/18/16

TRIAL BATCH -- DATA AND CALCULATIONS
(Saturated, Surface-dry Aggregates)

Specification				Date:	April 18, 2016	
Cement Content:	658	lbs		Project:	**FAU - Fly Ash**	
W/CM (lbs/lbs):	**0.410**					
C. A. Gradation:	# 89			Weights by:		
Air Content (%):	1.5	to	5.0	Mixing By:		
Slump Range (in):	5	to	8	Design By:		
Fine Agg. SSD:	0.30	Lab =	0.00	Witness By:		
Coarse Agg. SSD:	4.60	Lab =	8.26			
Batch Size (ft^3):	6.0	C.F. =	0.2222			
Ratio of Fine Agg:	52.0 %	by volume				

MATERIAL	SOURCE	WT. PER YD^3 (LB)	SPECIFIC GRAVITY	VOL. PER YD^3 (CF)	WT. PER BATCH (LB)	ADJ. WT. PER BATCH (LB)	REMARKS
CEMENT	Cemex	526	3.15	2.68	116.9	116.9	
FLY ASH		132	2.43	0.87	29.3	29.3	
GGBF SLAG							
ULTRA FINE FA							
METAKAOLIN							
SILICA FUME							
WATER	Local	270	1.00	4.33	60.0	49.7	
FINE AGG.	GA-397	1631	2.63	9.94	362.4	361.4	
COARSE AGG.	87-090	1404	2.45	9.18	312.0	323.4	
AIR ENTRAINER	WR Grace Darex AEA	3.3 oz			21.7 ml	21.7 ml	3 oz.cwt
ADMIXTURE	WR Grace WRDA 60	39.5 oz			259.6 ml	259.6 ml	6 oz.cwt
ADMIXTURE	ADVACAST 600	29.6 oz			194.5 ml	194.5 ml	See Remarks
TOTAL				27.00			

Plastic Property			
Slump (in):	5	Slump By:	
Air (%)	10.00%	Air By:	
Mix Temp (°F):	65	Temp By:	
Unit Weight (lb/ft^3):	130	Unit Weight By:	
Workability:		Cylinders By:	
Initial Set (min):		Air Temp (°F):	70.7
Final Set (min):		Final Bleed:	
Remarks:			

Moisture Calculations	
rock weight - wet(lb)	rock weight - dry (lb)
18.34	16.94

Table 45. T1 mix prepared on 8/16/16

TRIAL BATCH -- DATA AND CALCULATIONS
(Saturated, Surface-dry Aggregates)

Specification				Date:	July 1, 2016	
Cement Content:	658	lbs		Project:	**Ternary**	
W/CM (lbs/lbs):	**0.410**					
C. A. Gradation:	# 89			Weights by:		
Air Content (%):	1.5	to	5.0	Mixing By:		
Slump Range (in):	5	to	8	Design By:		
Fine Agg. SSD:	0.30	Lab =	0.00	Witness By:		
Coarse Agg. SSD:	4.60	Lab =	8.77			
Batch Size (ft^3):	6.5	C.F. =	0.2407			
Ratio of Fine Agg:	41.3 %	by volume				

MATERIAL	SOURCE	WT. PER YD^3 (LB)	SPECIFIC GRAVITY	VOL. PER YD^3 (CF)	WT. PER BATCH (LB)	ADJ. WT. PER BATCH (LB)	REMARKS
CEMENT	Cemex	198	3.15	1.01	47.6	47.6	
FLY ASH		132	2.39	0.88	31.7	31.7	20% FA
GGBF SLAG		329	2.86	1.84	79.2	79.2	50% Slag
ULTRA FINE FA							
METAKAOLIN							
SILICA FUME							
WATER	Local	270	1.00	4.33	65.0	50.5	
FINE AGG.	GA-397	1283	2.63	7.82	308.9	307.9	
COARSE AGG.	87-090	1701	2.45	11.13	409.5	426.6	
AIR ENTRAINER	WR Grace Darex AEA	13.2 oz			93.8 ml	93.8 ml	2 oz.cwt
ADMIXTURE	WR Grace WRDA 60	39.5 oz			281.3 ml	281.3 ml	6 oz.cwt
ADMIXTURE	ADVACAST 600	32.9 oz			234.4 ml	234.4 ml	5 oz cwt See
TOTAL				27.00			

Plastic Property			
Slump (in):	6.5	Slump By:	
Air (%)	12.40%	Air By:	
Mix Temp (°F):	74	Temp By:	
Unit Weight (lb/ft^3):	127.04	Unit Weight By:	
Workability:	Relatively Wet	Cylinders By:	
Initial Set (min):		Air Temp (°F):	
Final Set (min):		Final Bleed:	
Remarks:	use up to double this amount if needed		

Moisture Calculations	
rock weight - wet(lb)	rock weight - dry (lb)
18.6	17.1

Table 46. T2 mix prepared on 8/16/16

TRIAL BATCH -- DATA AND CALCULATIONS
(Saturated, Surface-dry Aggregates)

Specification				Date:	July 1, 2016	
Cement Content:	658	lbs		Project:	**Ternary**	
W/CM (lbs/lbs):	**0.370**	0.37 UPDTA				
C. A. Gradation:	# 89			Weights by:		
Air Content (%):	1.5	to	5.0	Mixing By:		
Slump Range (in):	5	to	8	Design By:		
Fine Agg. SSD:	0.30	Lab =	0.00	Witness By:		
Coarse Agg. SSD:	4.60	Lab =	8.77			
Batch Size (ft^3):	5.5	C.F. =	0.2037			
Ratio of Fine Agg:	41.3 %	by volume				

MATERIAL	SOURCE	WT. PER YD^3 (LB)	SPECIFIC GRAVITY	VOL. PER YD^3 (CF)	WT. PER BATCH (LB)	ADJ. WT. PER BATCH (LB)	REMARKS
CEMENT	Cemex	487	3.15	2.48	99.2	99.2	
FLY ASH		118	2.39	0.79	24.0	24.0	18% FA
GGBF SLAG			2.86				
ULTRA FINE FA							
METAKAOLIN							
SILICA FUME		53	2.20	0.39	10.8	10.8	8% SF
WATER	Local	230	1.00	3.69	46.9	32.7	+ 2.8 lbs
FINE AGG.	GA-397	1332	2.63	8.12	271.3	270.5	
COARSE AGG.	87-090	1764	2.45	11.54	359.3	374.3	
AIR ENTRAINER	WR Grace Darex AEA	13.2 oz			79.3 ml	79.3 ml	2 oz.cwt
ADMIXTURE	WR Grace WRDA 60	39.5 oz			237.8 ml	237.8 ml	6 oz.cwt
ADMIXTURE	ADVACAST 600	32.9 oz			198.2 ml	198.2 ml	5 oz cwt See Remarks
TOTAL				27.00			

Plastic Property			
Slump (in):	8	Slump By:	
Air (%)	20.00%	Air By:	
Mix Temp (°F):	77	Temp By:	
Unit Weight (lb/ft^3):	114.08	Unit Weight By:	
Workability:	Stiff Until Admix Added	Cylinders By:	
Initial Set (min):		Air Temp (°F):	
Final Set (min):		Final Bleed:	

Remarks: use up to double this amount if needed
Added 80 mL extra Advacast 600

Moisture Calculations	
rock weight - wet(lb)	rock weight - dry (lb)
18.6	17.1

Table 47. Mix design AO and CO

	AO	CO
Cement, kgs	113.5	113.4
Calcium Nitrite, kgs	0	5.2
Water, kgs	33.3	28.6
Coarse Aggregates, kgs	286.8	286.8
Coarse Aggregates, % excess moisture	2.06	2.5
Fine Aggregates, kgs	215.6	215.6
Fine Aggregates, % excess moisture	1.3	1.5
Unit Weight, kgs/m^3	2,292.5	2,276.4
w/cm ratio	0.37	0.367
RCP Average at 91 Days, C	4896 (High)	6285 (High)
Strength Avg. 28 days (MPa)	44.2	48.1
Cementitious per unit volume, kgs/m^3	399	394.4

Note: 1 kg/m^3 = 1.6842 lb/yd^3 , 1 kg = 2.205 lbs, 1MPa – 145.03 psi

Table 48. Mix design FA1, FA2, FA3, FA4

	FA1	FA2	FA3	FA4
Cement, kgs	90.8	73.8	56.7	73.8
Fly Ash, kgs	22.7	39.7	56.7	39.8
Calcium Nitrite, kgs	0	0	0	5.2
Water, kgs	27.6	27.8	28.0	24.4
Coarse Aggregates, kgs	287.4	287.4	287.4	288.4
Coarse Aggregates, % excess moisture	2.96	2.3	2.3	2.9
Fine Aggregates, kgs	212.4	206.0	199.6	203.8
Fine Aggregates, % excess moisture	2.68	3.68	3.68	3.0
Unit Weight, kgs/m^3	2,263.6	2,247.6	2,231.6	2,231.6
w/cm ratio	0.367	0.37	0.37	0.363
RCP Avg. 91 Days, C	989	713	731	NA
Strength Avg. 28 days (MPa)	45.5	42.7	36.3	34.2
Strength Avg. 91 days (MPa)	53.2	52.9	45.6	44.5
Cementitious per unit volume, kgs/m^3	399	400.4	401	396

Note: 1 kg/m^3 = 1.6842 lb/yd^3 , 1 kg = 2.205 lbs, 1MPa – 145.03 psi, Type F fly ash was used.

Table 49. Mix design SF1, SF2, SF3, SF4

	SF1	SF2	SF3	SF4
Cement, kgs	110.2	104.4	96.6	104.4
Silica Fume, kgs	7.2	19	35.6	19
Calcium Nitrite, kgs	0	0	0	2.68
Water, kgs	25	18.8	10.2	16.6
Coarse Aggregates, kgs	288.4	288.4	288.4	288.4
Coarse Aggregates, % excess moisture	2.65	2.7	2.9	2.9
Fine Aggregates, kgs	217.4	215.2	212.2	215.2
Fine Aggregates, % excess moisture	2.680	2.68	2.68	2.7
Unit Weight, kgs/m^3	2,279.6	2,273.2	2,262.0	*2,265.2*
w/cm Ratio	0.37	0.367	0.368	0.365
RCP Avg. 91 Days, C	2061	720	598	868
Strength Avg. 28 days (MPa)	48.7	50.8	52.6	48.8
Strength Avg. 91 days (MPa)	52.6	52.2	53.0	51.7
Cementitious per unit volume, kgs/m^3	397	397.6	399	396

Note: 1 kg/m^3 = 1.6842 lb/yd^3 , 1 kg, Silica Fume slurry was used and part of the mass counted towards the water.

Appendix C: Older Samples Single Rebar with 5-cm Concrete Cover.

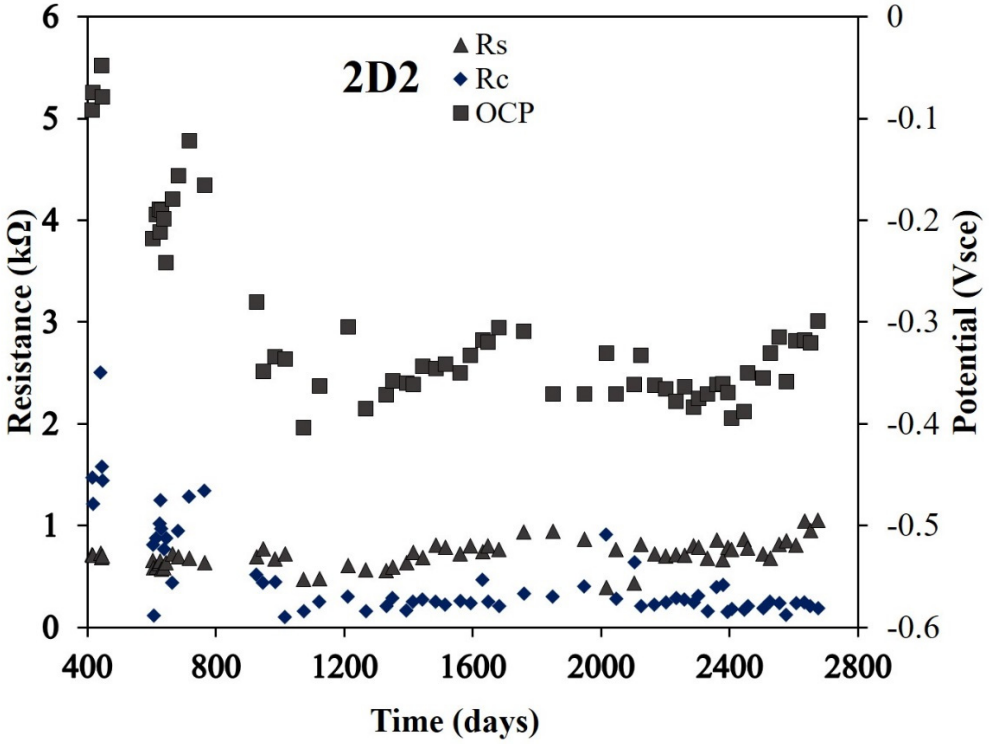

Figure 133. Rebar potentials, R_s, and R_c values measured on rebar in 2D2 specimen

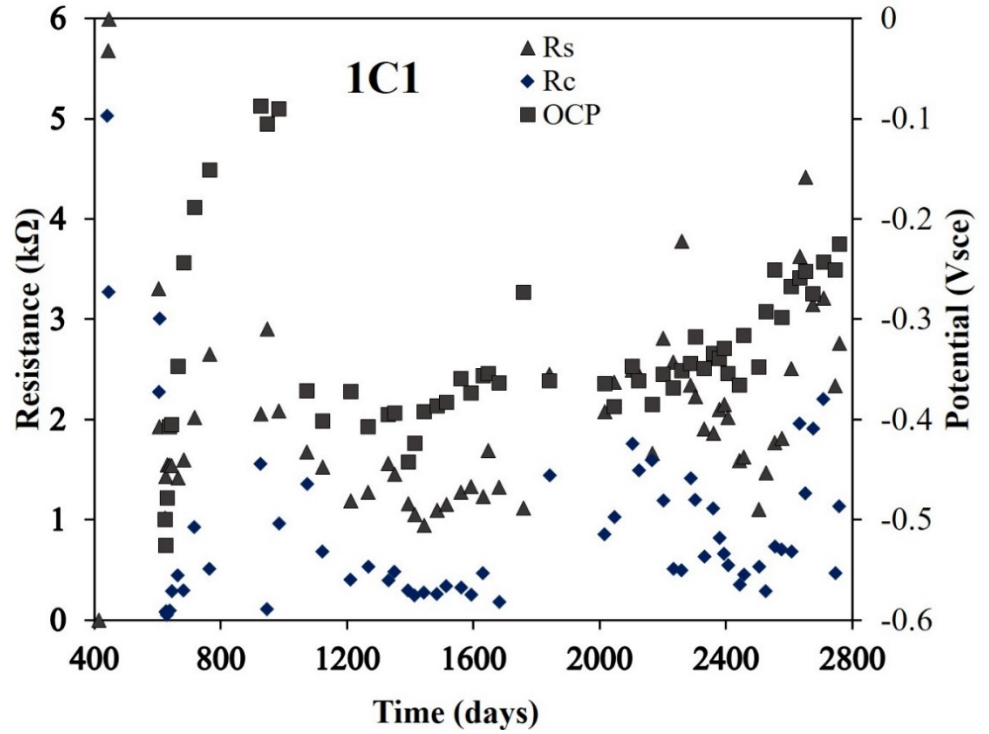

Figure 134. Rebar potentials, R_s, and R_c values measured on rebar in 1C1 specimen

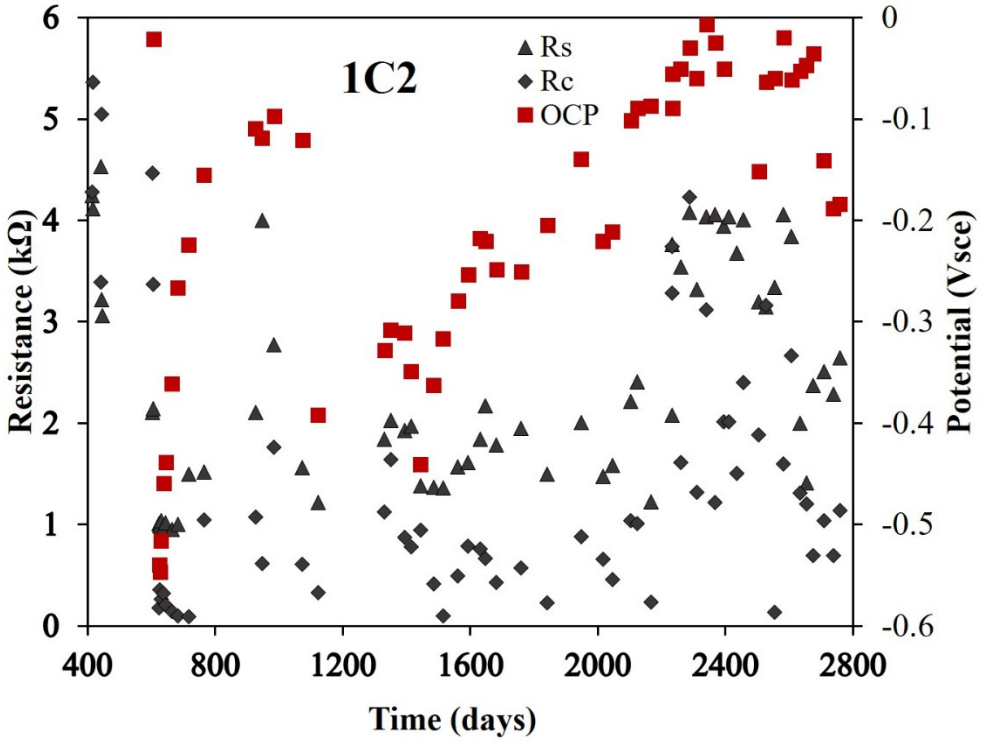

Figure 135. Rebar potentials, R_s, and R_c values measured on rebar in 1C2 specimen

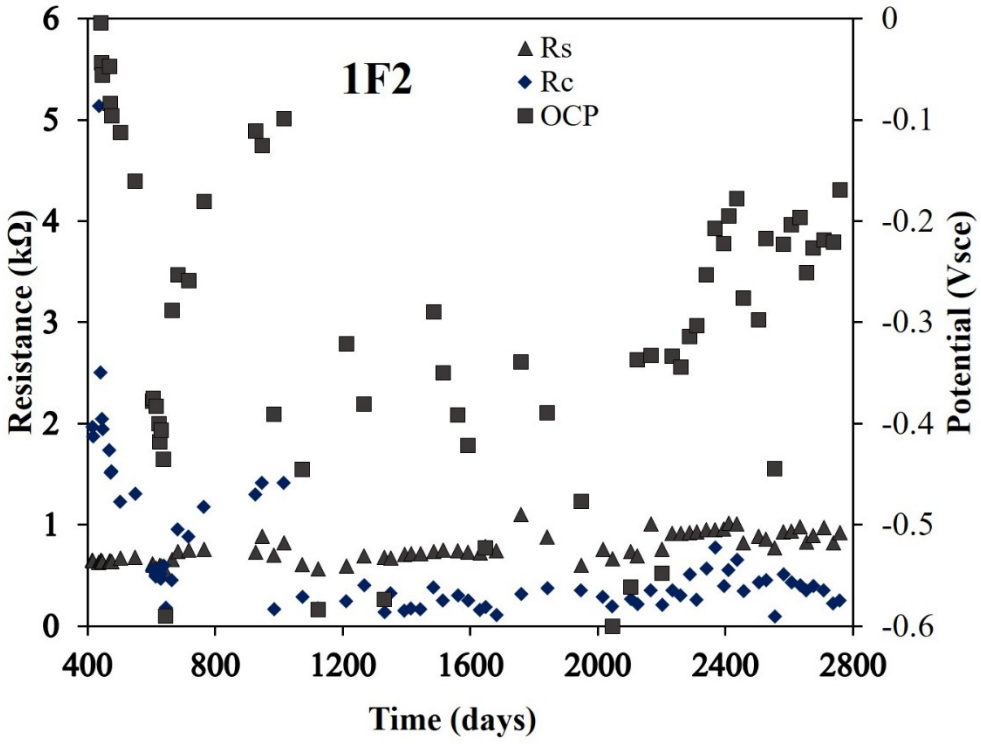

Figure 136. Rebar potentials, R_s, and R_c values measured on rebar in 1F2 specimen

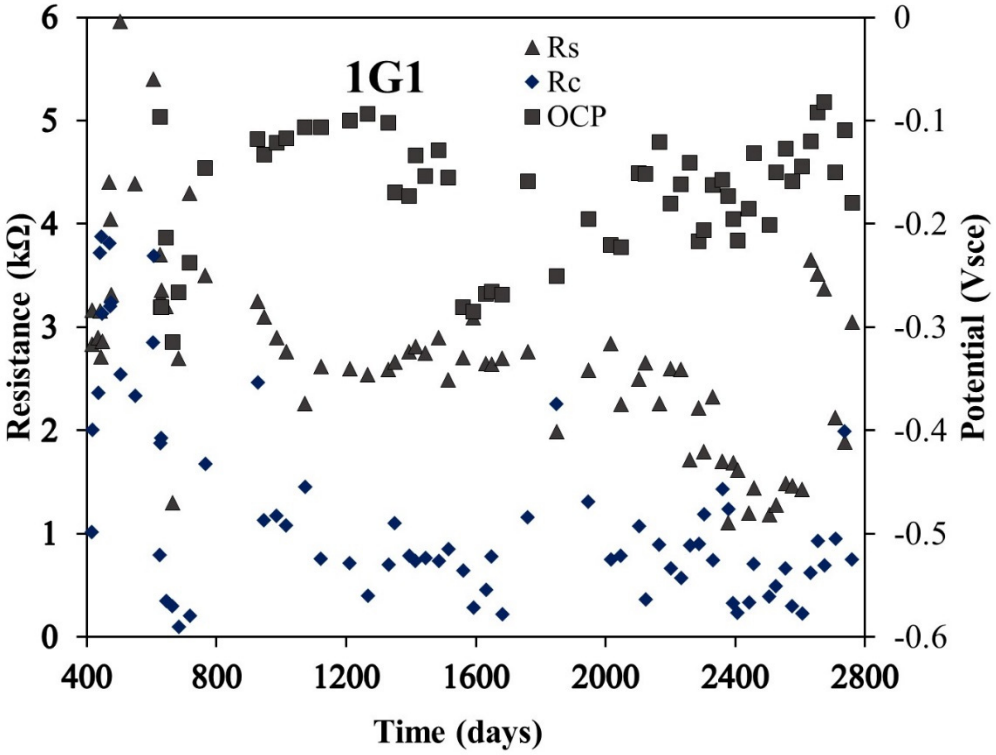

Figure 137. Rebar potentials, R_s, and R_c values measured on rebar in 1G1 specimen

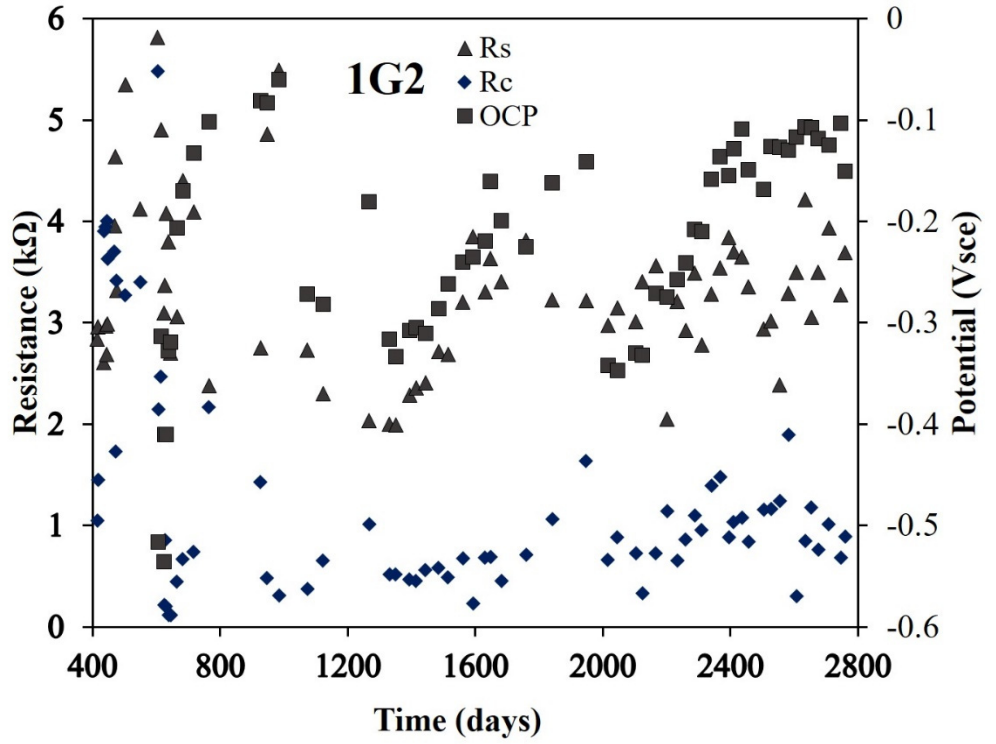

Figure 138. Rebar potentials, R_s, and R_c values measured on rebar in 1G2 specimen

Appendix D: SL Single Rebar and FA Single Rebar

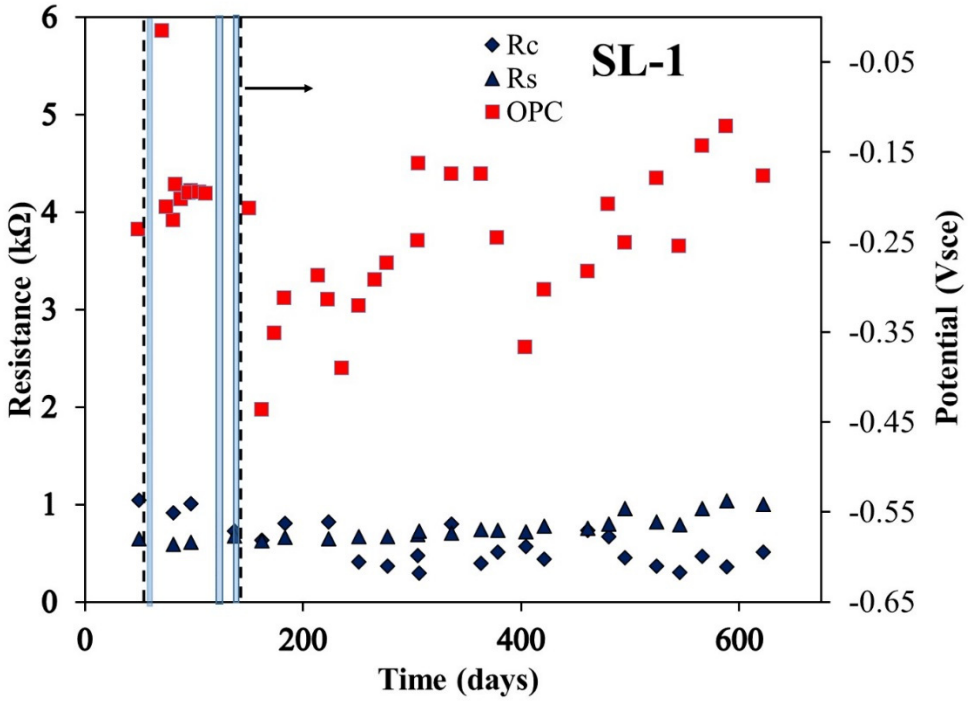

Figure 139. Rebar potentials, R_s, and R_c values measured on rebar in SL-1 specimen

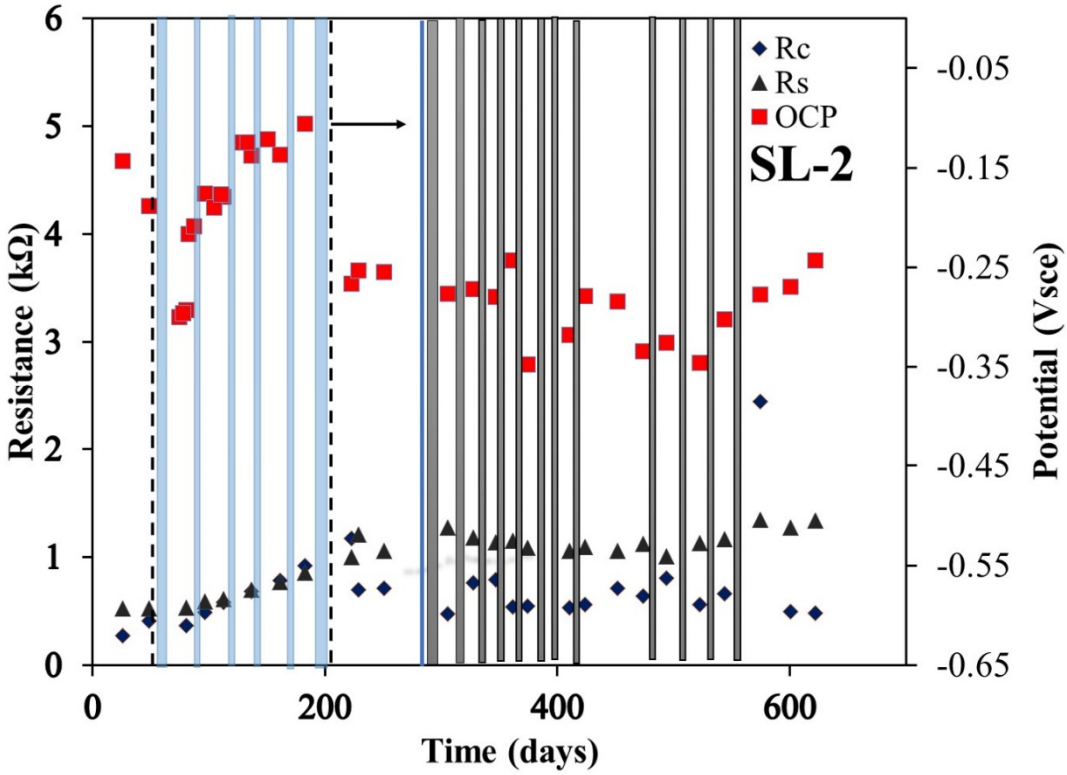

Figure 140. Rebar potentials, R_s, and R_c values measured on rebar in SL-2 specimen

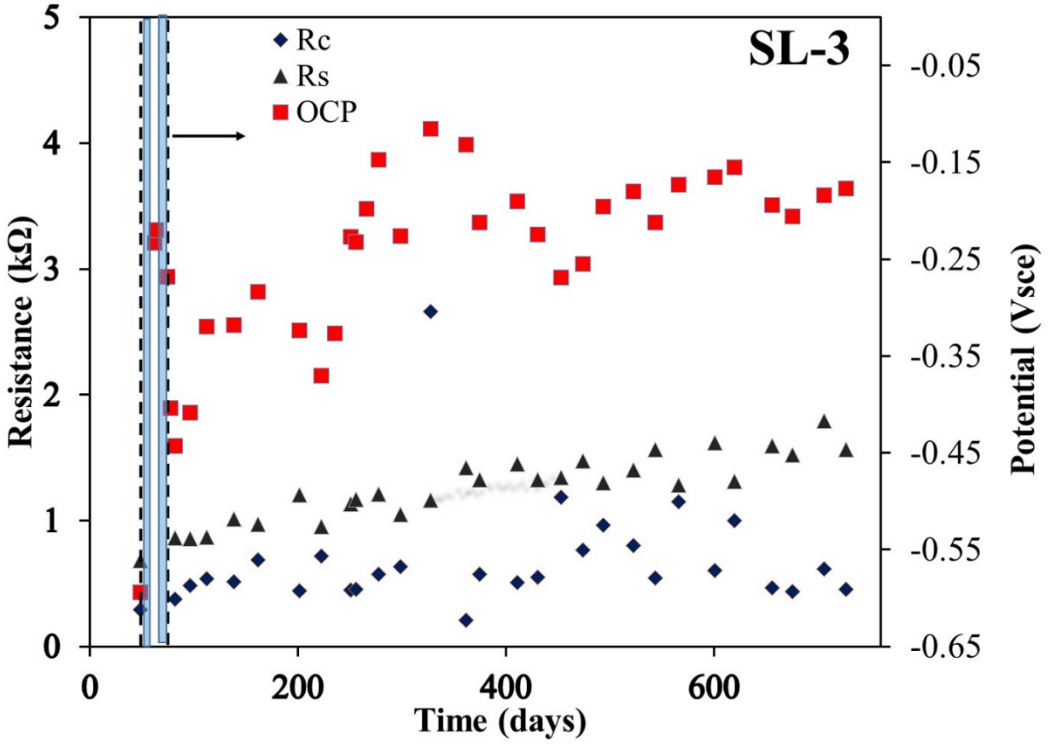

Figure 141. Rebar potentials, R_s, and R_c values measured on rebar in SL-3 specimen

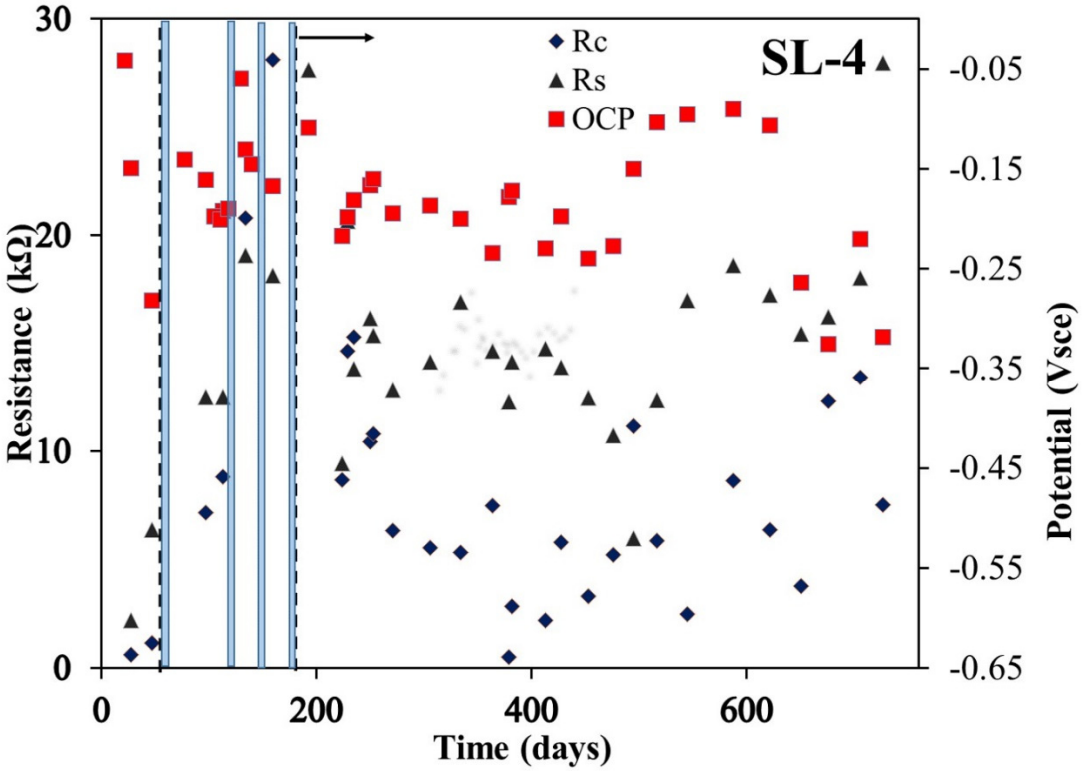

Figure 142. Rebar potentials, R_s, and R_c values measured on rebar in SL-4 specimen

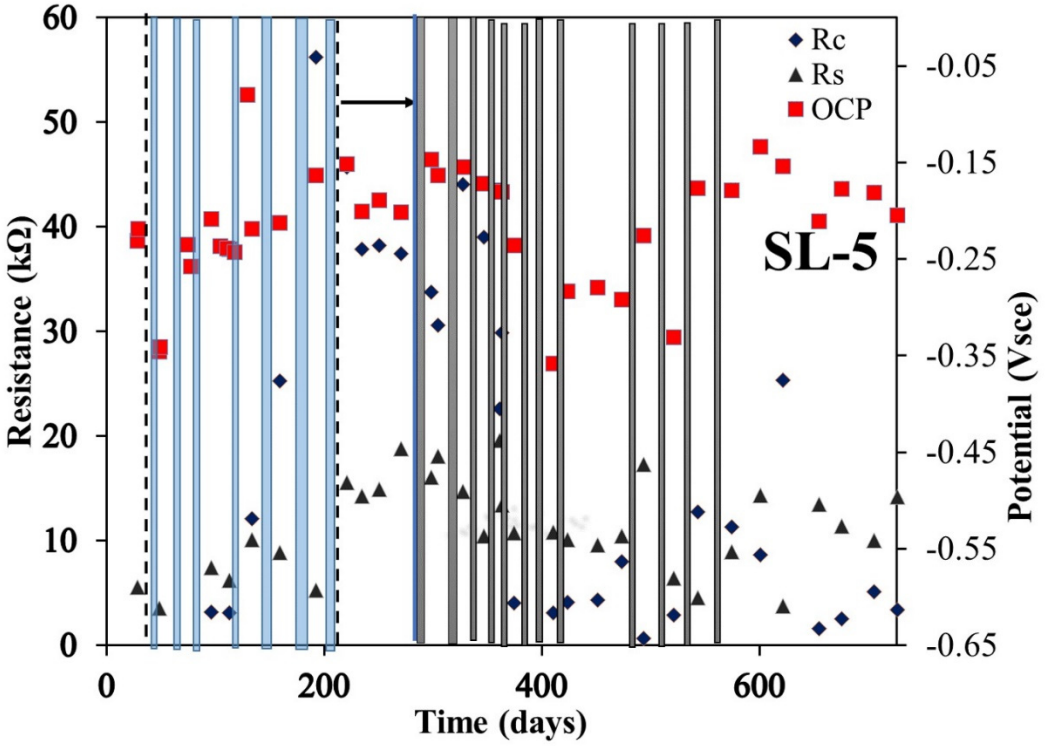

Figure 143. Rebar potentials, R_s, and R_c values measured on rebar in SL-5 specimen

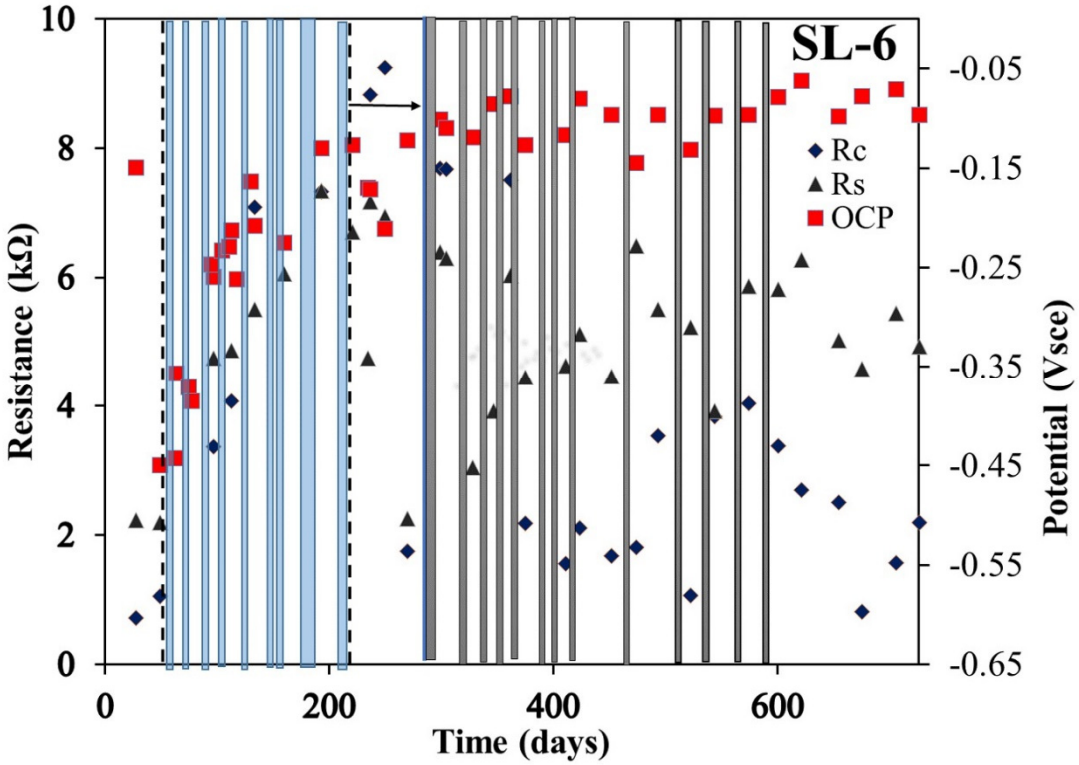

Figure 144. Rebar potentials, R_s, and R_c values measured on rebar in SL-6 specimen

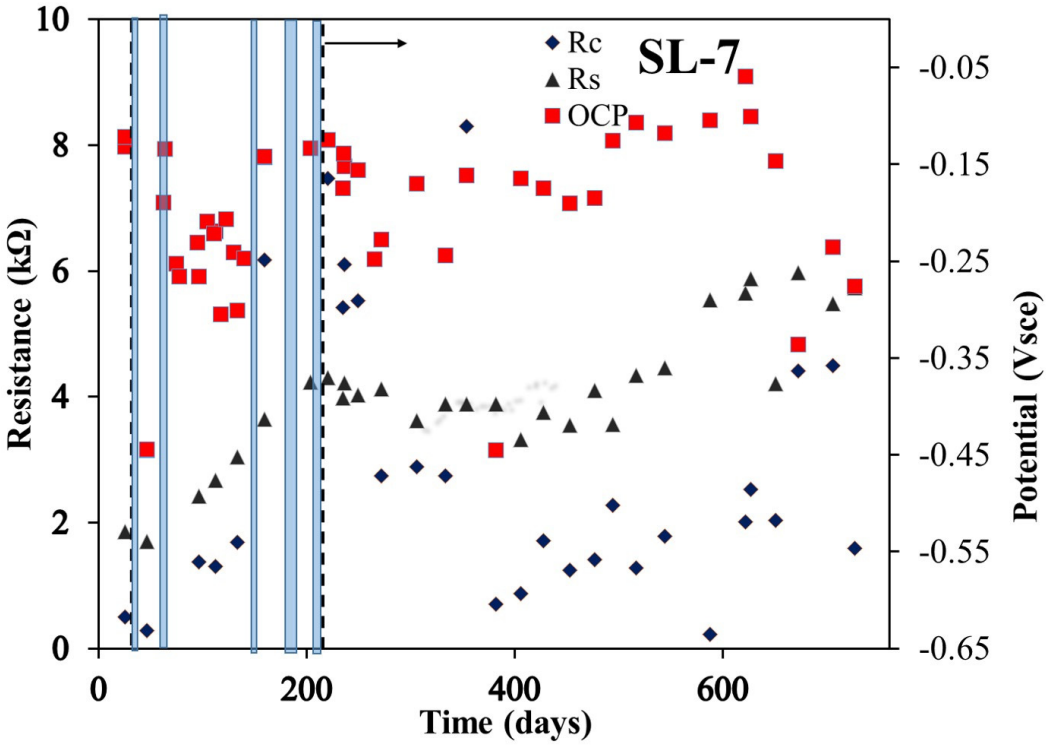

Figure 145. Rebar potentials, R_s, and R_c values measured on rebar in SL-7 specimen

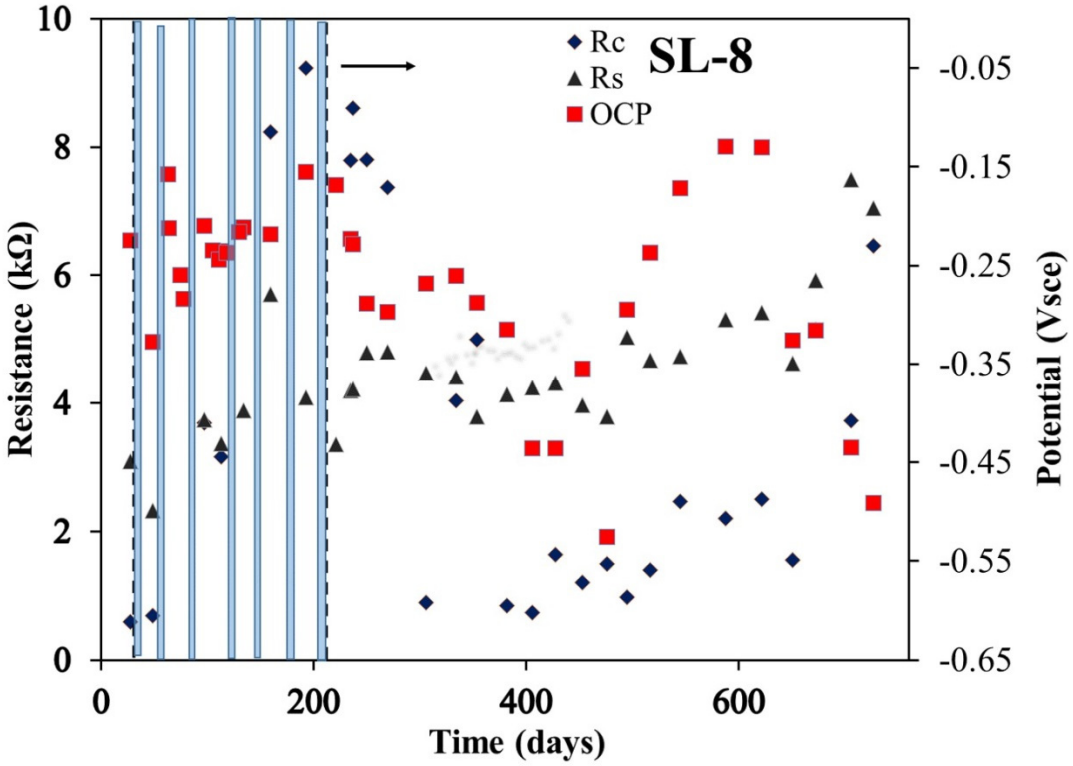

Figure 146. Rebar potentials, R_s, and R_c values measured on rebar in SL-8 specimen

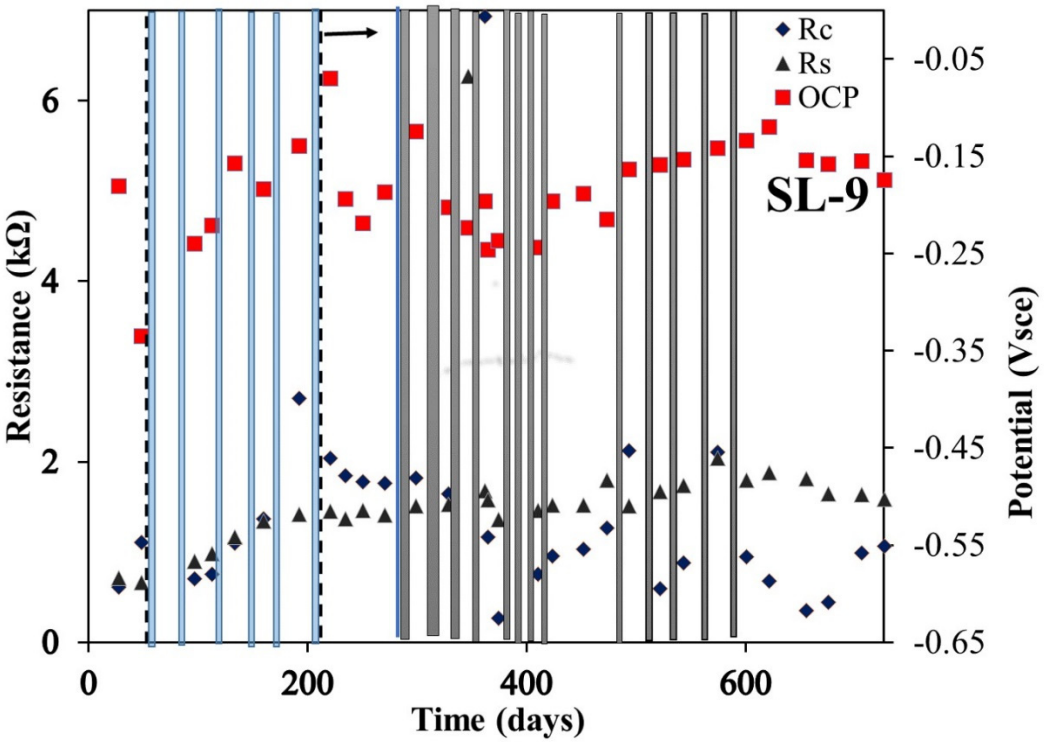

Figure 147. Rebar potentials, R_s, and R_c values measured on rebar in SL-9 specimen

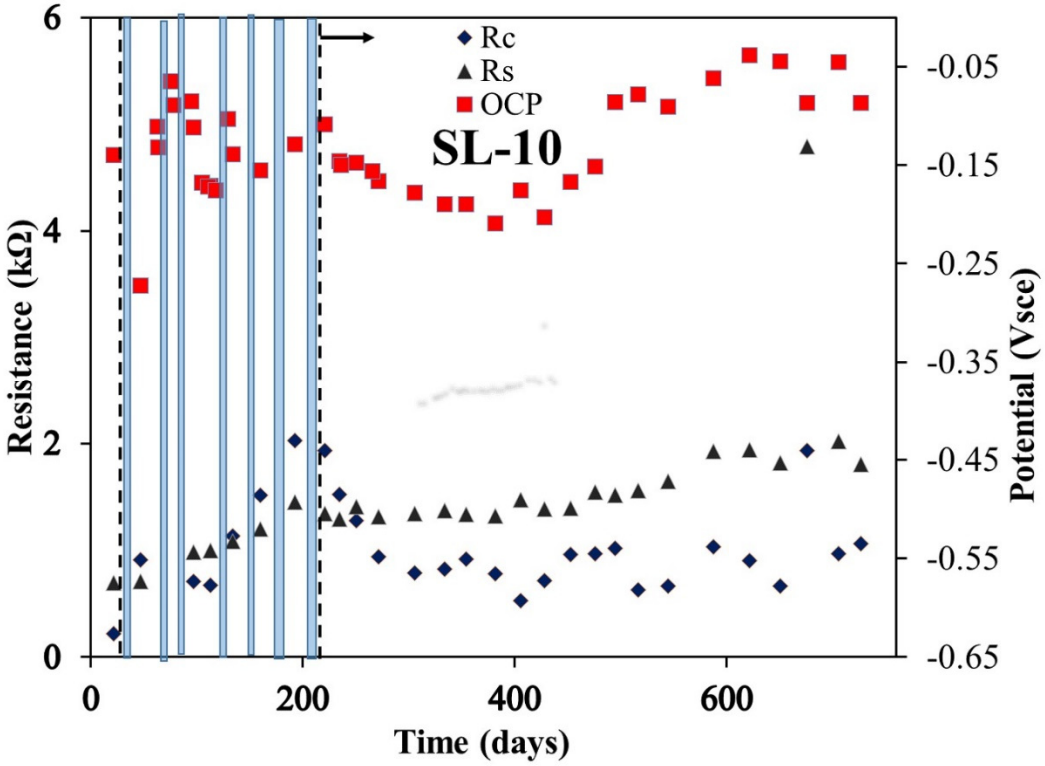

Figure 148. Rebar potentials, R_s, and R_c values measured on rebar in SL-10 specimen

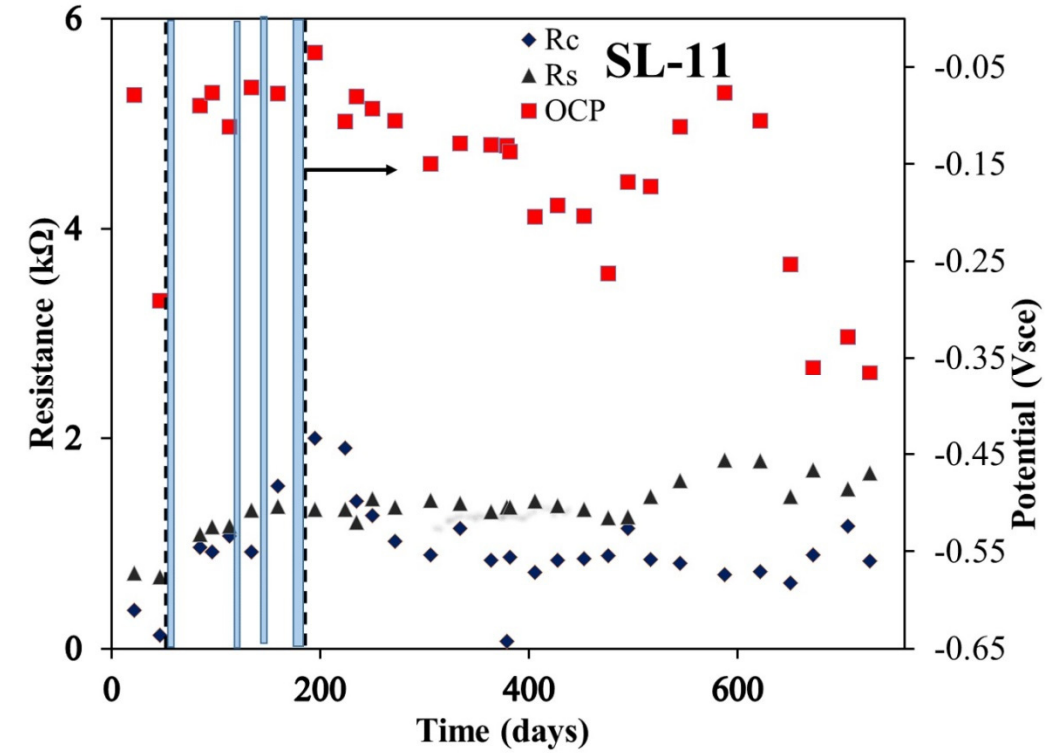

Figure 149. Rebar potentials, R_s, and R_c values measured on rebar in SL-11 specimen

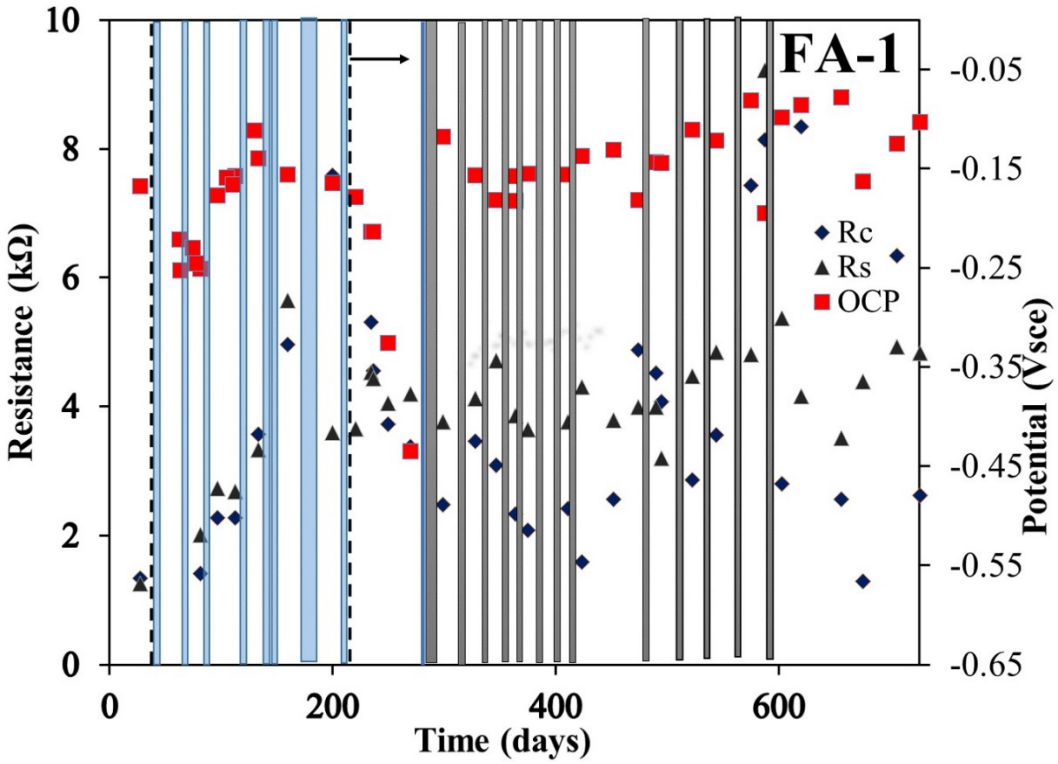

Figure 150. Rebar potentials, R_s, and R_c values measured on rebar in FA-1 specimen

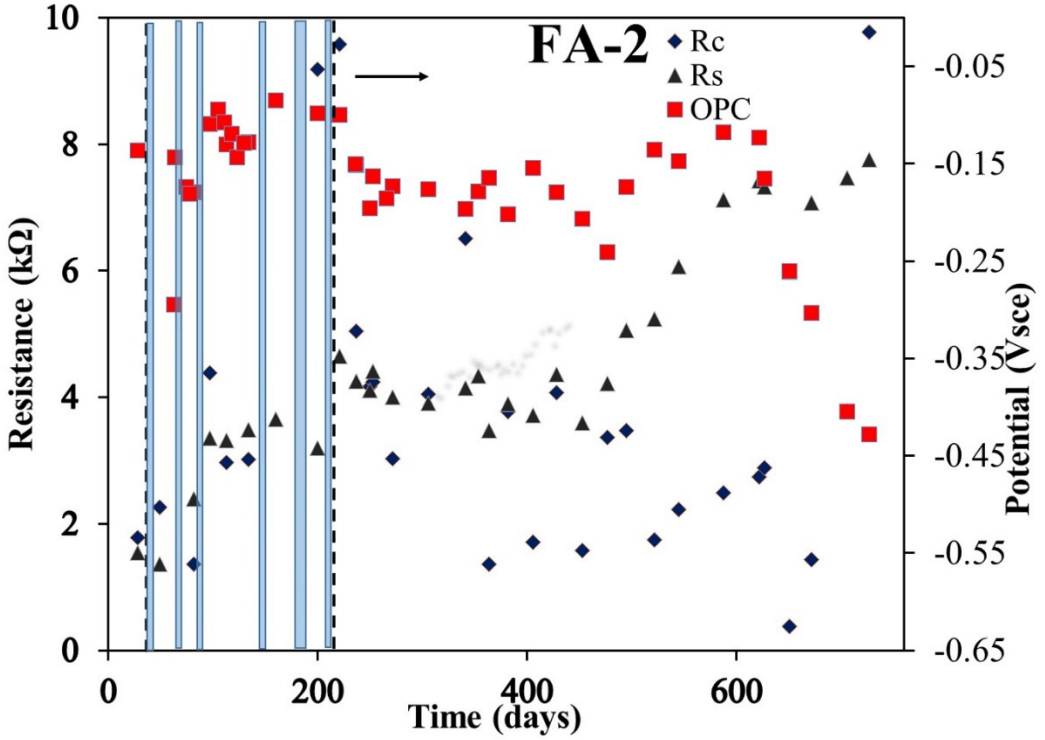

Figure 151. Rebar potentials, R_s, and R_c values measured on rebar in FA-2 specimen

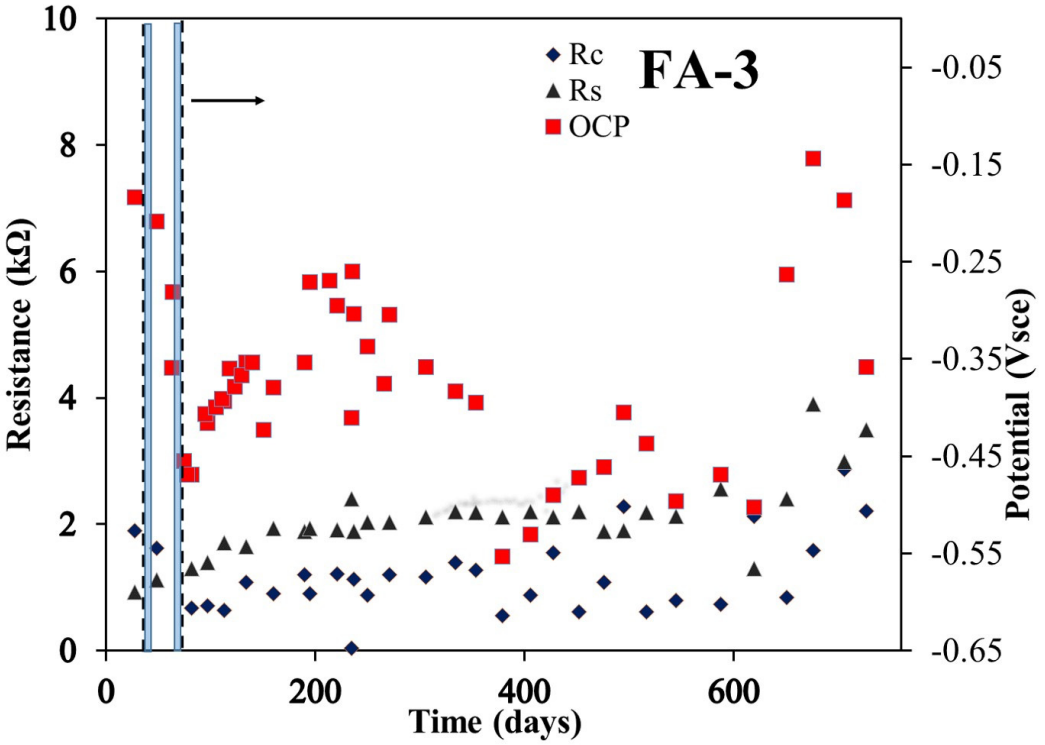

Figure 152. Rebar potentials, R_s, and R_c values measured on rebar in FA-3 specimen

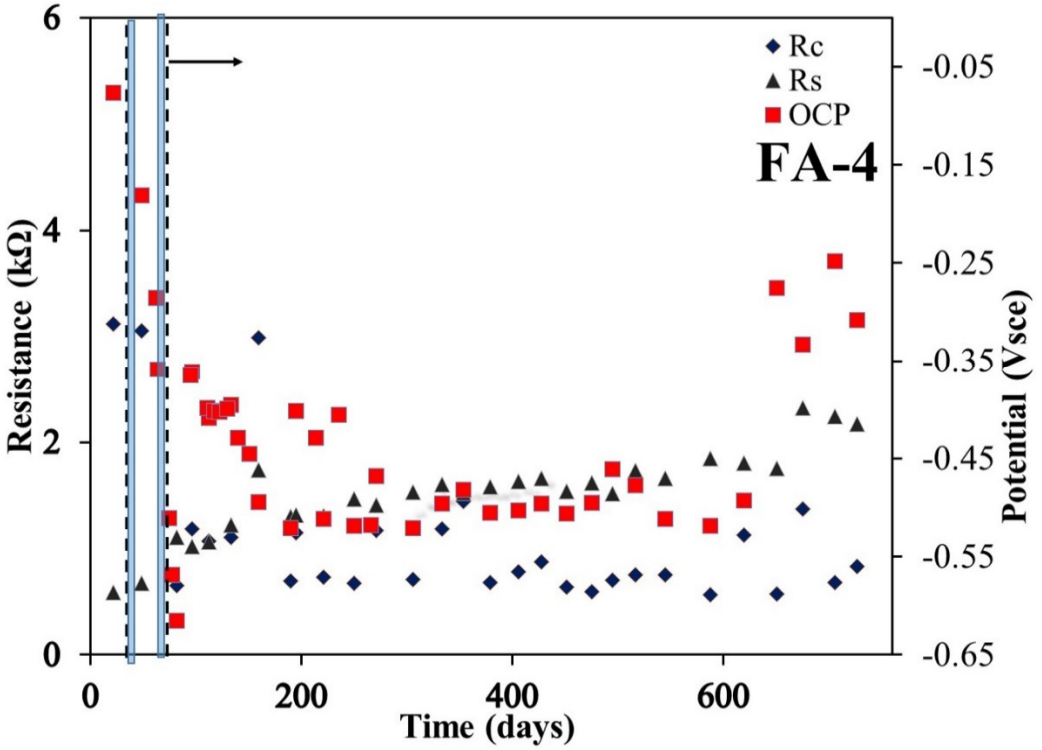

Figure 153. Rebar potentials, R_s, and R_c values measured on rebar in FA-4 specimen

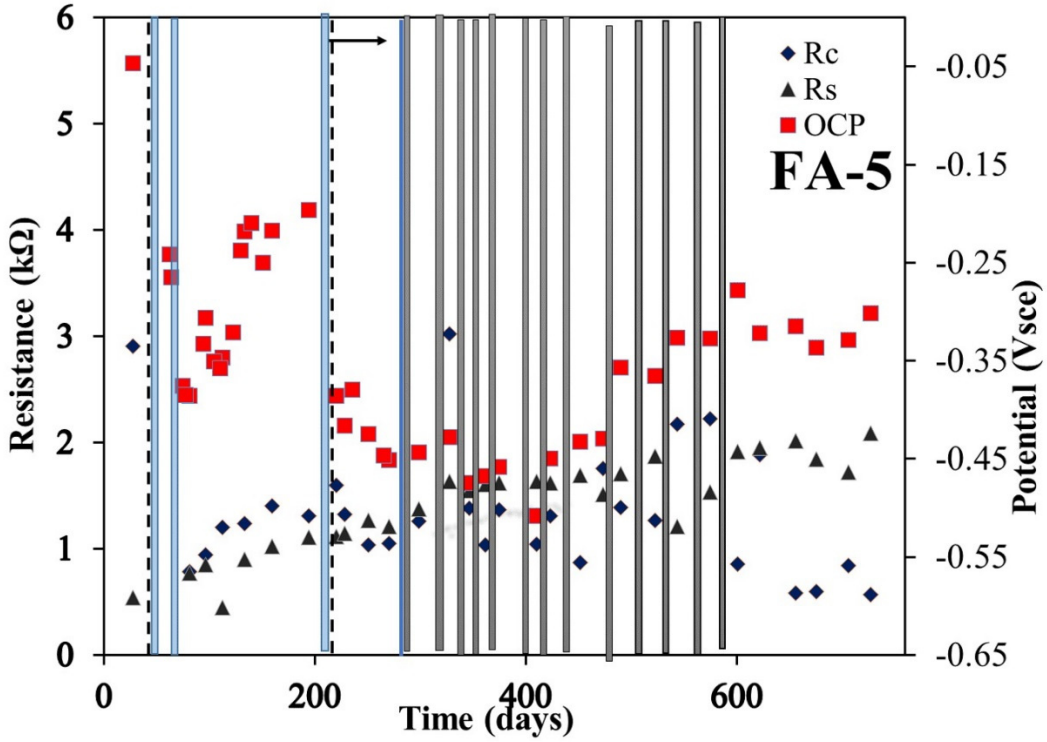

Figure 154. Rebar potentials, R_s, and R_c values measured on rebar in FA-5 specimen

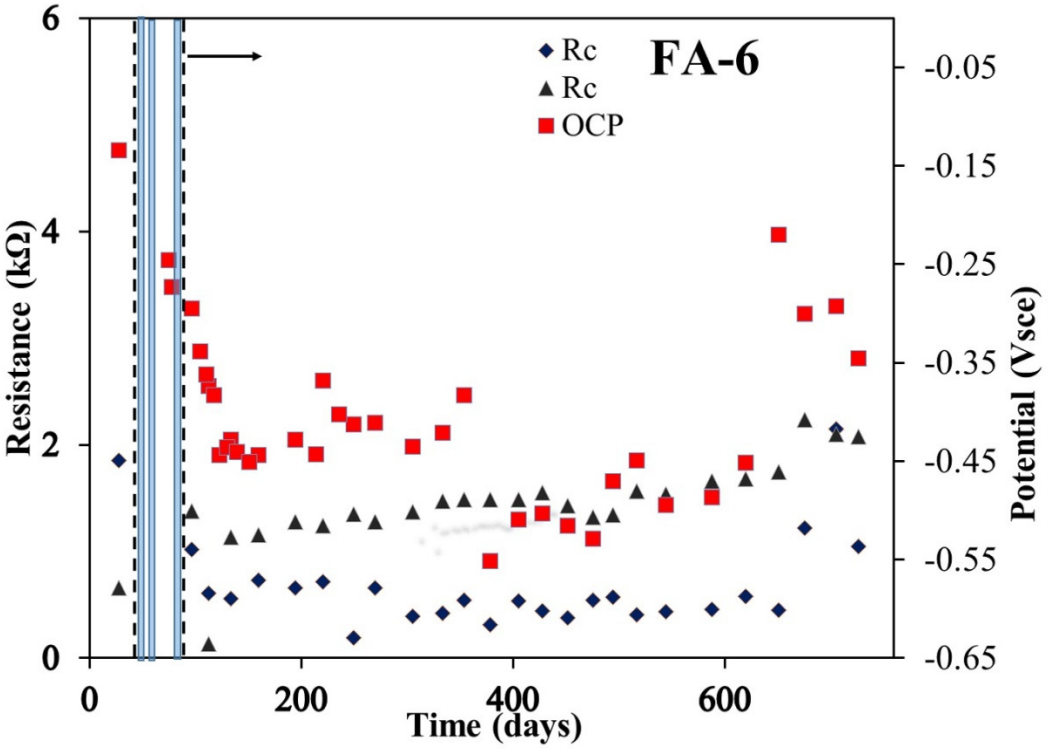

Figure 155. Rebar potentials, R_s, and R_c values measured on rebar in FA-6 specimen

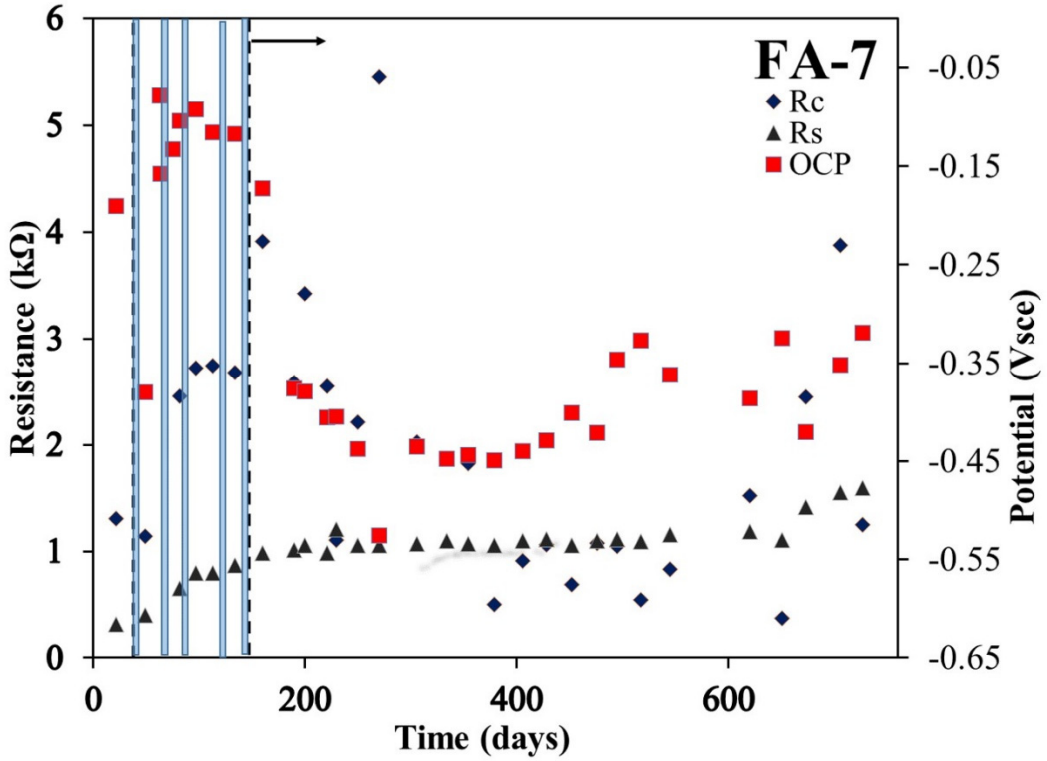

Figure 156. Rebar potentials, R_s, and R_c values measured on rebar in FA-7 specimen

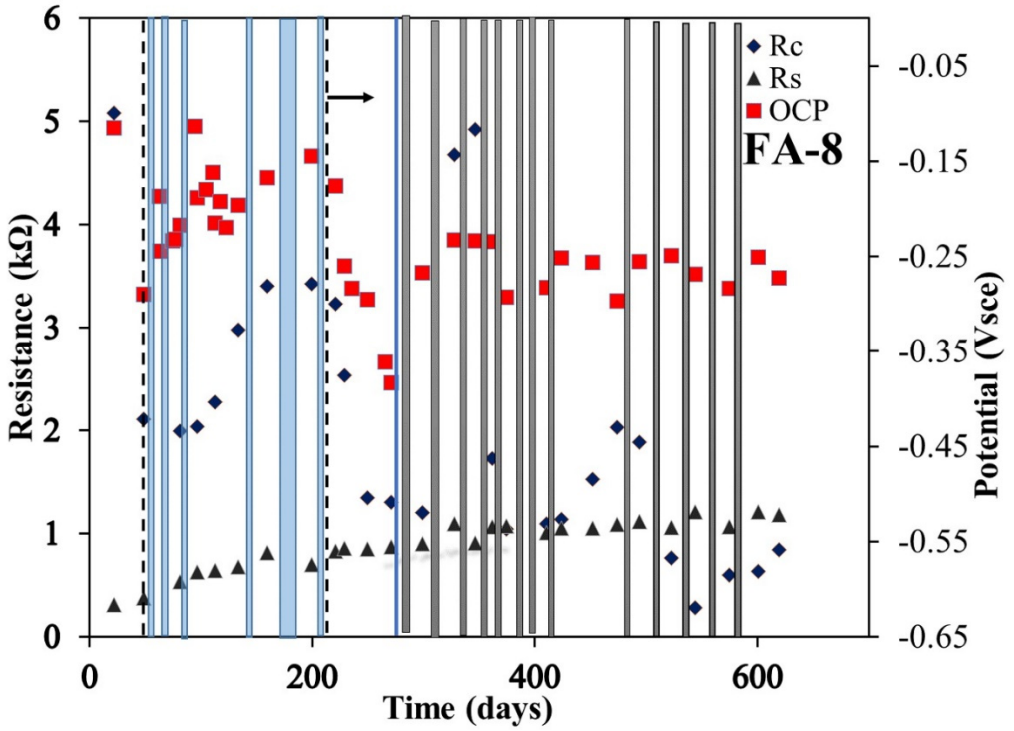

Figure 157. Rebar potentials, R_s, and R_c values measured on rebar in FA-8 specimen

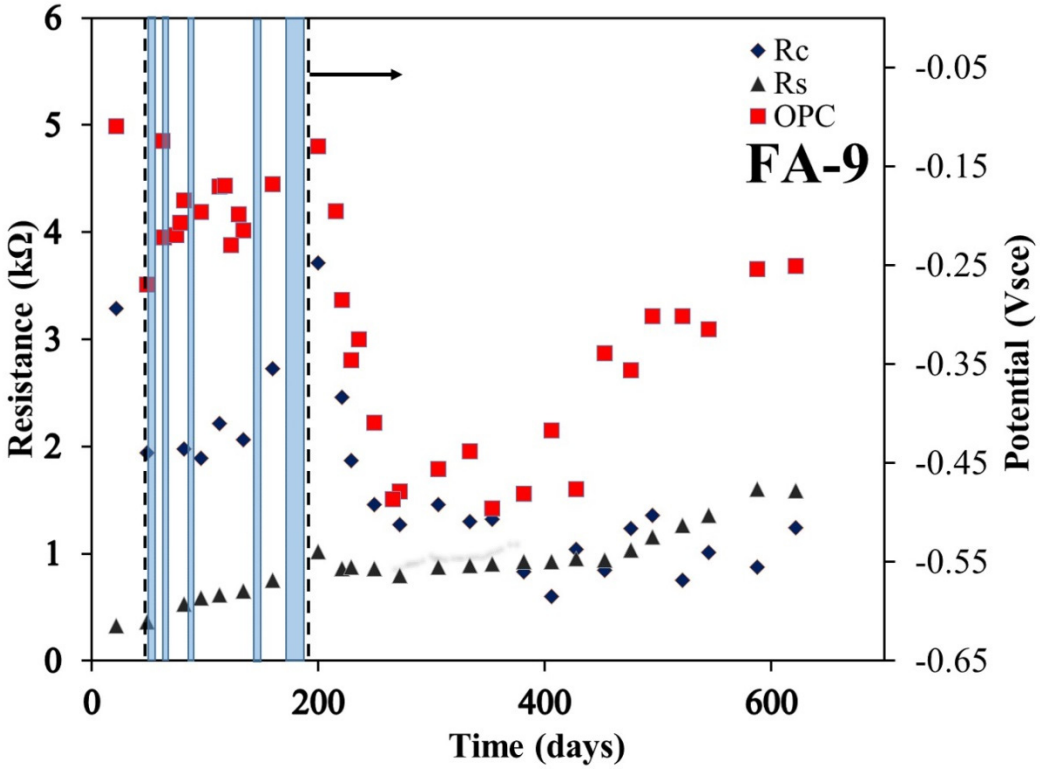

Figure 158. Rebar potentials, R_s, and R_c values measured on rebar in FA-9 specimen

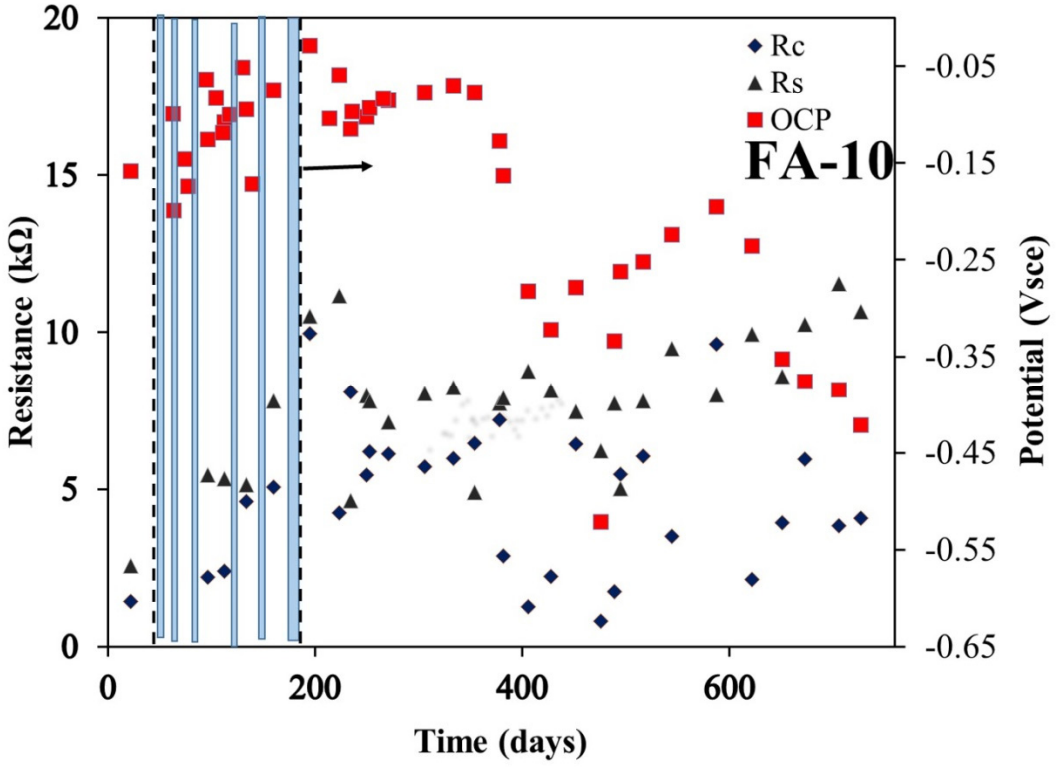

Figure 159. Rebar potentials, R_s, and R_c values measured on rebar in FA-10 specimen

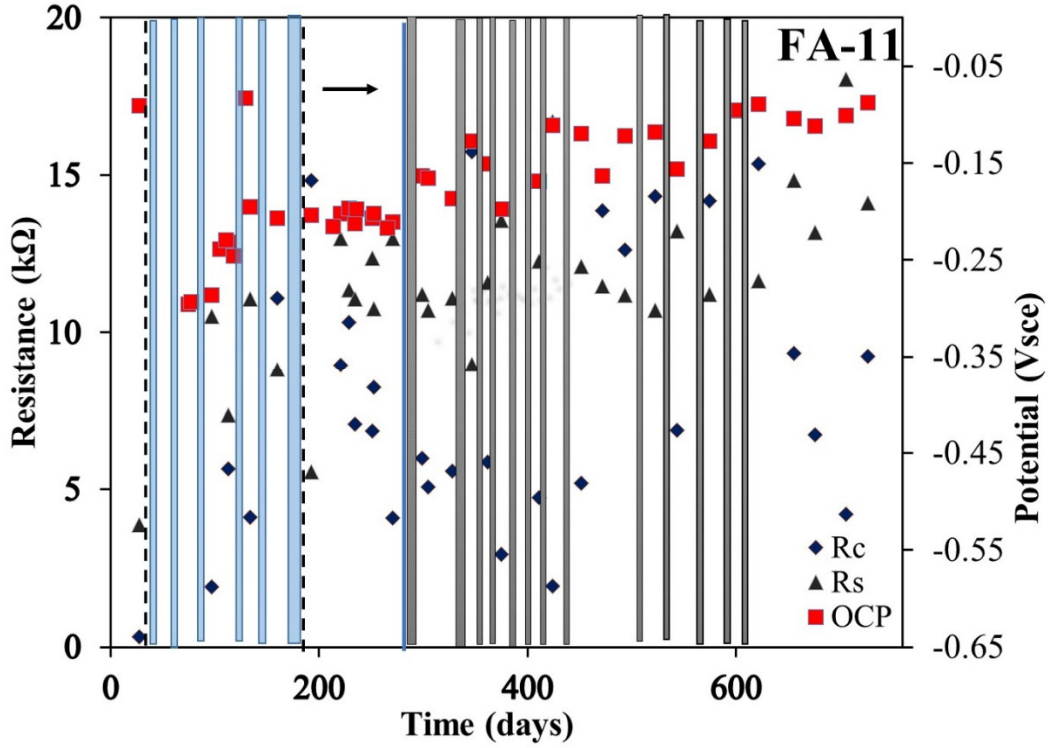

Figure 160. Rebar potentials, R_s, and R_c values measured on rebar in FA-11 specimen

Appendix E: T1 and T2 Single-rebar Samples

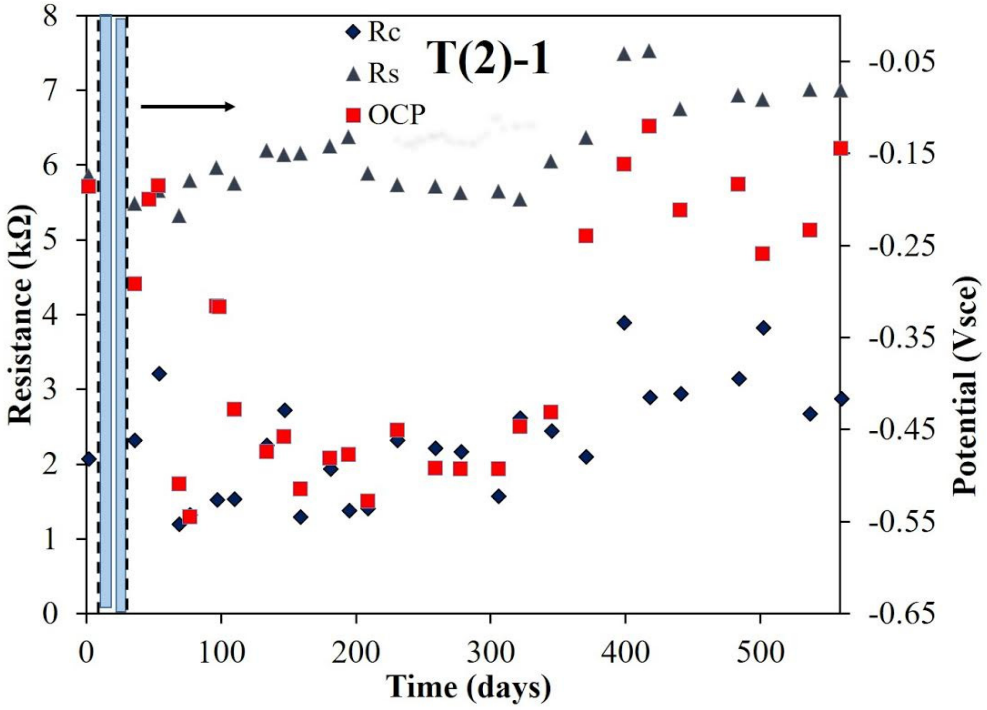

Figure 161. Rebar potentials, R_s, and R_c values measured on rebar in T2-1 specimen

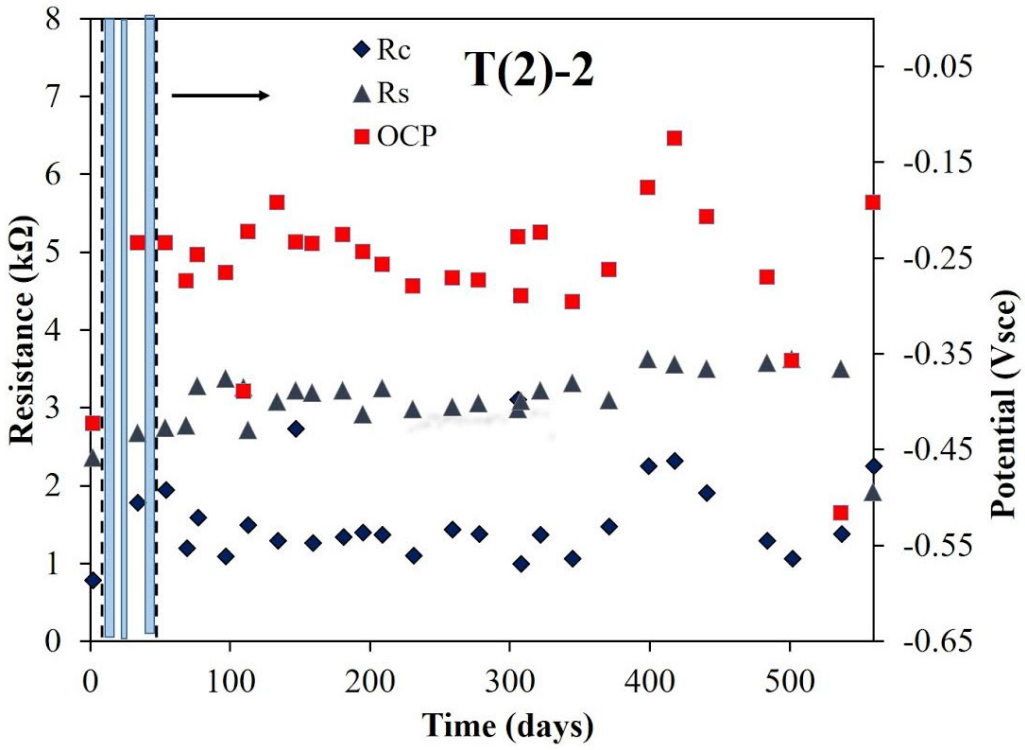

Figure 162. Rebar potentials, R_s, and R_c values measured on rebar in T2-2 specimen

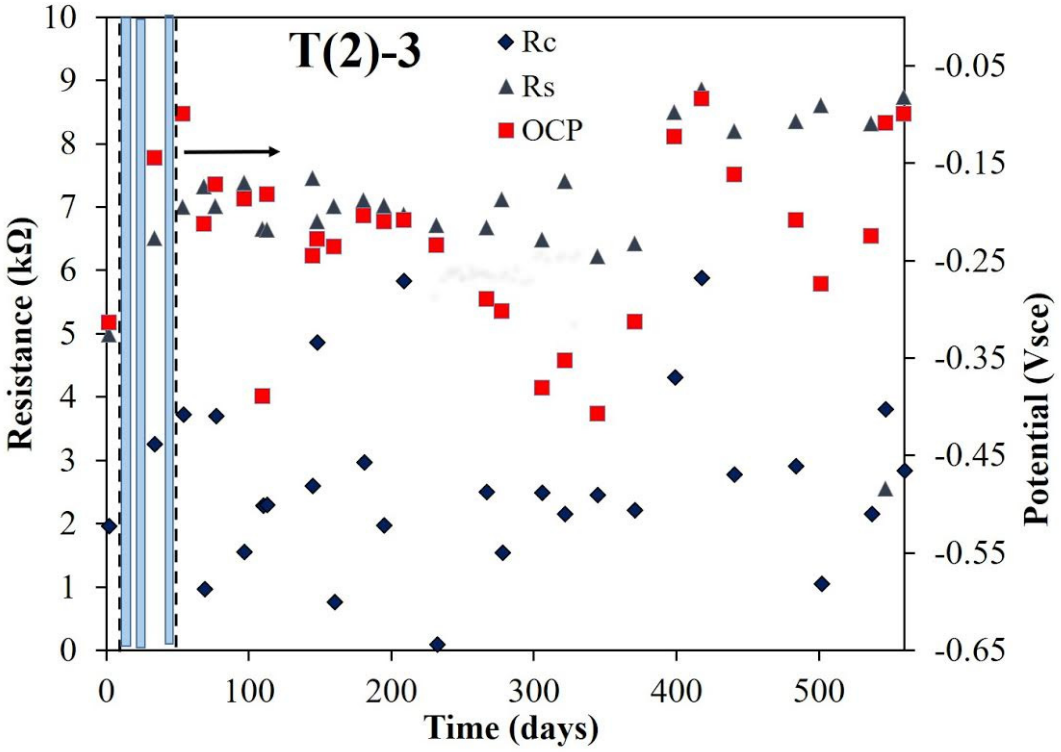

Figure 163. Rebar potentials, R_s, and R_c values measured on rebar in T2-3 specimen

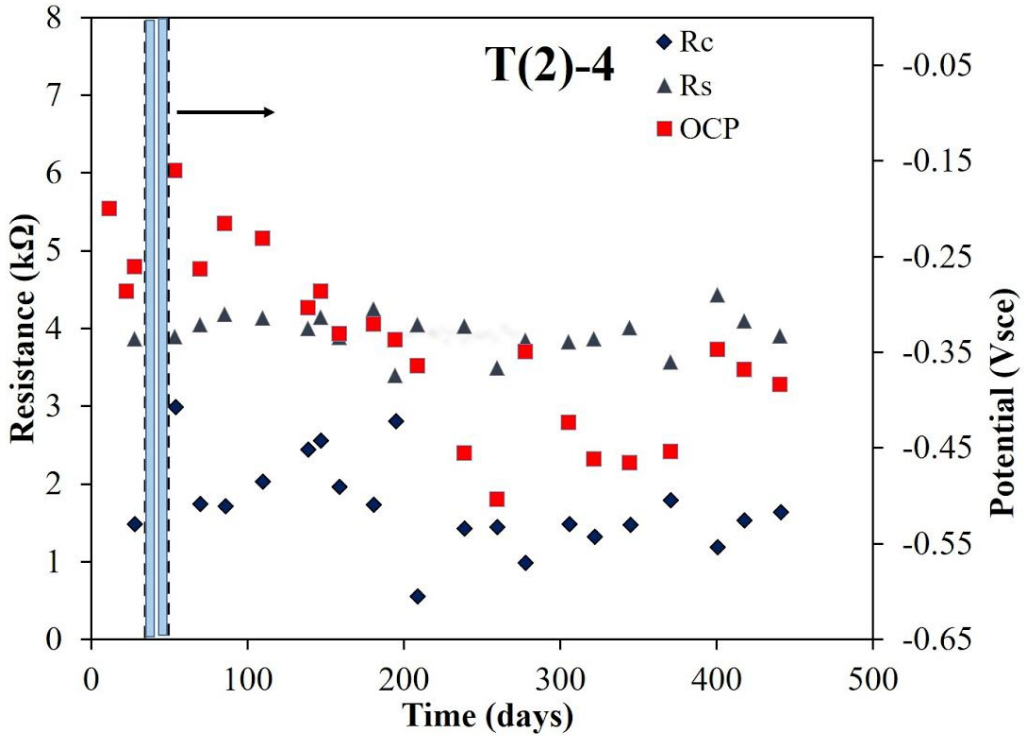

Figure 164. Rebar potentials, R_s, and R_c values measured on rebar in T2-4 specimen

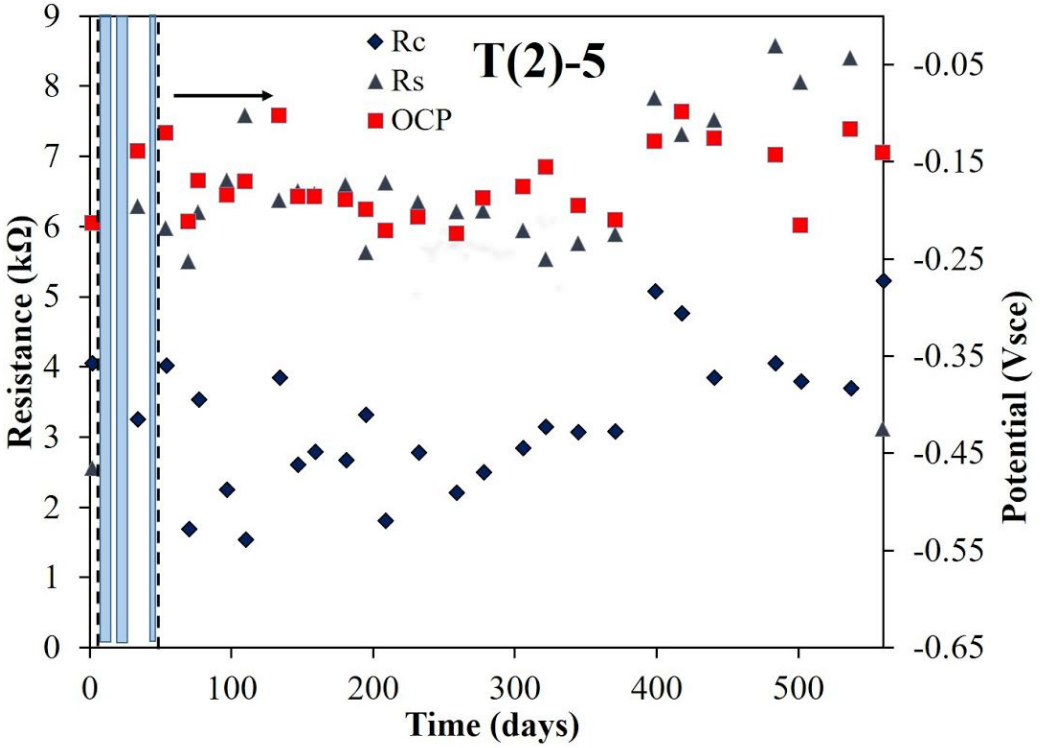

Figure 165. Rebar potentials, R_s, and R_c values measured on rebar in T2-5 specimen

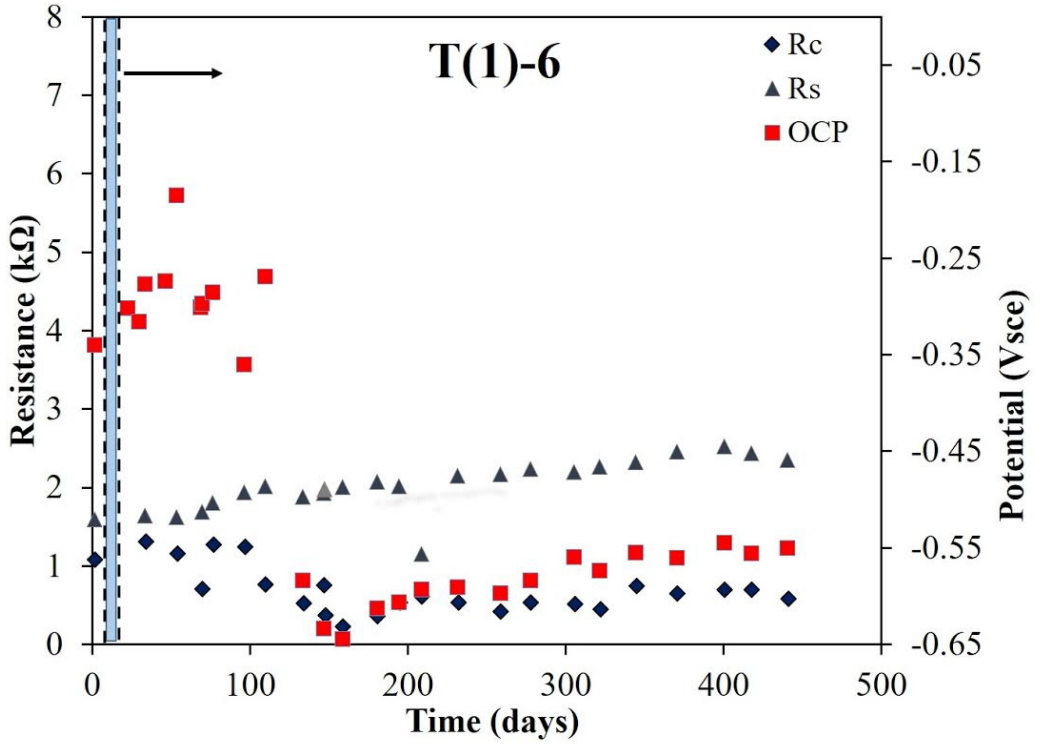

Figure 166. Rebar potentials, R_s, and R_c values measured on rebar in T1-6 specimen

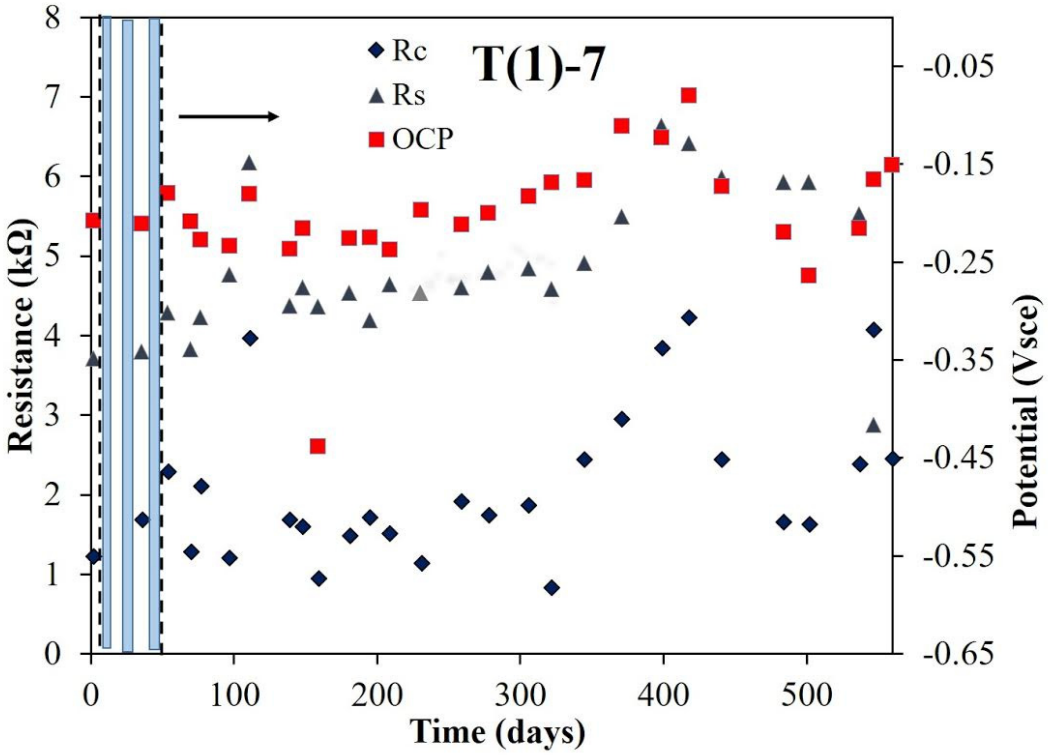

Figure 167. Rebar potentials, R_s, and R_c values measured on rebar in T1-7 specimen

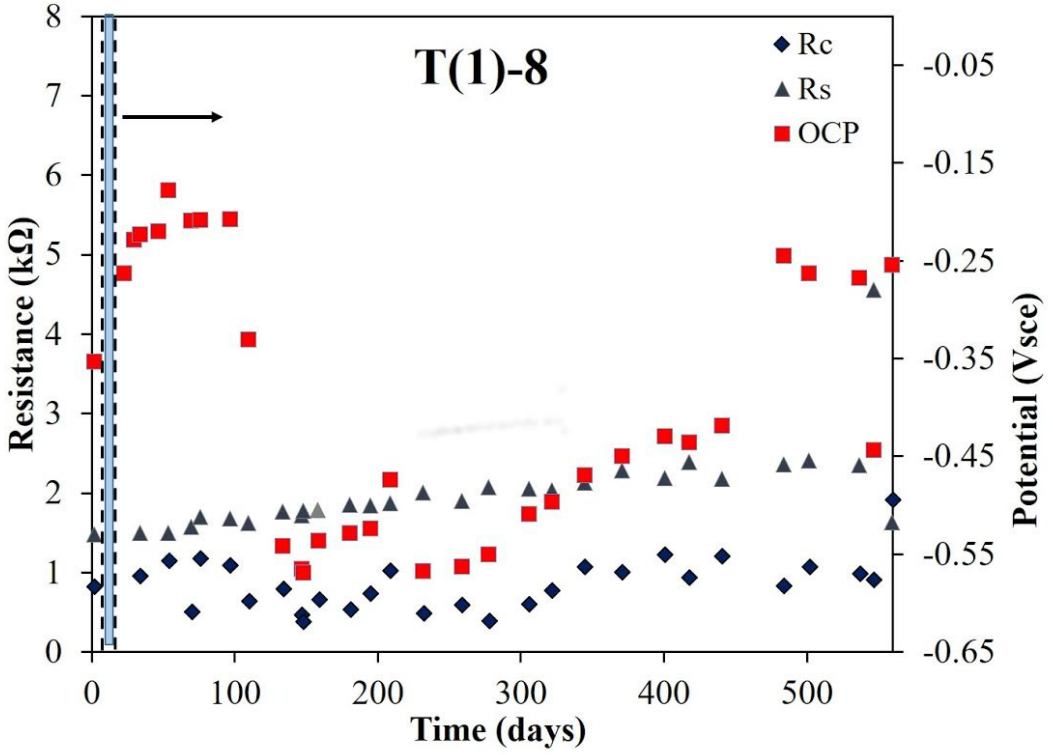

Figure 168. Rebar potentials, R_s, and R_c values measured on rebar in T1-8 specimen

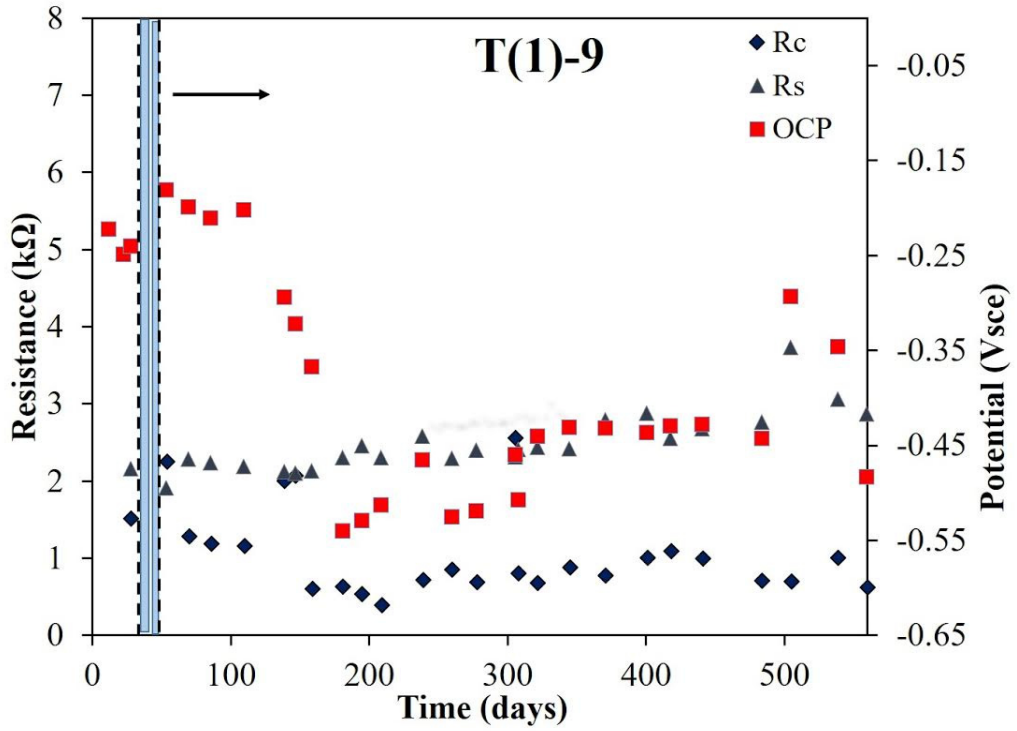

Figure 169. Rebar potentials, R_s, and R_c values measured on rebar in T1-9 specimen

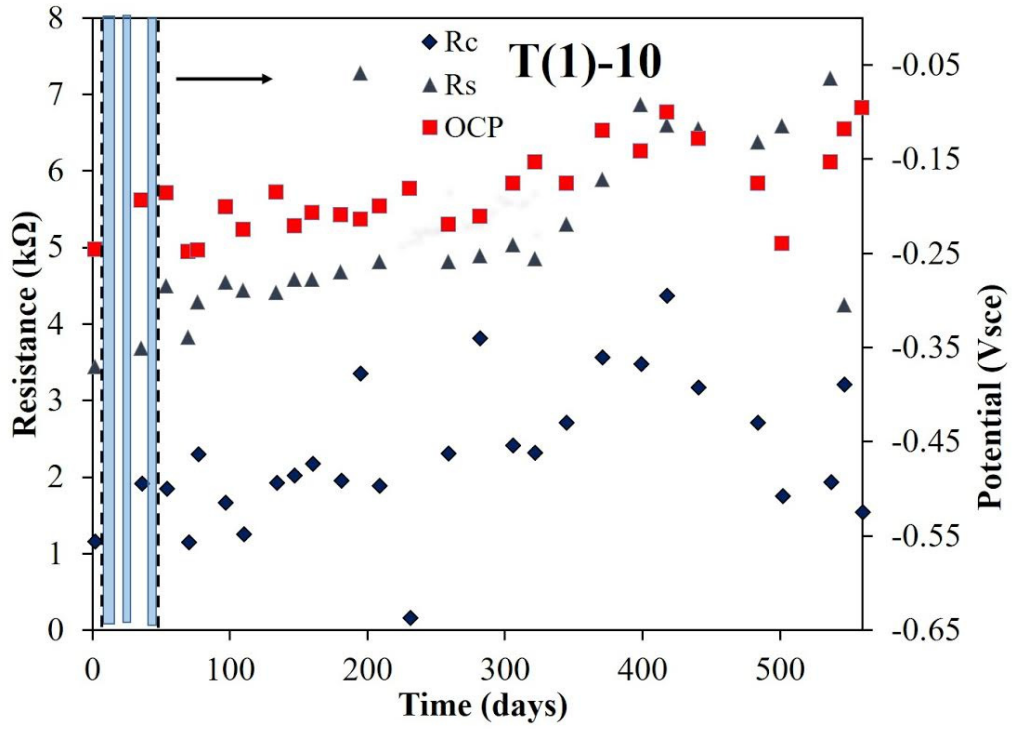

Figure 170. Rebar potentials, R_s, and R_c values measured on rebar in T1-10 specimen

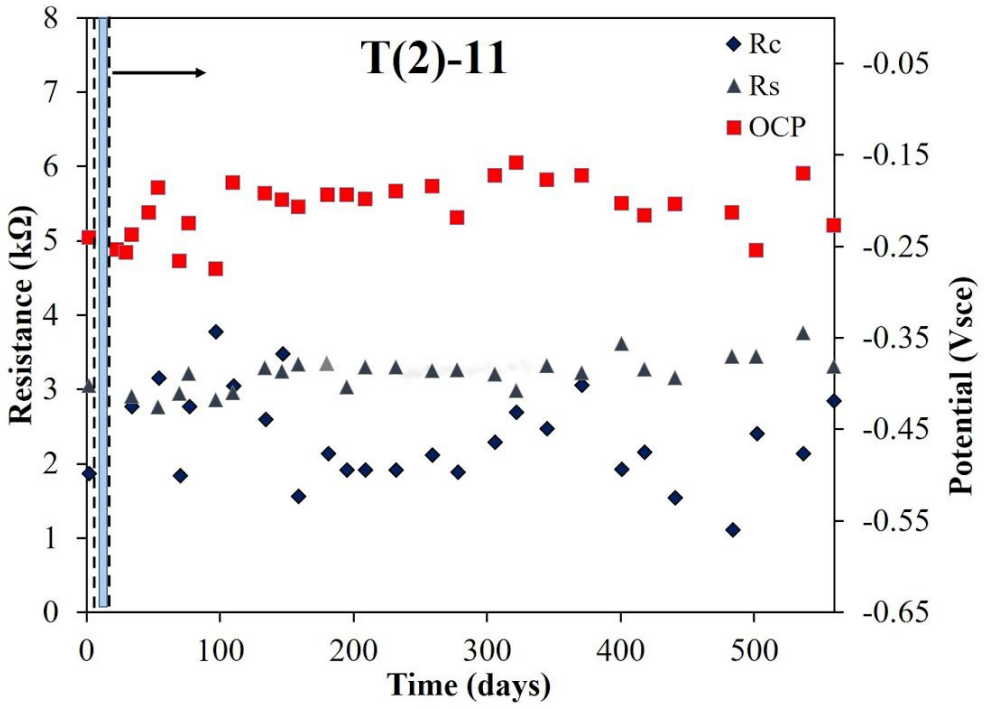

Figure 171. Rebar potentials, R_s, and R_c values measured on rebar in T2-11 specimen

Appendix F: Three-rebar Specimens (SL and FA Mixes)

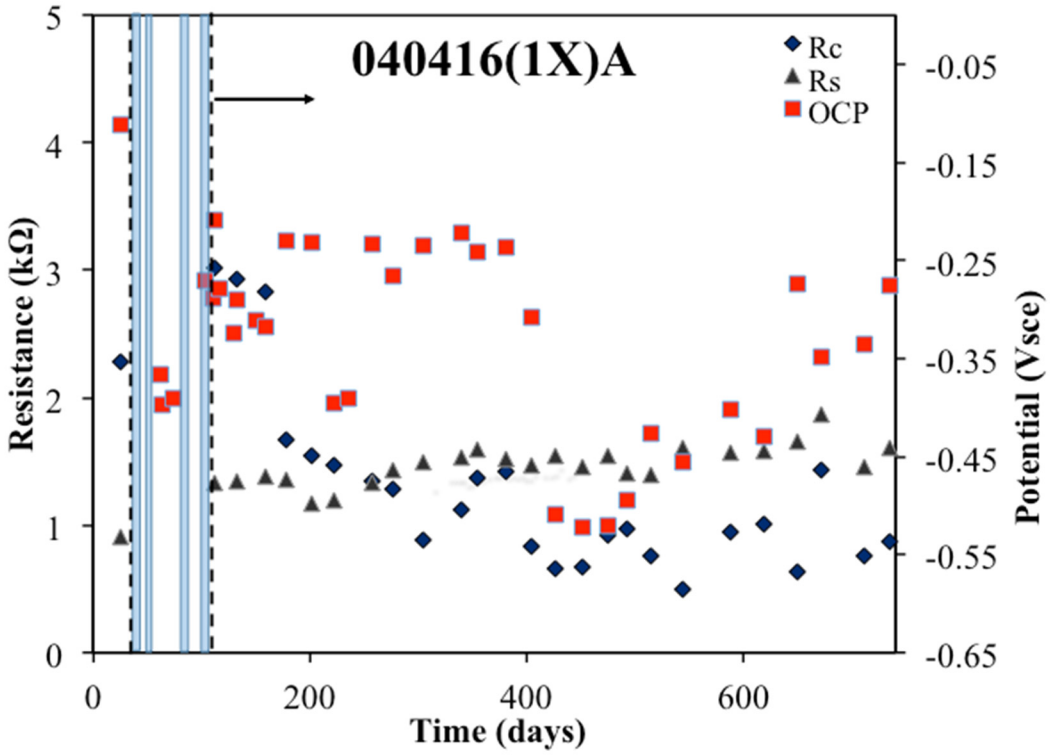

Figure 172. Rebar potentials, R_s, and R_c values measured on rebar 1X-A

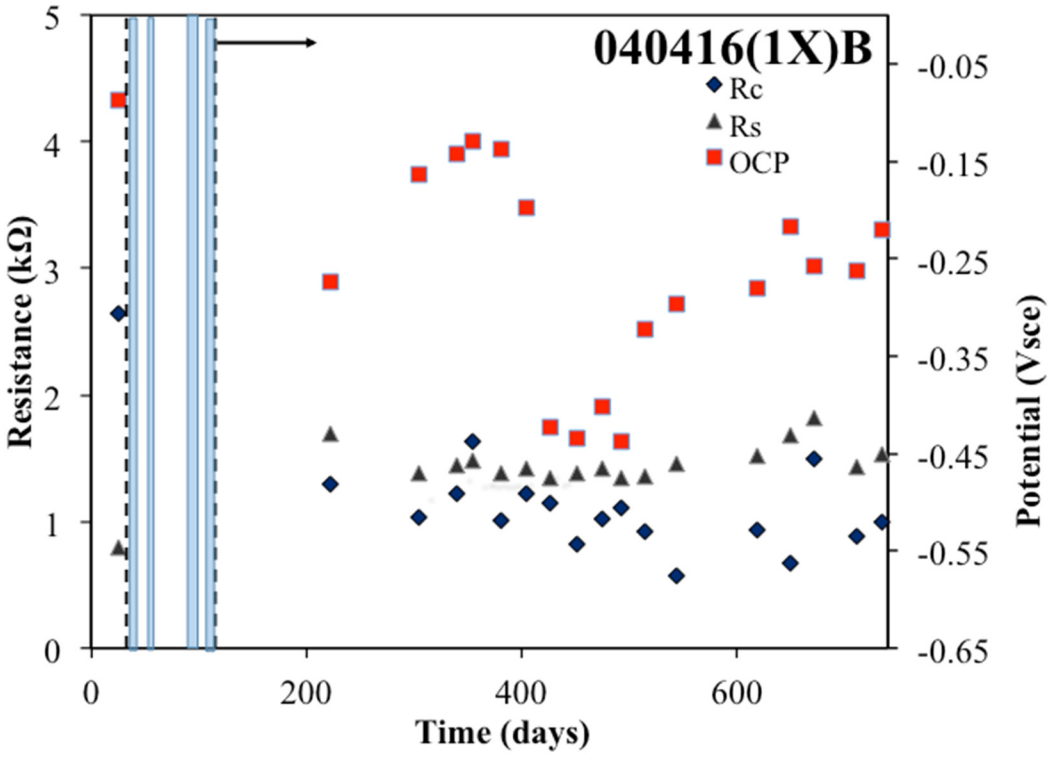

Figure 173. Rebar potentials, R_s, and R_c values measured on rebar 1X-B

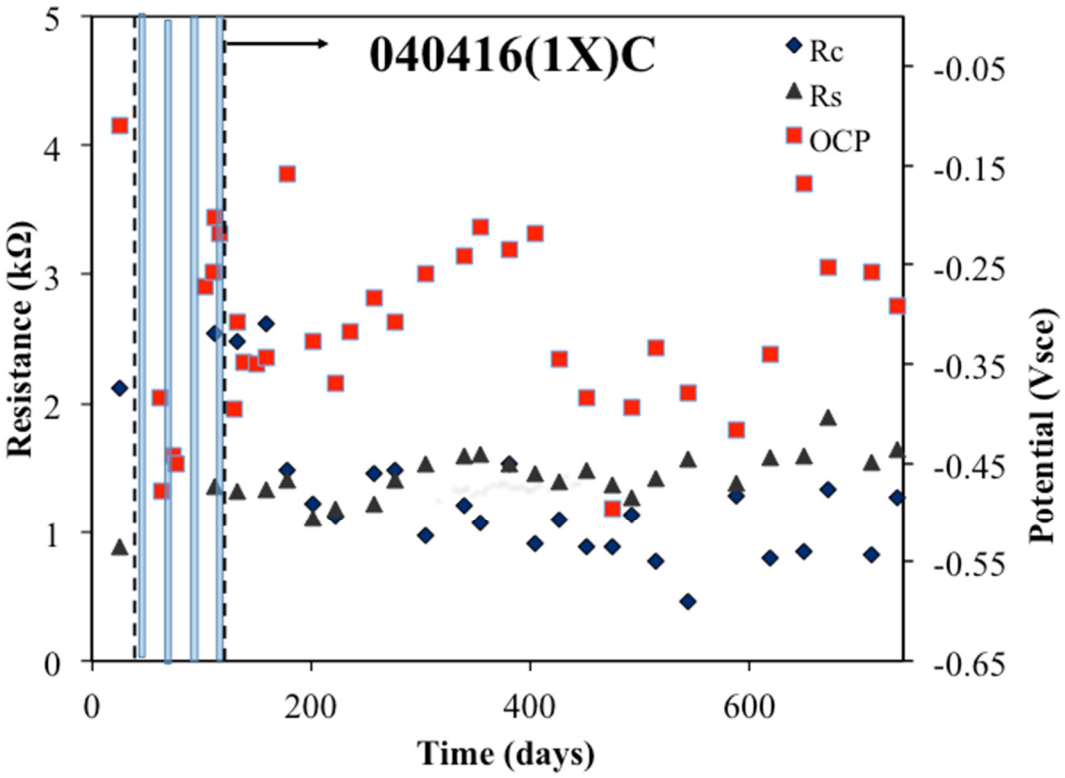

Figure 174. Rebar potentials, R_s, and R_c values measured on rebar 1X-C

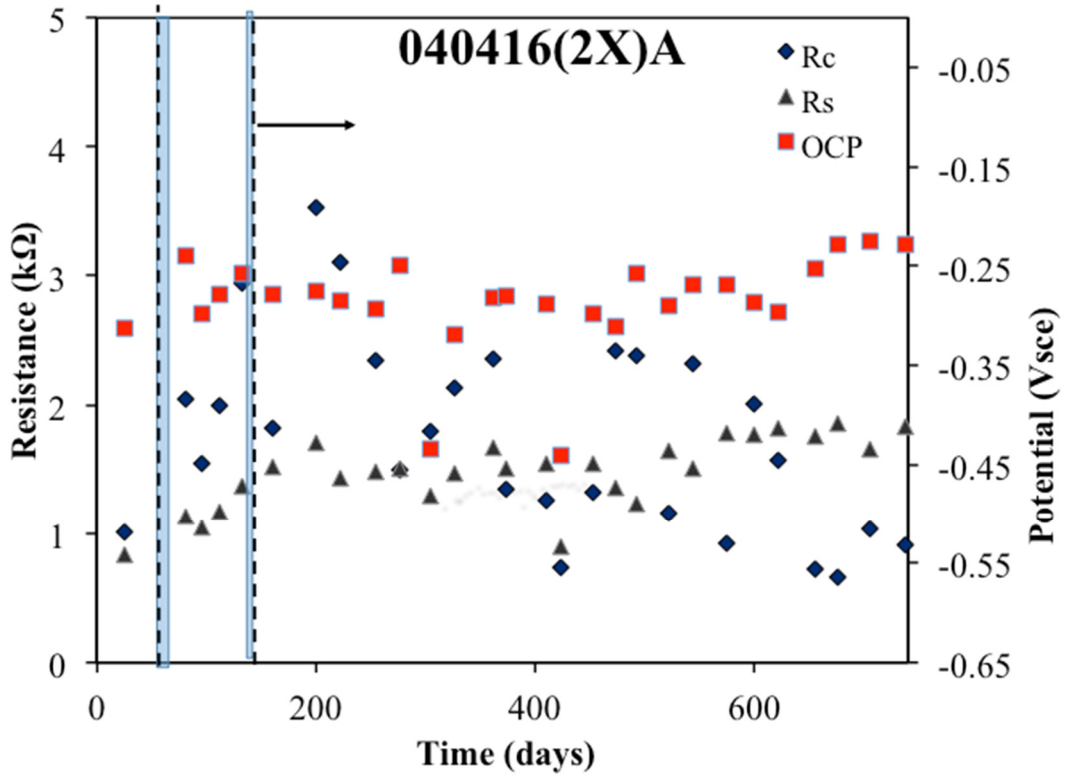

Figure 175. Rebar potentials, R_s, and R_c values measured on rebar 2X-A

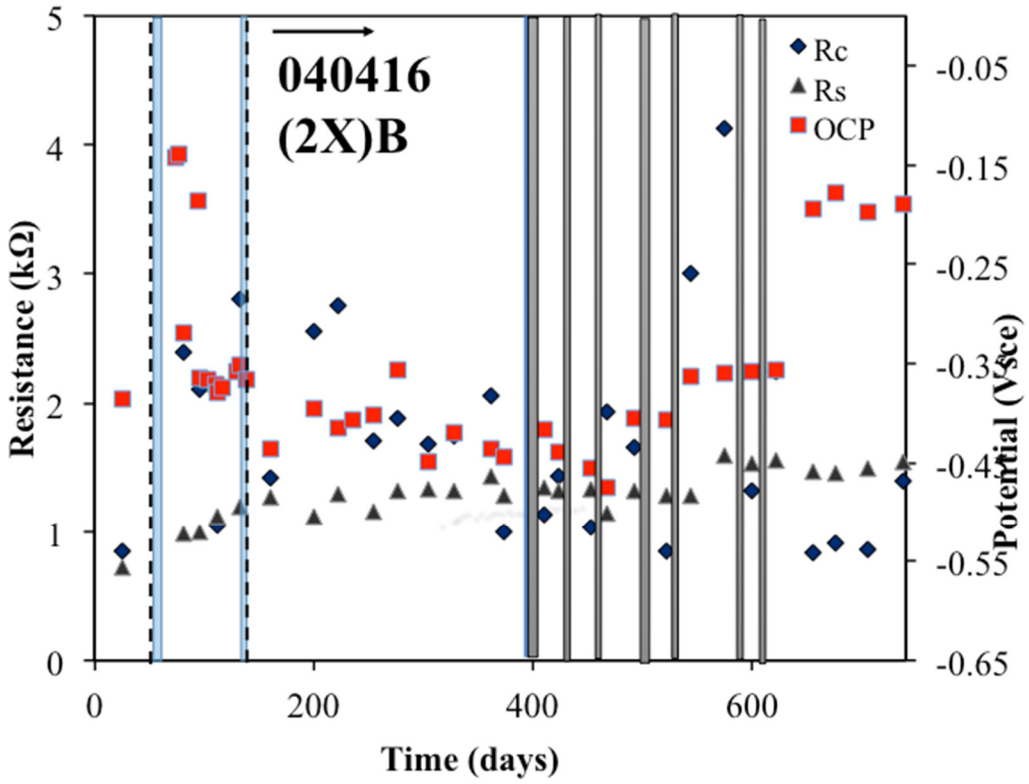

Figure 176. Rebar potentials, R_s, and R_c values measured on rebar 2X-B

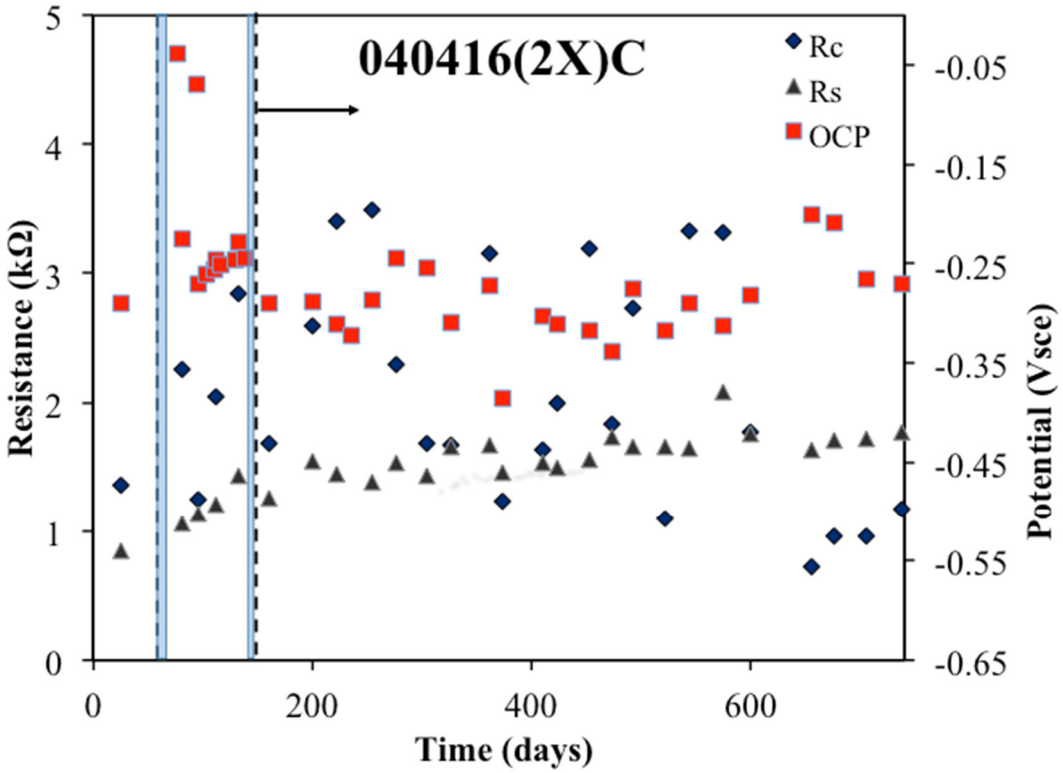

Figure 177. Rebar potentials, R_s, and R_c values measured on rebar 2X-C

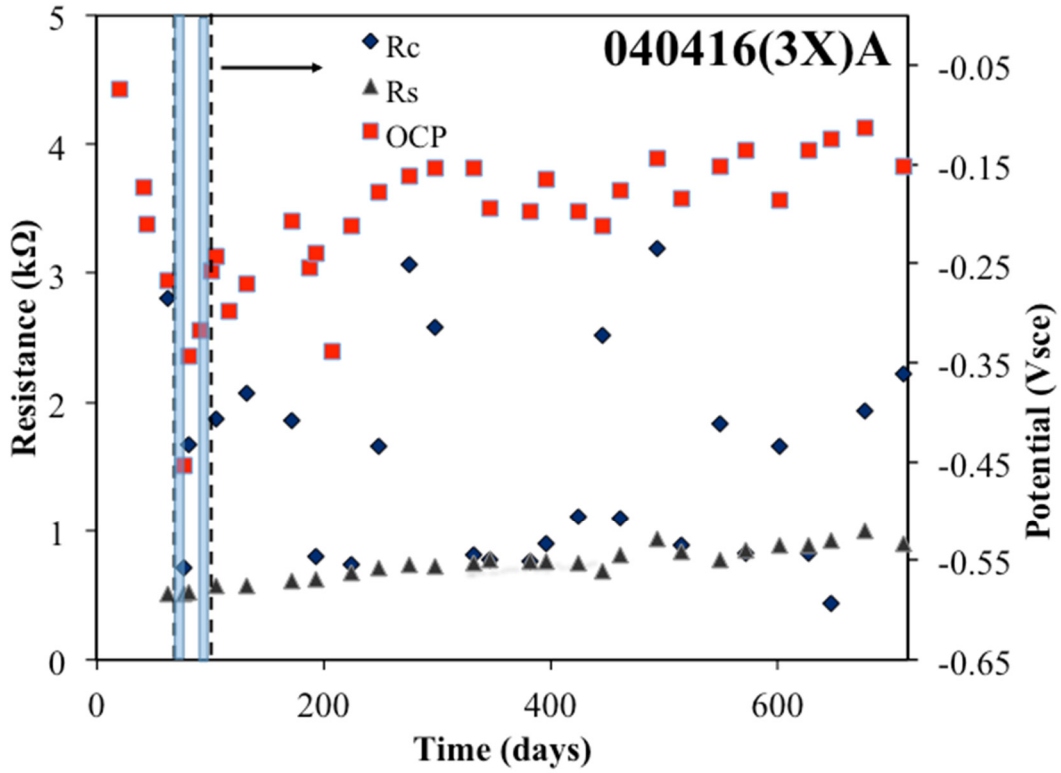

Figure 178. Rebar potentials, R_s, and R_c values measured on rebar 3X-A

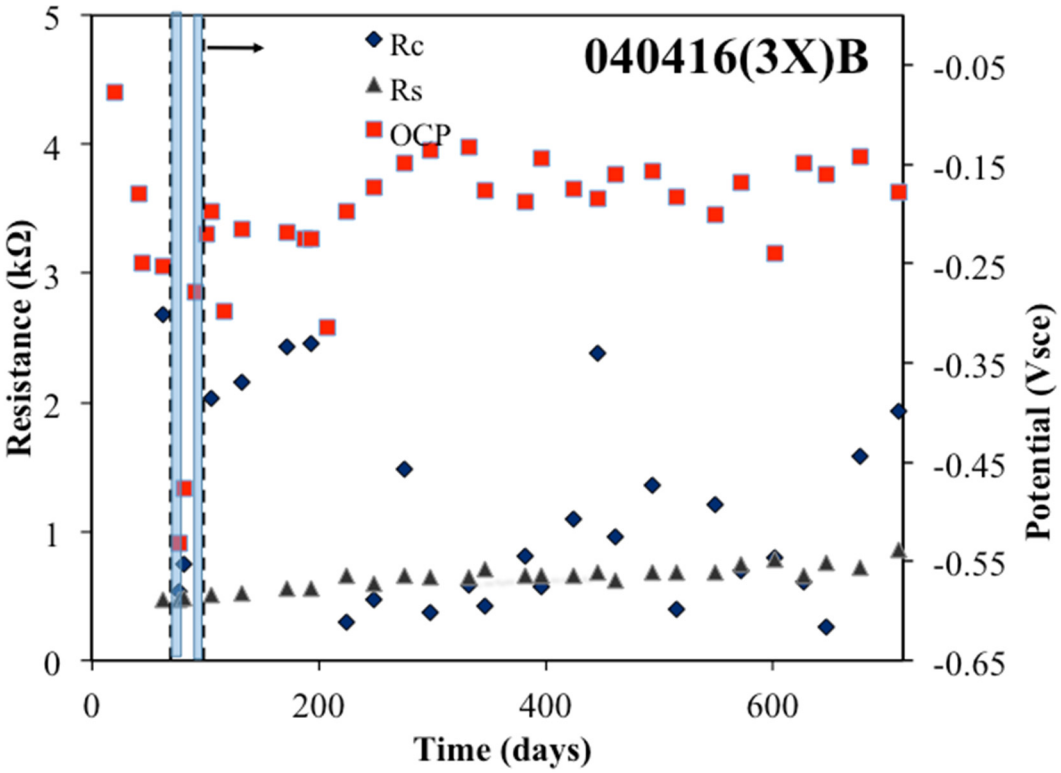

Figure 179. Rebar potentials, R_s, and R_c values measured on rebar 3X-B

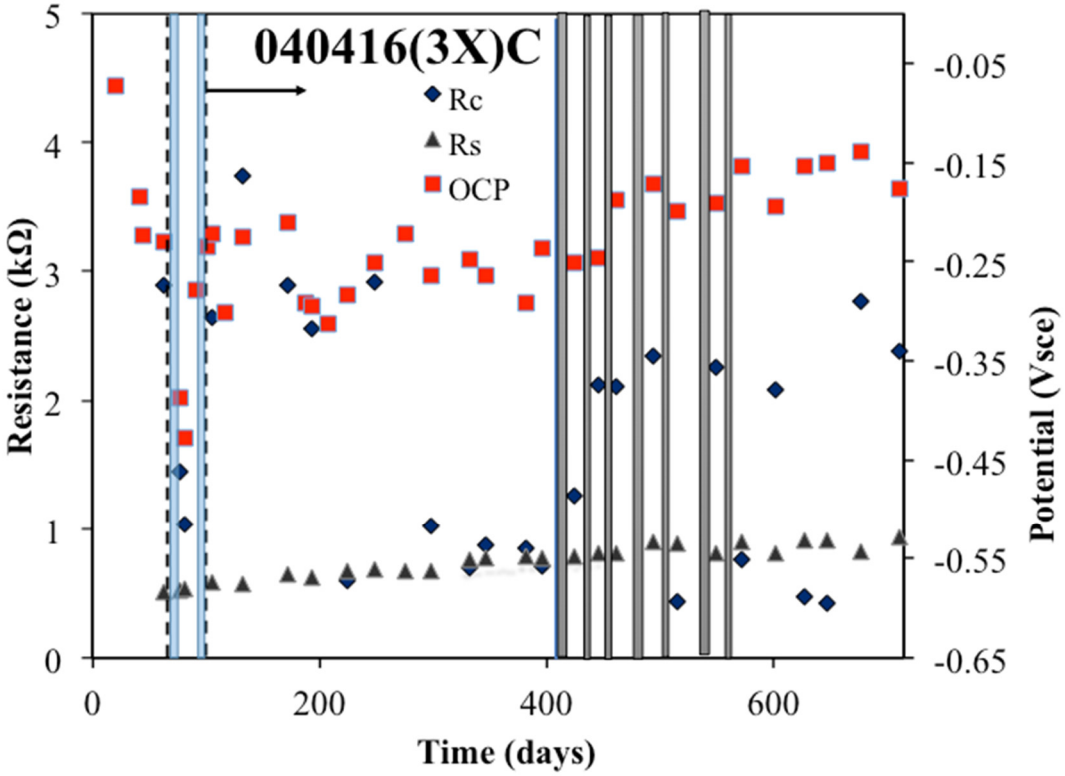

Figure 180. Rebar potentials, R_s, and R_c values measured on rebar 3X-C

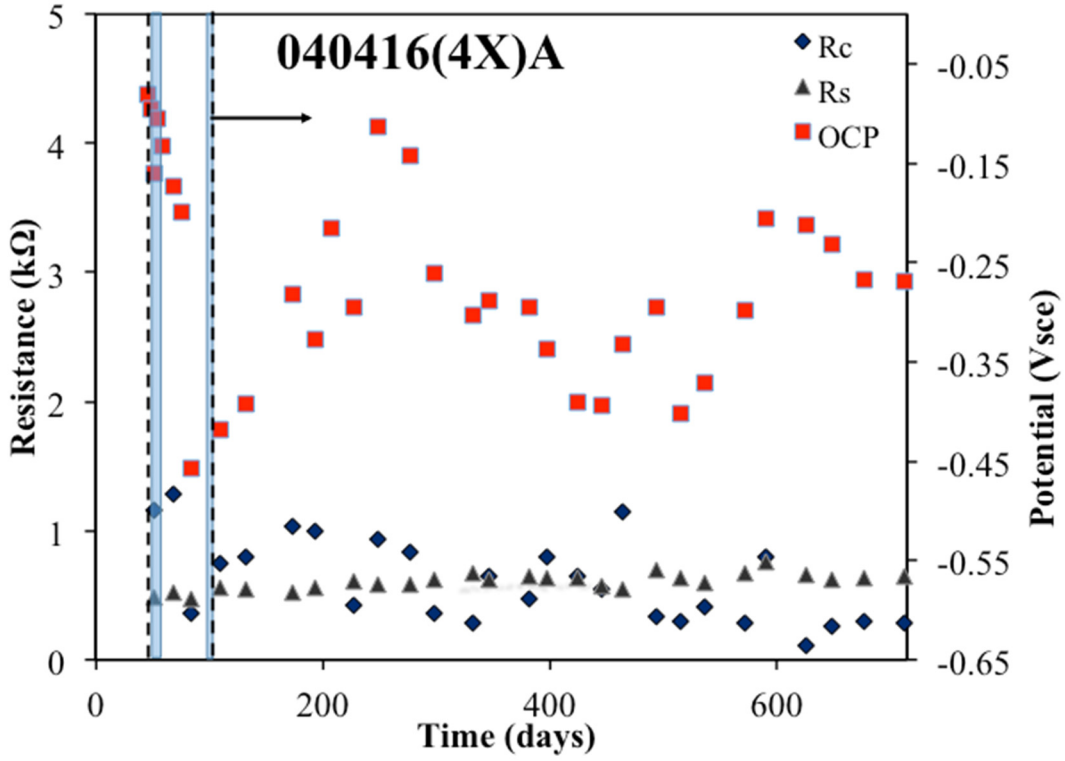

Figure 181. Rebar potentials, R_s, and R_c values measured on rebar 4X-A

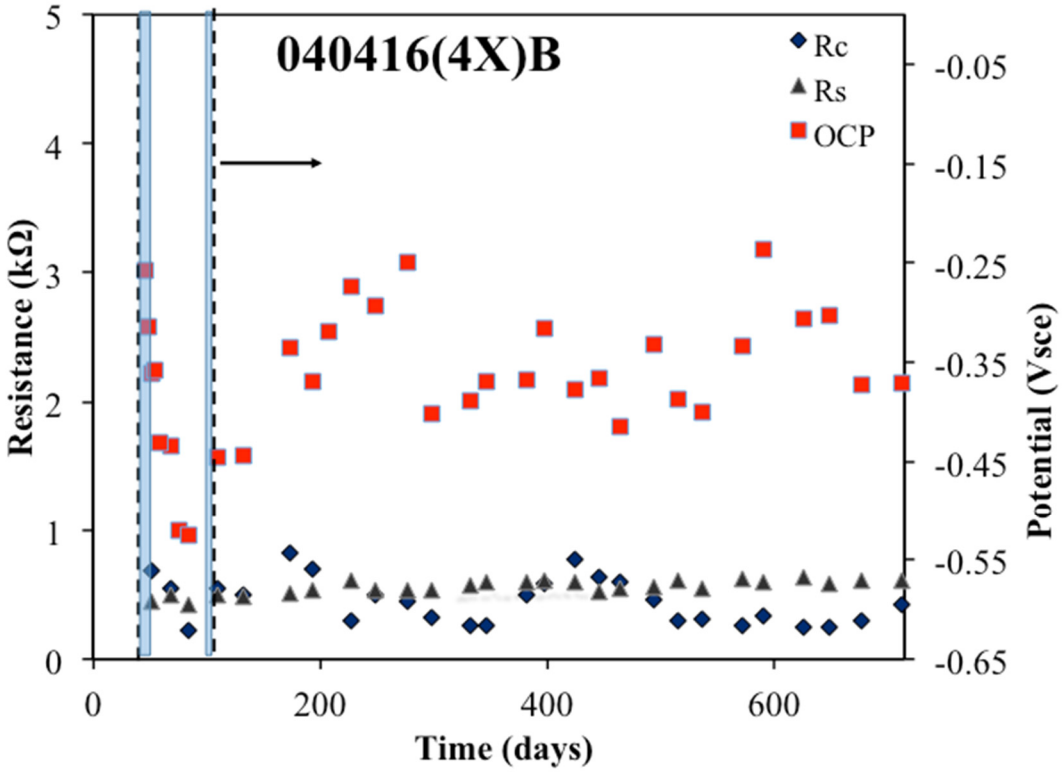

Figure 182. Rebar potentials, R_s, and R_c values measured on rebar 4X-B

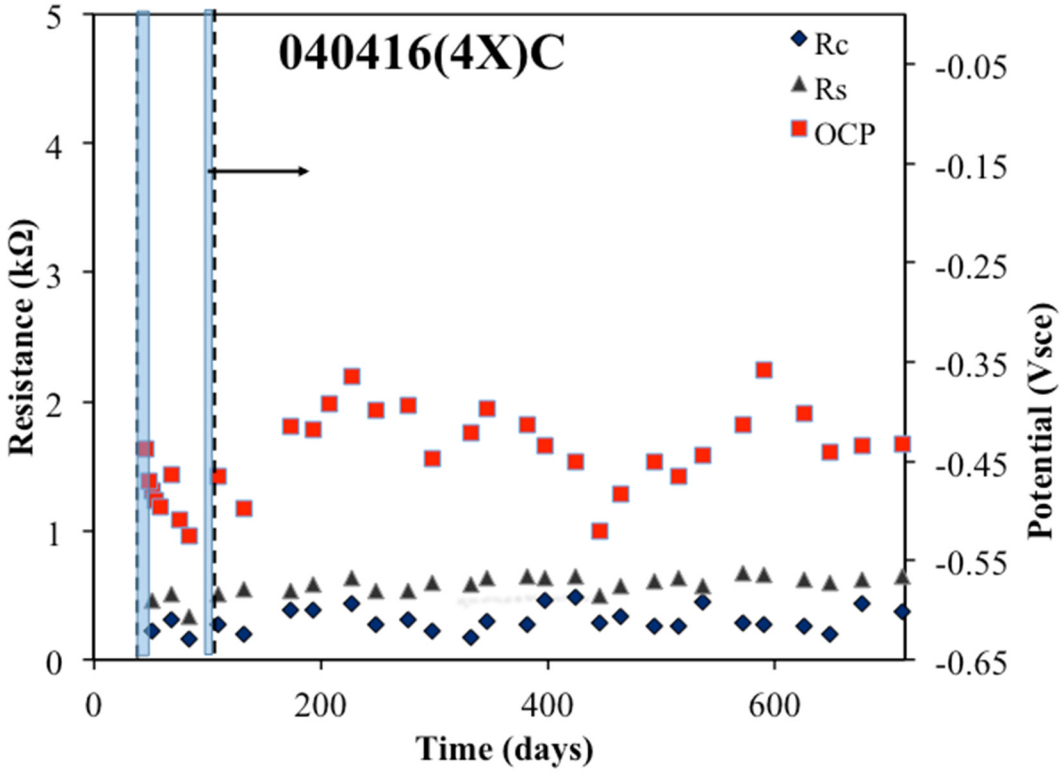

Figure 183. Rebar potentials, R_s, and R_c values measured on rebar 4X-C

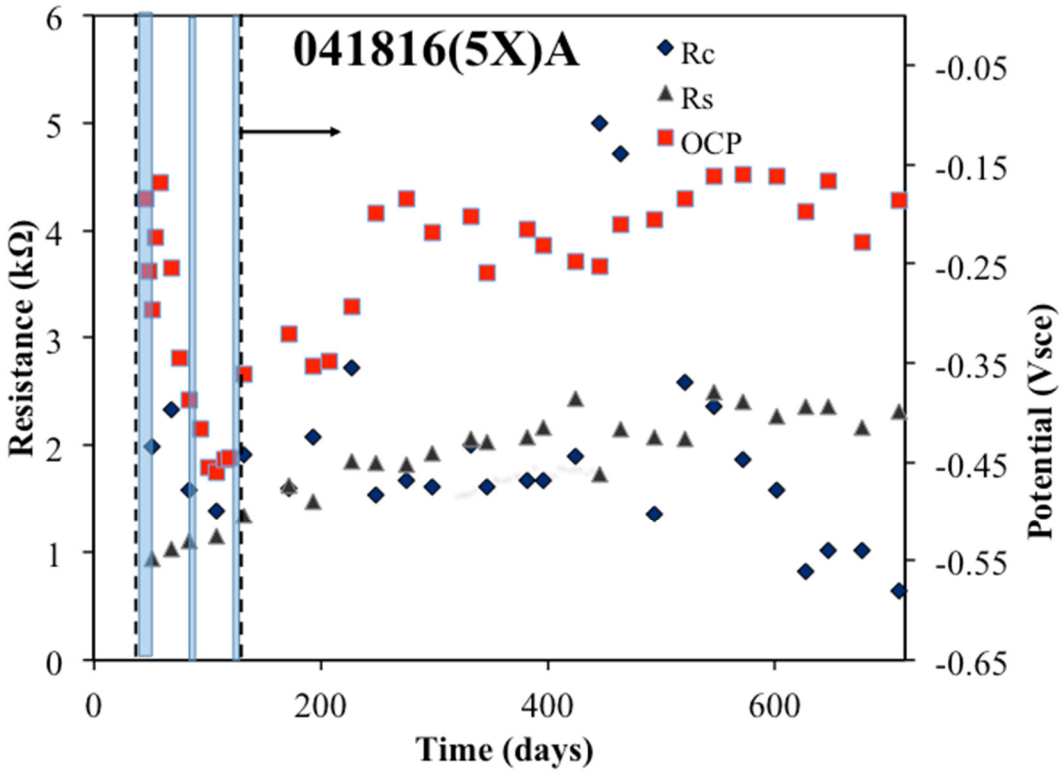

Figure 184. Rebar potentials, R_s, and R_c values measured on rebar 5X-A

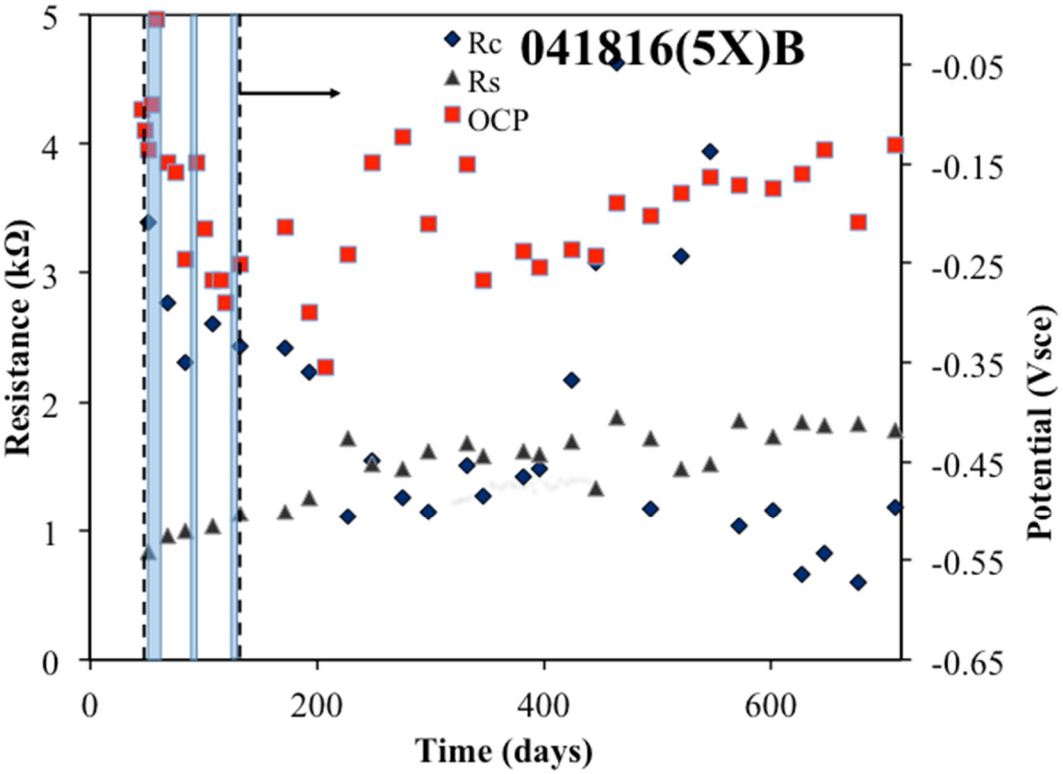

Figure 185. Rebar potentials, R_s, and R_c values measured on rebar 5X-B

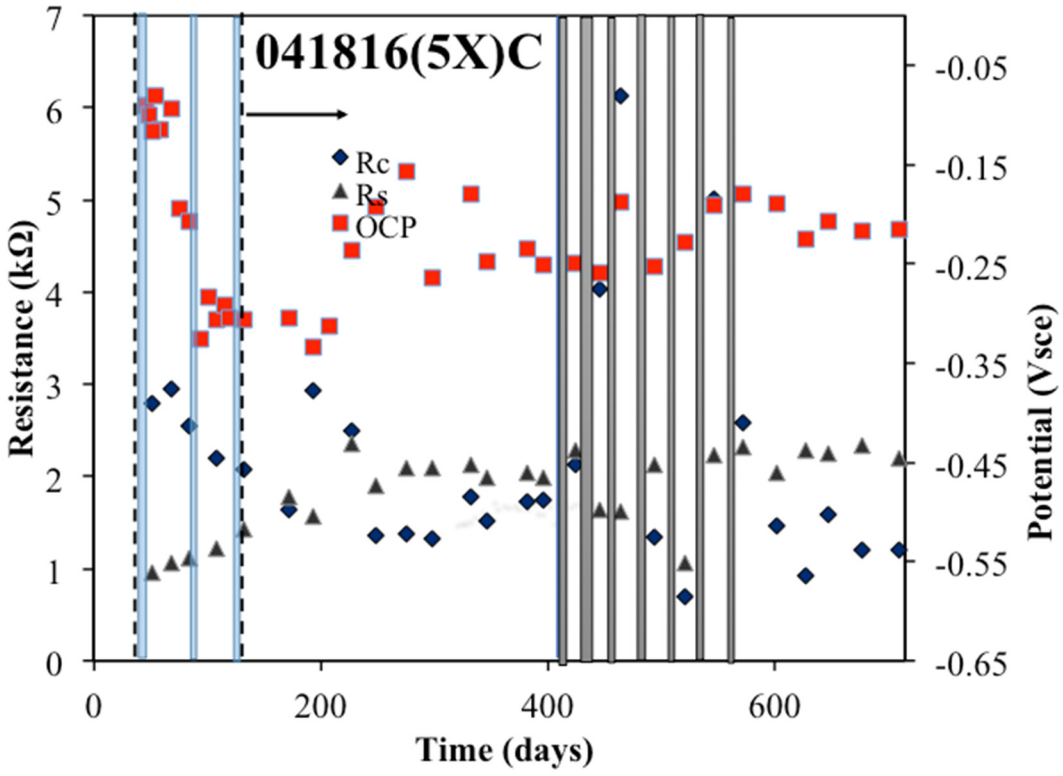

Figure 186. Rebar potentials, R_s, and R_c values measured on rebar 5X-C

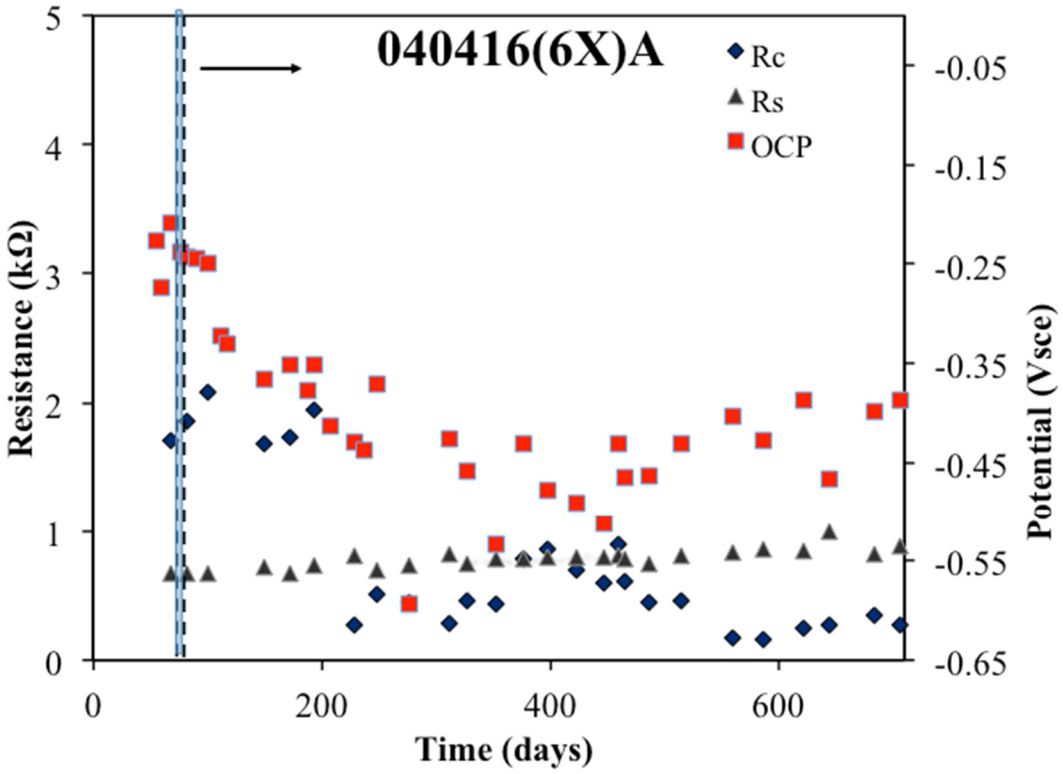

Figure 187. Rebar potentials, R_s, and R_c values measured on rebar 6X-A

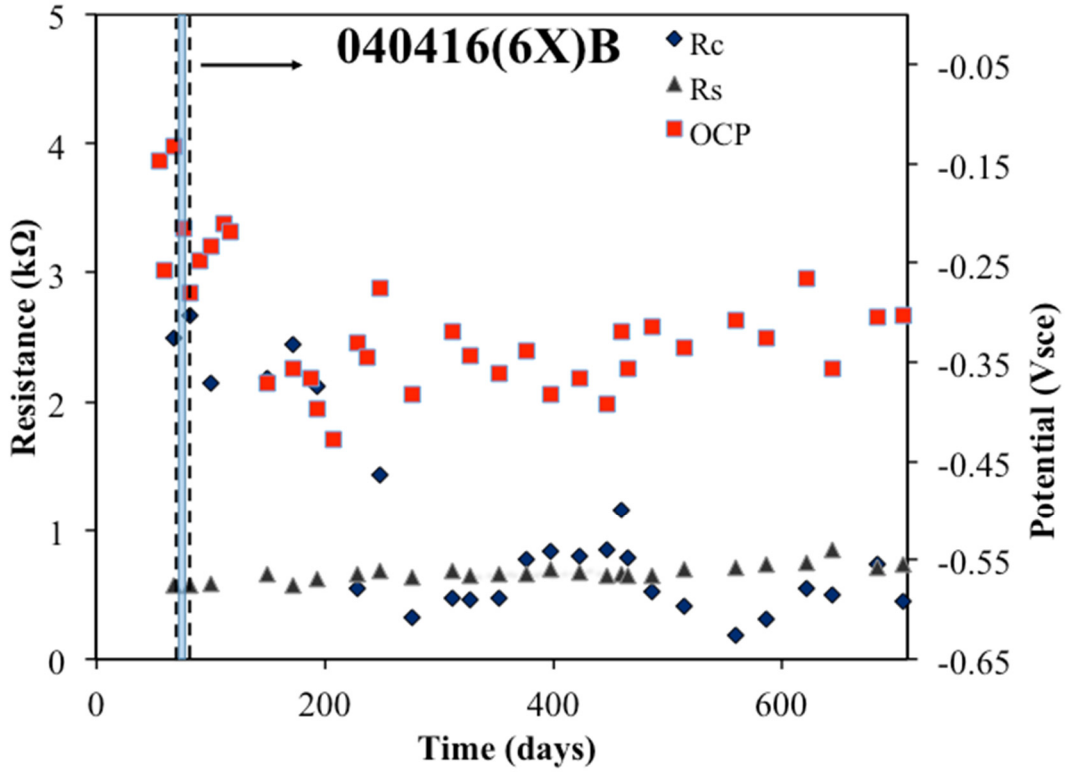

Figure 188. Rebar potentials, R_s, and R_c values measured on rebar 6X-B

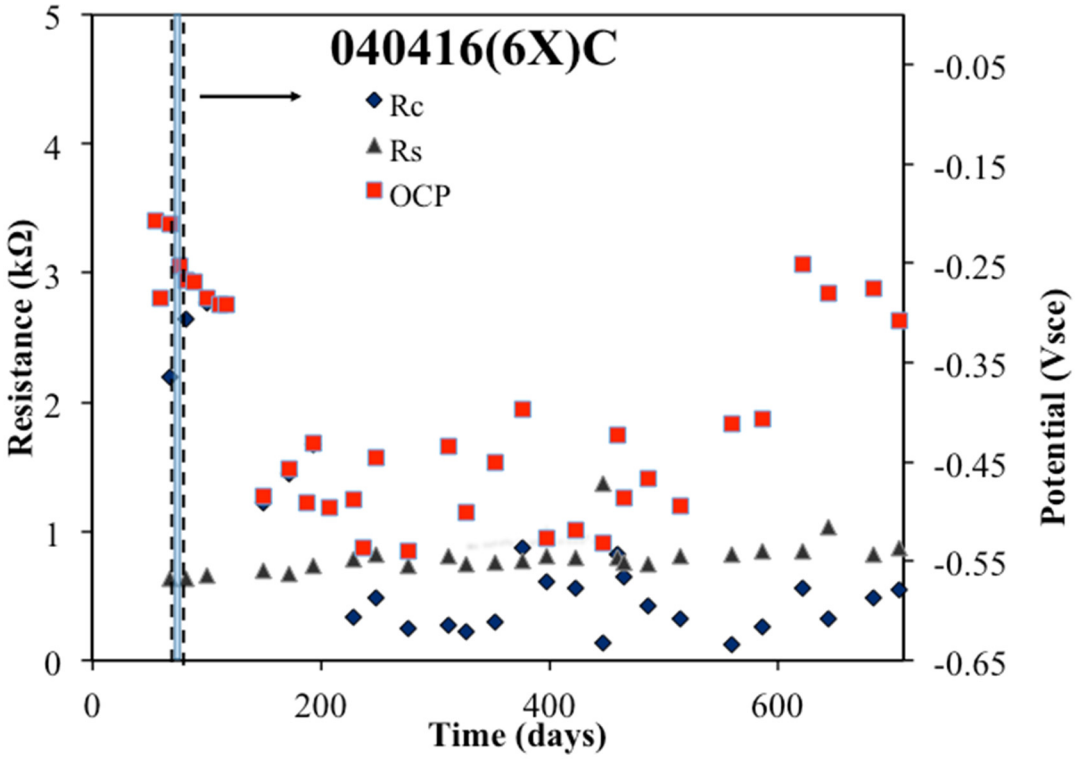

Figure 189. Rebar potentials, R_s, and R_c values measured on rebar 6X-C

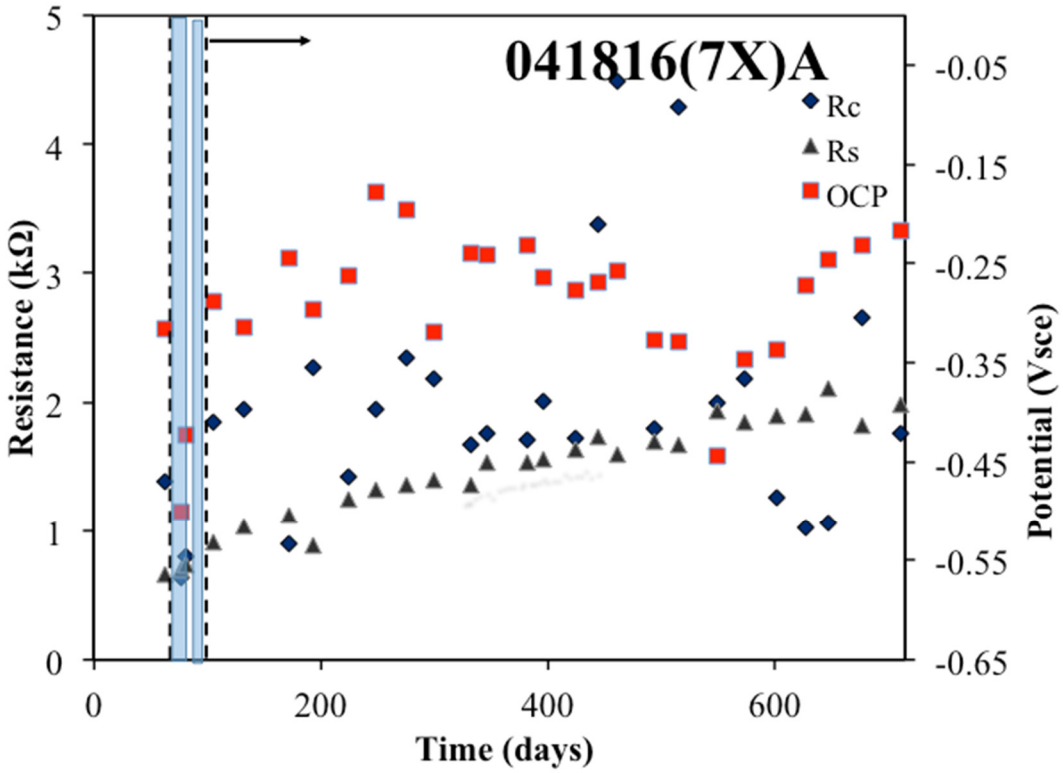

Figure 190. Rebar potentials, R_s, and R_c values measured on rebar 7X-A

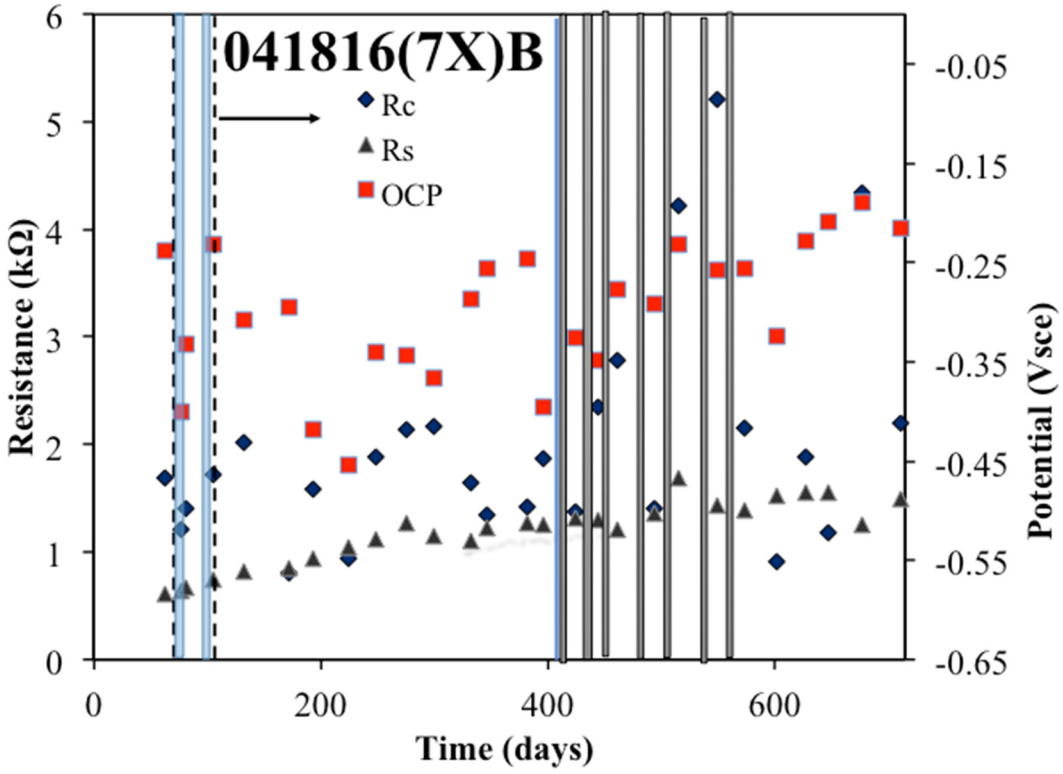

Figure 191. Rebar potentials, R_s, and R_c values measured on rebar 7X-B

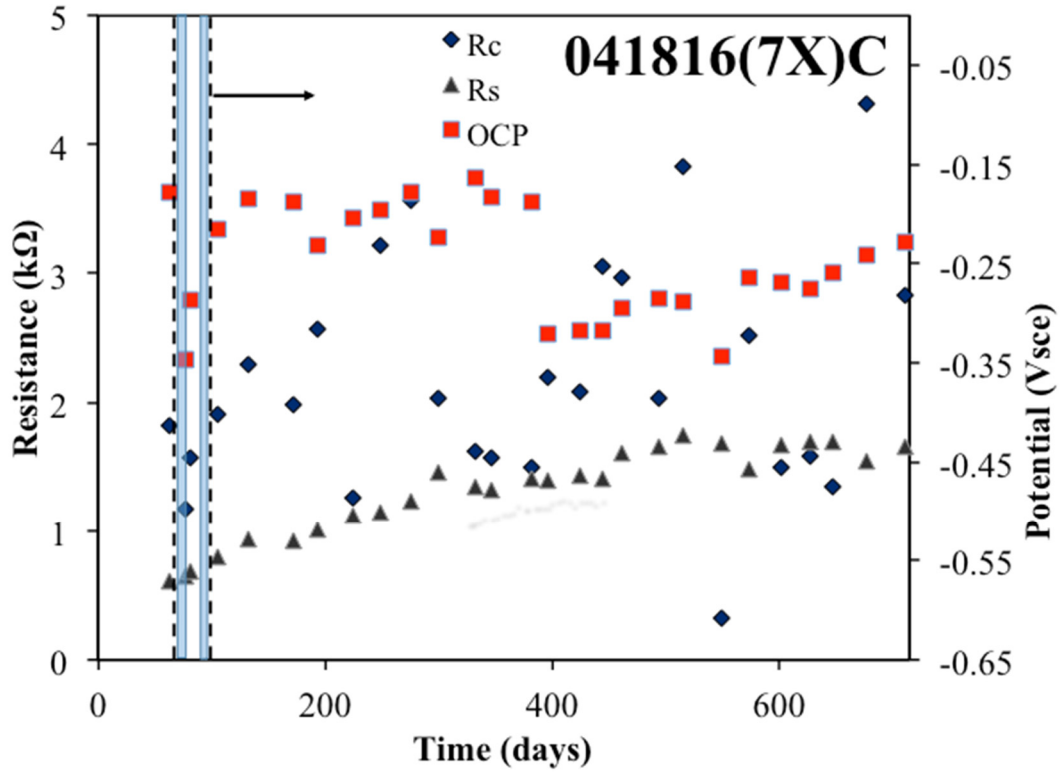

Figure 192. Rebar potentials, R_s, and R_c values measured on rebar 7X-C

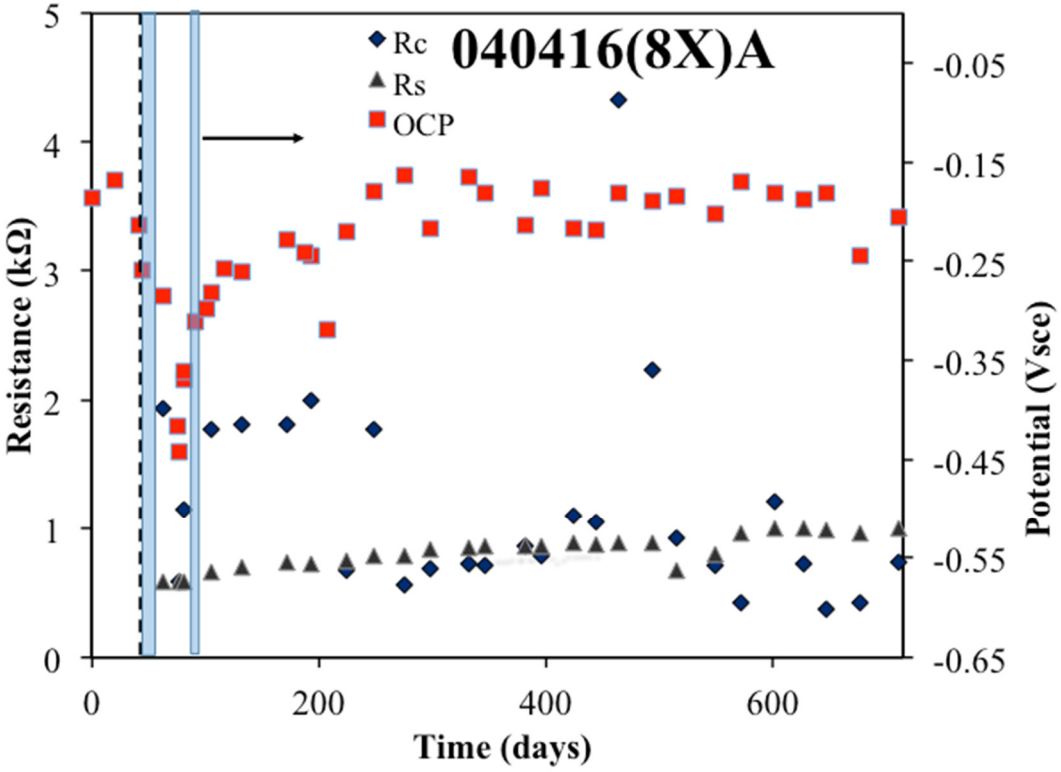

Figure 193. Rebar potentials, R_s, and R_c values measured on rebar 8X-A

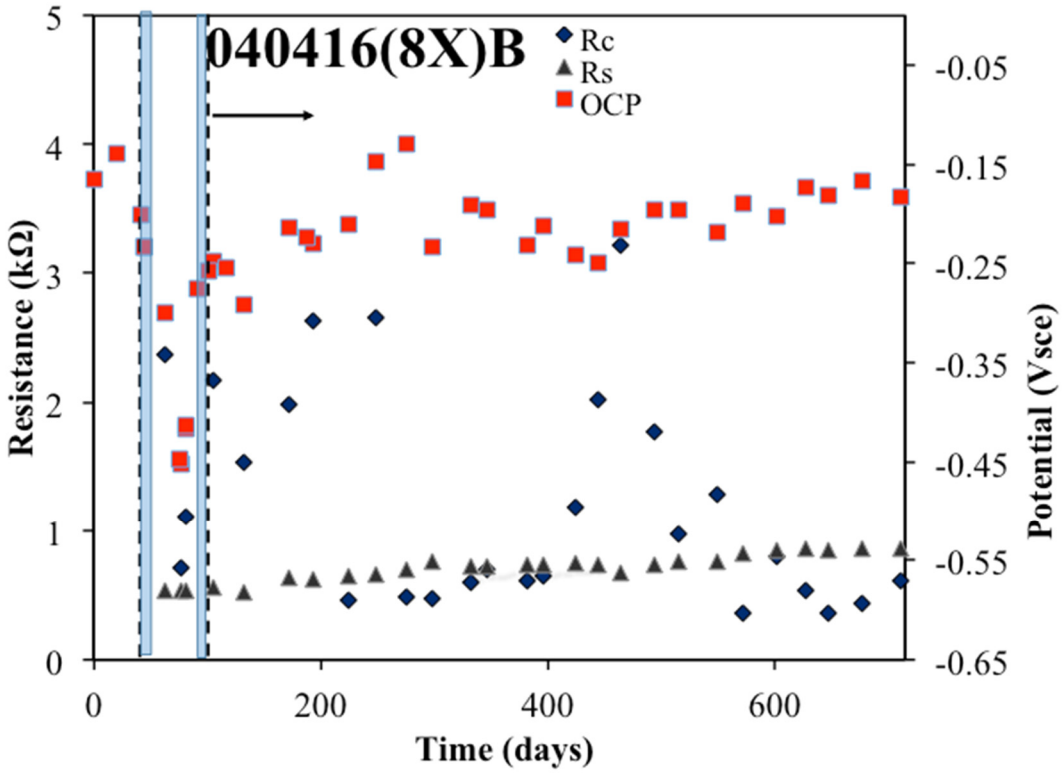

Figure 194. Rebar potentials, R_s, and R_c values measured on rebar 8X-B

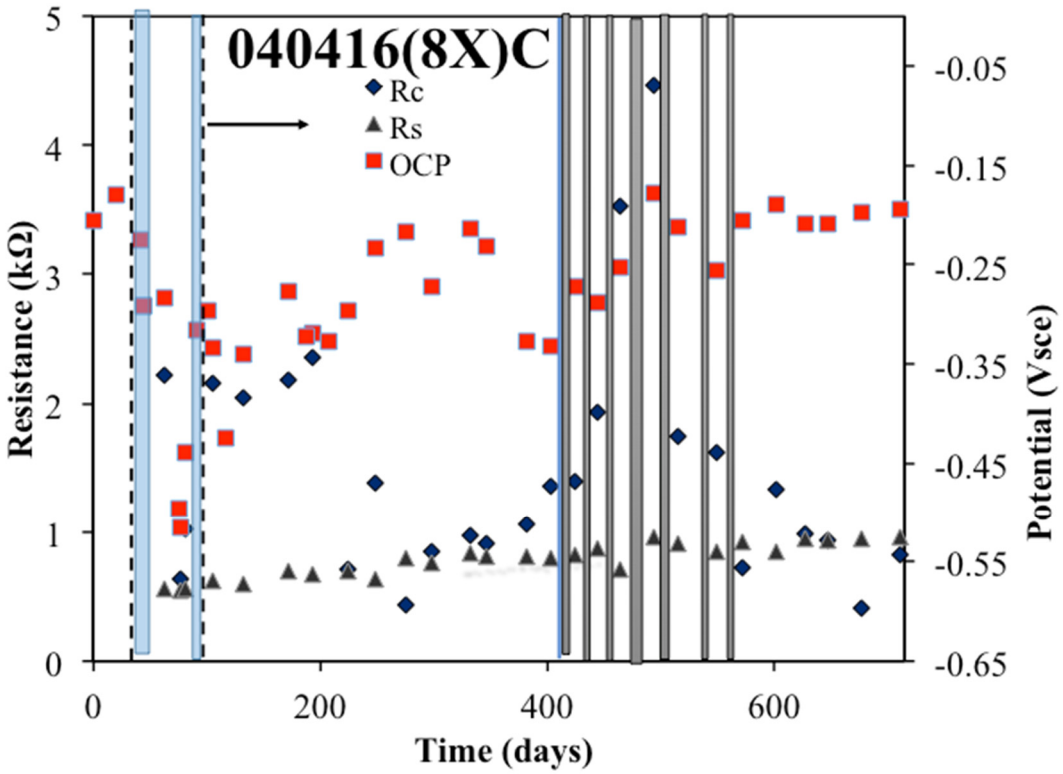

Figure 195. Rebar potentials, R_s, and R_c values measured on rebar 8X-C

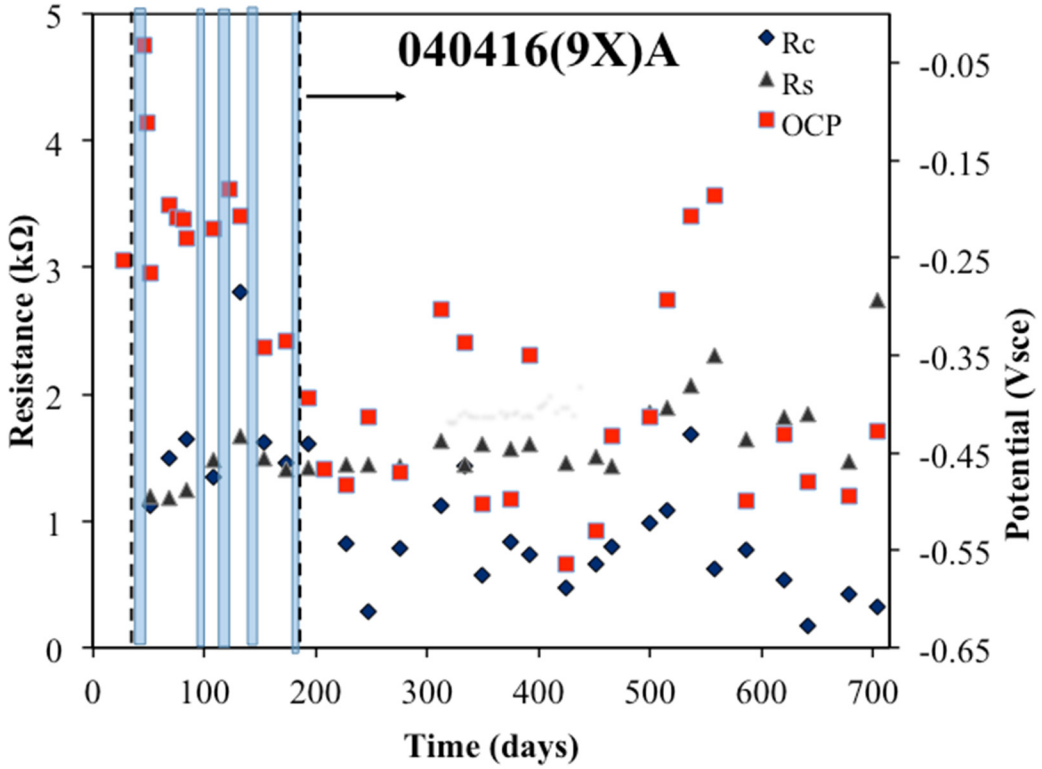

Figure 196. Rebar potentials, R_s, and R_c values measured on rebar 9X-A

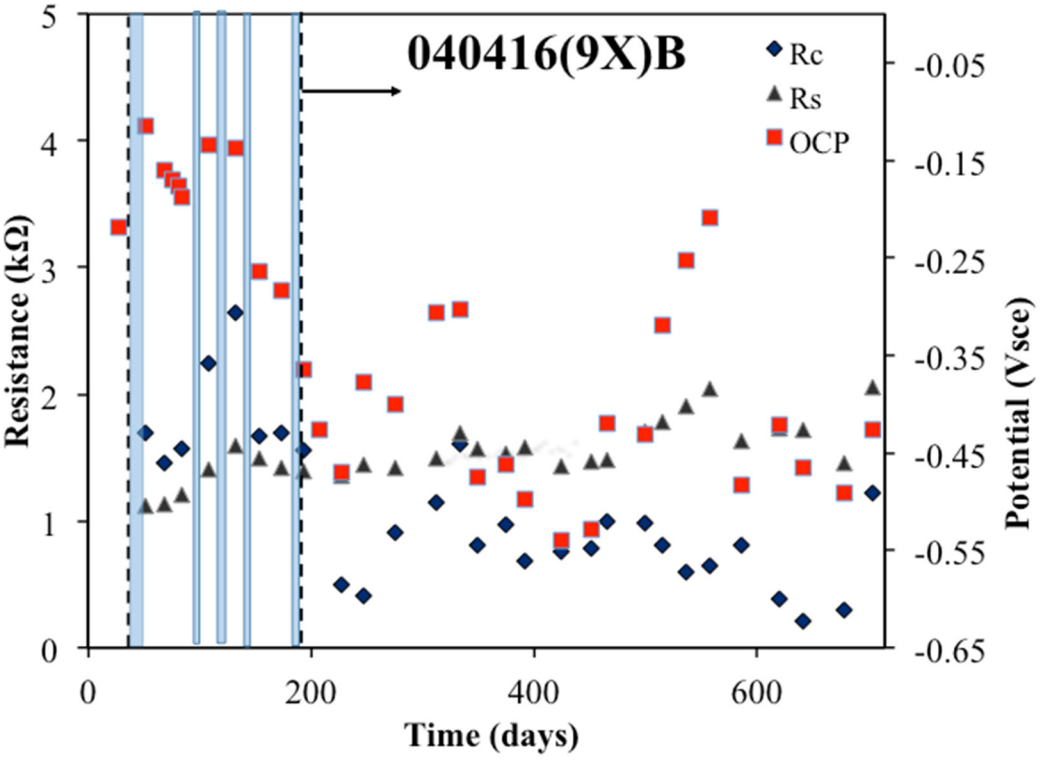

Figure 197. Rebar potentials, R_s, and R_c values measured on rebar 9X-B

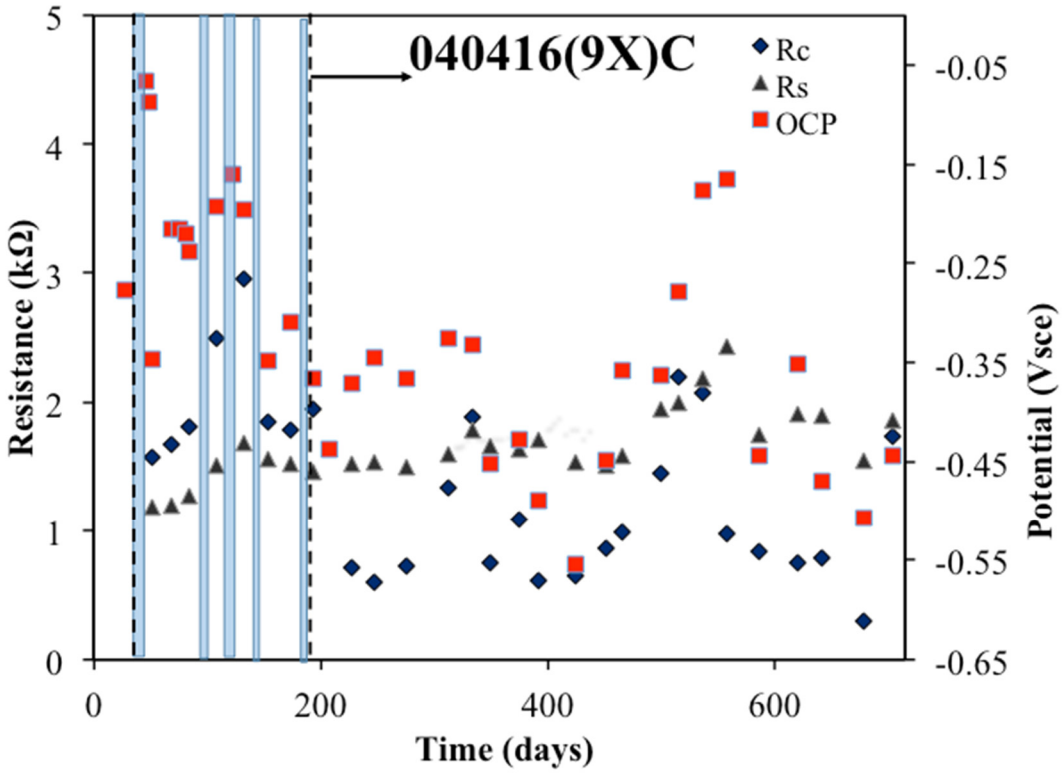

Figure 198. Rebar potentials, R_s, and R_c values measured on rebar 9X-C

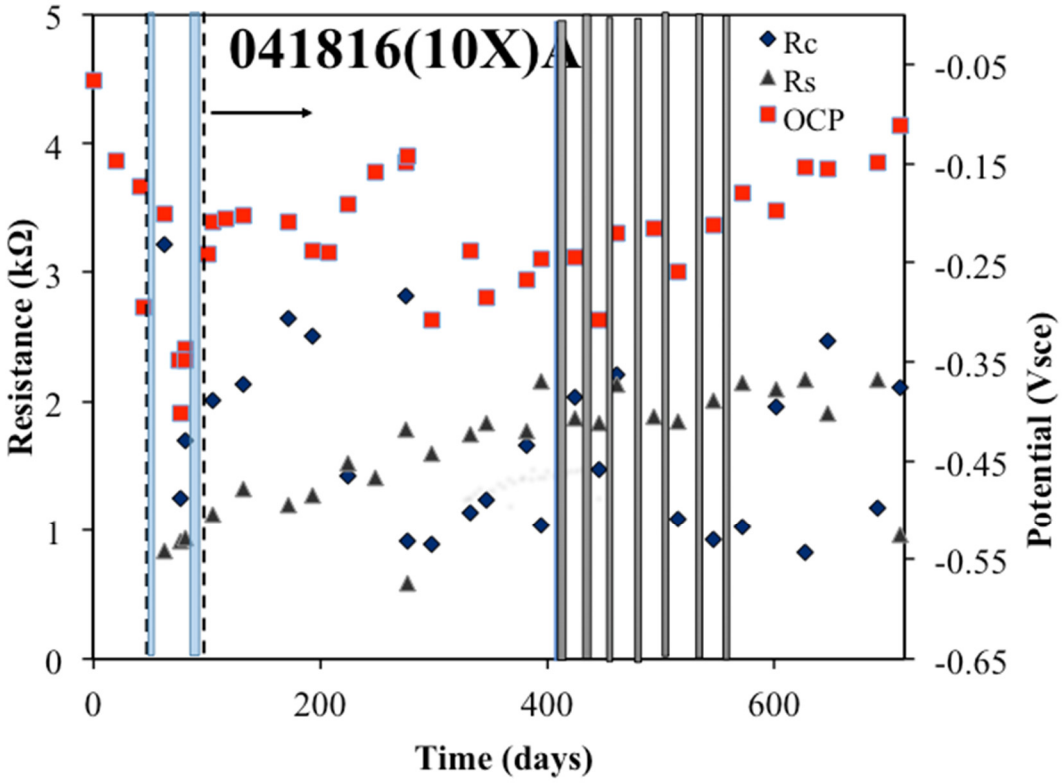

Figure 199. Rebar potentials, R_s, and R_c values measured on rebar 10X-A

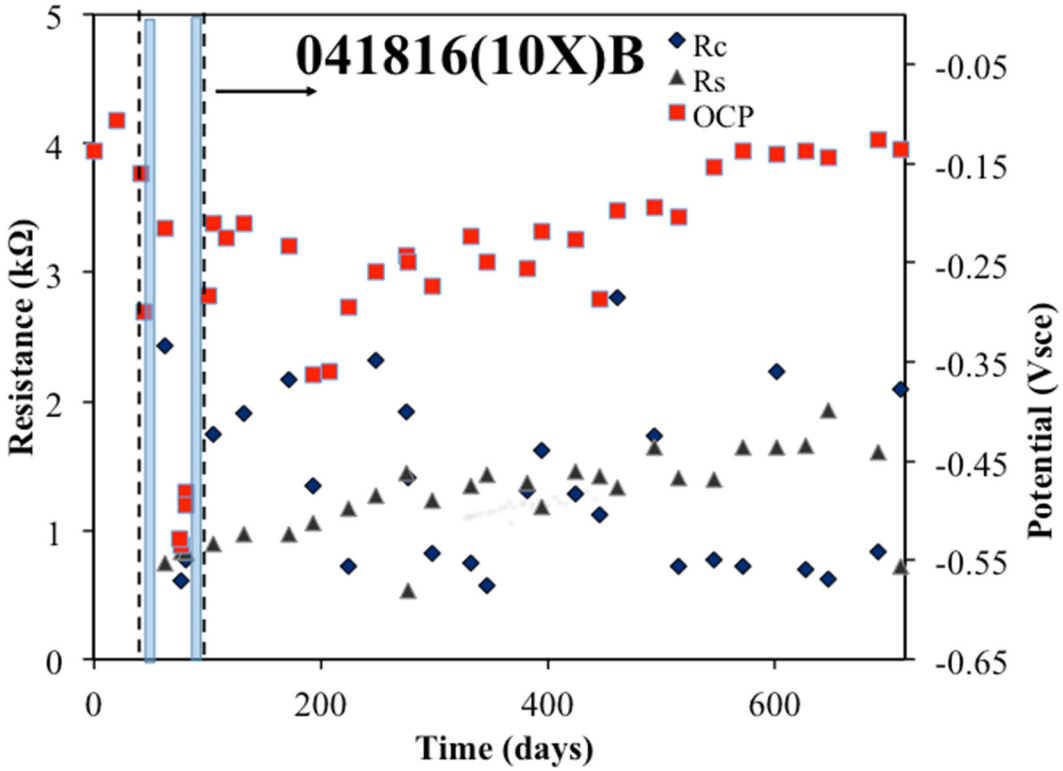

Figure 200. Rebar potentials, R_s, and R_c values measured on rebar 10X-B

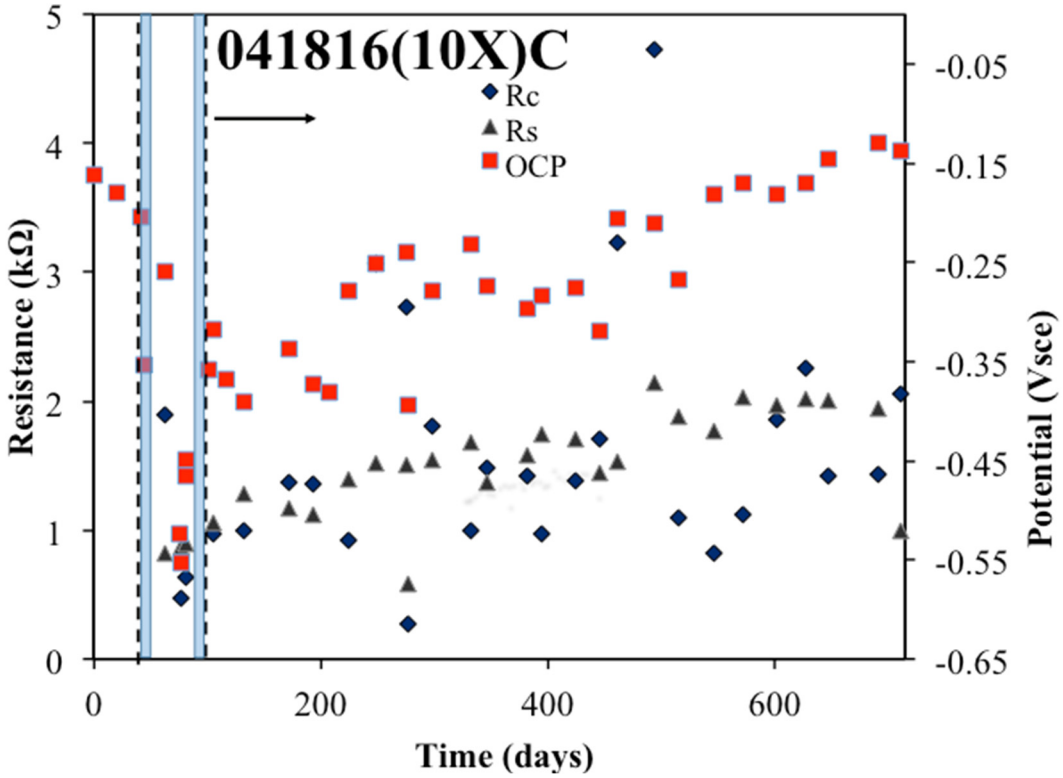

Figure 201. Rebar potentials, R_s, and R_c values measured on rebar 10X-C

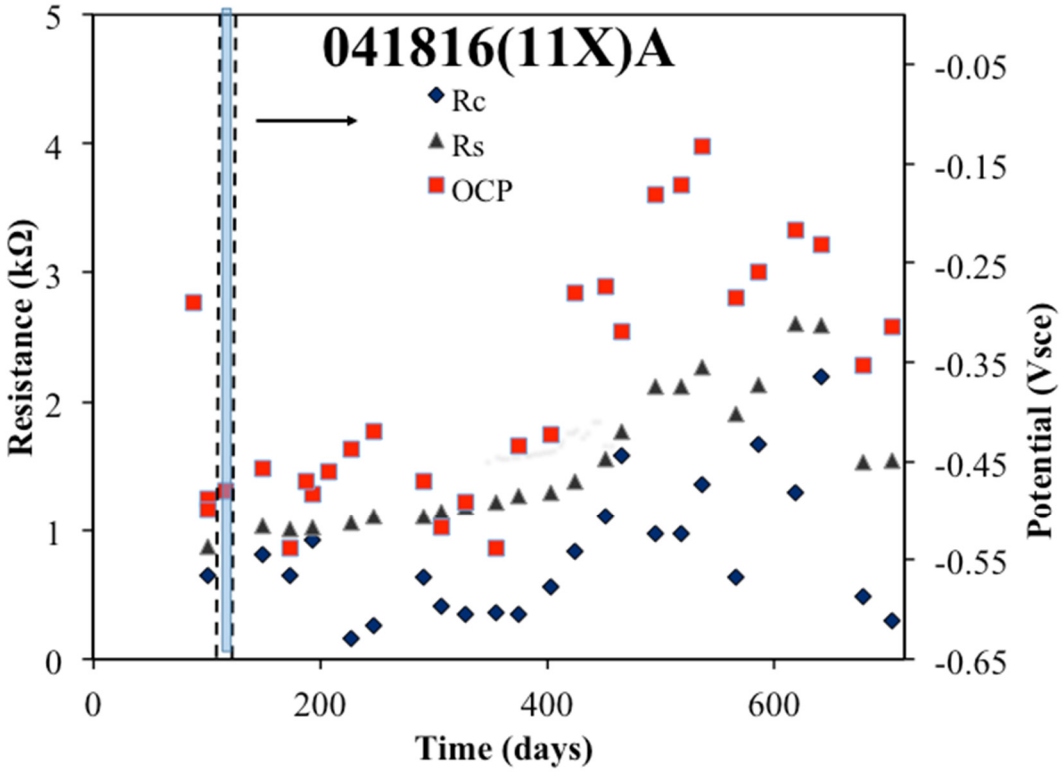

Figure 202. Rebar potentials, R_s, and R_c values measured on rebar 11X-A

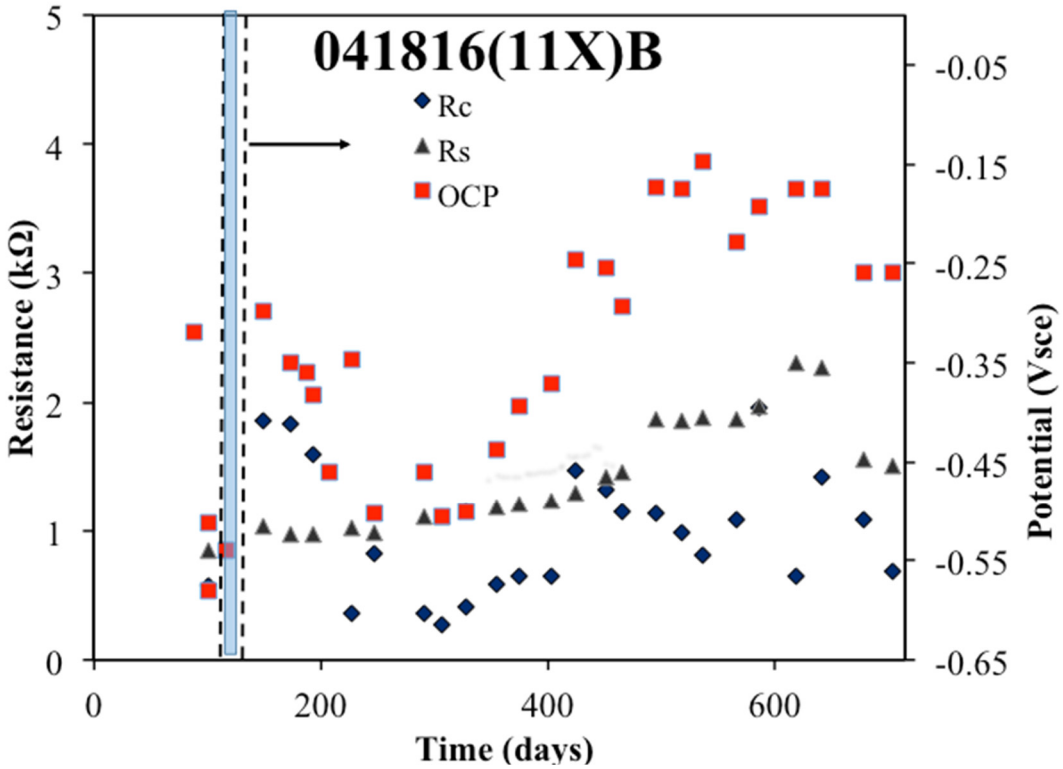

Figure 203. Rebar potentials, R_s, and R_c values measured on rebar 11X-B

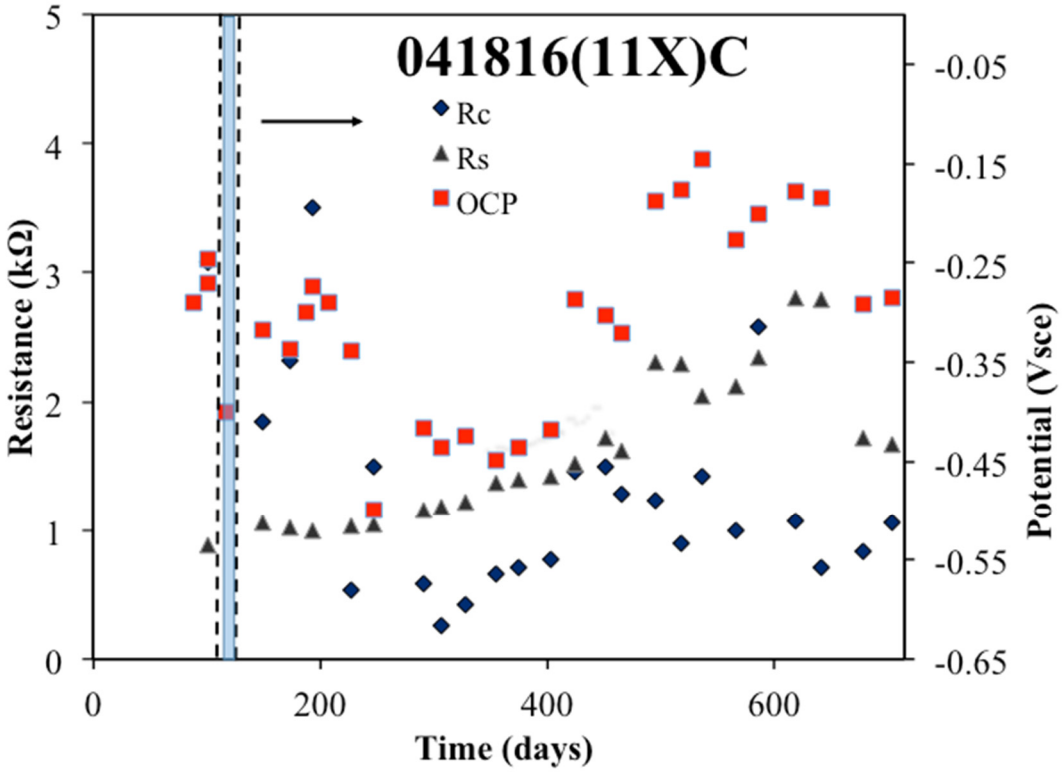

Figure 204. Rebar potentials, R_s, and R_c values measured on rebar 11X-C

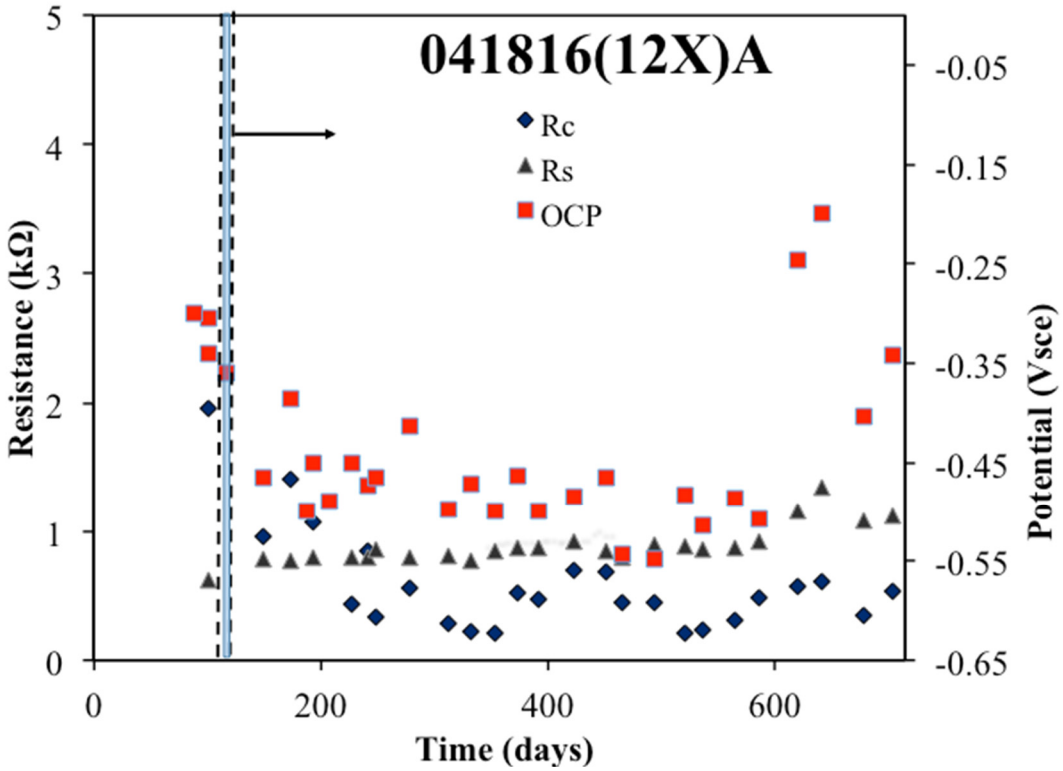

Figure 205. Rebar potentials, R_s, and R_c values measured on rebar 12X-A

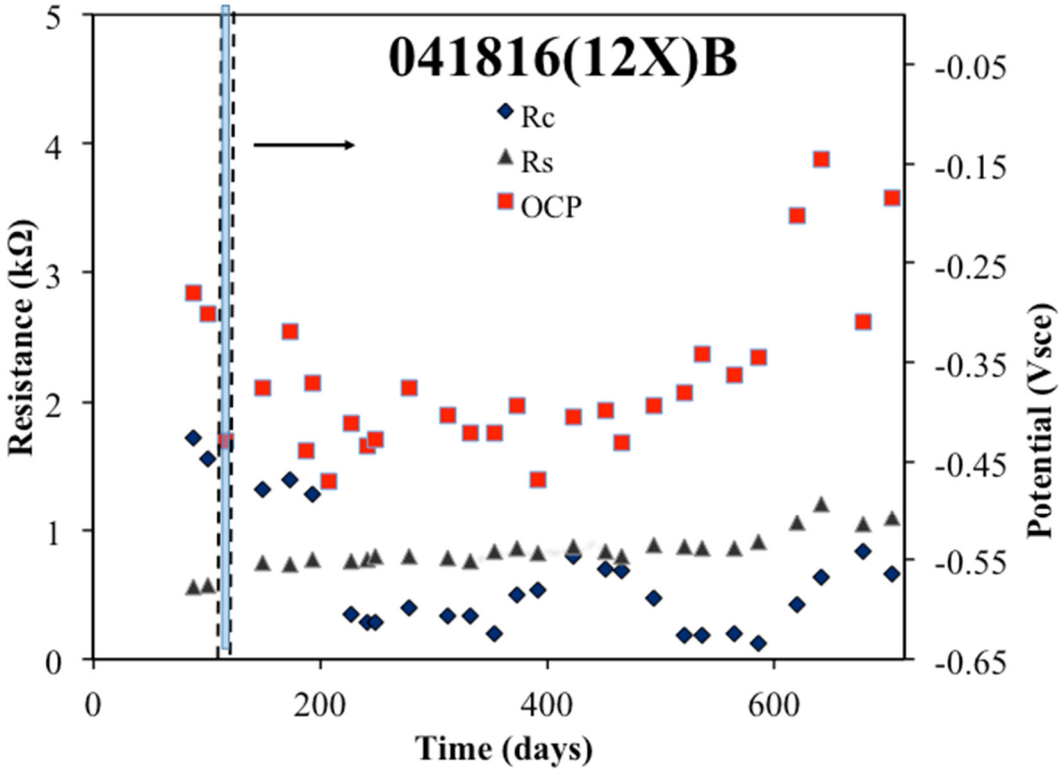

Figure 206. Rebar potentials, R_s, and R_c values measured on rebar 12X-B

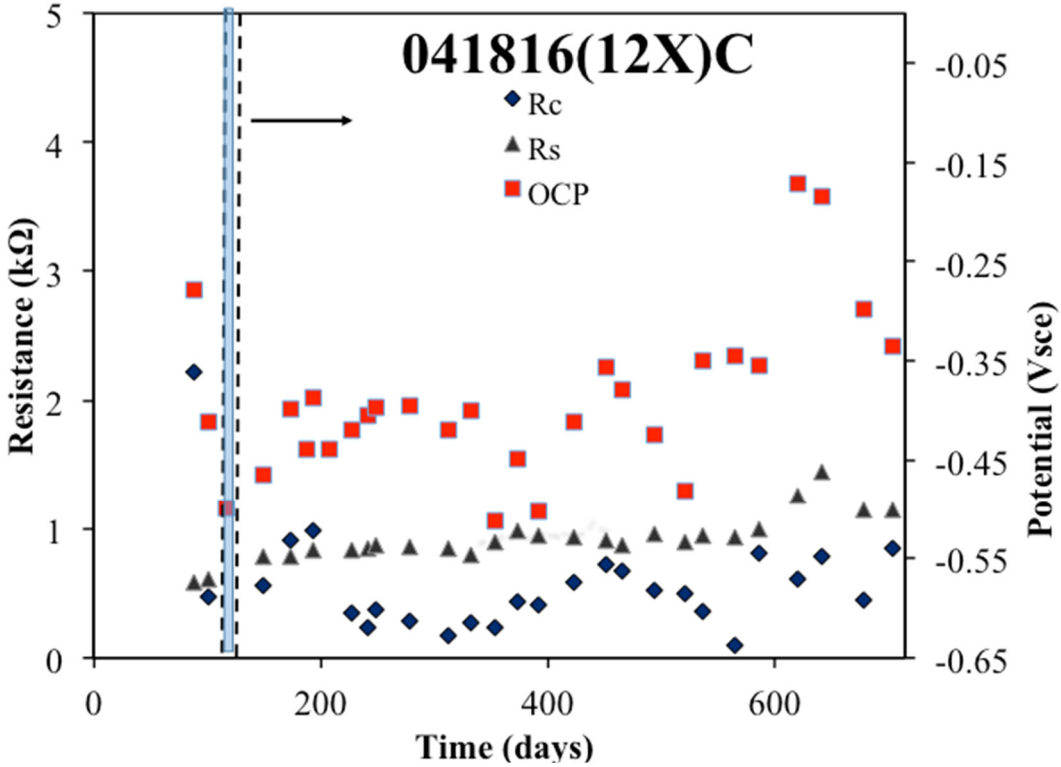

Figure 207. Rebar potentials, R_s, and R_c values measured on rebar 12X-C

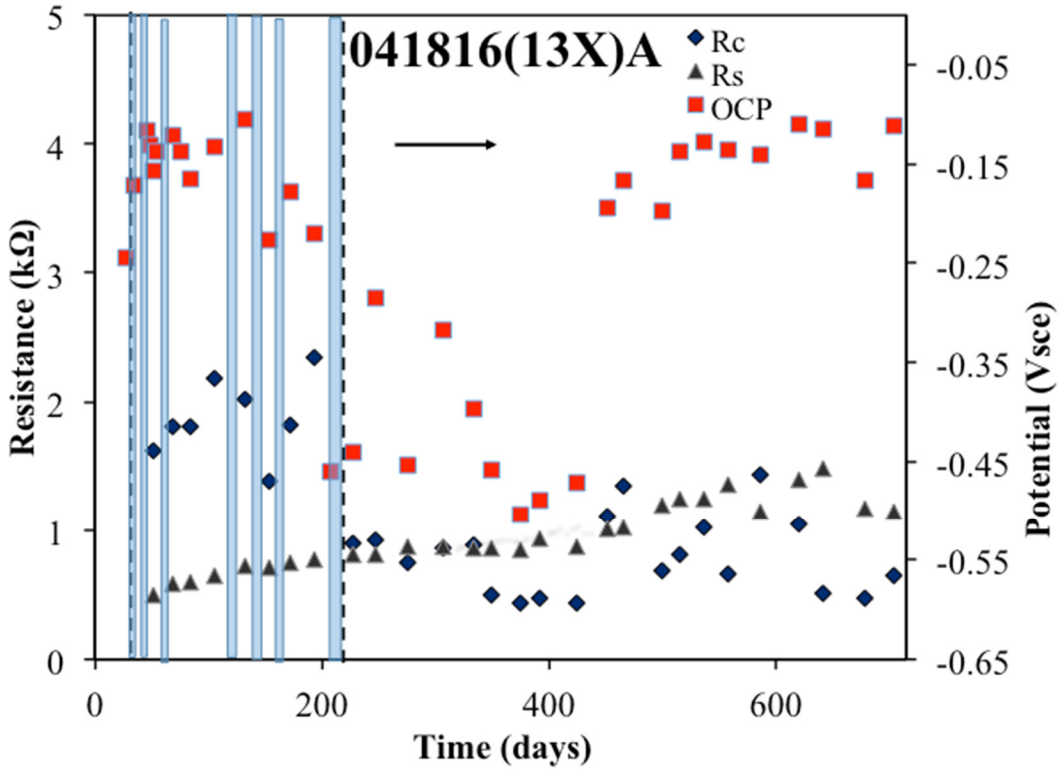

Figure 208. Rebar potentials, R_s, and R_c values measured on rebar 13X-A

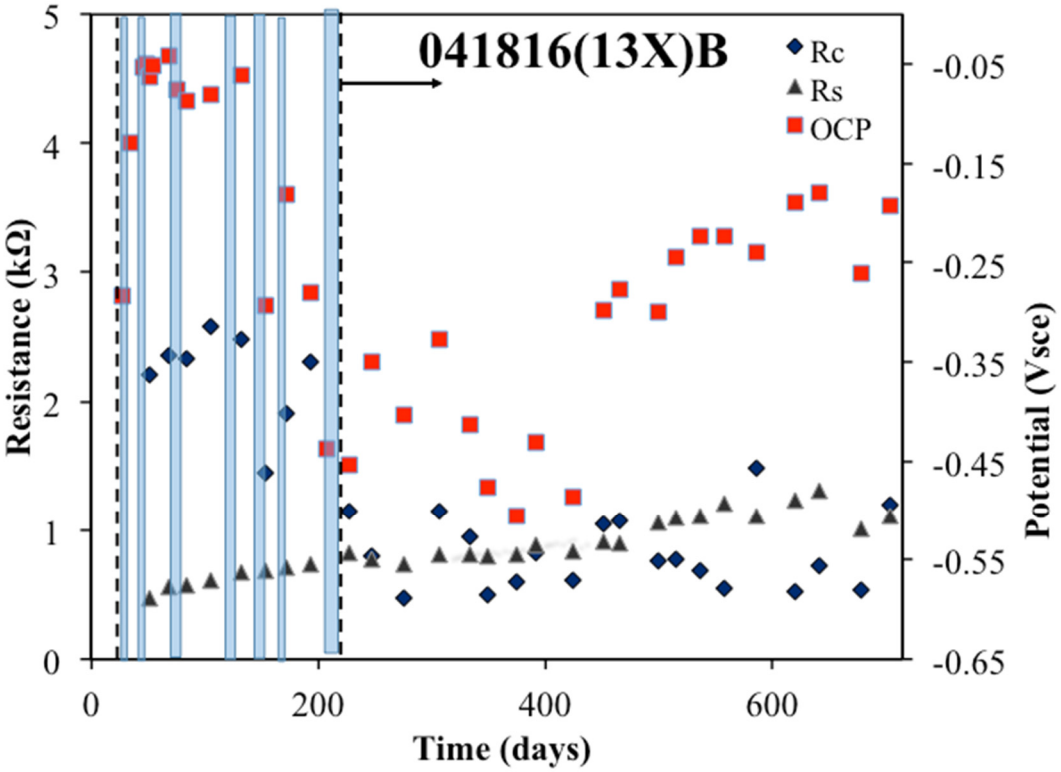

Figure 209. Rebar potentials, R_s, and R_c values measured on rebar 13X-B

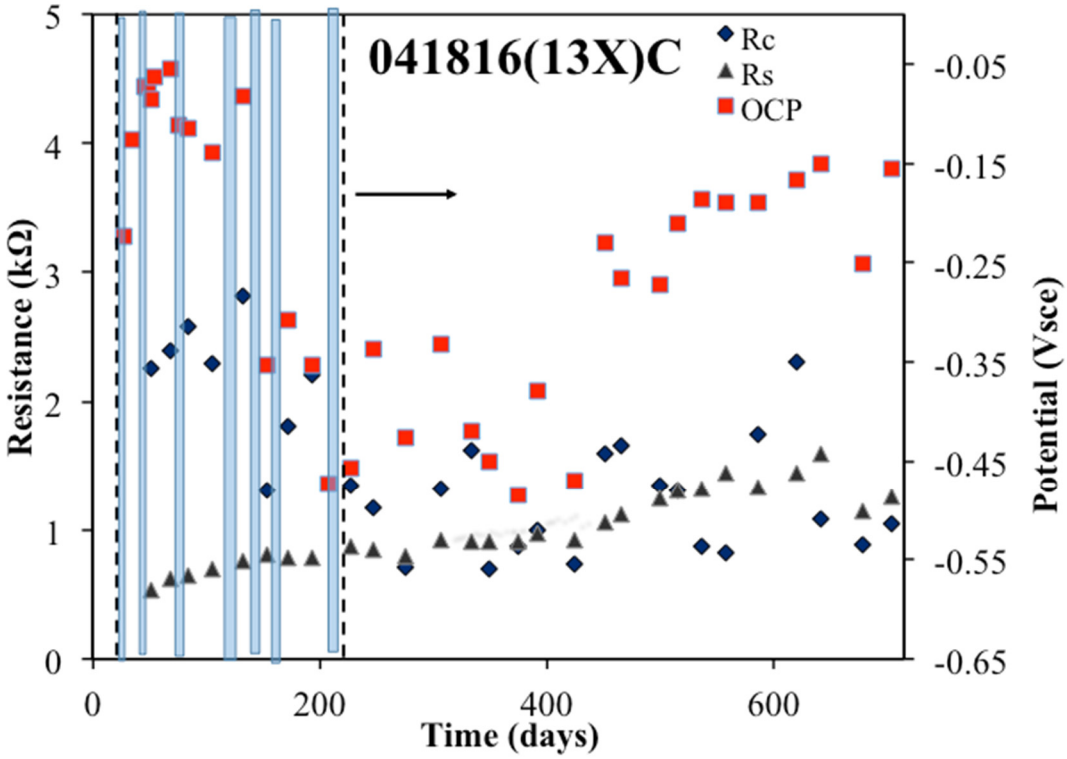

Figure 210. Rebar potentials, R_s, and R_c values measured on rebar 13X-C

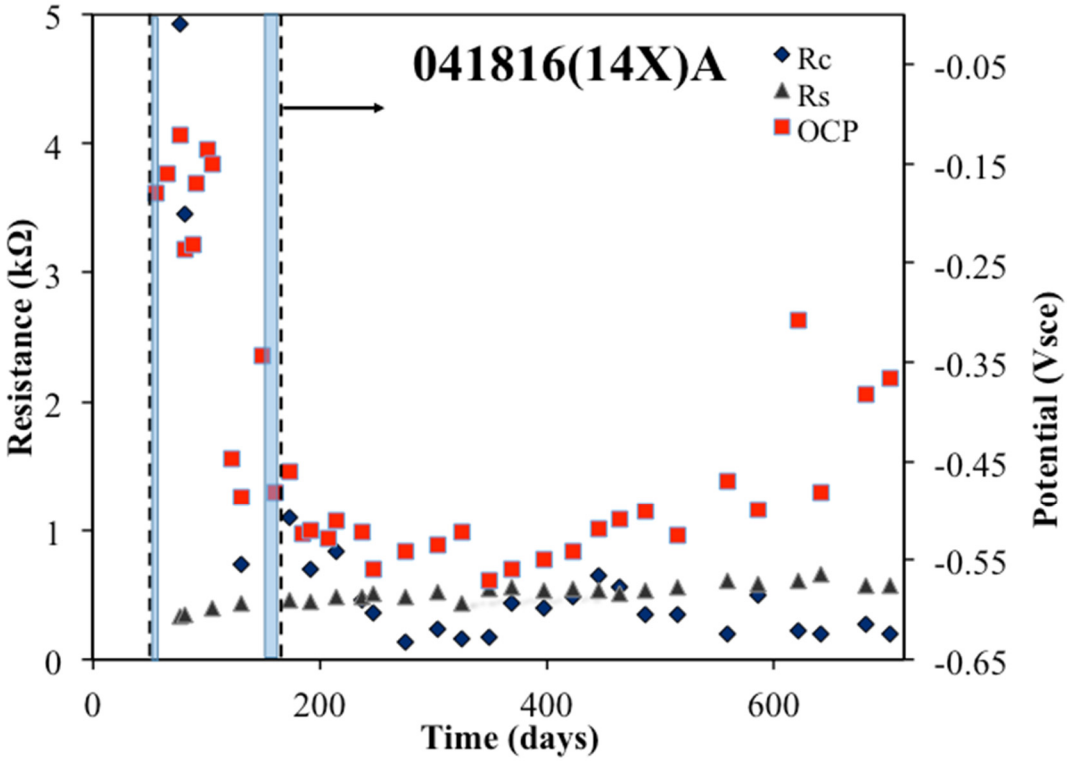

Figure 211. Rebar potentials, R_s, and R_c values measured on rebar 14X-A

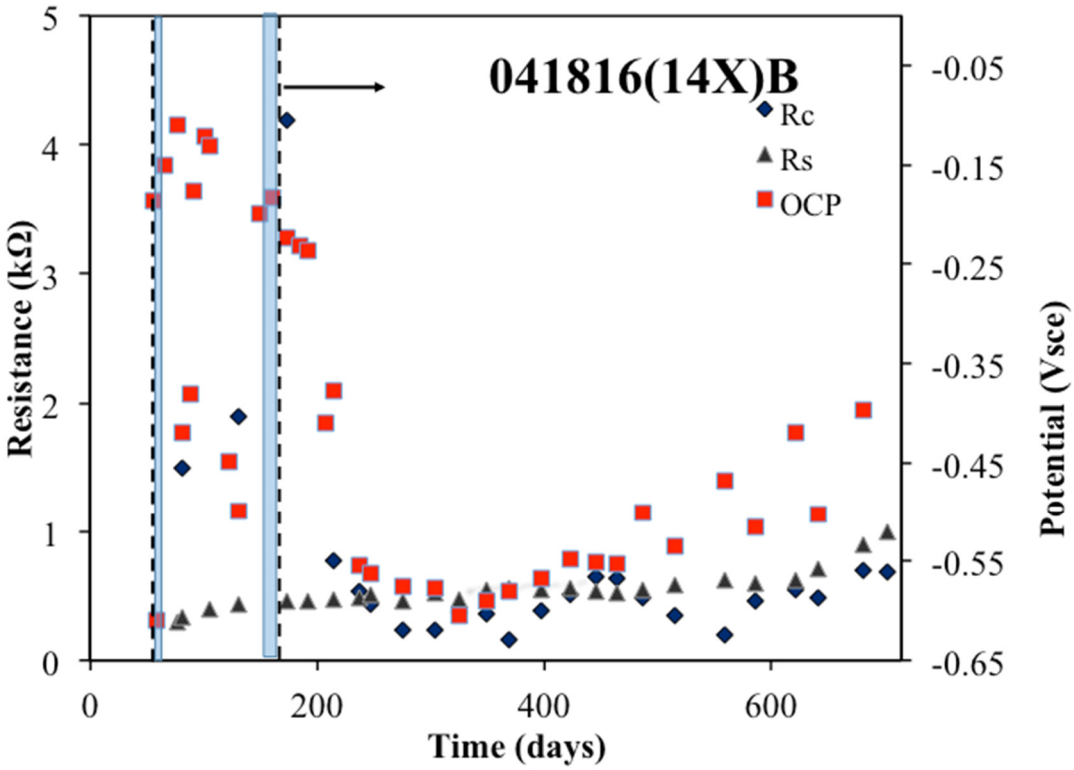

Figure 212. Rebar potentials, R_s, and R_c values measured on rebar 14X-B

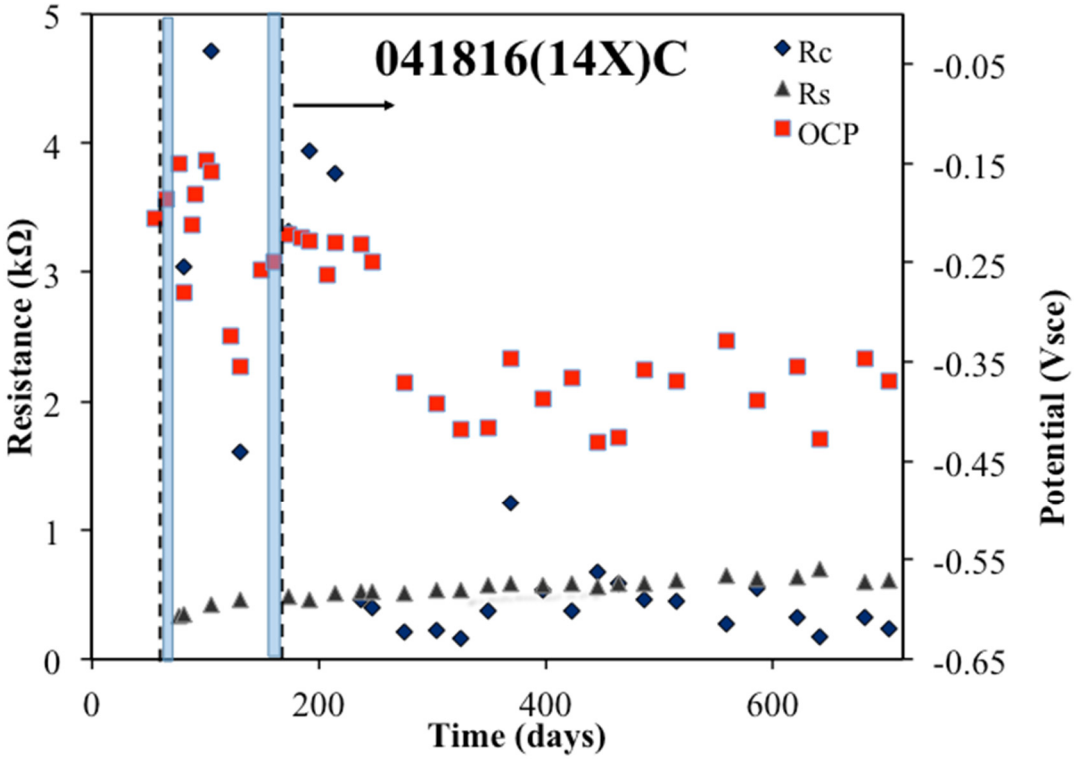

Figure 213. Rebar potentials, R_s, and R_c values measured on rebar 13X-B

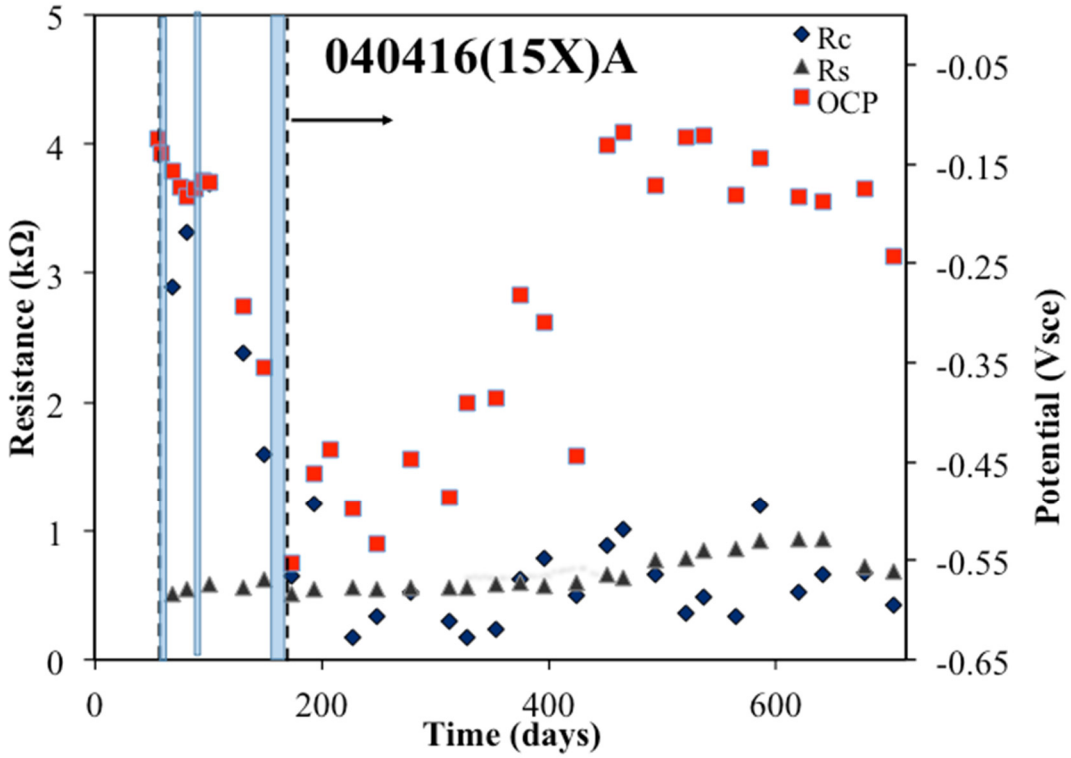

Figure 214. Rebar potentials, R_s, and R_c values measured on rebar 15X-A

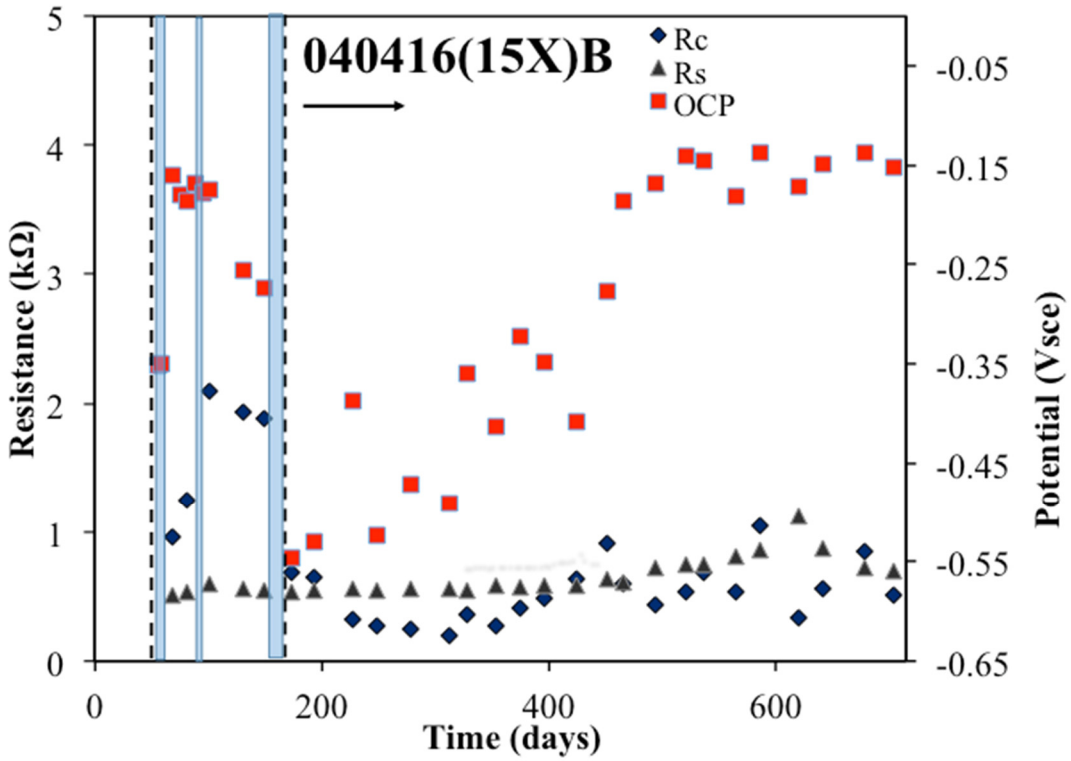

Figure 215. Rebar potentials, R_s, and R_c values measured on rebar 15X-B

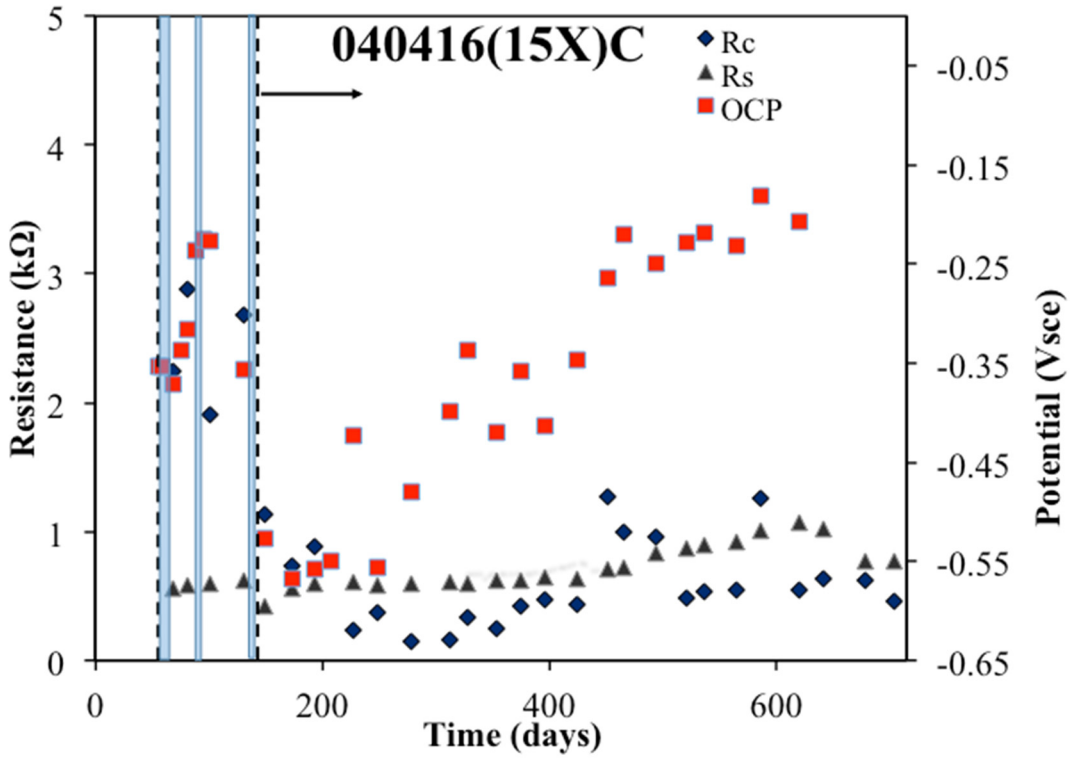

Figure 216. Rebar potentials, R_s, and R_c values measured on rebar 15X-C

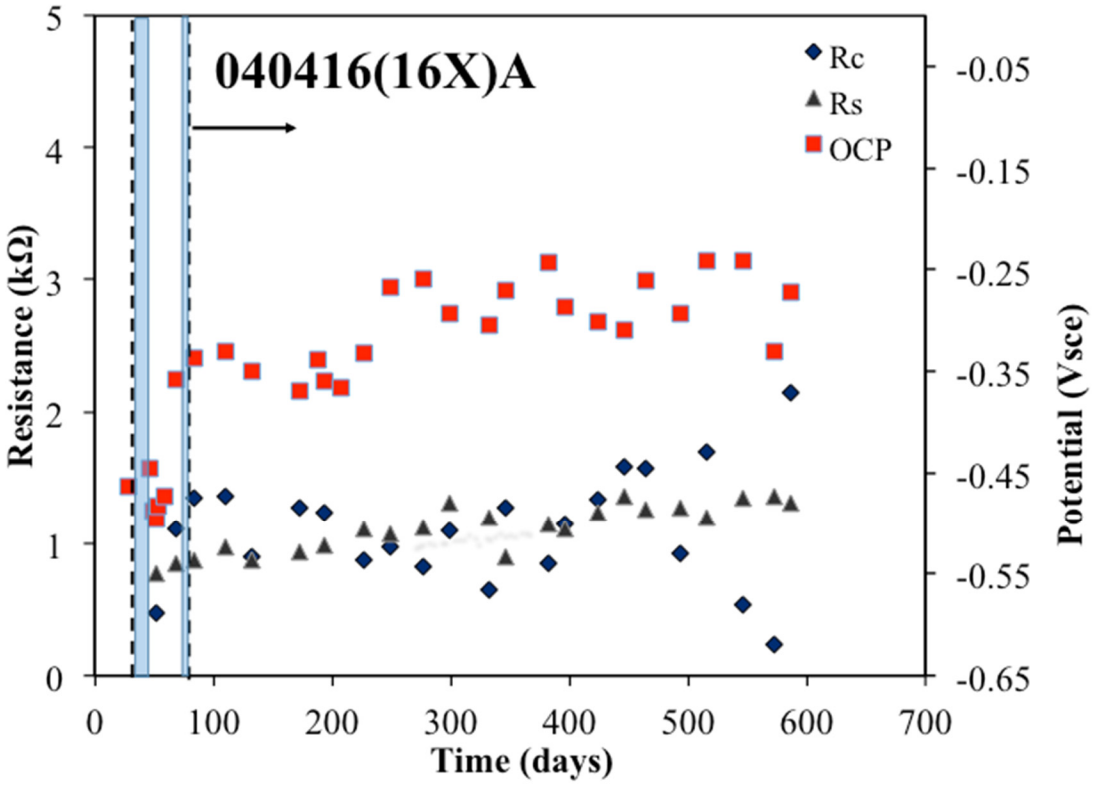

Figure 217. Rebar potentials, R_s, and R_c values measured on rebar 16X-A

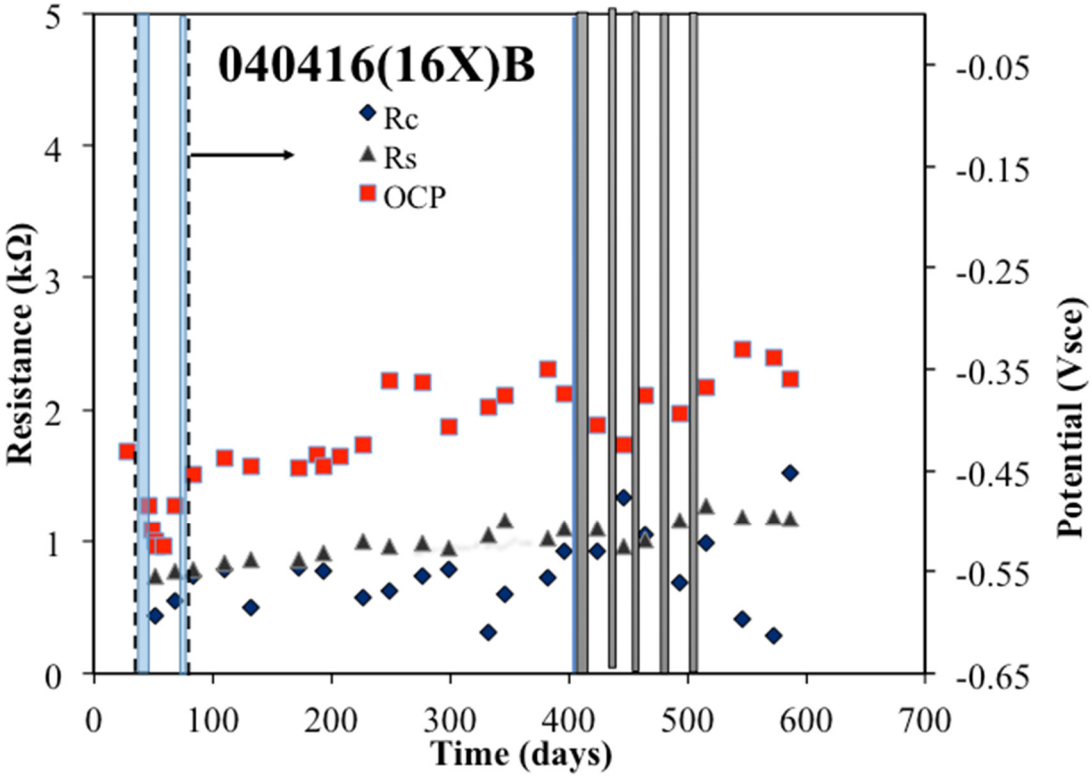

Figure 218. Rebar potentials, R_s, and R_c values measured on rebar 16X-B

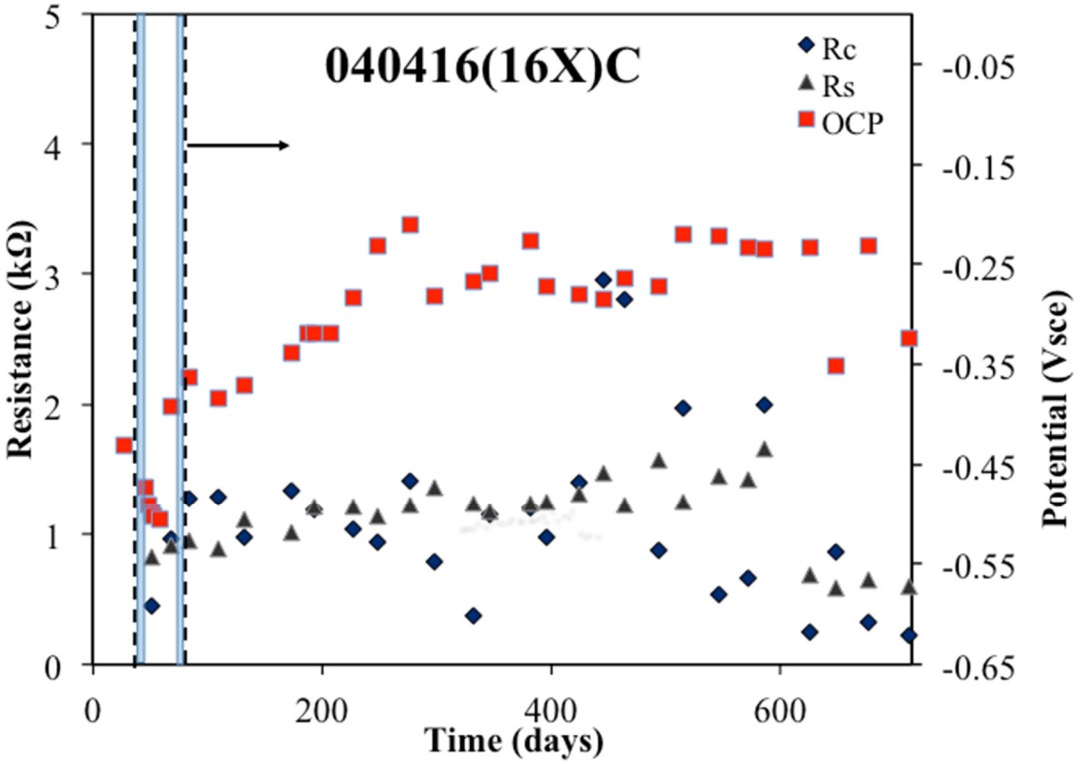

Figure 219. Rebar potentials, R_s, and R_c values measured on rebar 16X-C

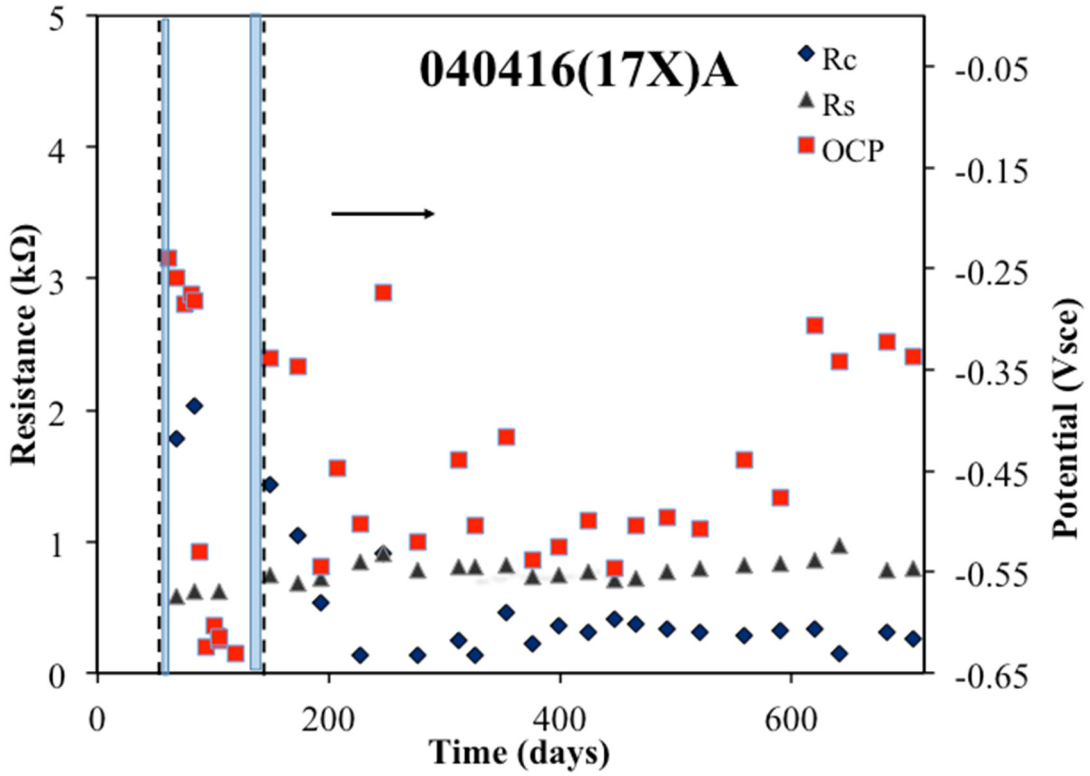

Figure 220. Rebar potentials, R_s, and R_c values measured on rebar 17X-A

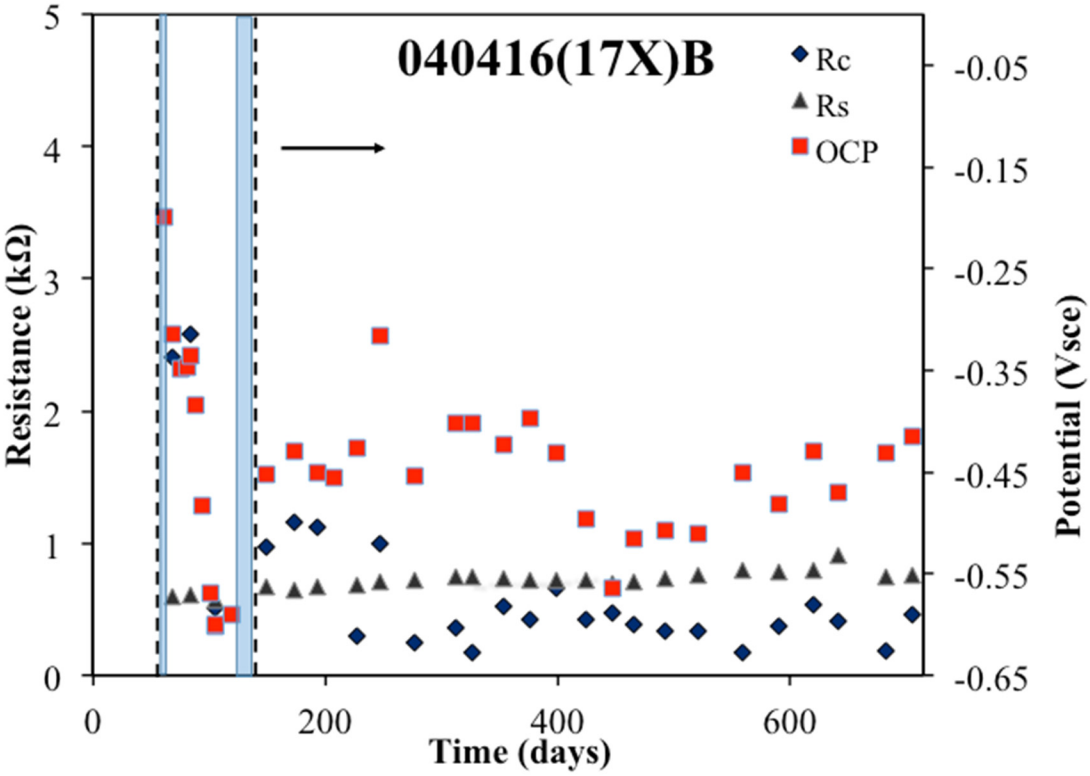

Figure 221. Rebar potentials, R_s, and R_c values measured on rebar 17X-B

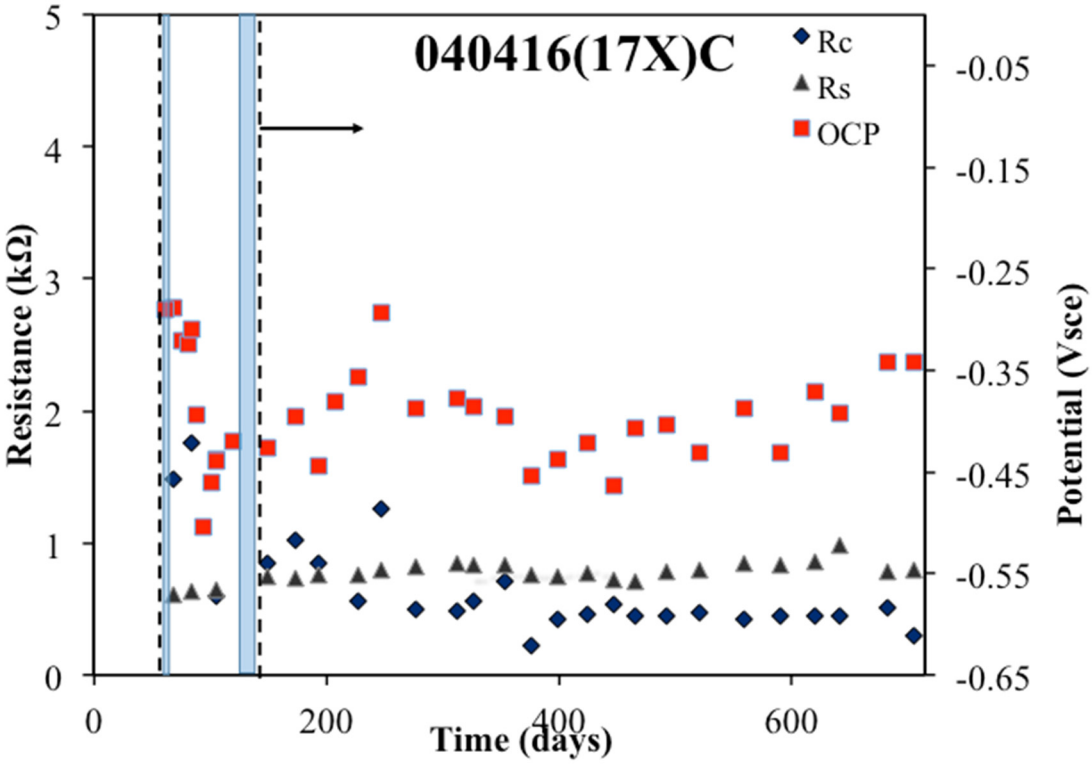

Figure 222. Rebar potentials, R_s, and R_c values measured on rebar 17X-C

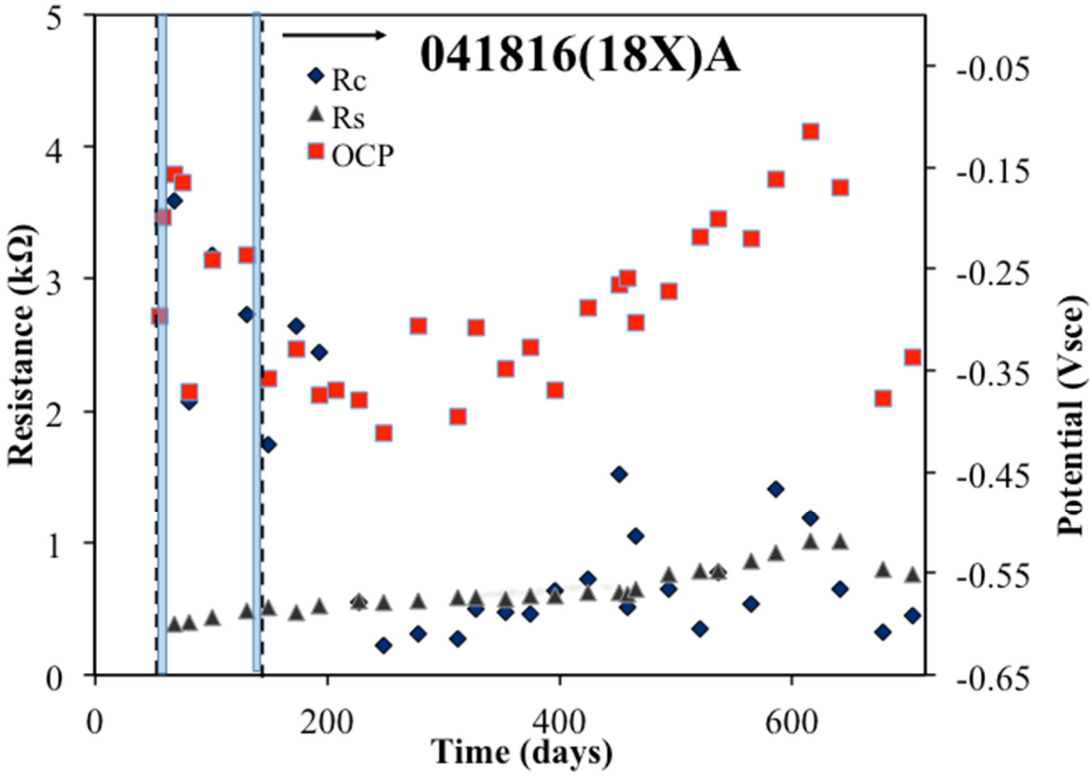

Figure 223. Rebar potentials, R_s, and R_c values measured on rebar 17X-B

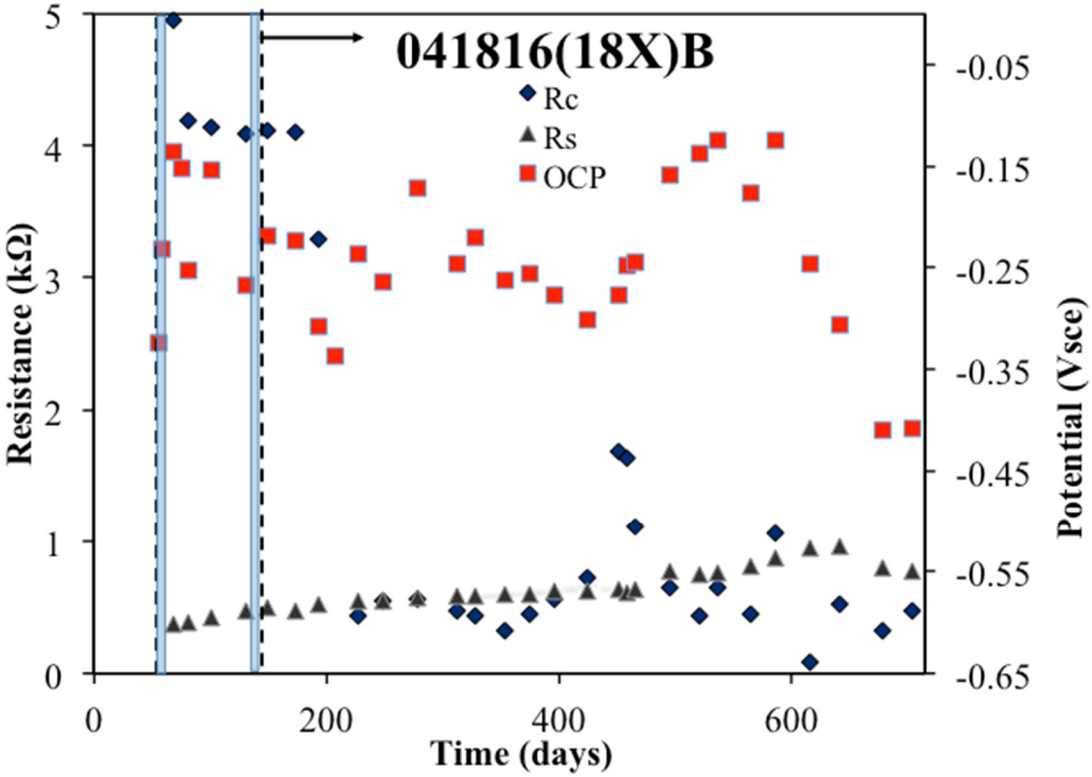

Figure 224. Rebar potentials, R_s, and R_c values measured on rebar 18X-B

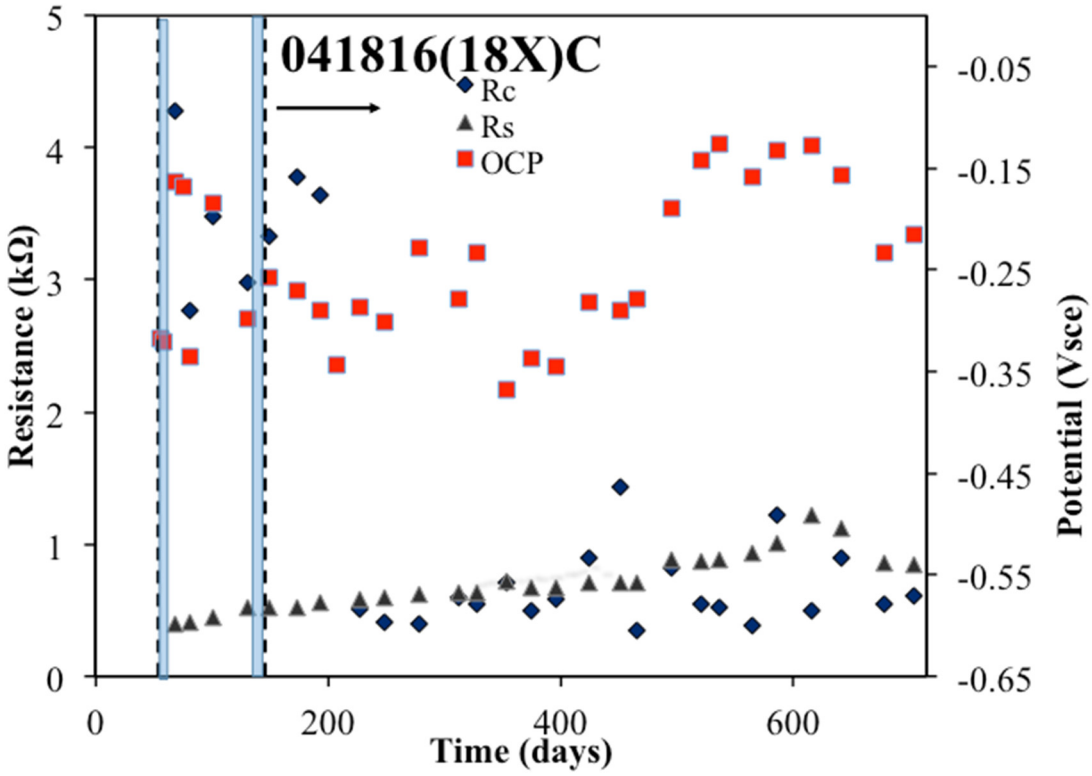

Figure 225. Rebar potentials, R_s, and R_c values measured on rebar 18X-C

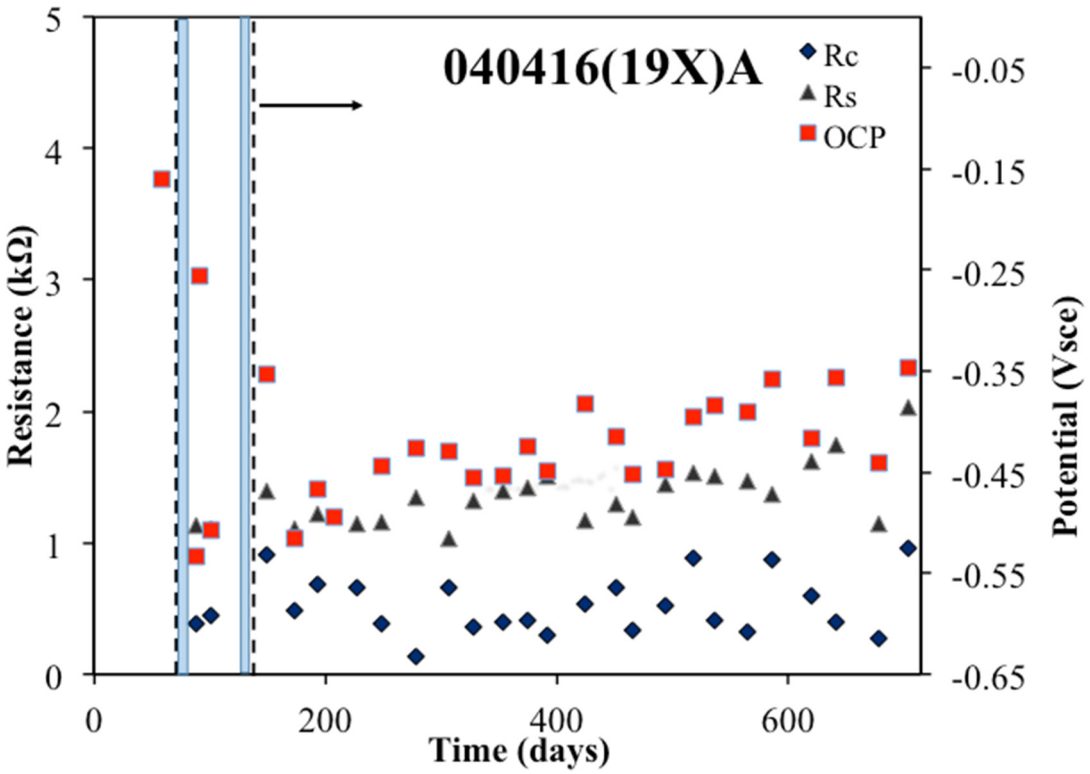

Figure 226. Rebar potentials, R_s, and R_c values measured on rebar 19X-A

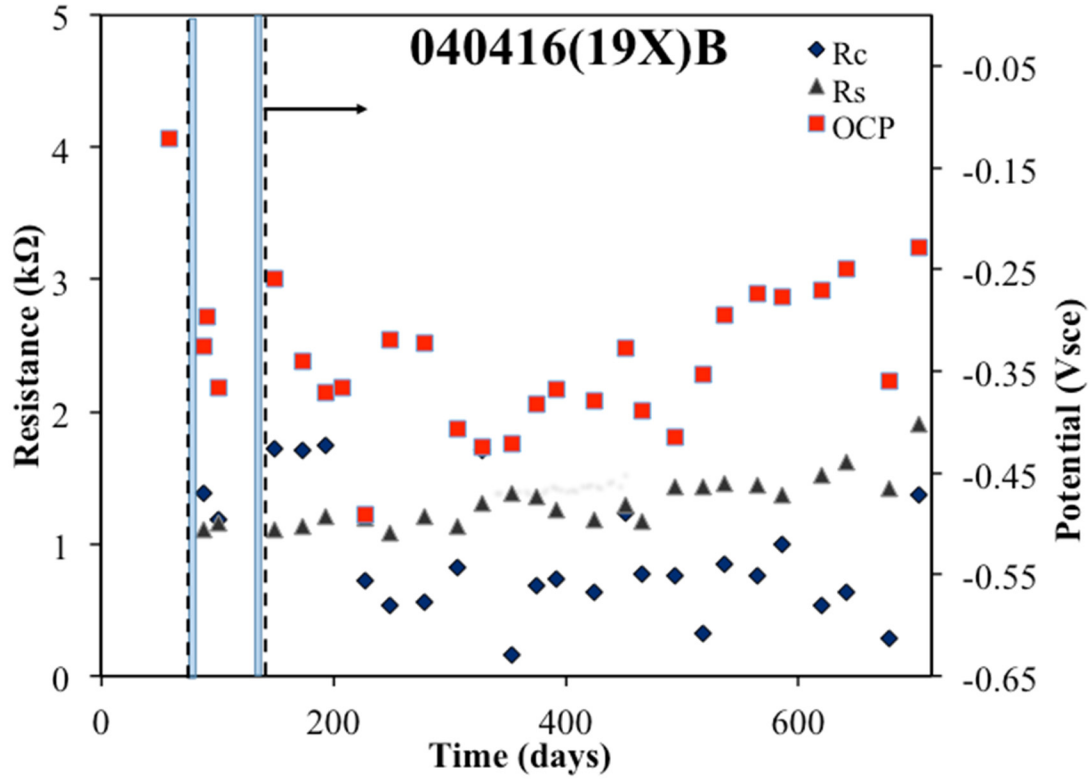

Figure 227. Rebar potentials, R_s, and R_c values measured on rebar 19X-B

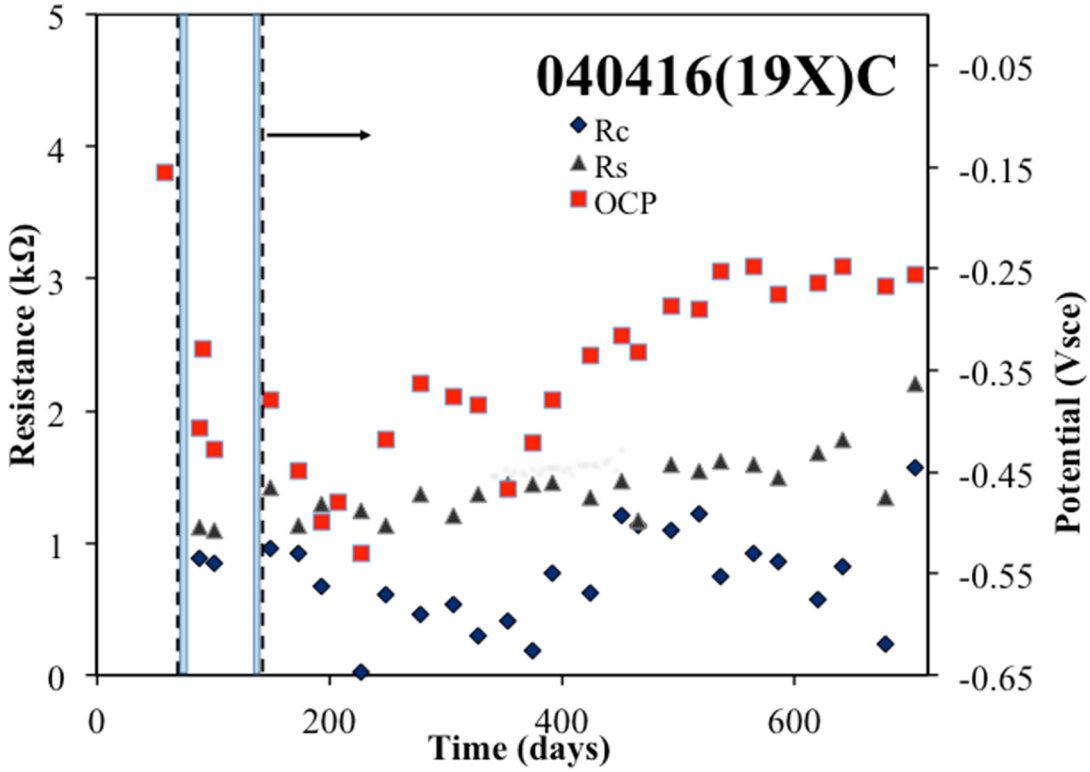

Figure 228. Rebar potentials, R_s, and R_c values measured on rebar 19X-C

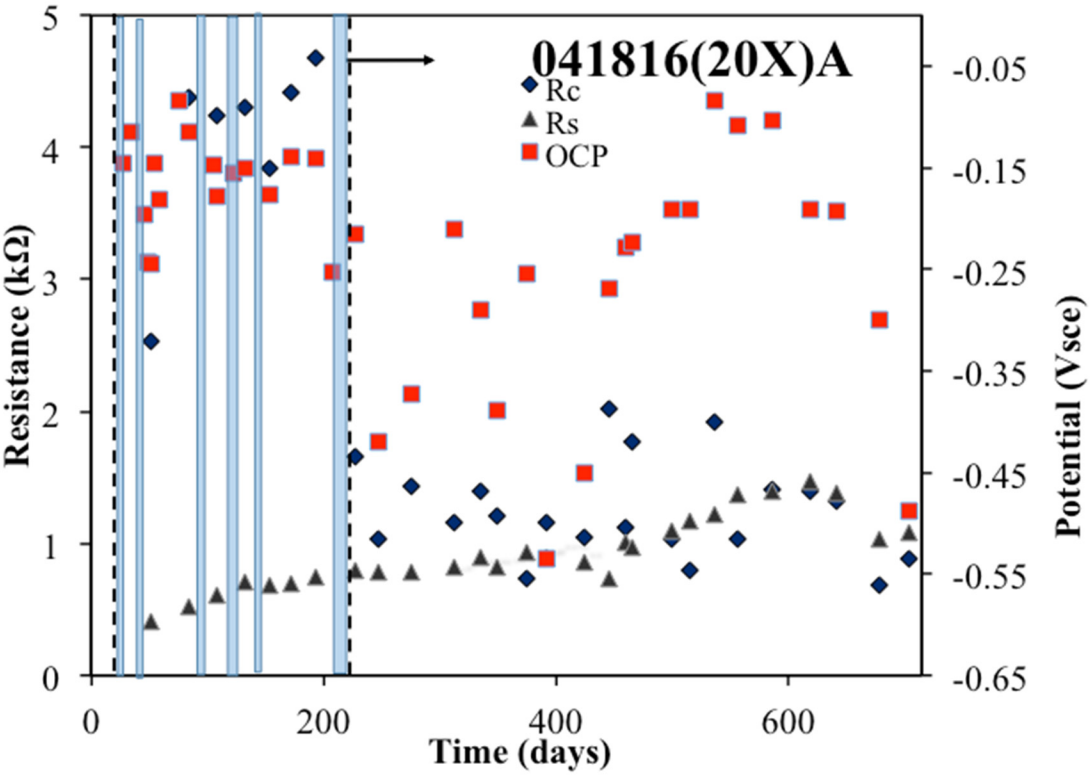

Figure 229. Rebar potentials, R_s, and R_c values measured on rebar 20X-A

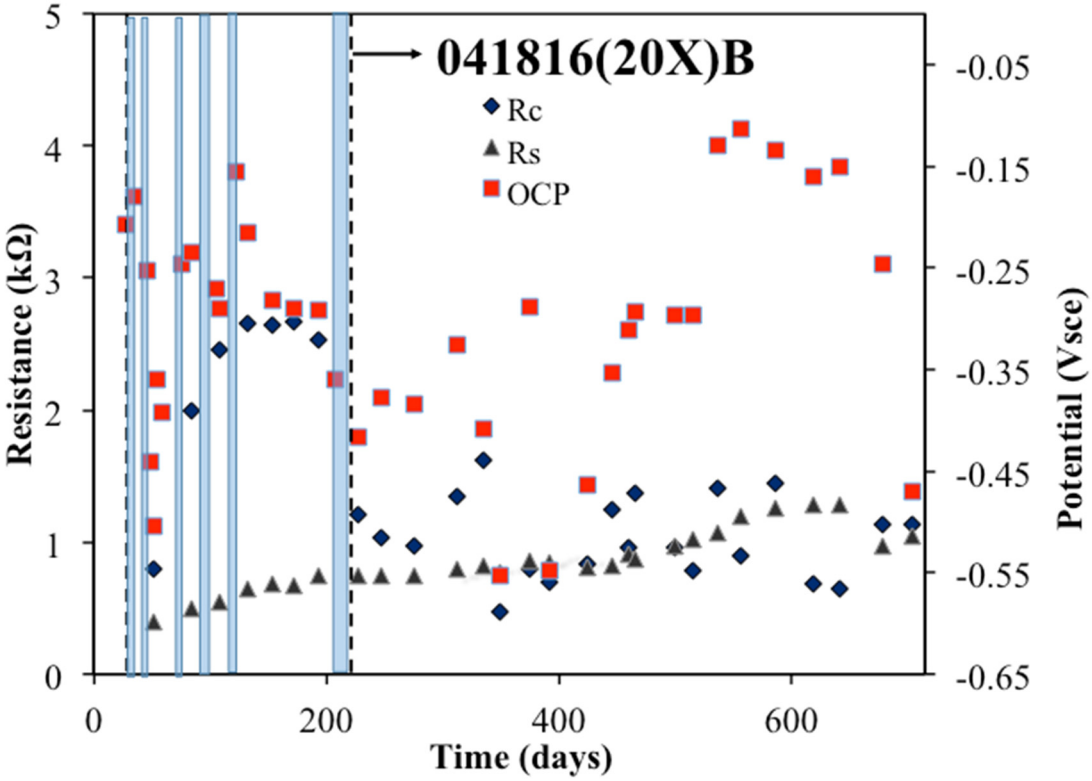

Figure 230. Rebar potentials, R_s, and R_c values measured on rebar 20X-B

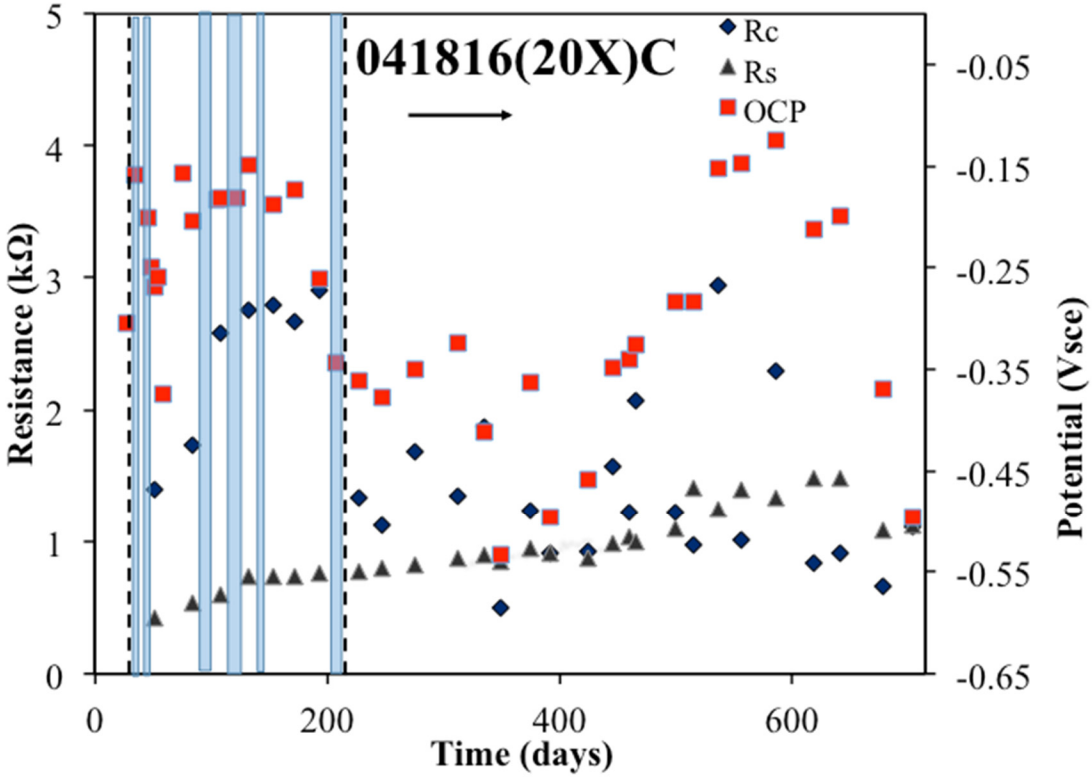

Figure 231. Rebar potentials, R_s, and R_c values measured on rebar 20X-C

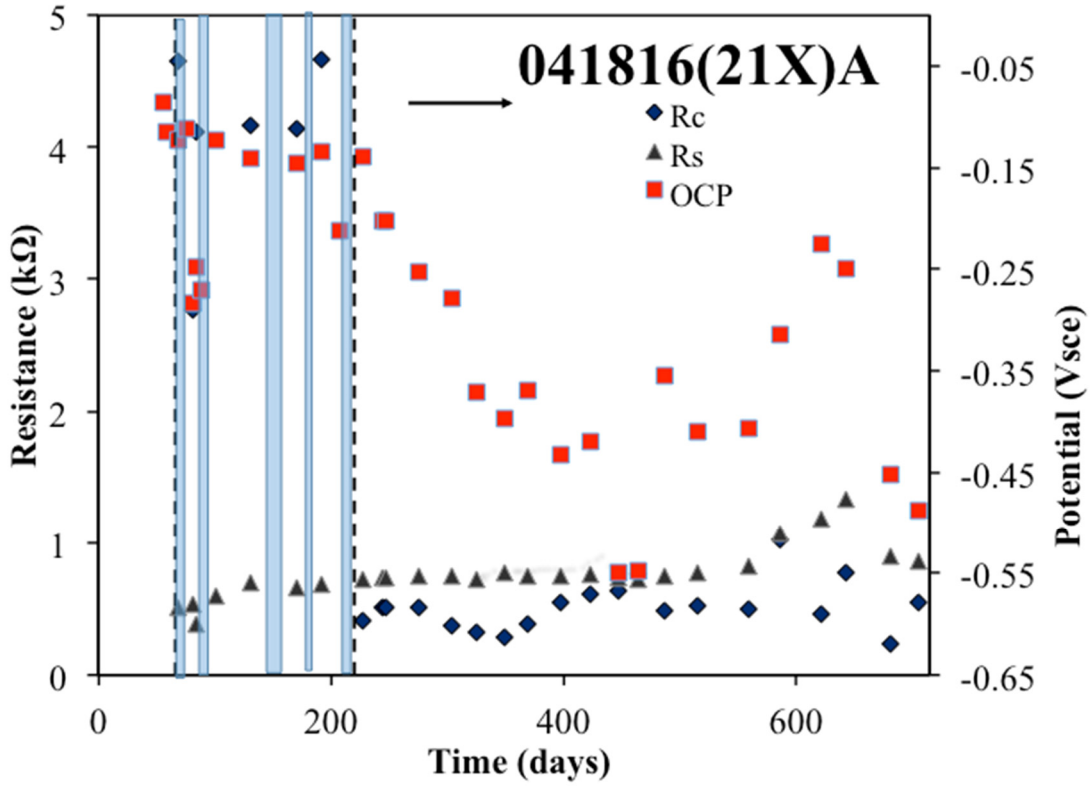

Figure 232. Rebar potentials, R_s, and R_c values measured on rebar 21X-A

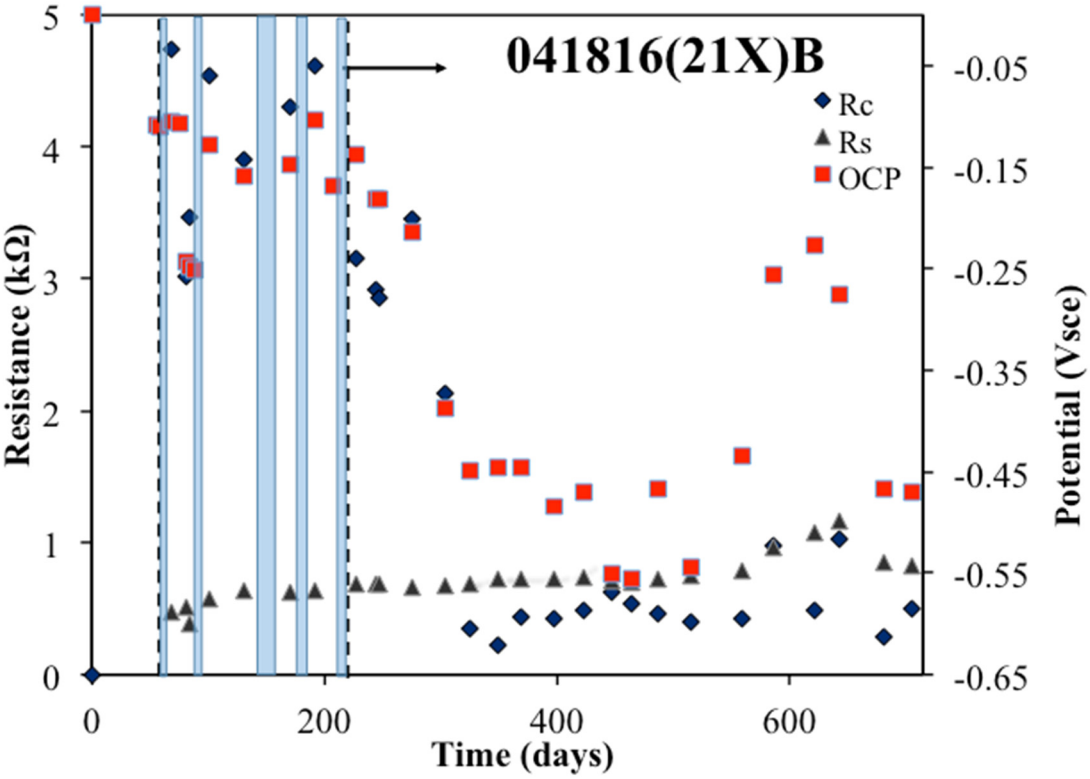

Figure 233. Rebar potentials, R_s, and R_c values measured on rebar 21X-B

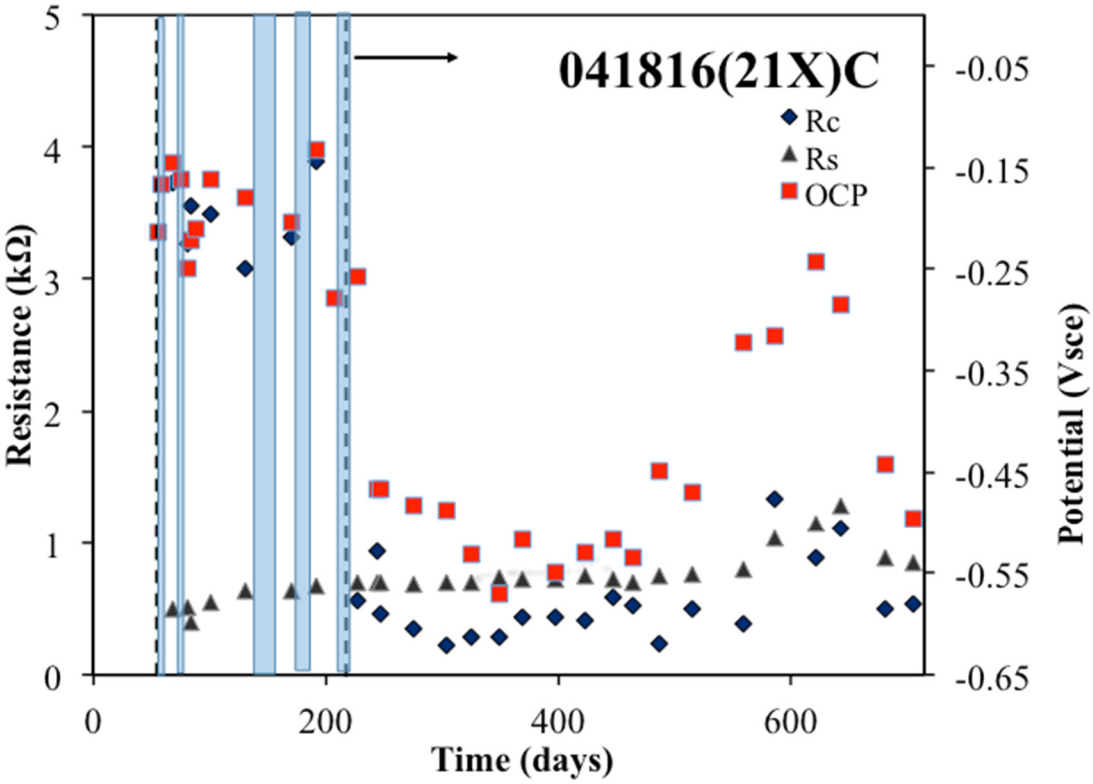

Figure 234. Rebar potentials, R_s, and R_c values measured on rebar 21X-C

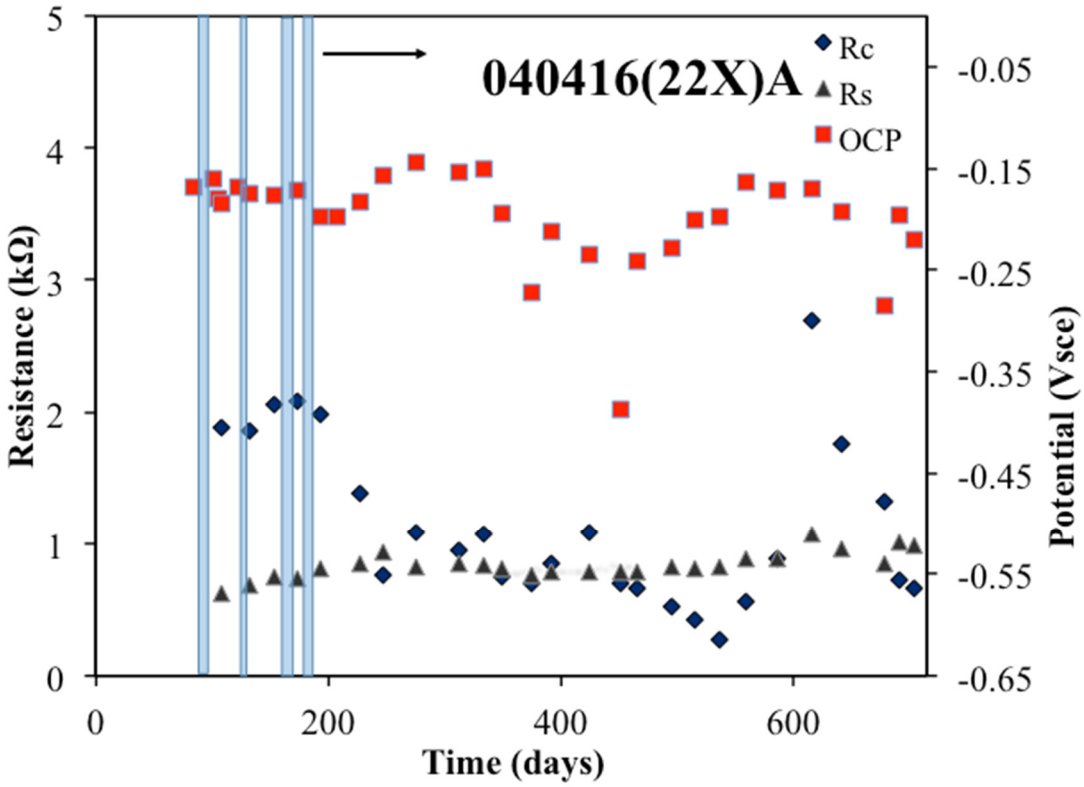

Figure 235. Rebar potentials, R_s, and R_c values measured on rebar 22X-A

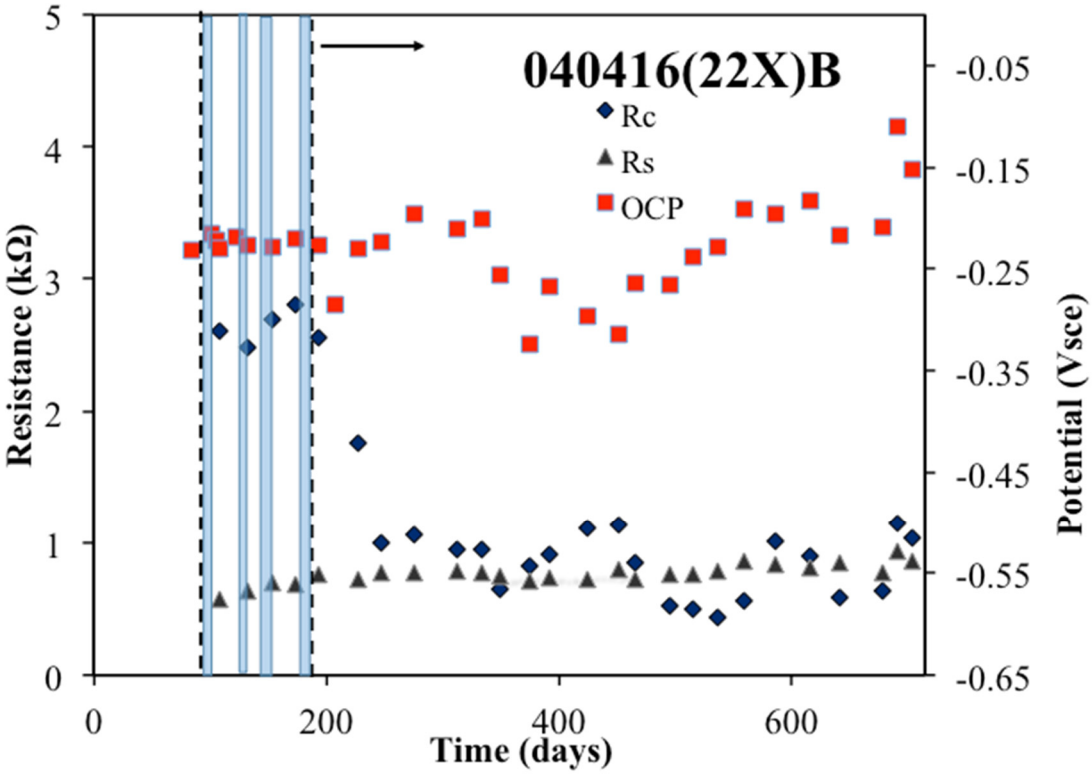

Figure 236. Rebar potentials, R_s, and R_c values measured on rebar 22X-B

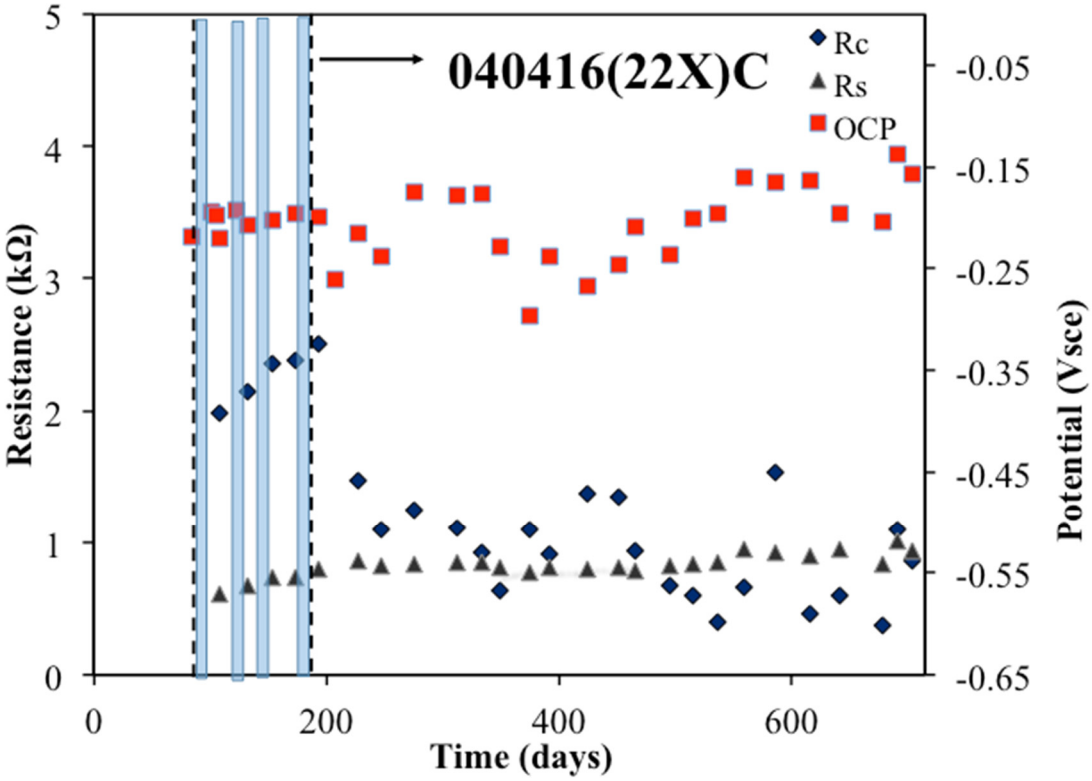

Figure 237. Rebar potentials, R_s, and R_c values measured on rebar 22X-C

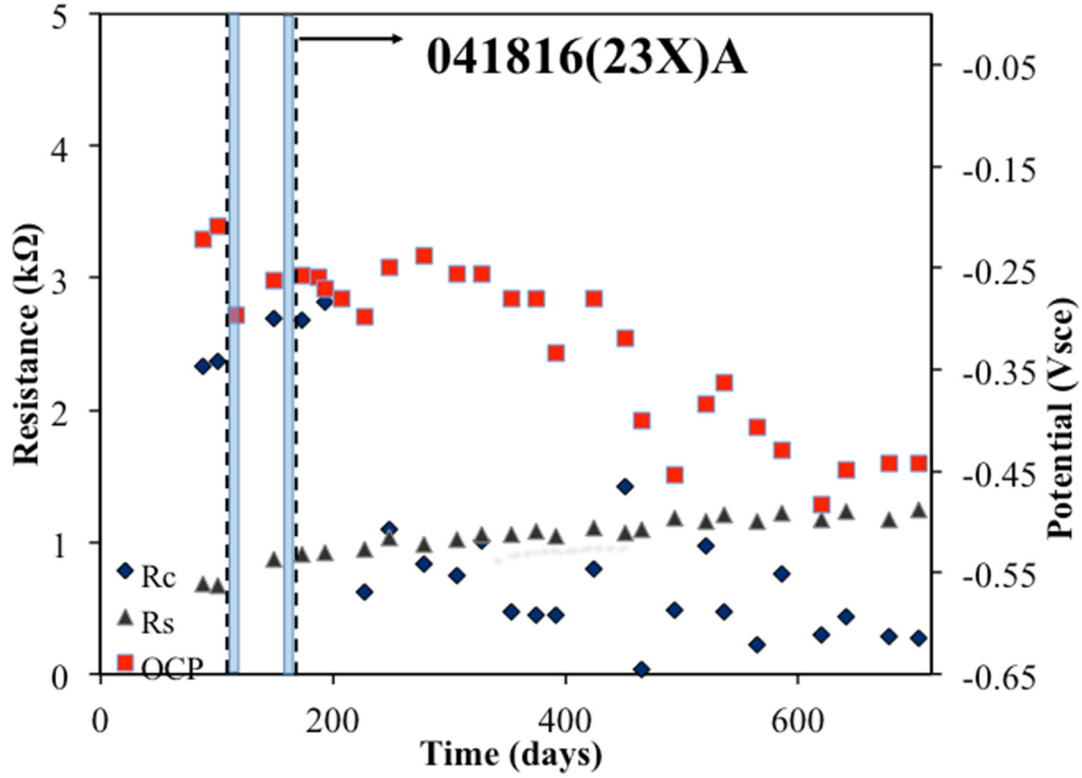

Figure 238. Rebar potentials, R_s, and R_c values measured on rebar 23X-A

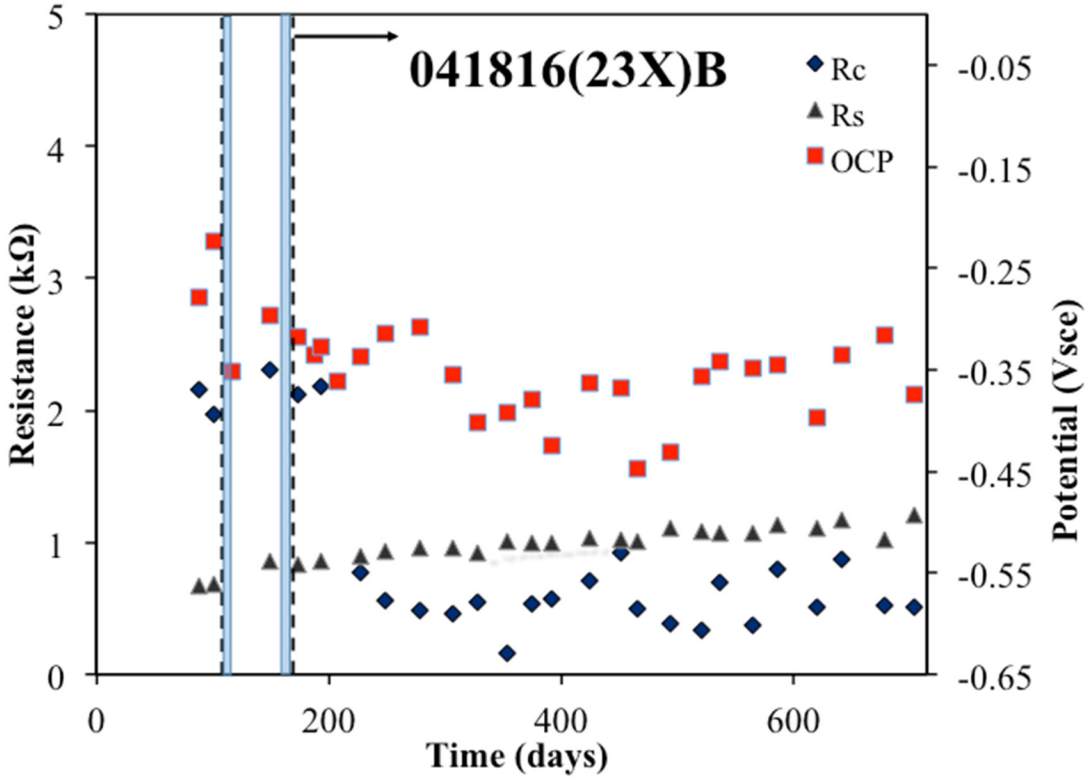

Figure 239. Rebar potentials, R_s, and R_c values measured on rebar 23X-B

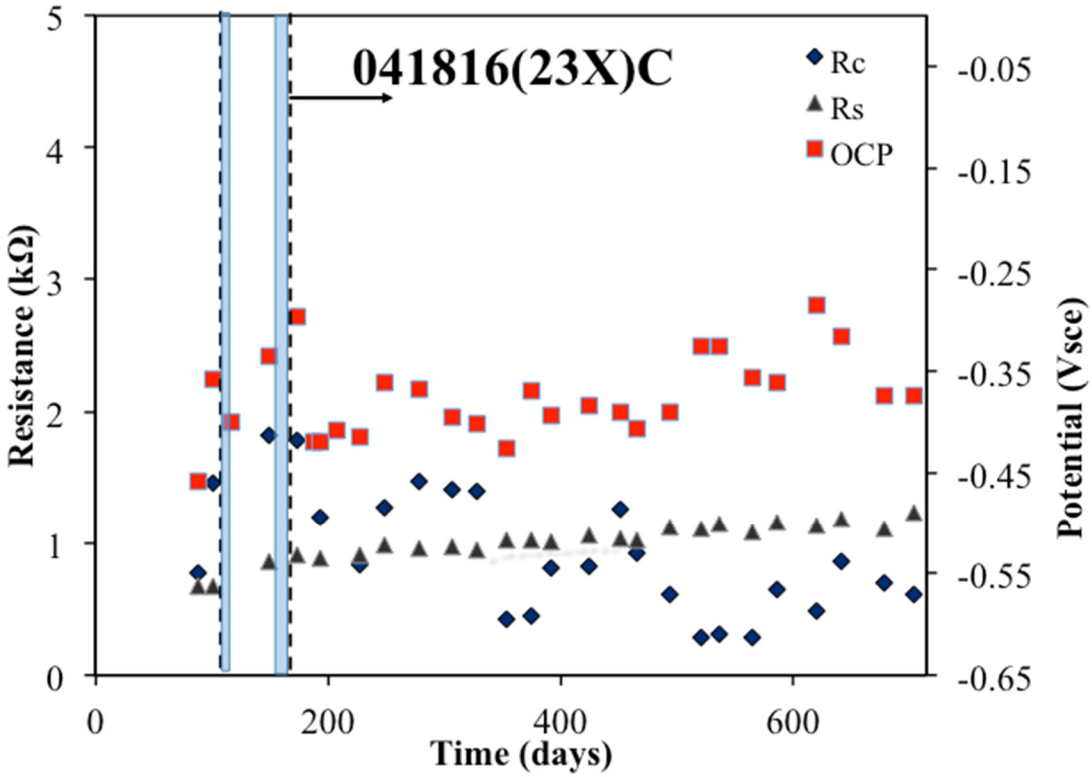

Figure 240. Rebar potentials, R_s, and R_c values measured on rebar 23X-C

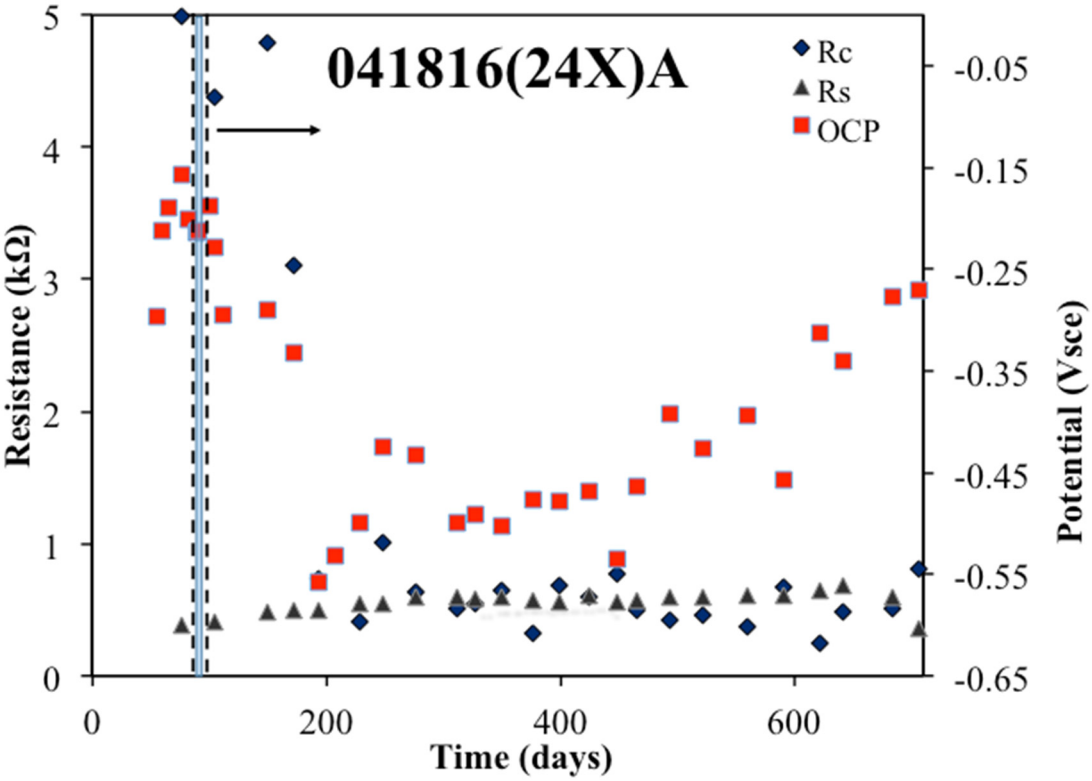

Figure 241. Rebar potentials, R_s, and R_c values measured on rebar 24X-A

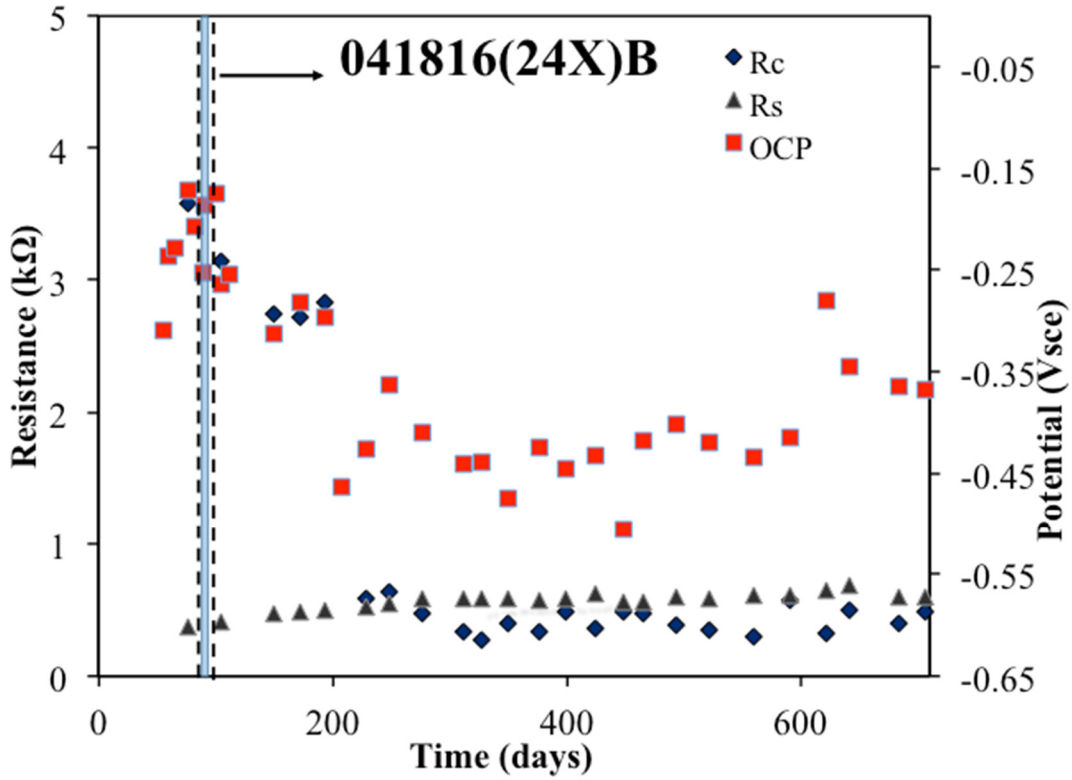

Figure 242. Rebar potentials, R_s, and R_c values measured on rebar 24X-B

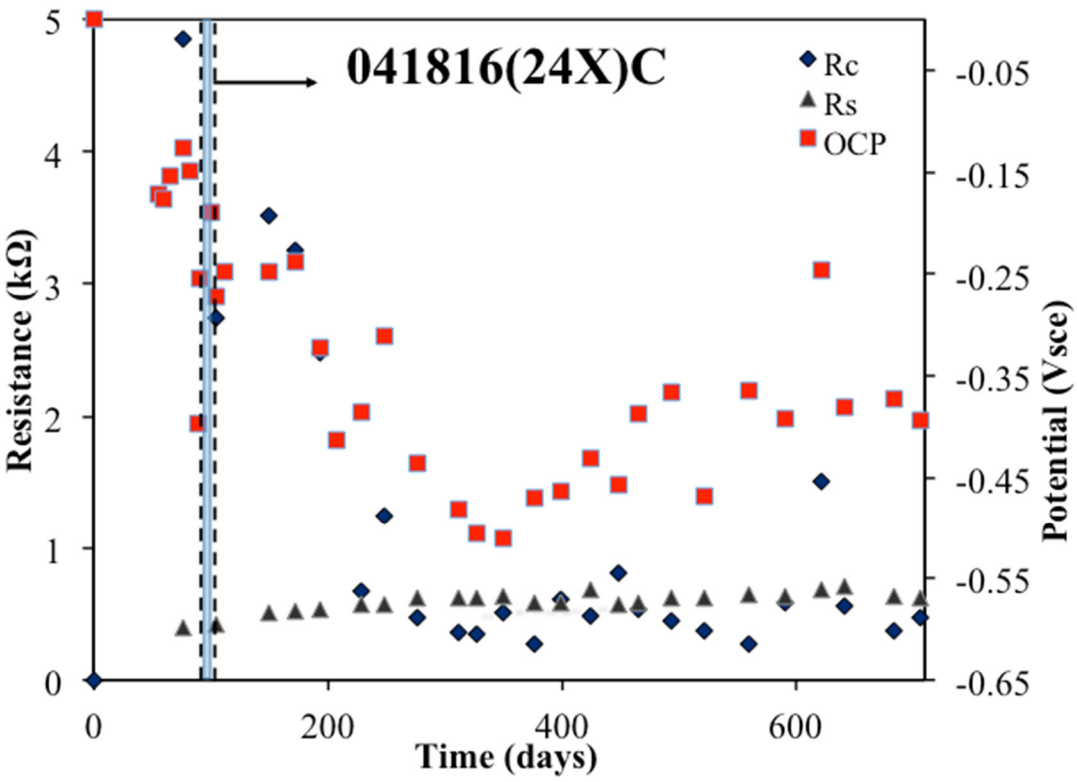

Figure 243. Rebar potentials, R_s, and R_c values measured on rebar 24X-C

Appendix G: T1 and T2 Three-rebar Samples

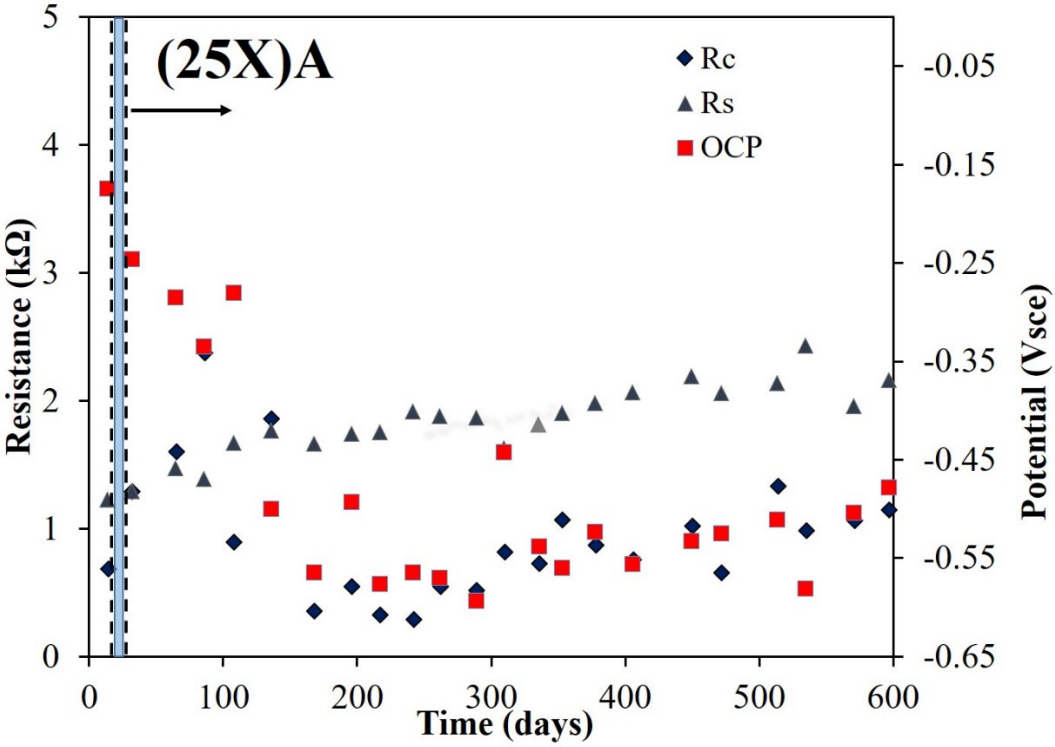

Figure 244. Rebar potentials, R_s, and R_c values measured on rebar 25X-A

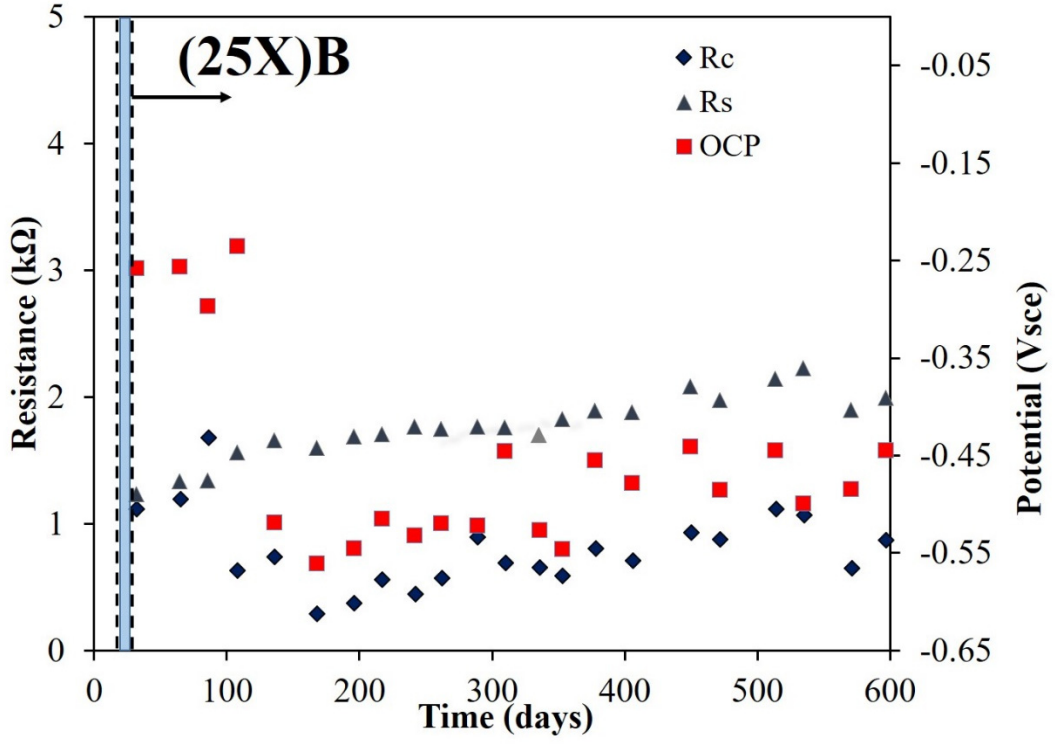

Figure 245. Rebar potentials, R_s, and R_c values measured on rebar 25X-B

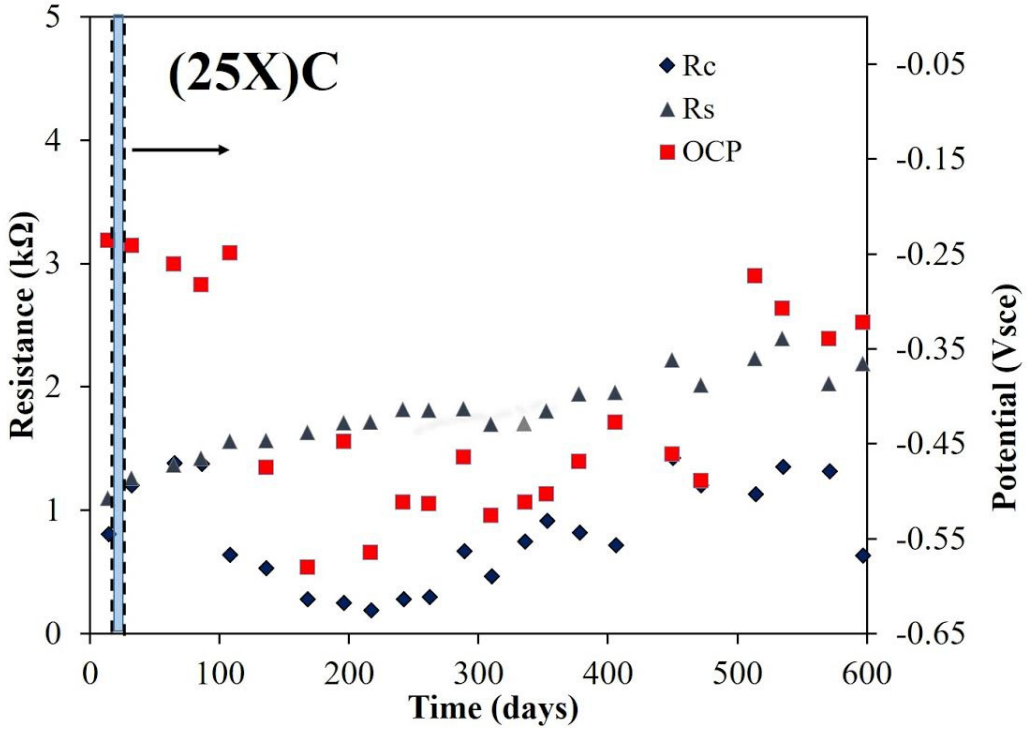

Figure 246. Rebar potentials, R_s, and R_c values measured on rebar 25X-C

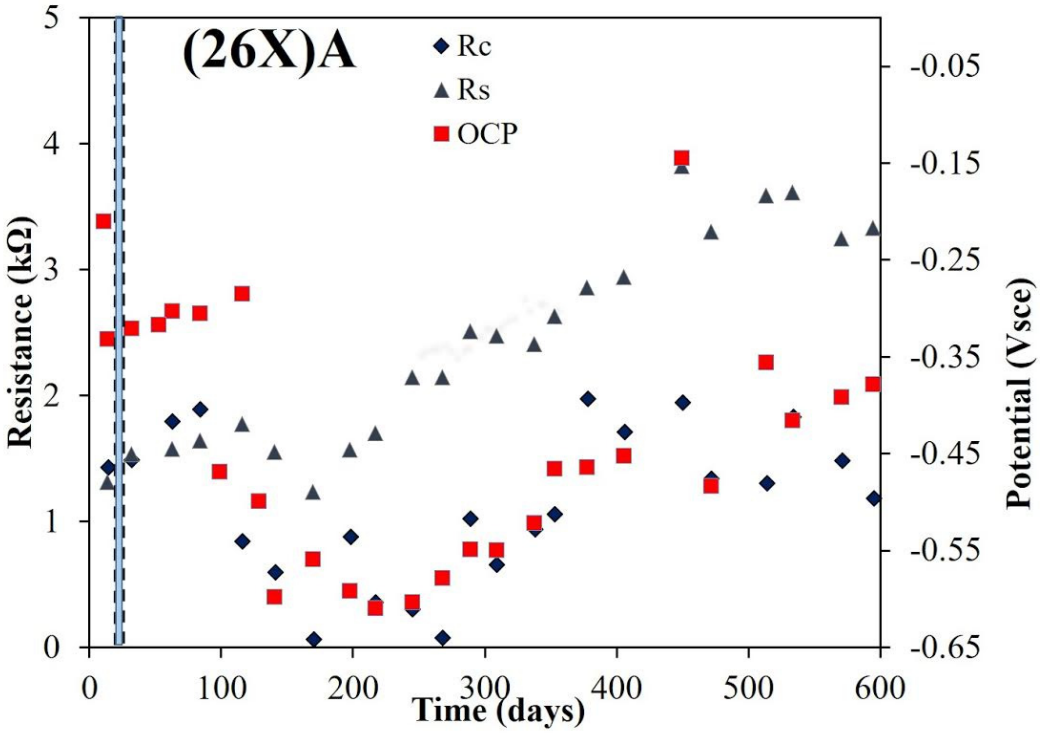

Figure 247. Rebar potentials, R_s, and R_c values measured on rebar 26X-A

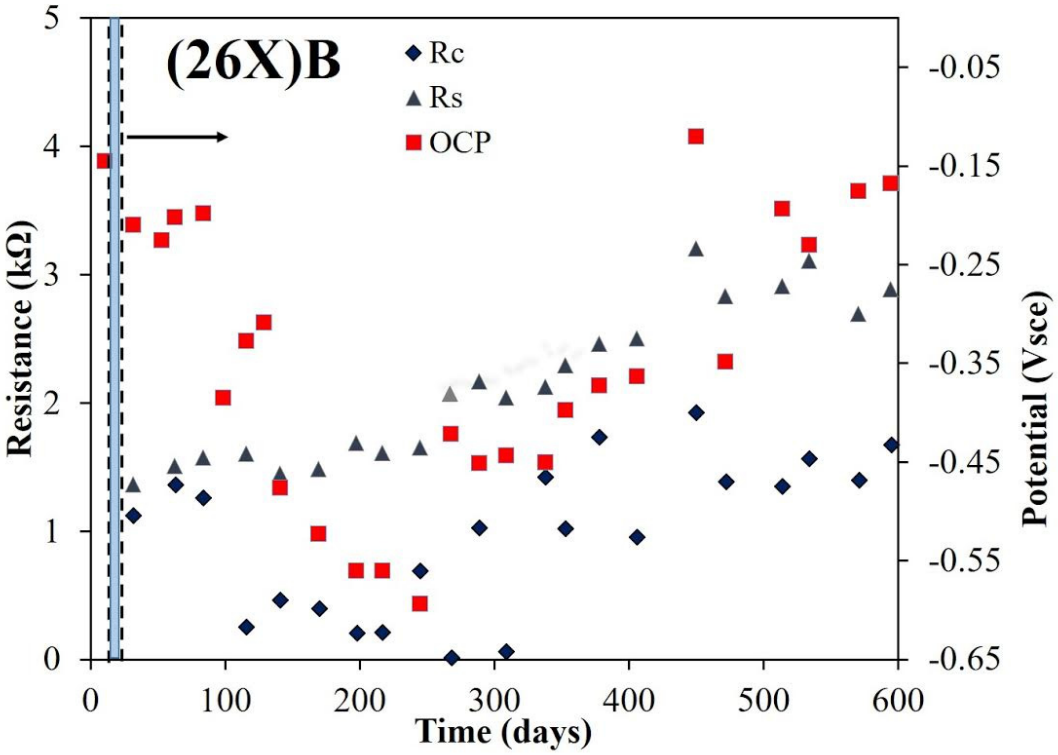

Figure 248. Rebar potentials, R_s, and R_c values measured on rebar 26X-B

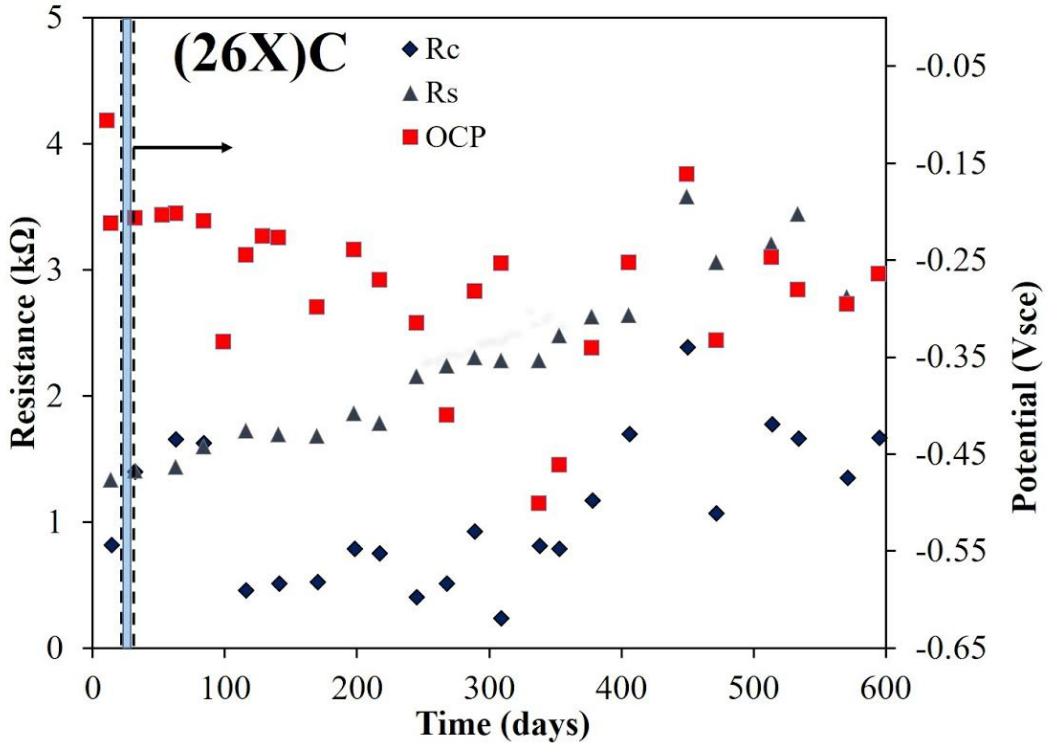

Figure 249. Rebar potentials, R_s, and R_c values measured on rebar 26X-C

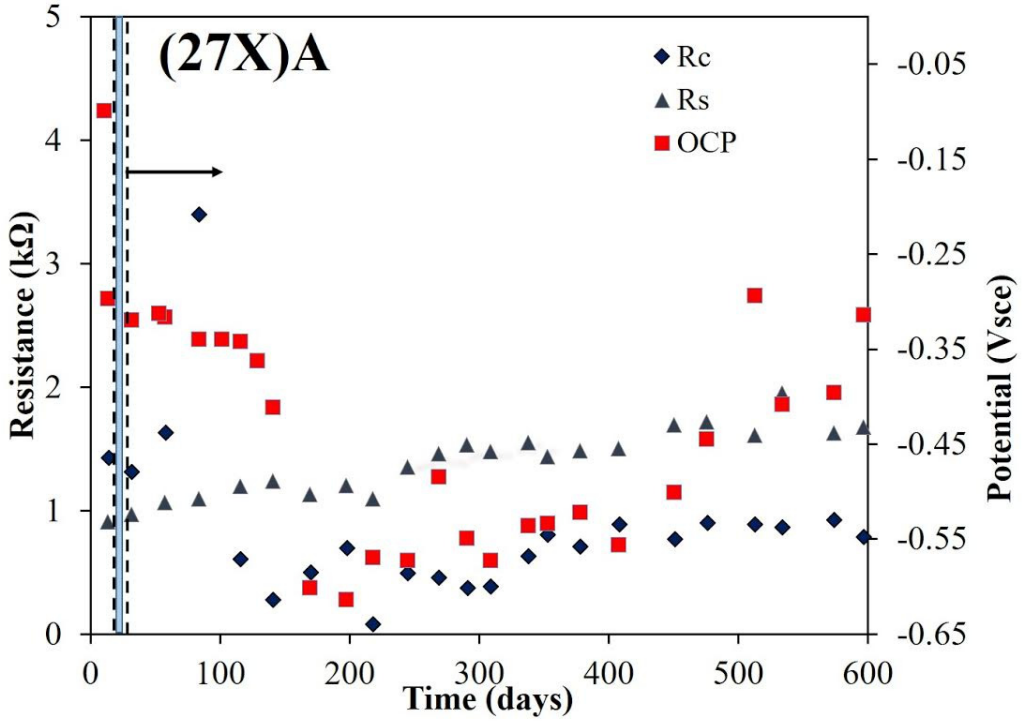

Figure 250. Rebar potentials, R_s, and R_c values measured on rebar 27X-A

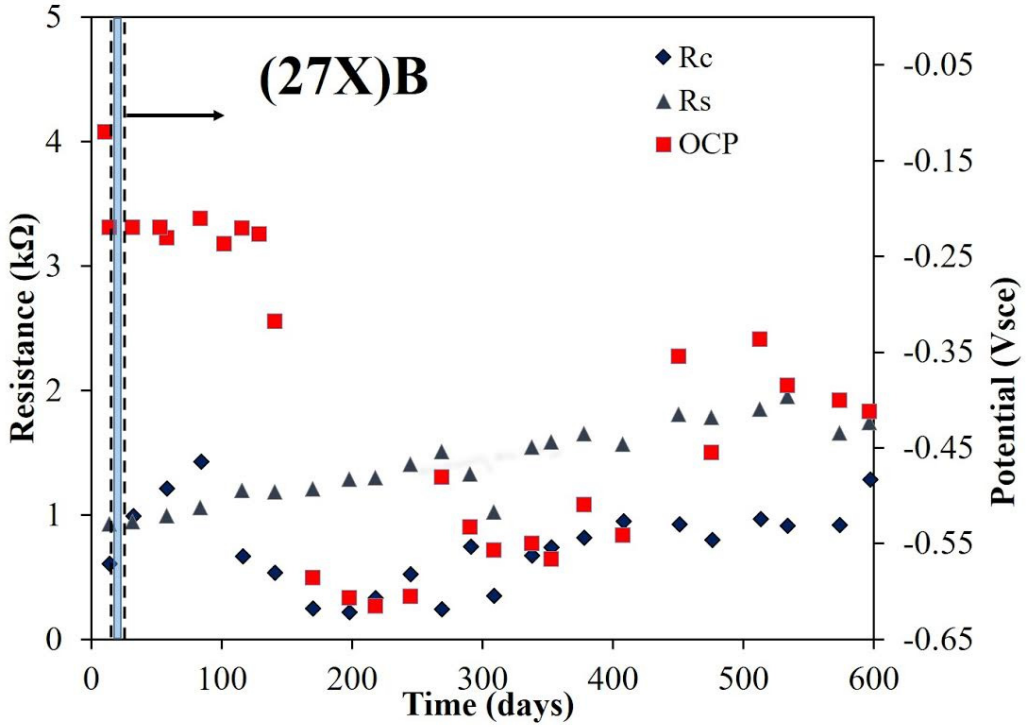

Figure 251. Rebar potentials, R_s, and R_c values measured on rebar 27X-B

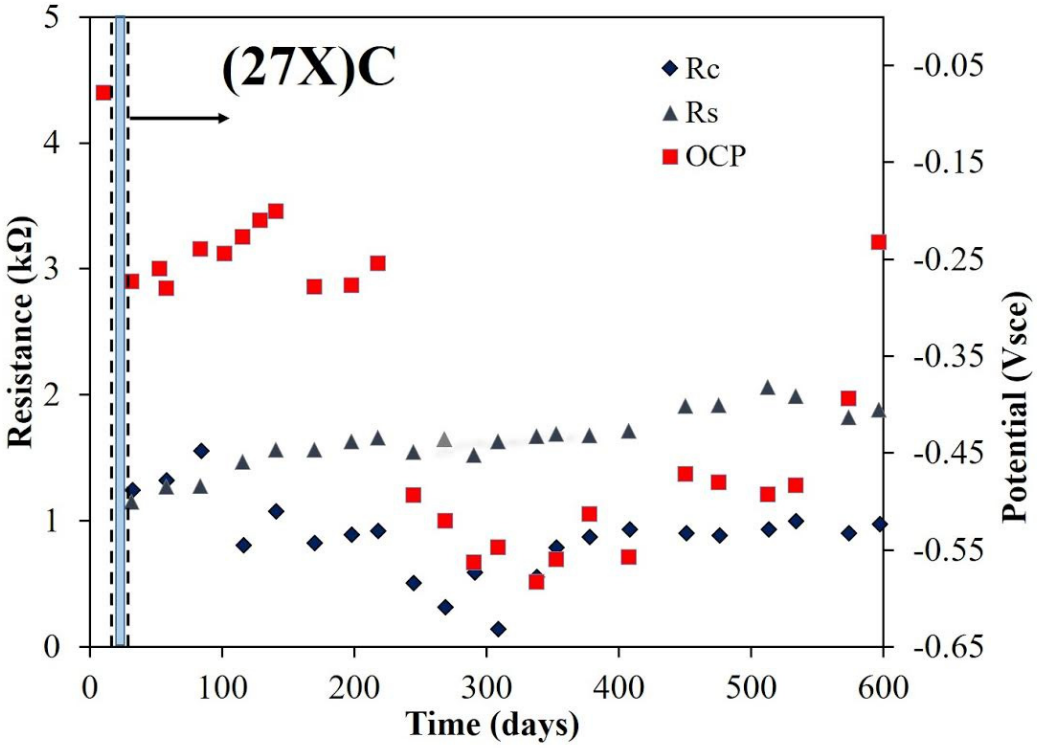

Figure 252. Rebar potentials, R_s, and R_c values measured on rebar 27X-C

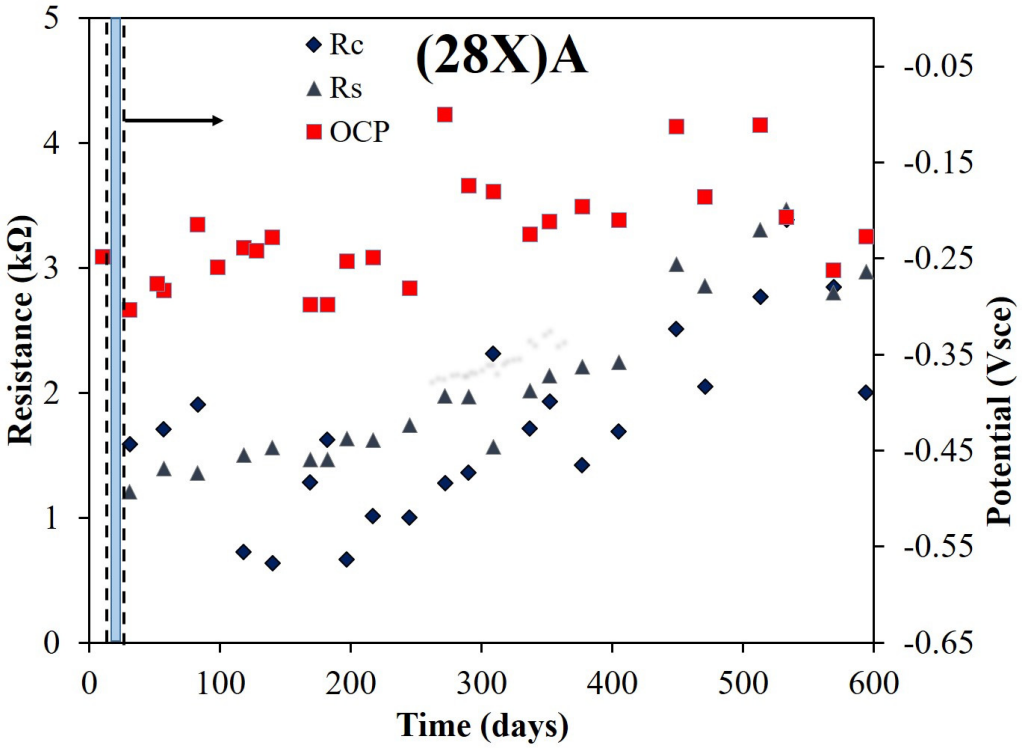

Figure 253. Rebar potentials, R_s, and R_c values measured on rebar 28X-A

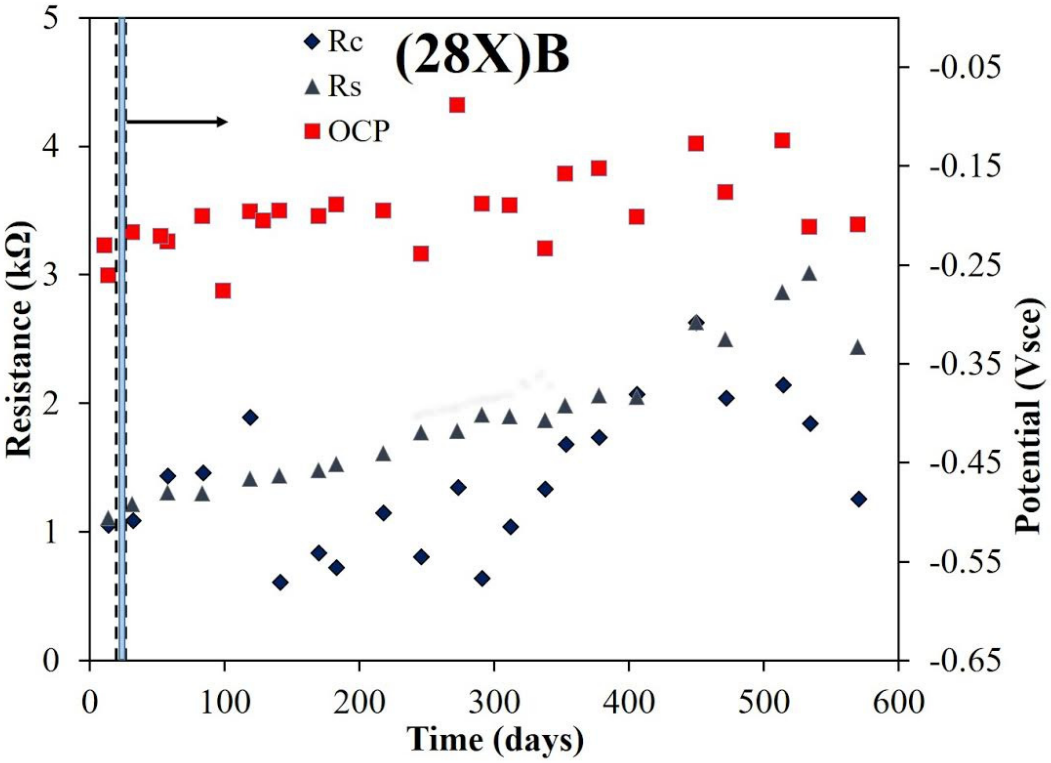

Figure 254. Rebar potentials, R_s, and R_c values measured on rebar 28X-B

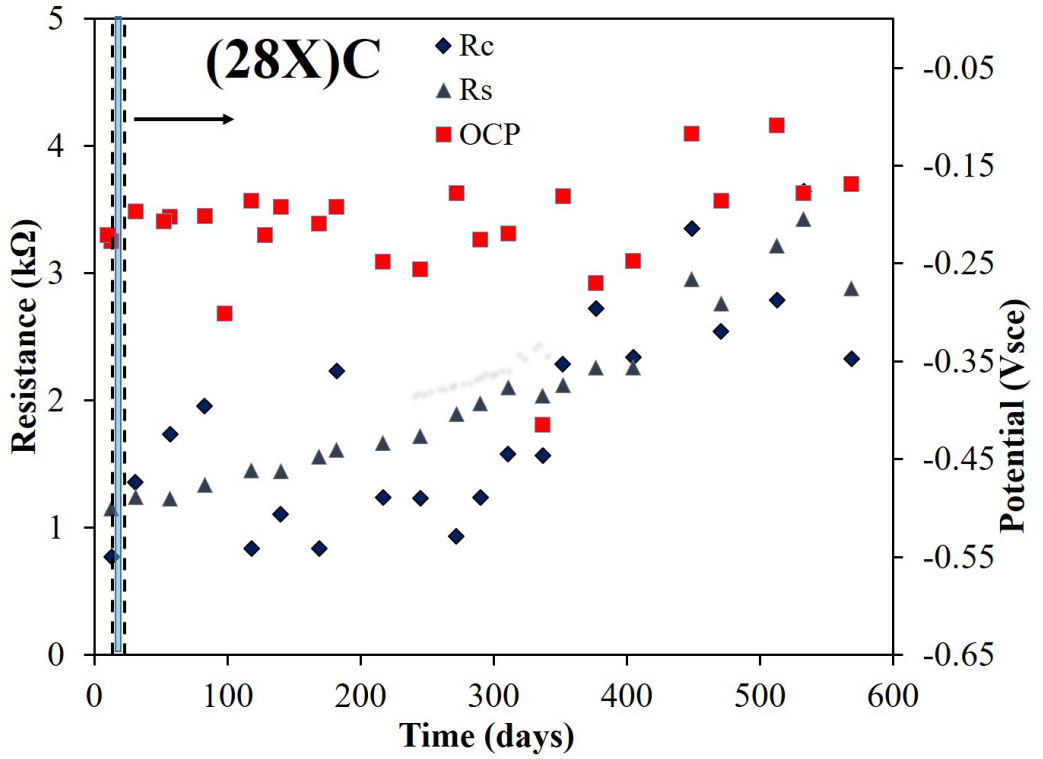

Figure 255. Rebar potentials, R_s, and R_c values measured on rebar 28X-C

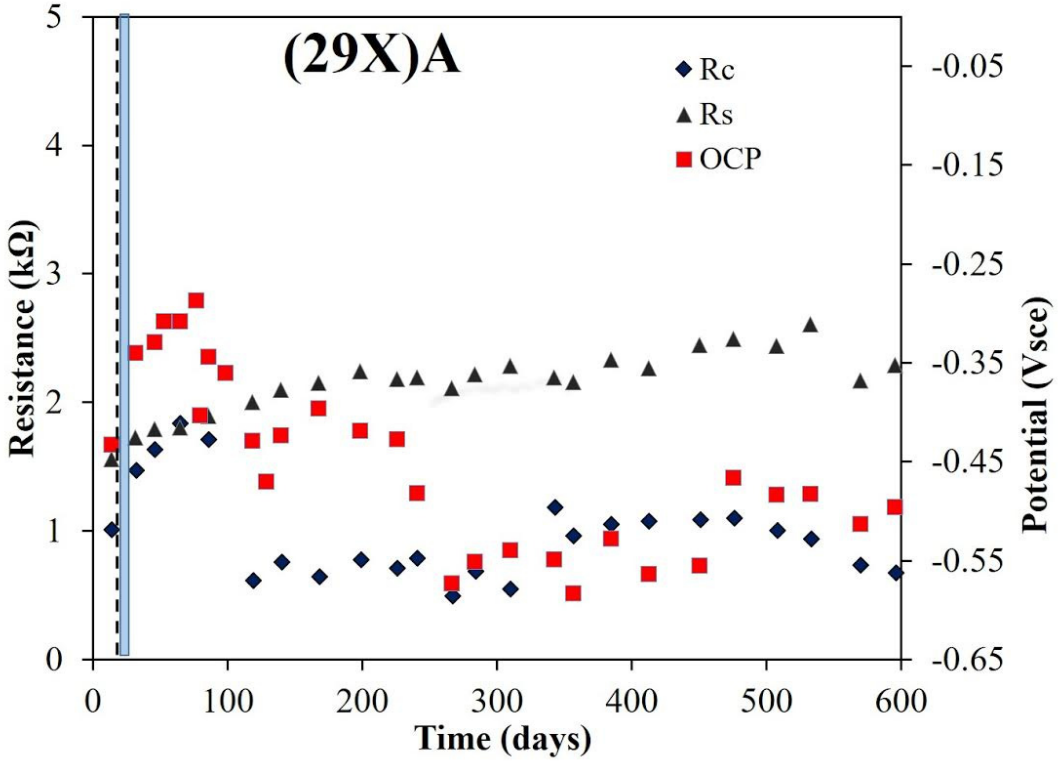

Figure 256. Rebar potentials, R_s, and R_c values measured on rebar 29X-A

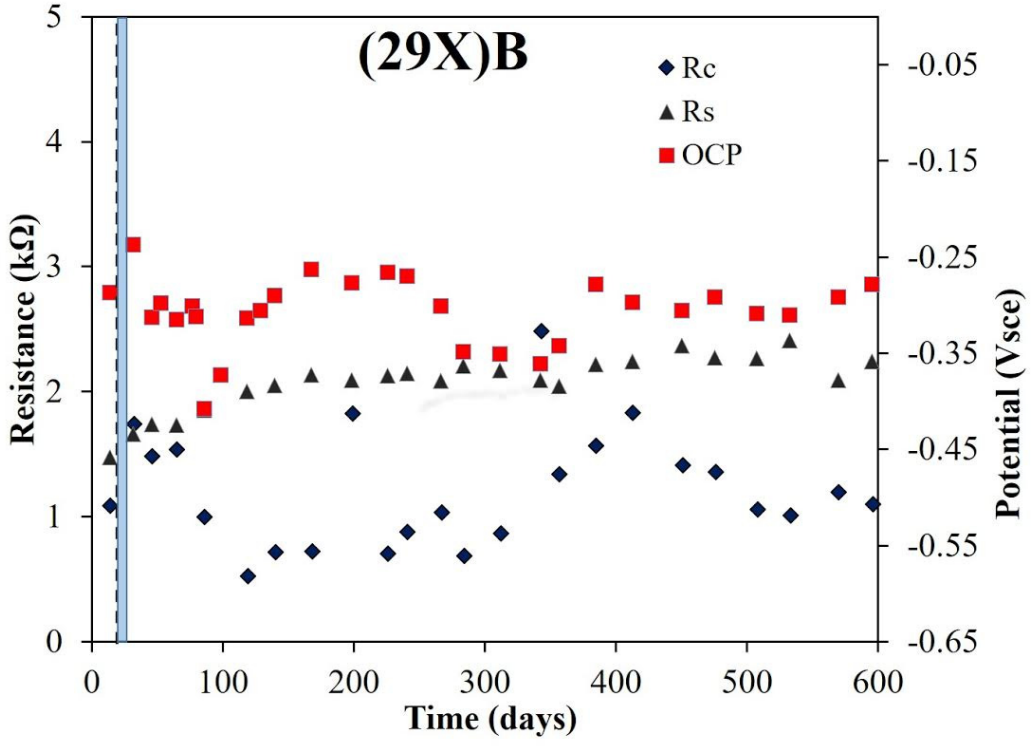

Figure 257. Rebar potentials, R_s, and R_c values measured on rebar 29X-B

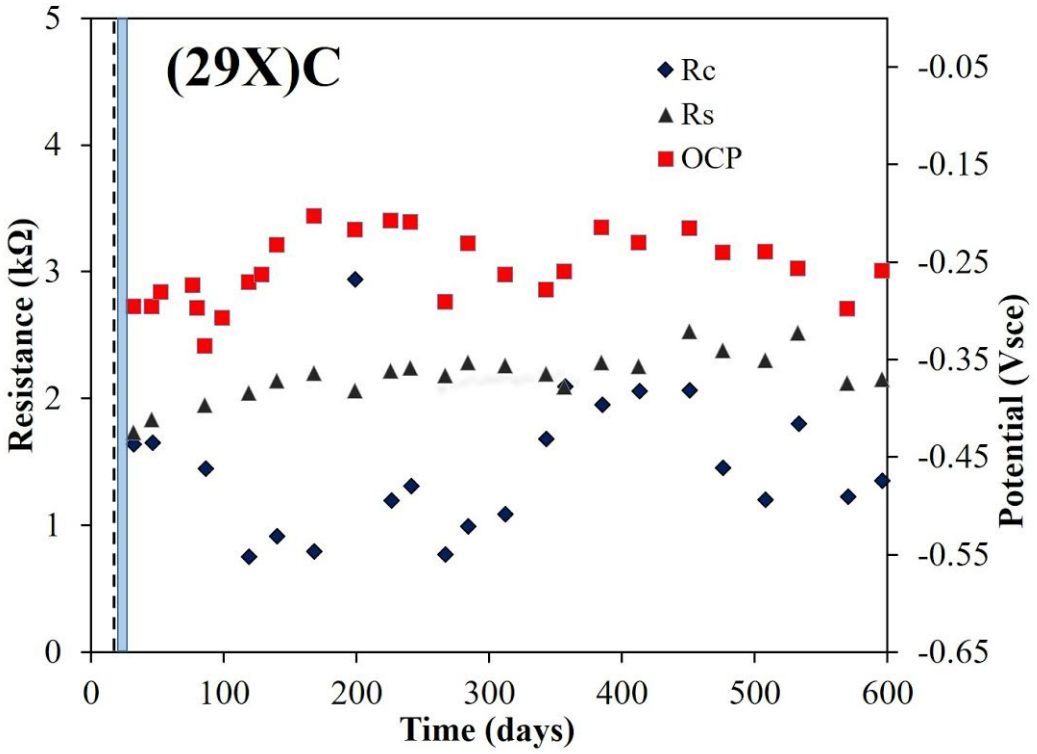

Figure 258. Rebar potentials, R_s, and R_c values measured on rebar 29X-C

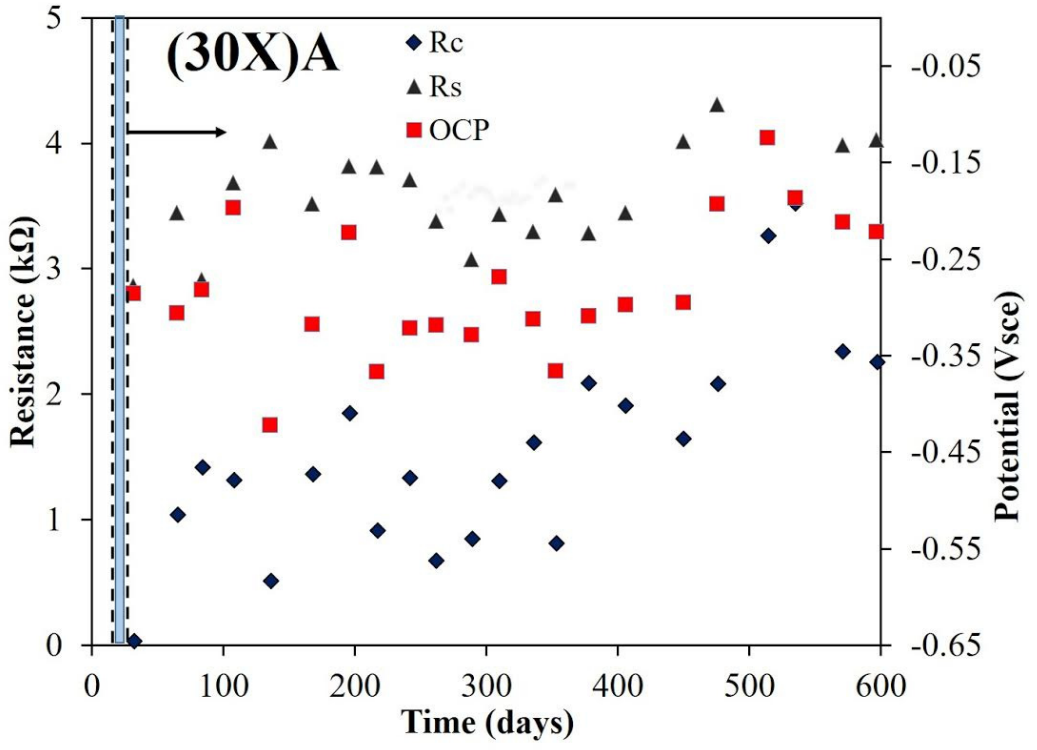

Figure 259. Rebar potentials, R_s, and R_c values measured on rebar 30X-A

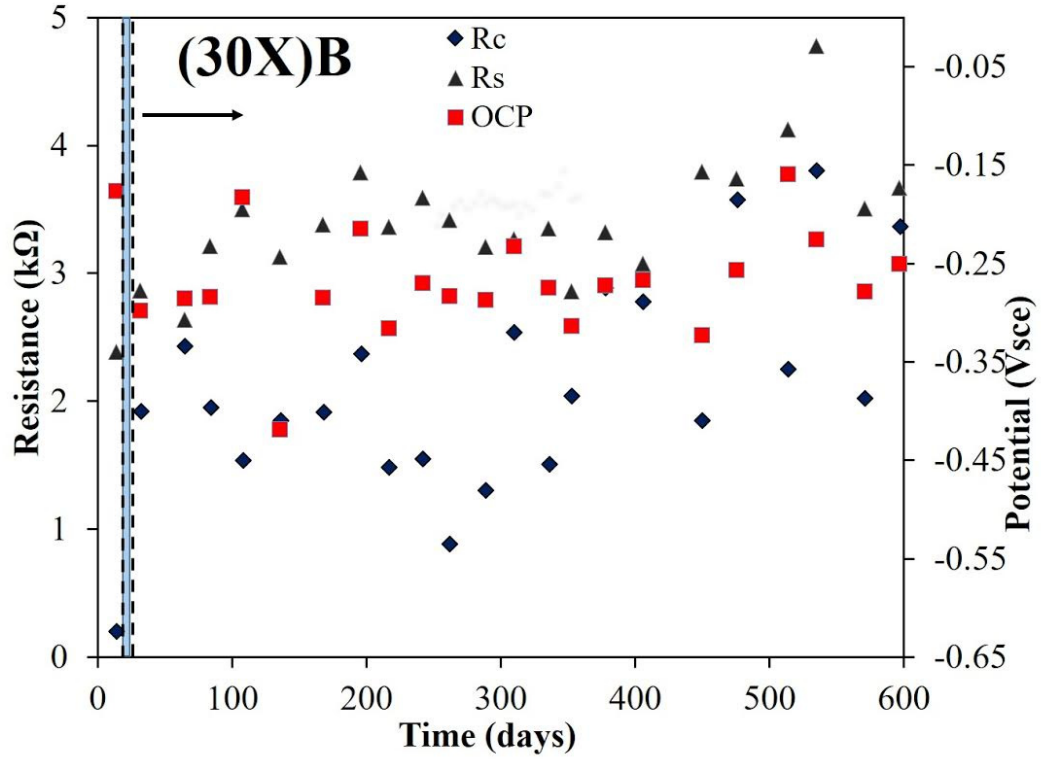

Figure 260. Rebar potentials, R_s, and R_c values measured on rebar 30X-B

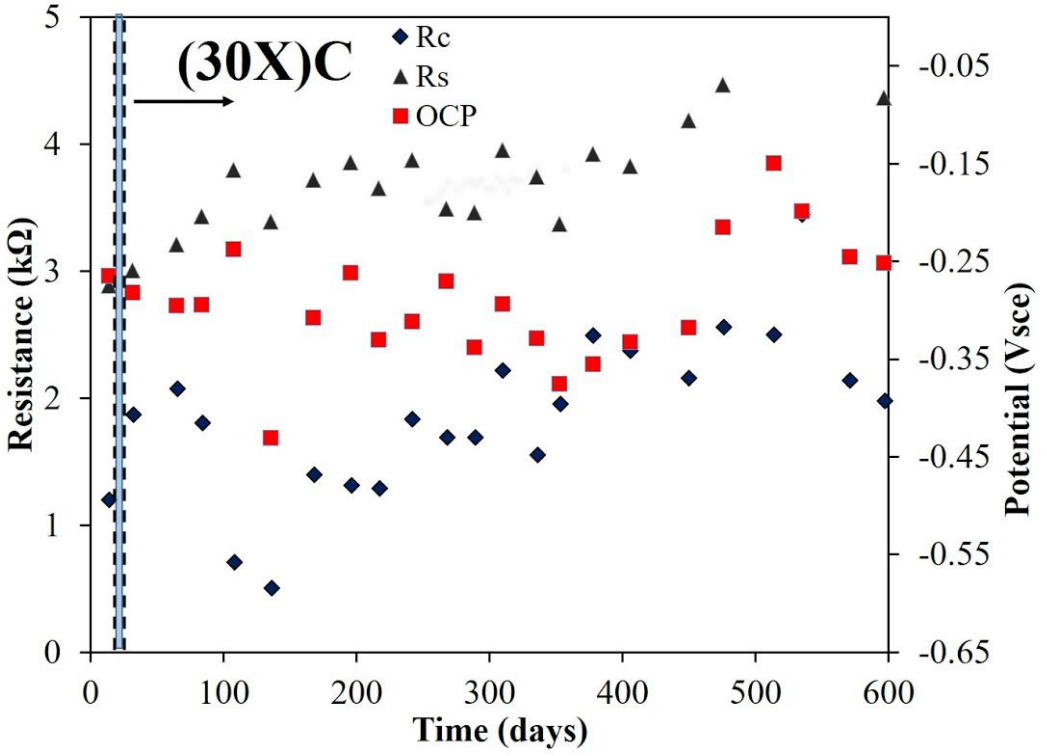

Figure 261. Rebar potentials, R_s, and R_c values measured on rebar 30X-C

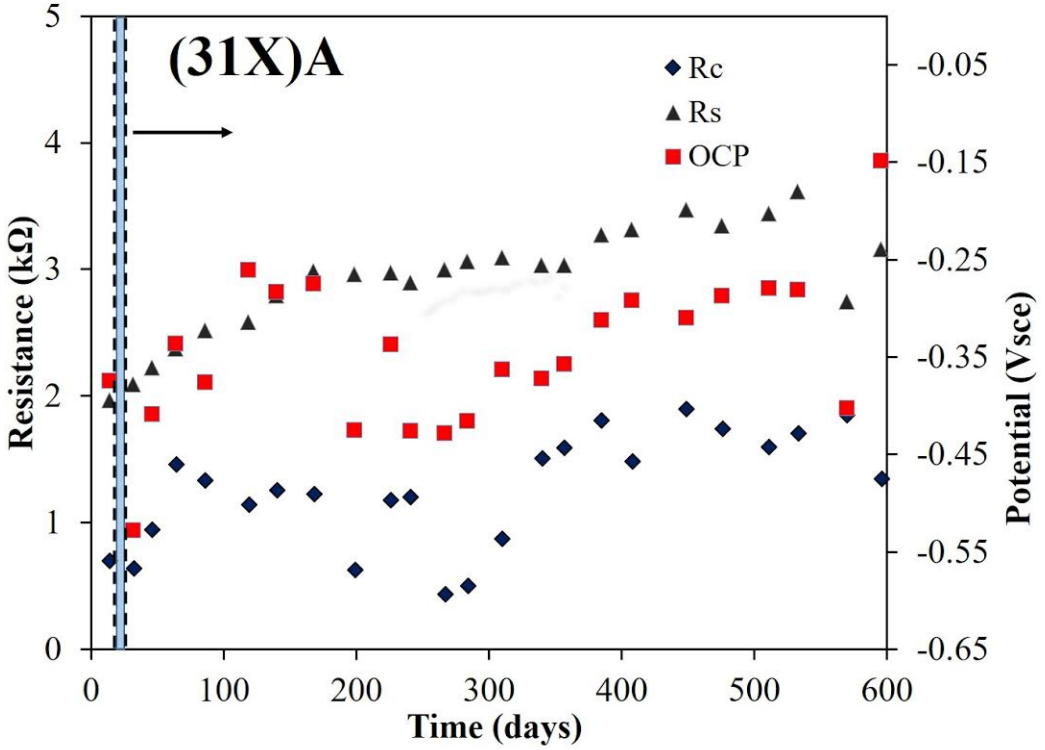

Figure 262. Rebar potentials, R_s, and R_c values measured on rebar 31X-A

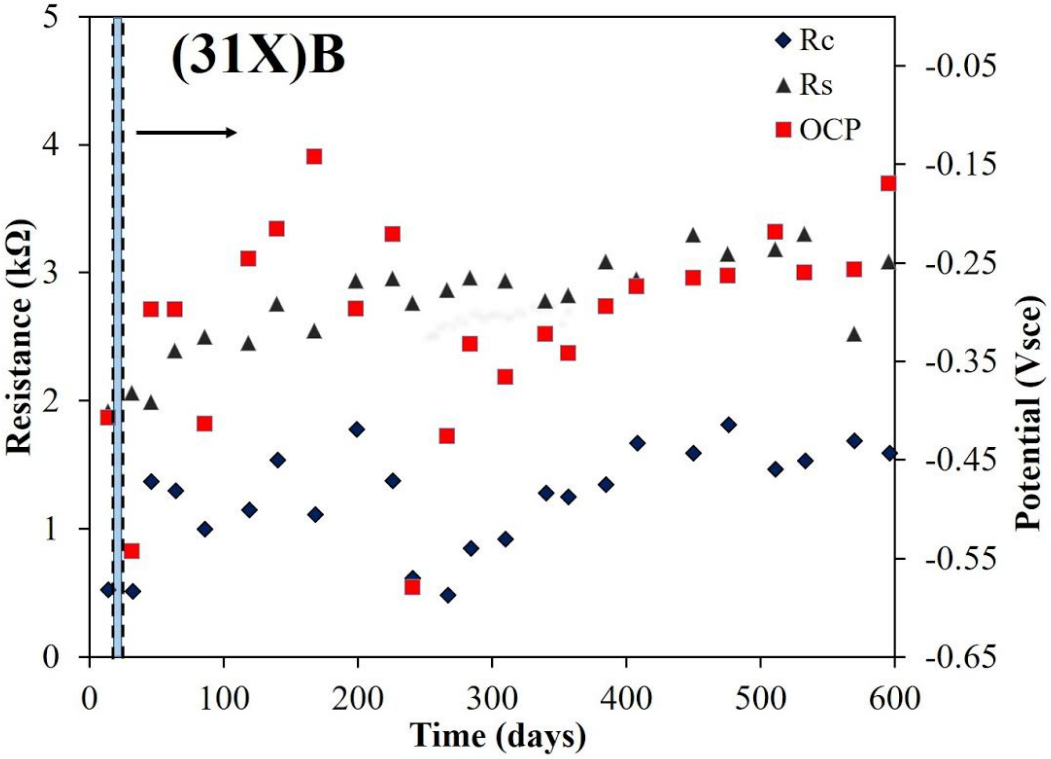

Figure 263. Rebar potentials, R_s, and R_c values measured on rebar 31X-B

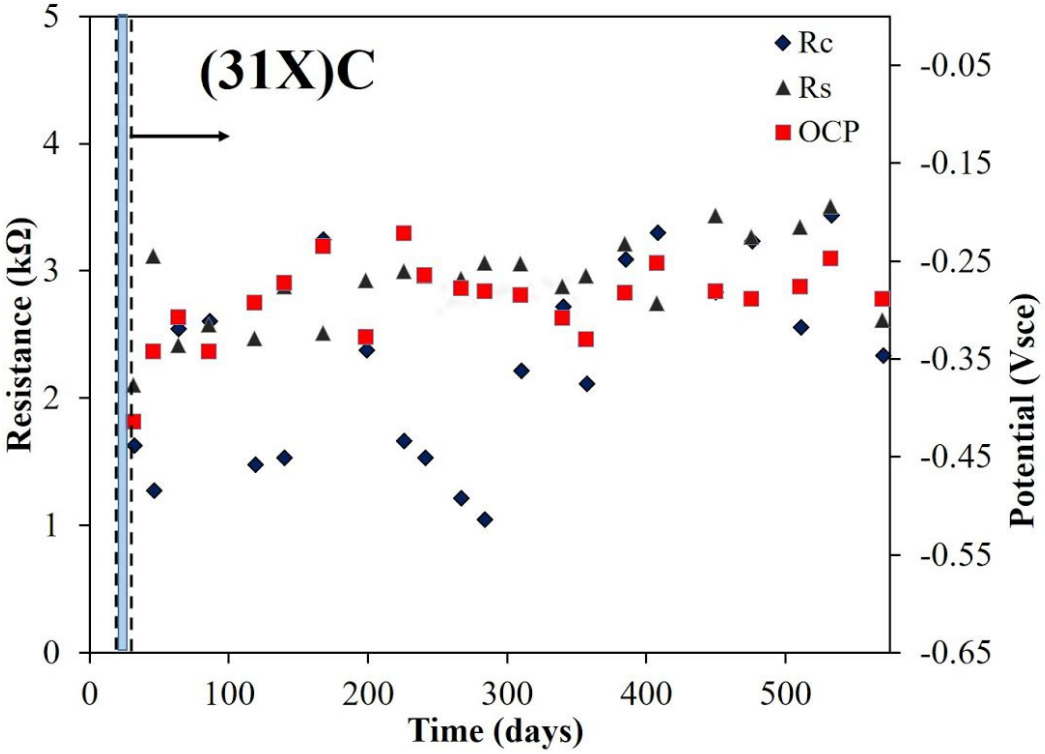

Figure 264. Rebar potentials, R_s, and R_c values measured on rebar 31X-C

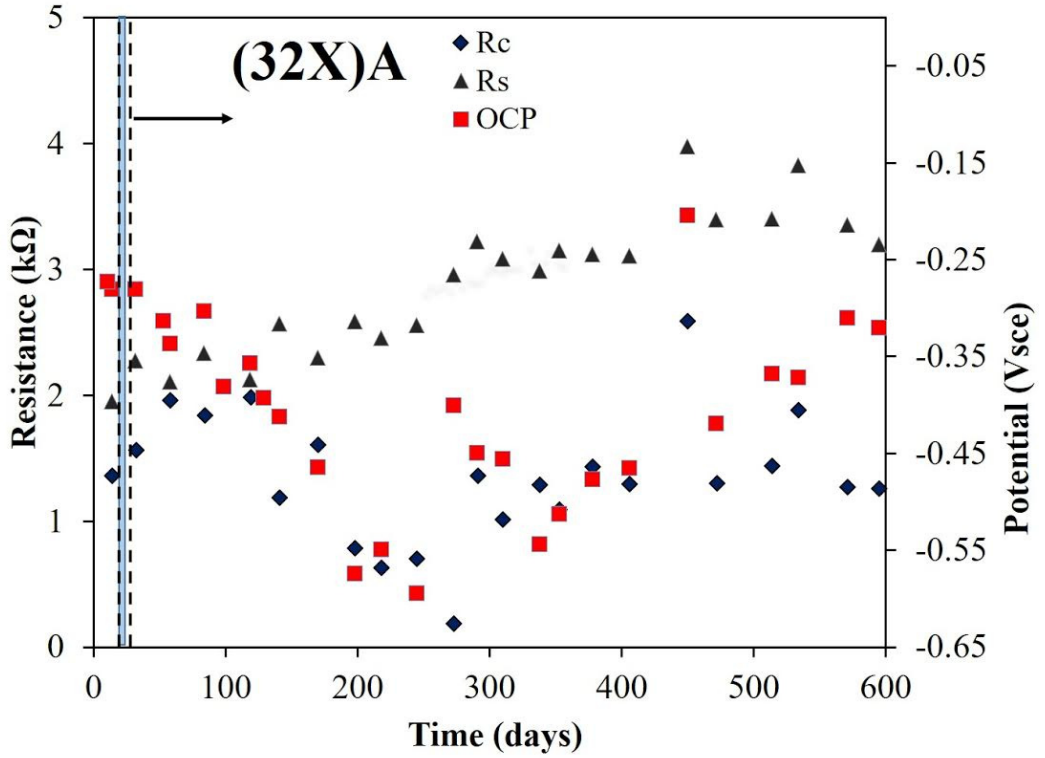

Figure 265. Rebar potentials, R_s, and R_c values measured on rebar 32X-A

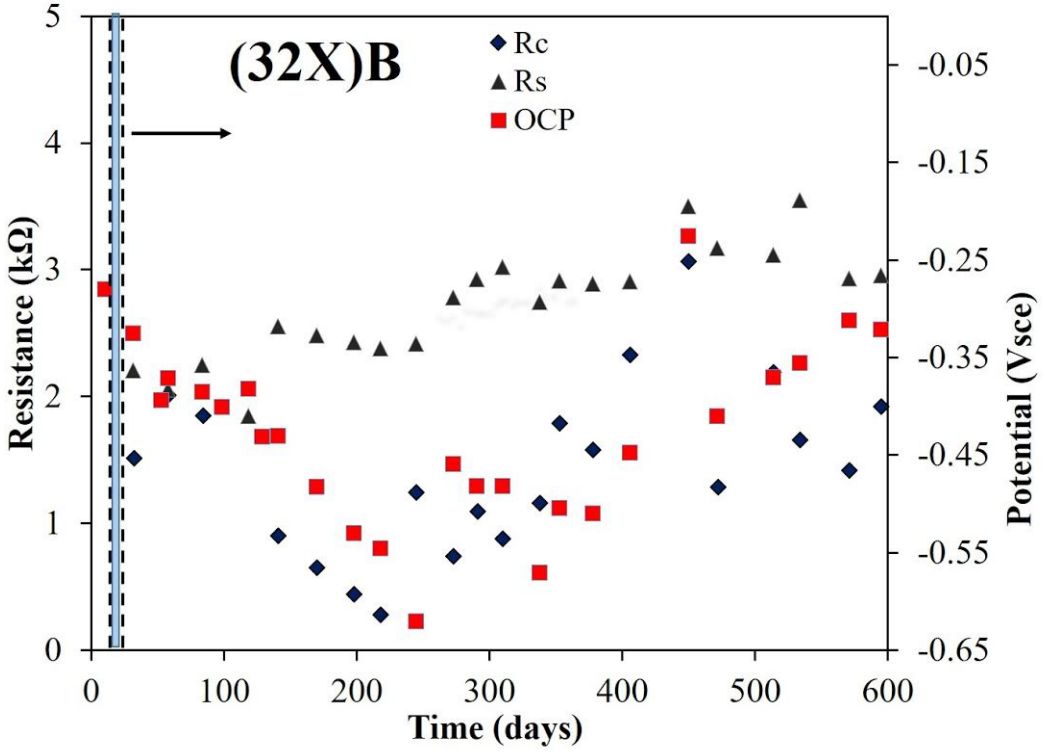

Figure 266. Rebar potentials, R_s, and R_c values measured on rebar 32X-B

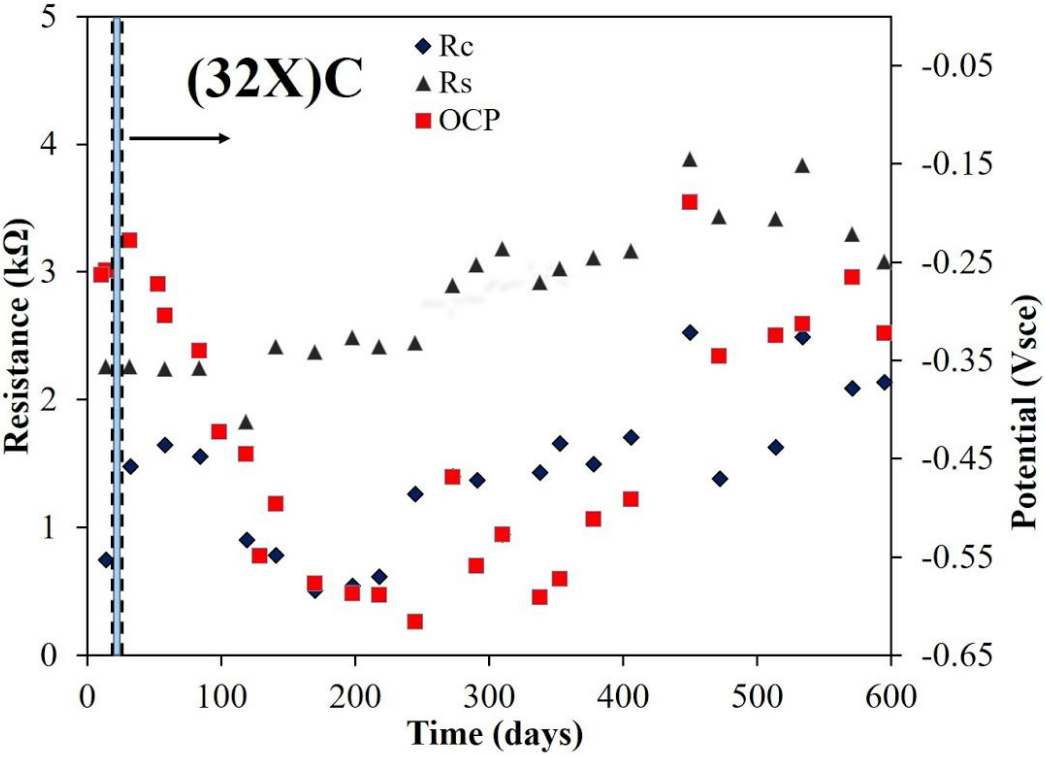

Figure 267. Rebar potentials, R_s, and R_c values measured on rebar 32X-C

Appendix H: Rebar Potential vs. Time (24-years-old Samples)

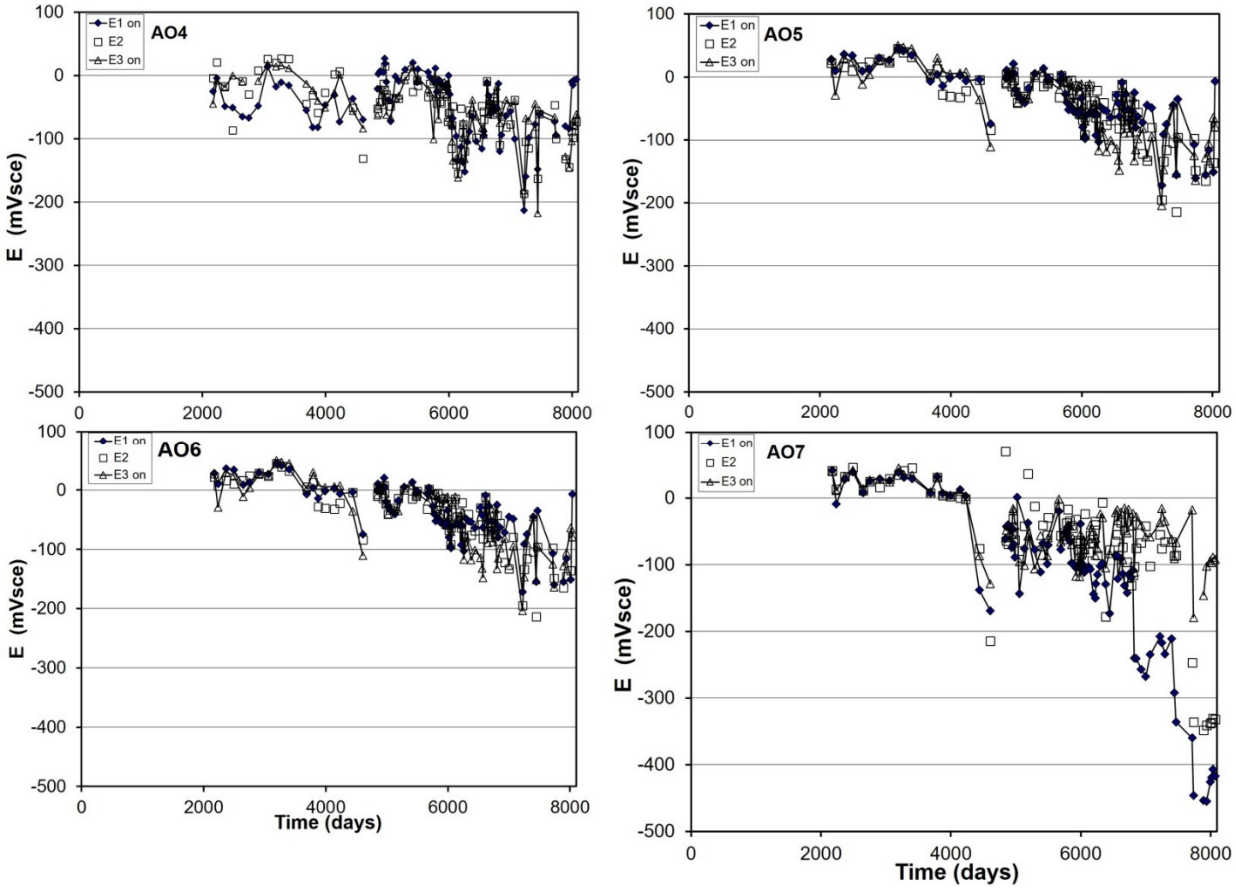

Figure 268. Rebar potentials measured on specimens AO4, AO5, AO6 and AO7

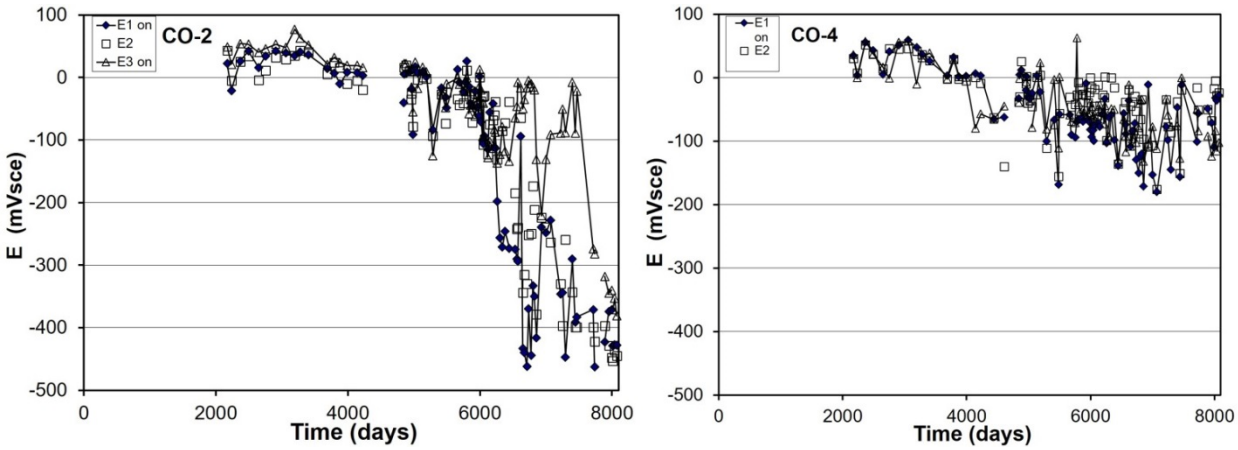

Figure 269. Rebar potentials measured on specimens CO2, and CO4

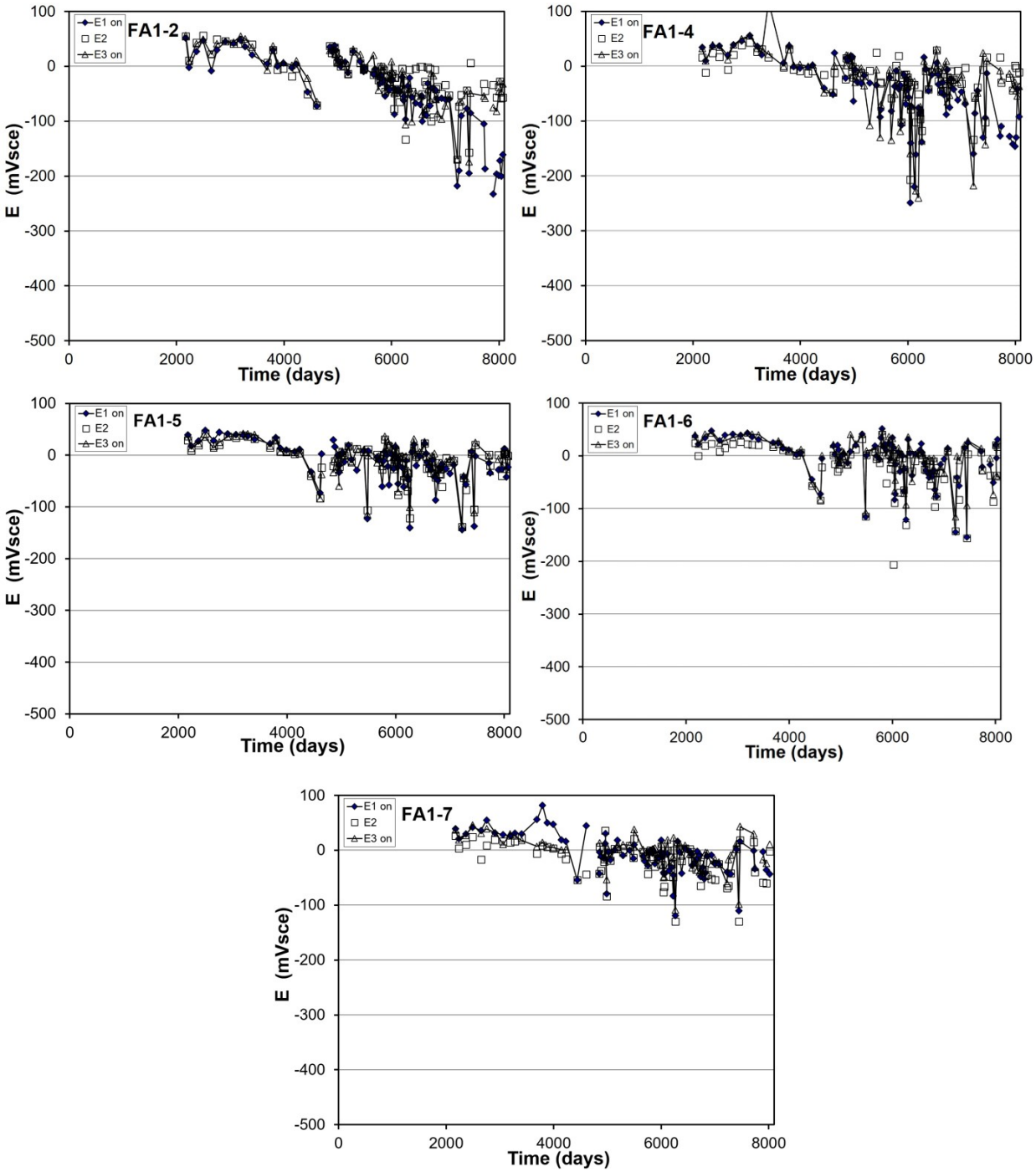

Figure 270. Rebar potentials measured on specimens FA1-2, FA1-4, FA1-5, FA1-6 and FA1-7

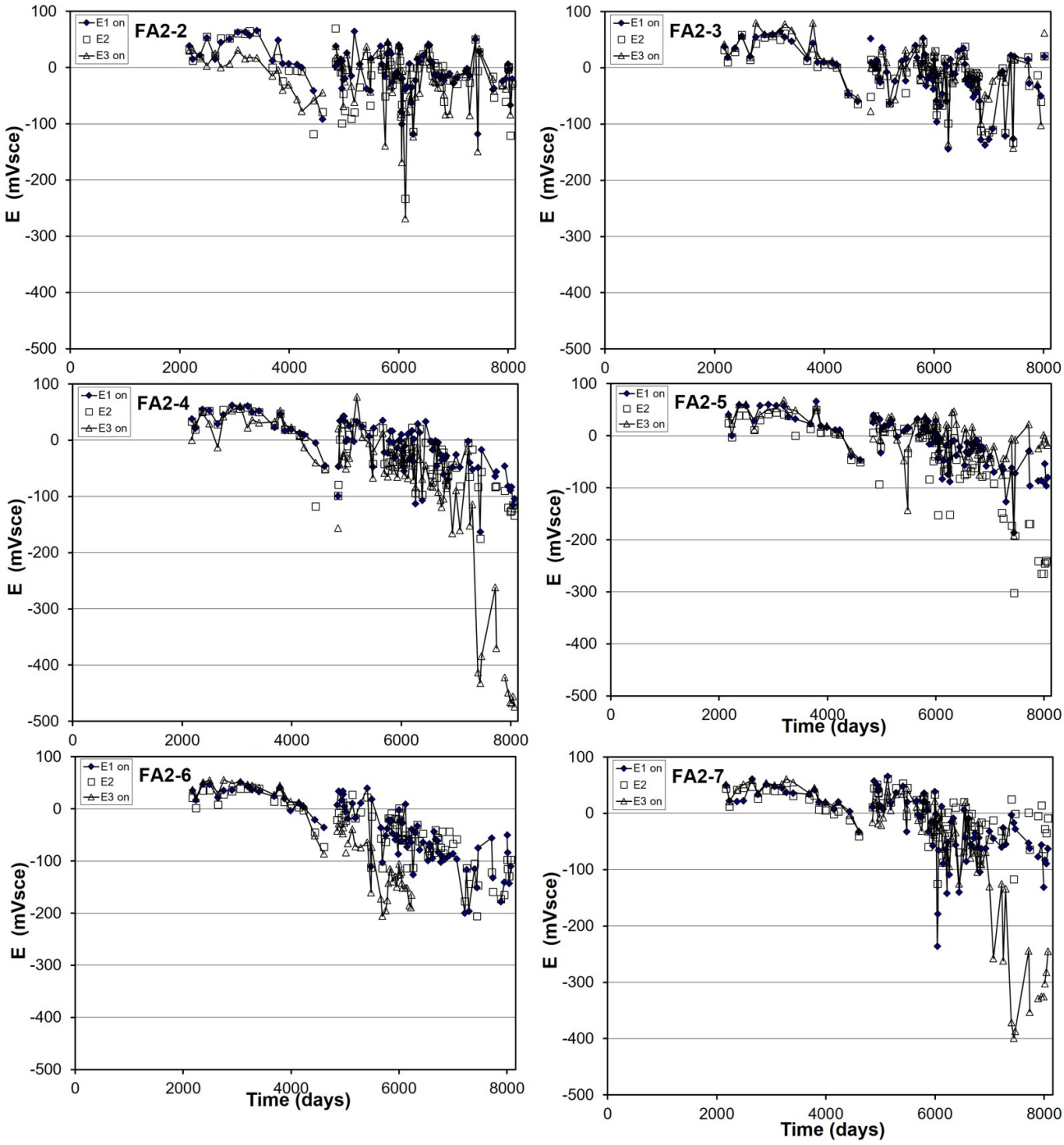

Figure 271. Rebar potentials measured on specimens FA2-2, FA2-3, FA2-4, FA2-5, FA2-6 and FA2-7

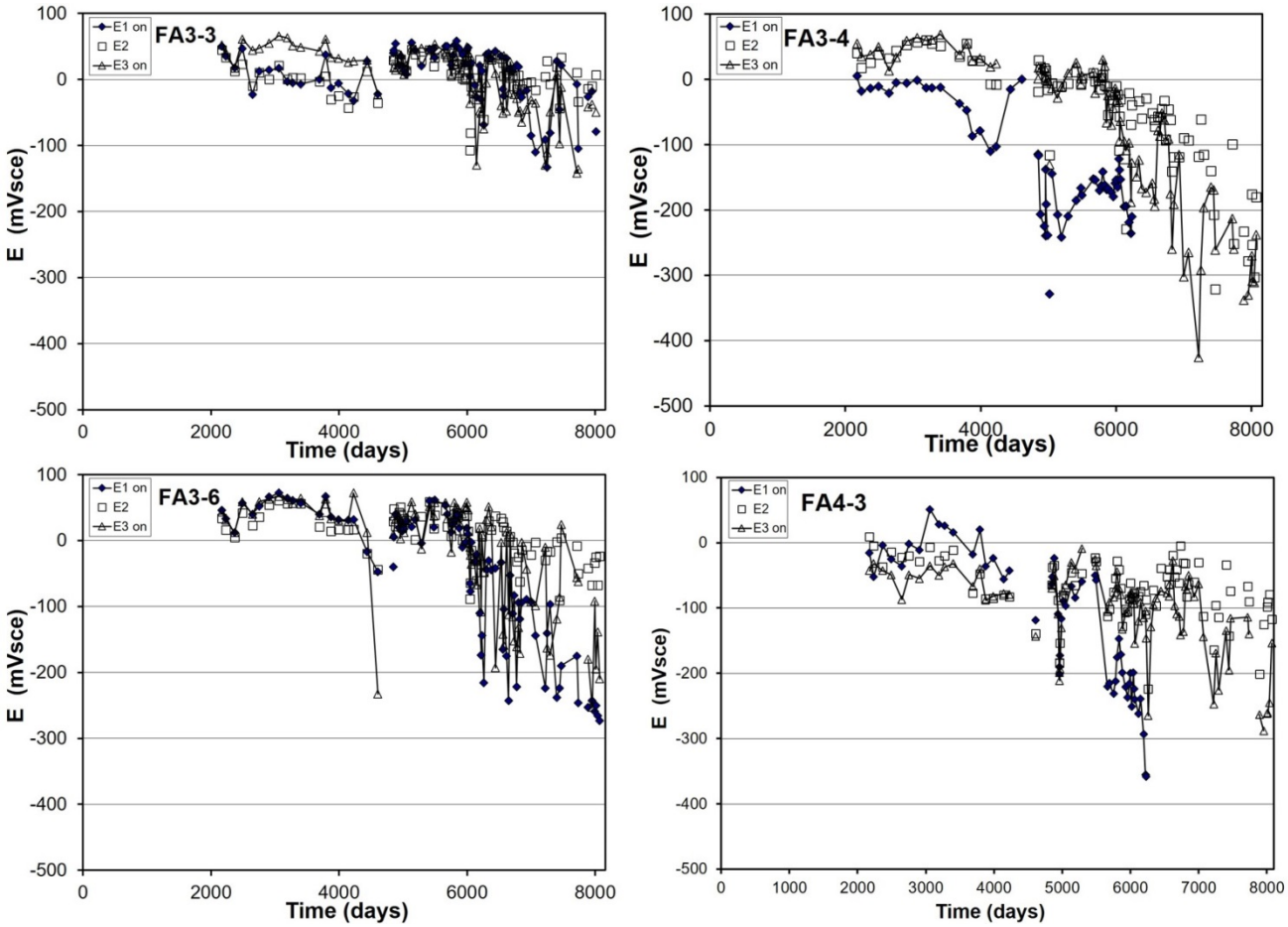

Figure 272. Rebar potentials measured on specimens FA3-3, FA3-4, FA3-6, and FA4-3

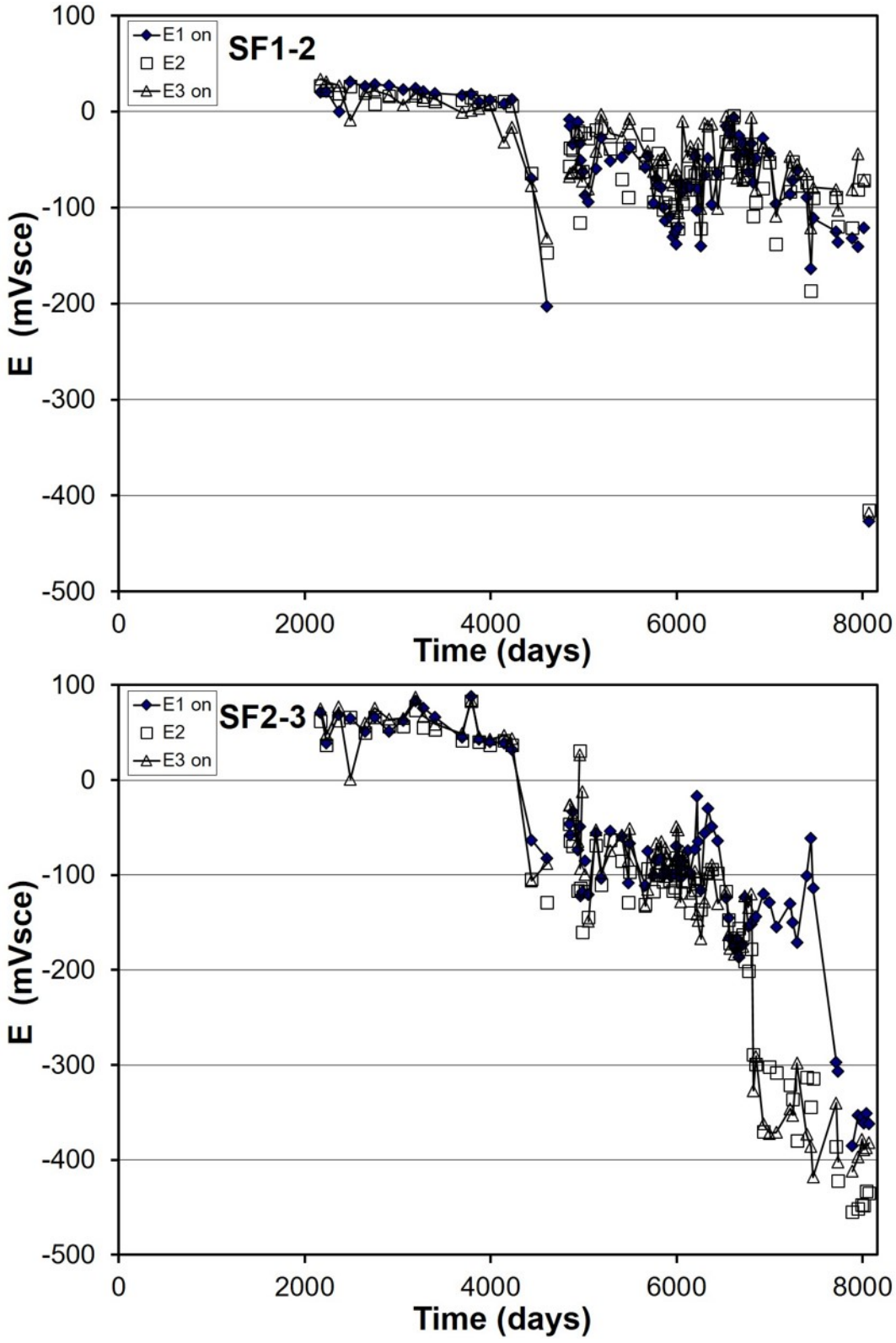

Figure 273. Rebar potentials measured on specimens SF1-2, and SF2-3

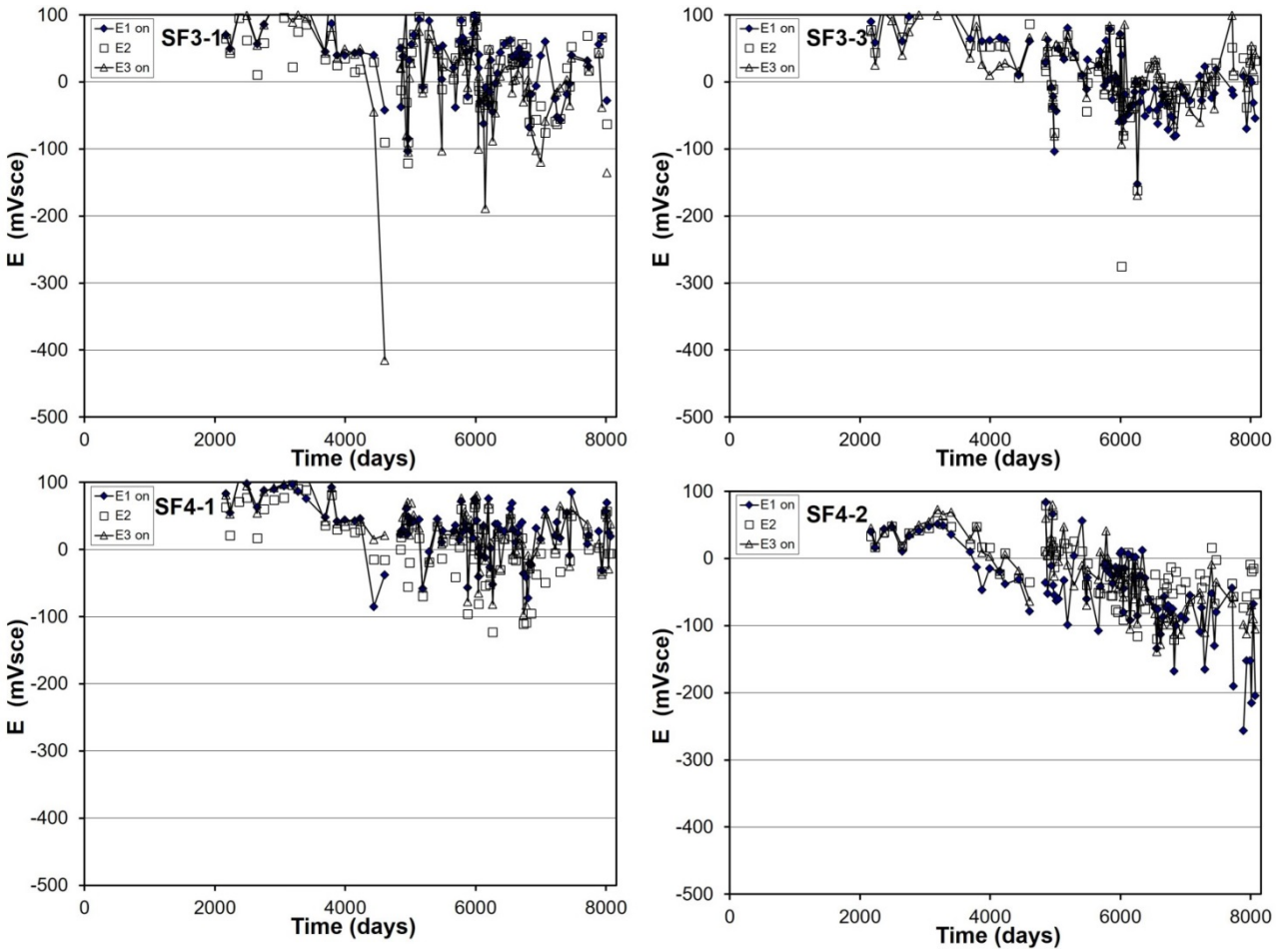

Figure 274. Rebar potentials measured on specimens SF3-1, SF3-3, SF4-1 and SF4-2

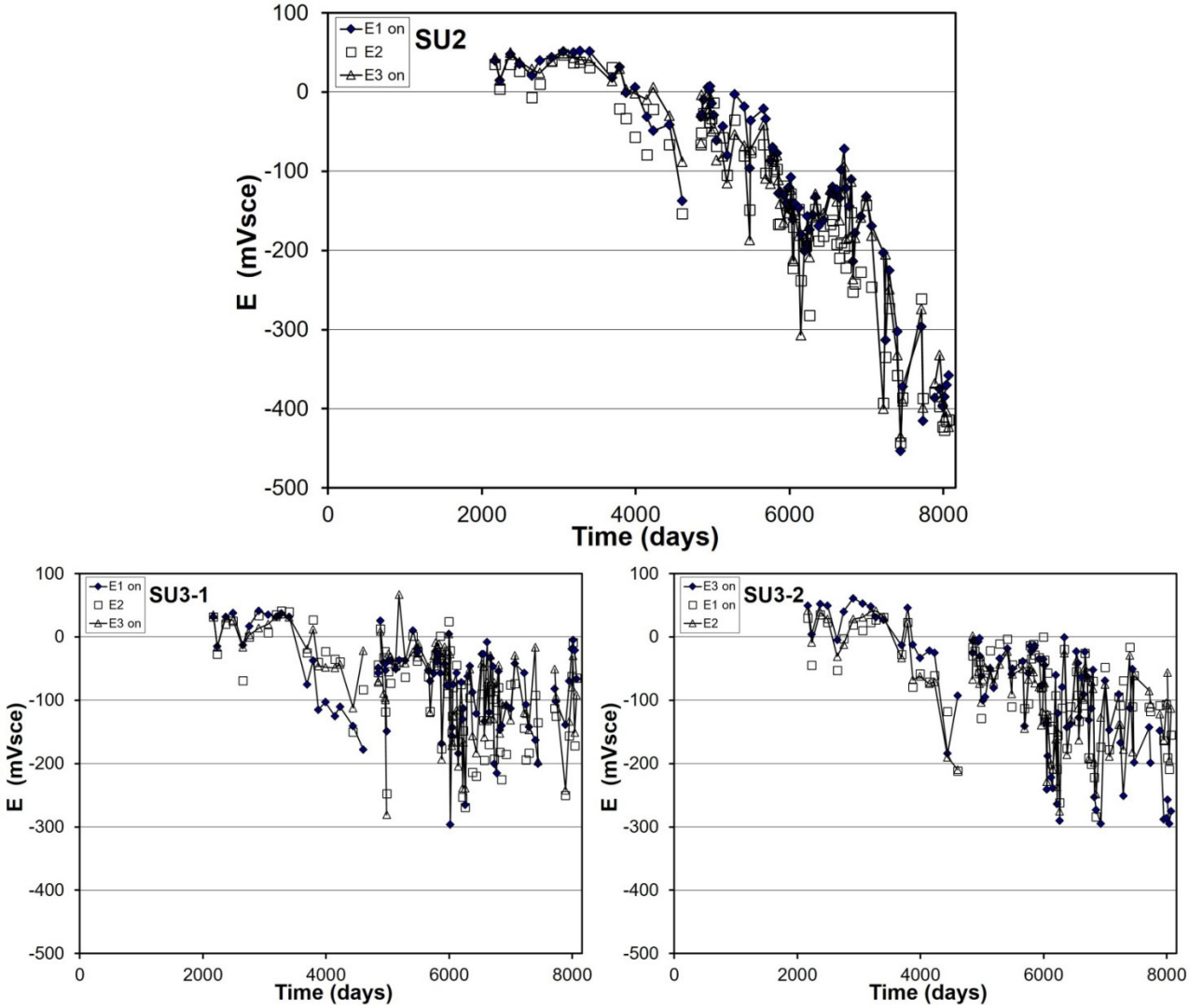

Figure 275. Rebar potentials measured on specimens SU2, SU3-1, and SU3-2

Appendix I: Forensic Examination of Specimens CO–2 (61B) and SU–2 (14B)

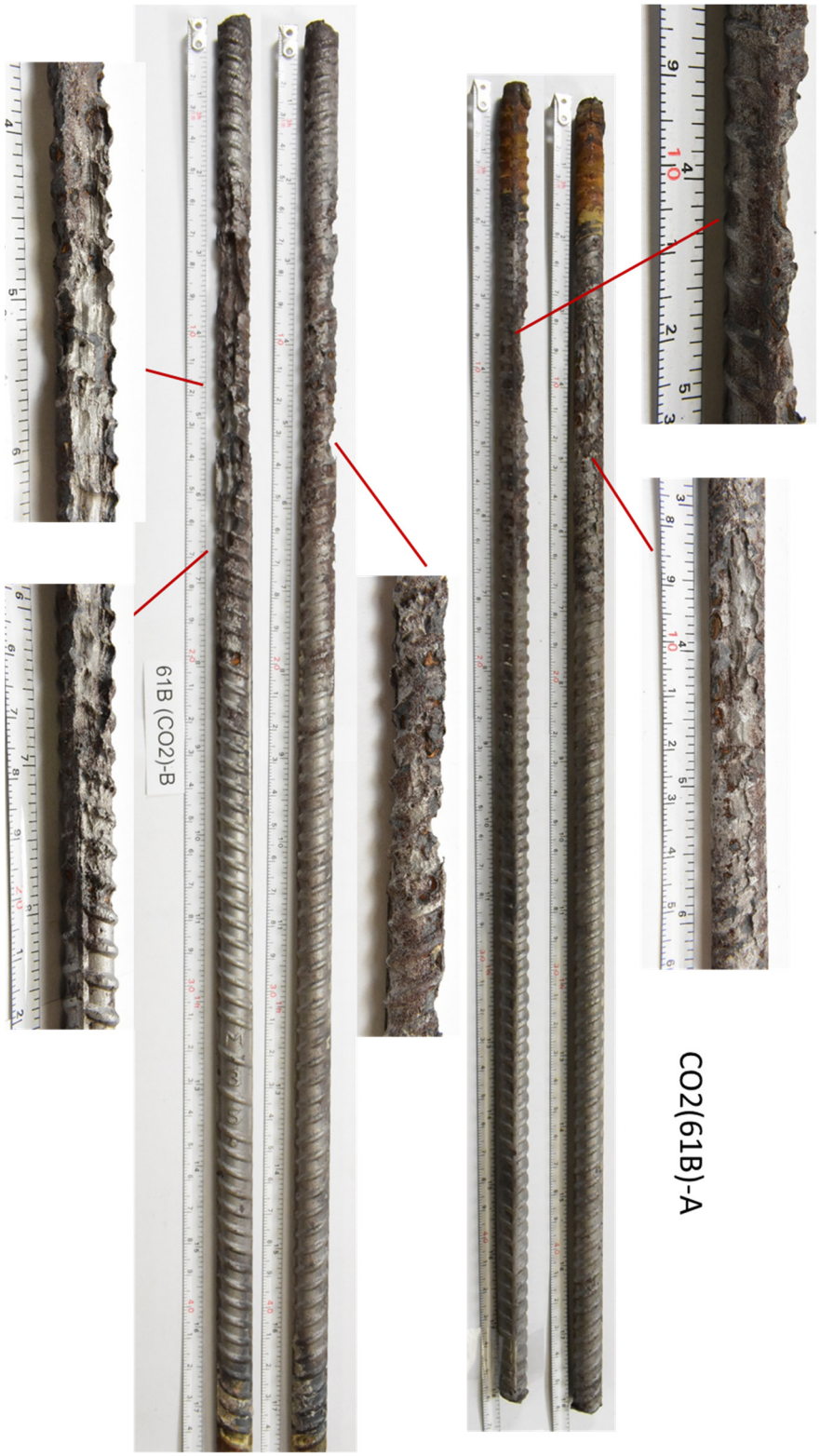

Figure 276. Visual inspection of rebar CO2-A and CO2-B

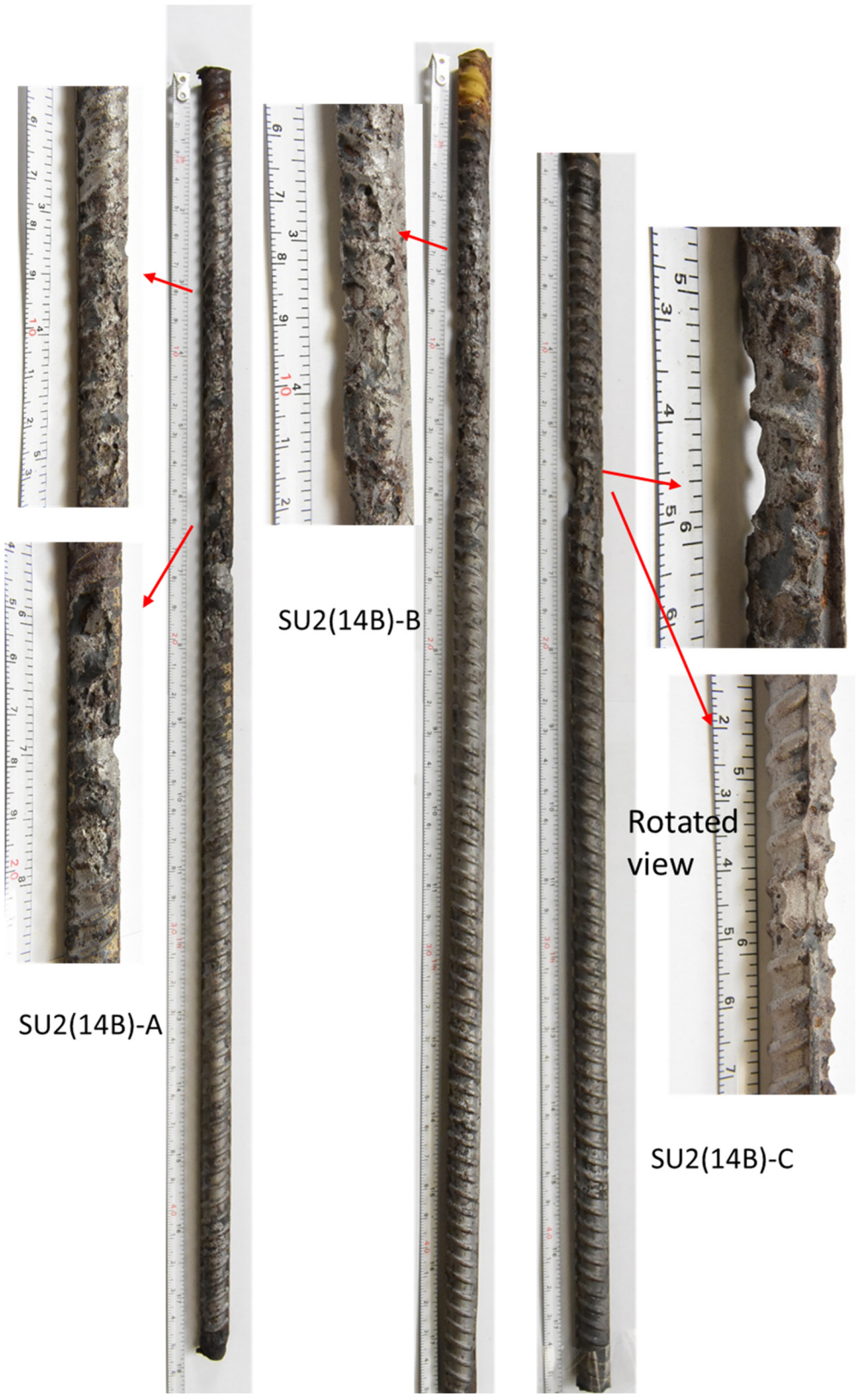

Figure 277. Visual inspection of rebar SU2-B and SU2-C